BEHAVIOR OF MATERIALS AT CRYOGENIC TEMPERATURES

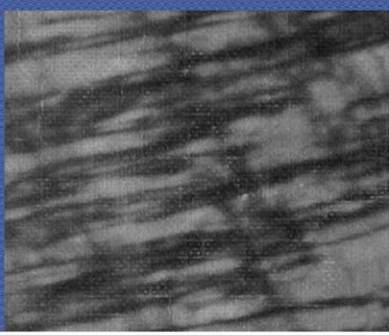

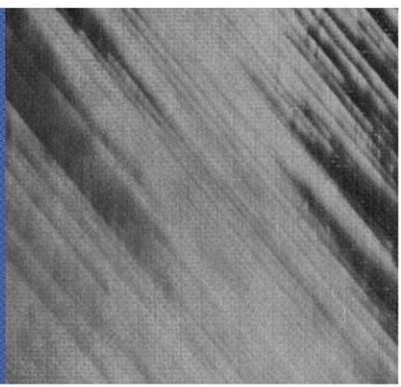

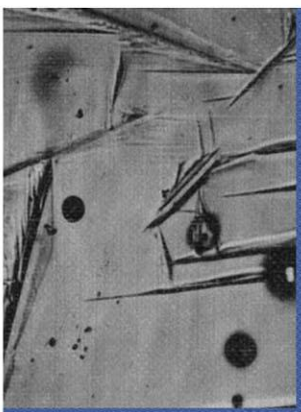

ASTM

AMERICAN SOCIETY FOR TESTING AND MATERIALS

BEHAVIOR OF MATERIALS AT CRYOGENIC TEMPERATURES

A symposium
presented at the
Sixty-eighth Annual Meeting
AMERICAN SOCIETY FOR
TESTING AND MATERIALS
Lafayette, Ind., June 13–18, 1965

ASTM SPECIAL TECHNICAL PUBLICATION NO. 387

Price $8.50; to members $5.95

published by the
AMERICAN SOCIETY FOR TESTING AND MATERIALS
1916 Race Street, Philadelphia, Pa. 19103

Library of Congress Catalog Card Number: 66-16603

NOTE

The Society is not responsible, as a body,
for the statements and opinions
advanced in this publication.

Printed in Baltimore, Md.
March, 1966

Foreword

The Symposium on the Behavior of Materials at Cryogenic Temperatures was conducted in two sessions at the ASTM Annual Meeting in Lafayette, Ind., on June 14, 1965. The first session included papers primarily associated with the mechanical behavior of materials. The second session emphasized physical behavior. One of the papers presented at the meeting, "Effect of Metallurgical Variables on the Superconducting Properties of Metals and Alloys," by H. W. Schadler and J. W. Livingston, has been published elsewhere and is included in this volume by abstract only. This symposium was sponsored by the Division of Material Sciences. Fred R. Schwartzberg, Martin Co., Denver, Colo., served as symposium chairman and presided over the afternoon session; James E. Campbell, Battelle Memorial Inst., presided over the evening session.

Related ASTM Publications

Low-Temperature Properties of High-Strength Aircraft and Missile Materials, STP 287 (1960), $7.00

Physical Properties of Metals and Alloys from Cryogenic to Elevated Temperatures, DS 22 (1961), $4.75

Evaluation of Metallic Materials in Design for Low-Temperature Service, STP 302 (1961), $7.50

Contents

This page intentionally left blank

Fred R. Schwartzberg[1]

Introduction

The behavior of materials at cryogenic temperatures has become an important area of our technology during the last decade. In recent years, a wealth of data, particularly mechanical property data, has been generated on the properties of numerous materials at very low temperatures. These data have been primarily of a phenomenological nature; significantly less attention has been devoted to gaining an understanding of these phenomena.

As our first entry into the area of cryogenics, the phenomenological approach was justified, particularly since many materials were suitable for cryogenic service and merely required testing to determine design properties. However, future developments in the cryogenic materials field will require more thorough fundamental understanding of behavior. The objective of this symposium was to provide the technical community with a convenient base for developing such an understanding.

In the first paper, Kula and DeSisto review the factors governing plastic behavior at low temperatures. Following a phenomenological presentation of behavior, such as serrated yielding and effect of crystal structure, the authors present fundamental discussions of the mechanisms associated with these characteristics. Wessel presents a discussion of the basic factors governing fracture of metals and then proceeds to show that fracture data can be used to establish performance characteristics of structures.

The third paper, by Reed and Breedis, is a very complete review and bibliography on the subject of the mechanisms of low-temperature phase transformations.

In his paper on thermophysical properties of metals, Powell treats the properties thermal conductivity and specific heat in a theoretical manner in order to provide a basis for prediction of materials behavior in the absence of great amounts of experimental data. In addition, pertinent experimental data are given and discussed. The paper by Schadler and Livingston on superconductivity was subject to prior publication and is incorporated in this volume in abstract form. This paper represents an excellent approach to superconductivity from the metallurgist's standpoint and is highly recommended for additional reading.

[1] Chief, Materials Research, Martin Company, Denver, Colorado; Chairman of Symposium.

This page intentionally left blank

E. B. Kula[1] *and T. S. DeSisto*[2]

Plastic Behavior of Metals at Cryogenic Temperatures

REFERENCE: E. B. Kula and T. S. DeSisto, "**Plastic Behavior of Metals at Cryogenic Temperatures,**" *Behavior of Materials at Cryogenic Temperatures, ASTM STP 387,* Am. Soc. Testing Mats., 1966, p. 3.

ABSTRACT: The serrated yielding exhibited by metals during tension tests at temperatures near absolute zero is the principal consideration of this paper. Stress-strain curves are presented for various metals including Armco iron, "K" Monel, and titanium at temperatures from +200 to −269 C. The variations of yield stress and ductility are shown to depend primarily on crystal structure. At −269 C, serrated yielding occurs in many metals. This is caused by adiabatic heating, and can occur independently of the deformation mechanism. A partial differential equation is derived relating load to strain hardening, strain rate, and thermal softening. At cryogenic temperatures, it is shown that thermal softening becomes so large that maximum load is exceeded, and discontinuous yielding occurs. During yielding, heating occurs, reducing the thermal-softening term, and serration ceases.

KEY WORDS: cryogenics, metals, crystal structure, yield strength, serrated yielding, strain hardening, strain rate, thermal softening

Recent years have seen a tremendous increase in studies of the behavior of materials at low temperatures. A prime factor has been the relative availability of refrigeration equipment for producing liquid helium, such as the Collins cryostat, so that low-temperature research can be carried out in many laboratories. Many interesting phenomena and applications of fundamental and practical significance have been discovered in the course of such research. The equipment required to operate at these low temperatures has led to a need for data on mechanical properties of structural materials at these temperatures.

A more important source of the demand for data on low-temperature mechanical properties has been the development of liquid-fuel rockets. The need for equipment to produce, transport, and contain large quantities of liquid oxygen and liquid hydrogen has spurred many development and evaluation programs on the mechanical properties of metals at these temperatures.

[1] Physical metallurgist, Materials Engineering Div., U. S. Army Materials Research Agency, Watertown, Mass.

[2] General engineer, Materials Engineering Div., U. S. Army Materials Research Agency, Watertown, Mass.

Beyond these rather practical requirements for mechanical property data lie some rather fundamental reasons for studying mechanical behavior at low temperatures. Changes in mechanical properties are observed with any change in temperature, and the difference between room-temperature mechanical properties and those at temperatures approaching absolute zero can be rather large. Beyond the normal temperature sensitivity found

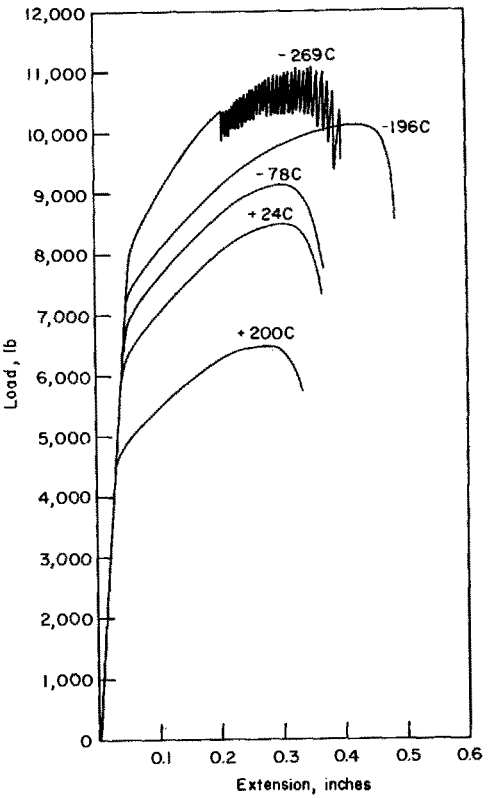

FIG. 1—*Load extension curves of cold-drawn and aged "K" Monel at the indicated temperatures.*

in all regions of the temperature scale, changes in deformation mechanism, such as from slip to twinning, and phase transitions not detected by room-temperature tests or perhaps even by cooling to low temperatures, can occur during testing at low temperatures causing marked or unexpected changes in properties. In fact, the low-temperature region approaching absolute zero is probably the most interesting on the whole temperature scale Two factors accounting for this are the low energy available from thermal fluctuations for thermally activated plastic deformation, and the very low specific heat of metals at these temperatures.

Considerable data exists on the mechanical properties of metals at low temperatures. Much of this is concerned with fracture behavior, especially brittle fracture, which is the subject of another paper in this volume.[3] One of the most comprehensive collections of strength data for structurally useful metals has been collected in the *Cryogenic Materials Data Handbook* [*1*].[4] This is an invaluable source of data with sections on: aluminum,

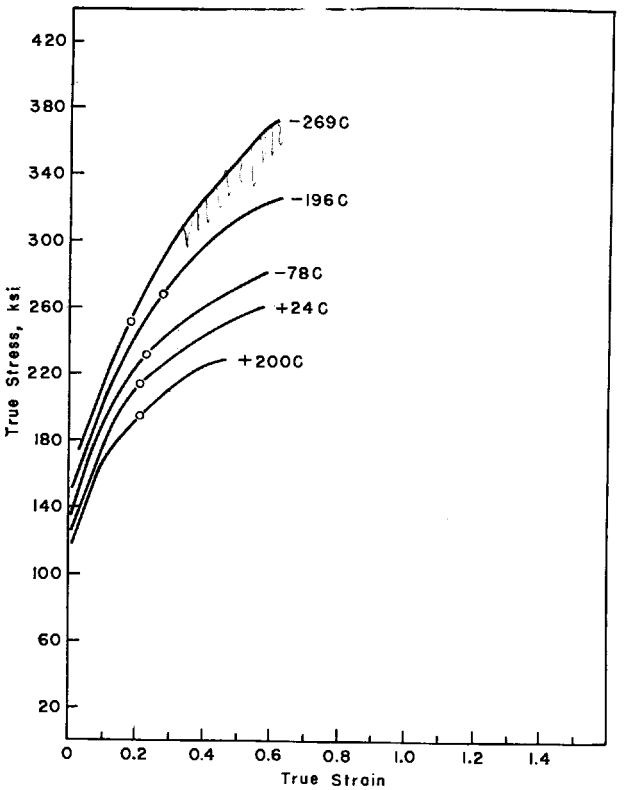

FIG. 2—*True stress-strain curves of cold-drawn and aged "K" Monel at the indicated temperatures.*

stainless steels, titanium, superalloys, alloy steels, miscellaneous metals and alloys, polymeric materials, fiber-reinforced plastics, and miscellaneous nonmetallics.

In 1958, Rosenberg published a review of the mechanical properties of metals at liquid-helium temperatures [*2*]. In addition to strength, he discusses elasticity, creep, fatigue, and internal friction.

[3] See p. 32.

[4] The italic numbers in brackets refer to the list of references appended to this paper.

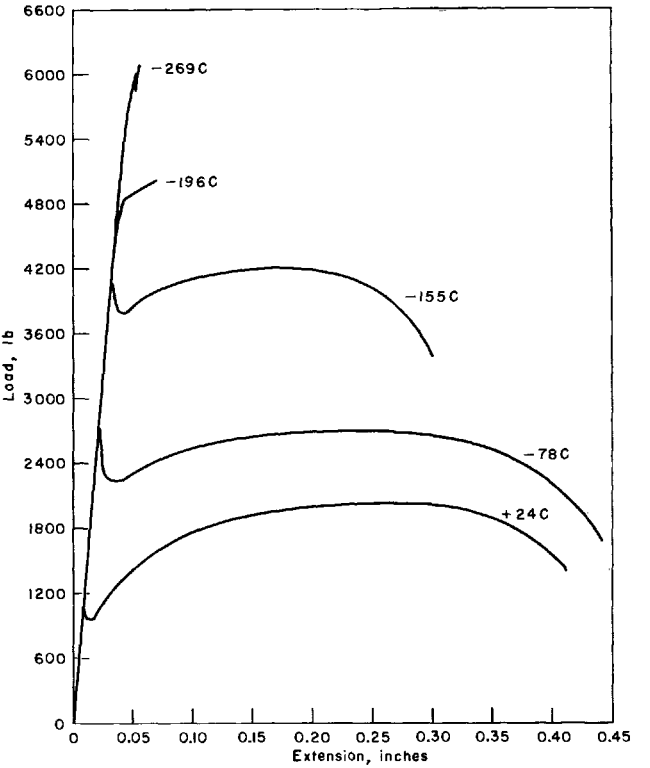

FIG. 3—*Load extension curves of annealed Armco iron at the indicated temperatures.*

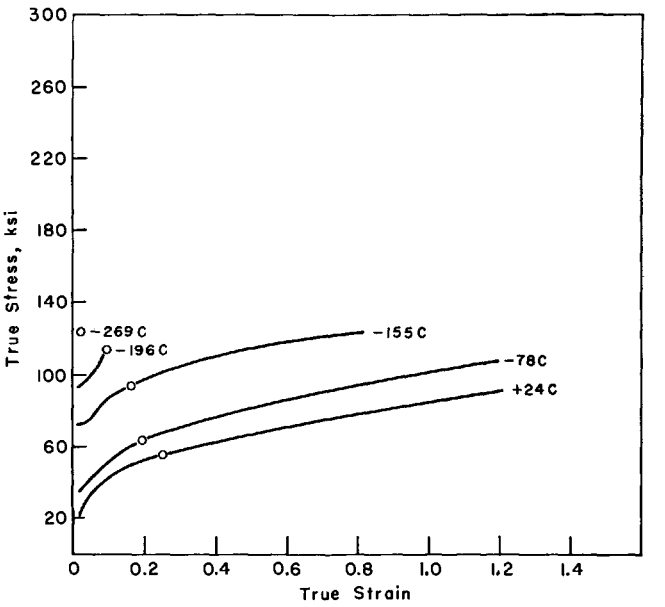

FIG. 4—*True stress-strain curves of annealed Armco iron at the indicated temperature.*

A very comprehensive review has been published by Conrad [*3*]. He not only surveys the mechanical properties of various commercially pure metals at low temperatures, but considers the structural changes occurring during deformation, and finally attempts to identify the exact dislocation mechanisms controlling plastic flow at low temperatures.

Since Refs. [*1*] and [*3*] are up-to-date and extensive in coverage, no

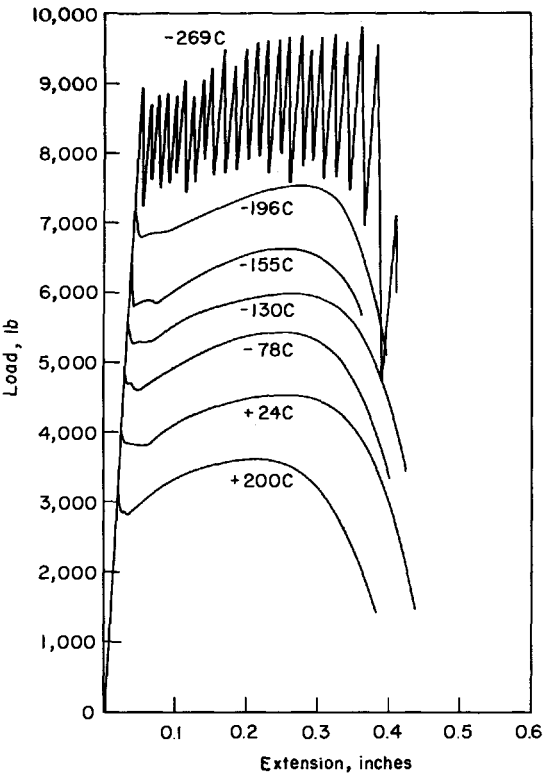

FIG. 5—*Load extension curves of annealed tantalum, 10 per cent tungsten at the indicated temperatures.*

attempt will be made here to review the voluminous data that may be pertinent to low-temperature plastic flow. Instead, we will attempt to show what happens to typical tensile stress-strain curves for metals of various crystal structures as the temperature is lowered, and how some of the properties determined from a stress-strain curve change with temperature. A brief discussion of the reasons for property changes with temperature will be made, utilizing Ref. [*3*] rather than the original references. Finally, the phenomenon of serrated yielding, so prominent in tests at liquid-helium temperature, will be discussed in some detail, and a modified interpretation of the reasons for serrated yielding will be made.

Low-Temperature Mechanical Behavior

A series of tensile stress-strain curves for "K" Monel, Armco iron, tantalum 10 per cent tungsten, and commercially pure titanium are presented in Figs. 1 to 8. The temperature range extends from −269 to +200 C. For each material a load-extension and a true stress-strain curve are shown. A diameter gage was used for the true stress-strain measure-

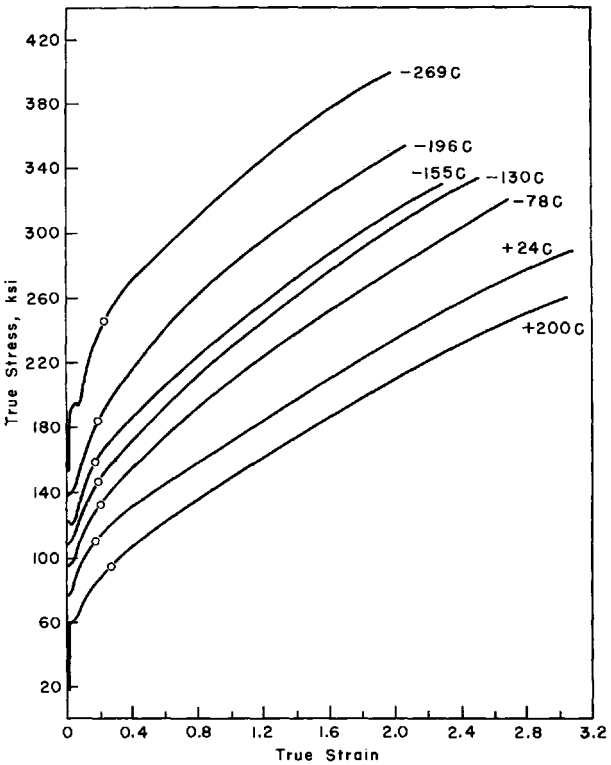

FIG. 6—*True stress-strain curves of annealed tantalum, 10 per cent tungsten at the indicated temperatures.*

ments. The extension represents length changes over a 1¼-in. reduced section on the 0.250-in.-diameter specimens.

Figures 1 and 2 show stress-strain curves for a face-centered cubic metal, the commercial alloy, "K" Monel. The yield and tensile strengths increase as the temperature is lowered, and the true stress-strain curves tend to diverge slightly. The ductility increases slightly with decreasing temperature down to −196 C, as does the strain at maximum load indicated by the circles in Fig. 2. At −269 C the ductility is slightly lower, but, more striking, a series of serrations appear after some strain. These are not shown in Fig. 2, which simply shows the upper envelope of the serrations.

Similar curves for Armco iron are shown in Figs. 3 and 4. A sharp yield point is present at all temperatures, and the ductility is reduced at low temperatures, so that premature fracture occurs on yielding at −269 C. This reduced ductility is shown not only by the reduced elongation and fracture strain, but also by decreasing values of strain at maximum load.

This premature failure is typical of many body-centered cubic metals at low temperatures. The behavior of another body-centered cubic alloy,

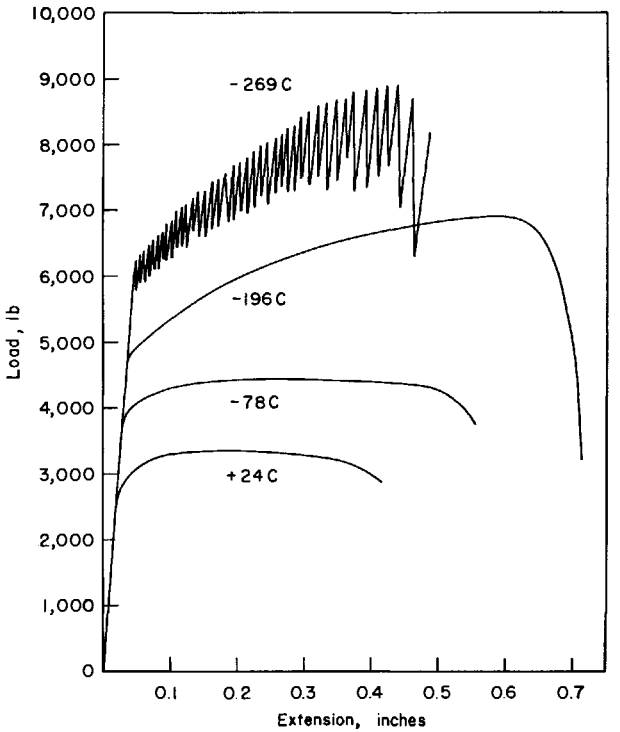

FIG. 7—*Load extension curves of annealed commercially pure titanium at the indicated temperatures.*

the single-phase Ta-10W alloy, is shown in Figs. 5 and 6. The strain at maximum load changes very little with temperature, and the fracture ductility is only slightly reduced at low temperature. This alloy shows a yield point, and the yield and tensile strengths increase with decreasing temperature. The true stress-strain curves are approximately parallel, in contrast to the "K" Monel in Fig. 2, and the change with temperature appears to be somewhat greater. At −269 C, serrations are observed immediately upon yielding.

The behavior of a hexagonal close-packed metal, commercially pure titanium, is shown in Figs. 7 and 8. The strength increases as the tempera-

ture is lowered, at a rate similar to that for the body-centered cubic metal in Figs. 5 and 6. The ductility, especially the strain at maximum load, increases as the temperature is lowered in the same manner as the face-centered cubic "K" Monel. Again, the stress-strain curve for −269 C is serrated.

The stress-strain curves shown in Figs. 1 to 8 exhibit features typical of

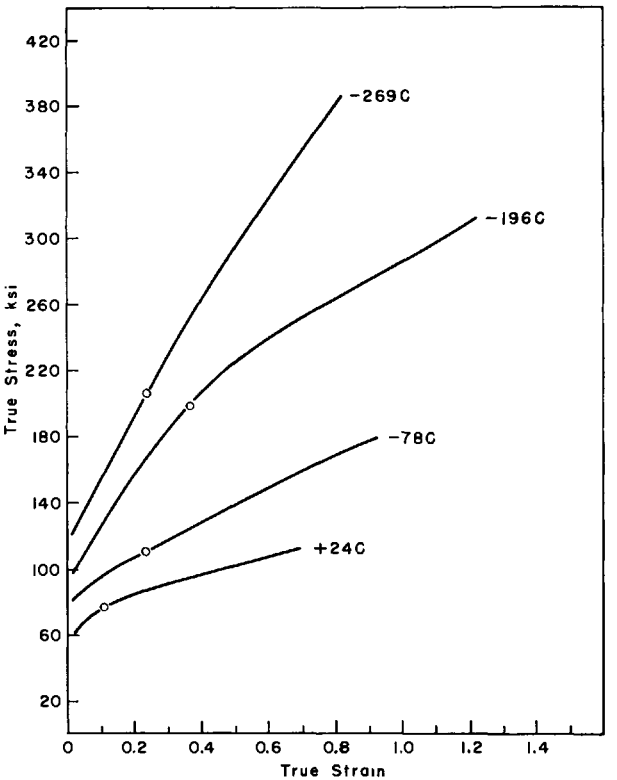

FIG. 8—*True stress-strain curves of annealed commercially pure titanium at the indicated temperatures.*

a number of metals of the given crystal structure. Specifically, metals of the same crystal structure often show similar rates of increase of flow stress with decreasing temperature and similar changes of ductility with temperature. Serrated yielding, on the other hand, occurs with metals of several different structures.

Figure 9 shows the yield strength of a number of commercial-purity metals in the low-temperature range. Where data were taken from the literature, the source is indicated by a reference after the symbol. The stresses are plotted against the homologous temperature, which is the ratio

of the test temperature T to the melting point T_m. These results show that the face-centered cubic metals, nickel and aluminum, show only a small change of stress with temperature. The body-centered cubic metals, tantalum, columbium, vanadium, and iron, show a very strong rise in yield stress, especially below a T/T_m ratio of 0.1. The hexagonal close-packed metal titanium shows a temperature sensitivity higher than the face-centered cubic metals, but lower than the body-centered cubic metals. These results are typical, although within any one group variations may be

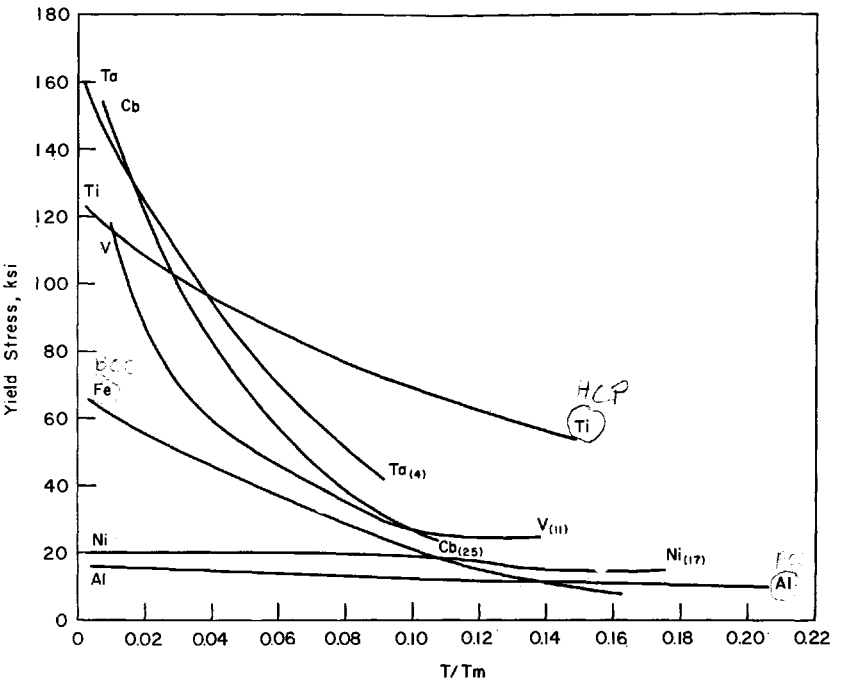

FIG. 9—*Yield stress versus T/T_m for various commercially pure metals. (The numbers in parentheses refer to references.)*

found depending on grain size, impurities, stacking-fault energy, and shear modulus. It is known from dislocation theory, for example, that the strength should depend on the shear modulus.

This distinction between crystal structures is not restricted to high-purity or commercial-purity metals, but also exists for many commercial alloys. Figures 10 to 12 show plots of yield strength versus test temperature for a number of commercial alloys. Some of the data were taken from Ref. [*1*], the remainder from tests conducted at the U. S. Army Materials Research Agency. Included in these plots are data for single-phase substitutional alloys as well as alloys where a second phase is present in the structure. Some of the data are for alloys in various heat-treated conditions.

In spite of this wide variation in composition and structure, the same behavior is exhibited for the pure metals. Again, the body-centered cubic metals show the highest temperature sensitivity, the face-centered cubic metals the lowest, and the hexagonal close-packed metals an intermediate behavior.

One group of commercially important metals that have been excluded

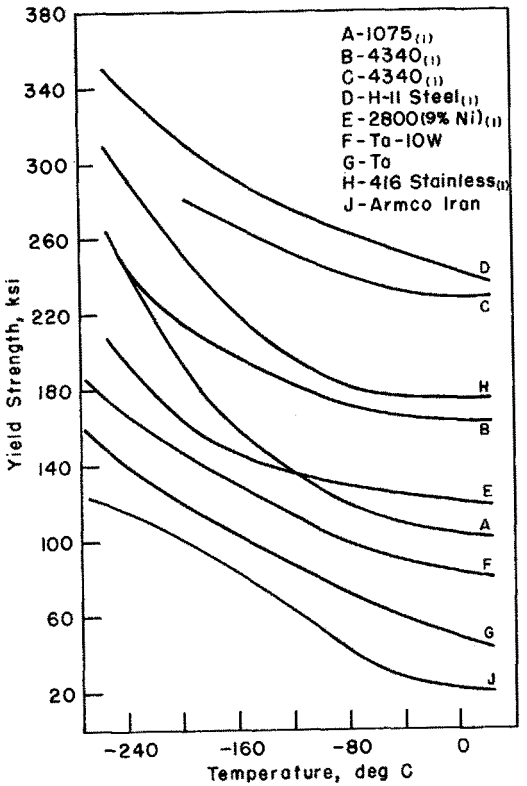

FIG. 10—*Yield stress versus temperature for various BCC commercial alloys.*

from these plots are the metastable stainless steels. These steels are face-centered cubic austenite at room temperature, but may transform to a body-centered cubic martensite or hexagonal epsilon phase either on cooling, or on straining at low temperature. Since the martensite and epsilon are significantly stronger than the austenite, this may lead to an apparently high variation of strength with temperature. Such a variation with temperature is not reversible. Martensite formation in metastable stainless steels is discussed in another paper in this volume.[5]

[5] See p. 60.

In describing the ductility, it is recognized that there are two separate factors that must be considered: the reduction of area, and the elongation. During any given test, both these quantities increase with strain. But over a range of temperature, the elongation and reduction of area at fracture may show rather different trends. The reduction of area, or fracture strain, is a measure of termination of plastic flow by brittle fracture or by

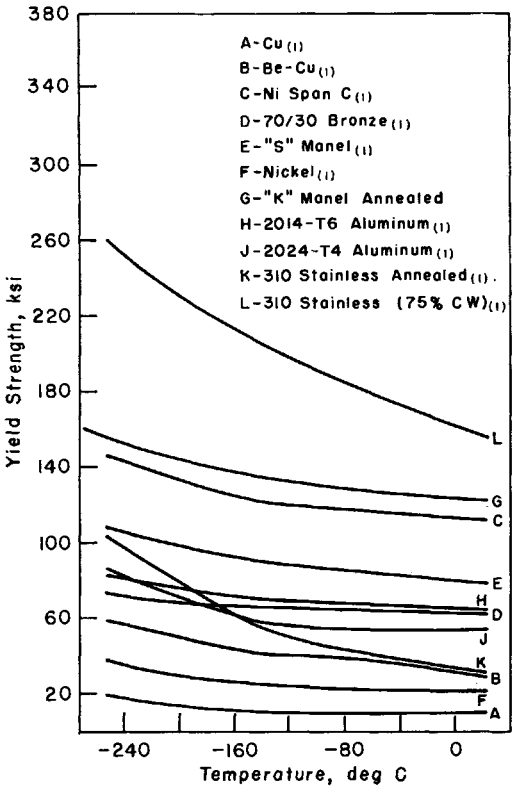

FIG. 11—*Yield stress versus temperature for various FCC commercial alloys.*

a ductile-rupture process. It is strongly influenced by the presence of inclusions. The elongation, on the other hand, is strongly controlled by the strain at maximum load. On straining beyond maximum load, the deformation is restricted to the necked region and contributes relatively little to the total elongation. The strain at maximum load is related to the work-hardening properties, since it is generally equal to the strain-hardening exponent, n, in the power law relating stress and strain, $\sigma = k\,\epsilon^n$.

This difference is shown graphically in Fig. 13, which shows ductility of tantalum as a function of test temperature [*4*]. The strain-hardening exponent, n, undergoes a sharp transition below room temperature and is

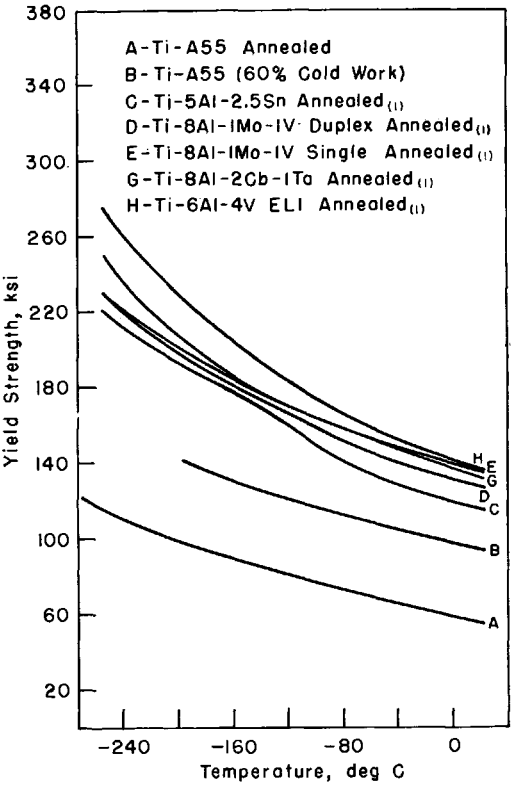

FIG. 12—*Yield stress versus temperature for various HCP commercial alloys.*

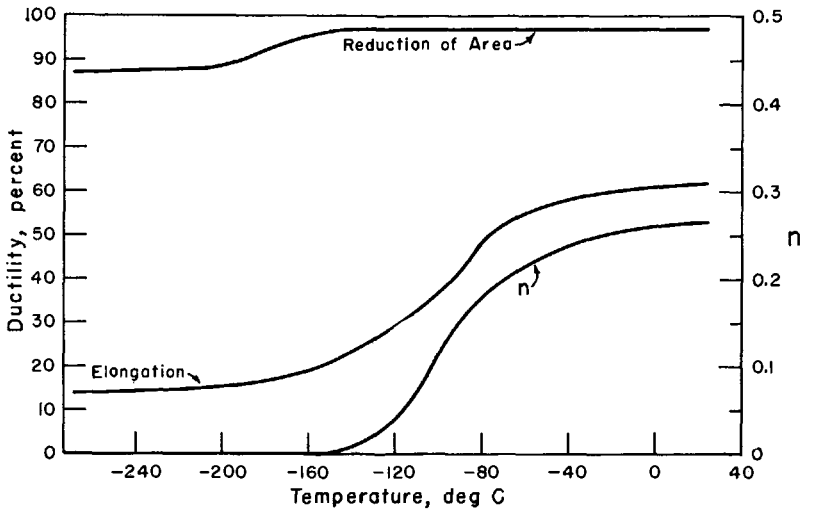

FIG. 13—*Ductility of annealed tantalum.*

essentially zero below −150 C. The elongation goes through a transition in the same temperature range, while reduction of area shows only a minor decrease. From the point of view of elongation, tantalum is not ductile at the lowest temperature, yet it exhibits excellent reduction of area. Such behavior is frequently encountered at low temperatures in body-centered cubic metals, especially if they are of high purity.

Since the strain at maximum load, or strain-hardening exponent, is a measure of the strain-hardening behavior, it is not unexpected that metals of the same crystal structure should show similar behavior with respect to

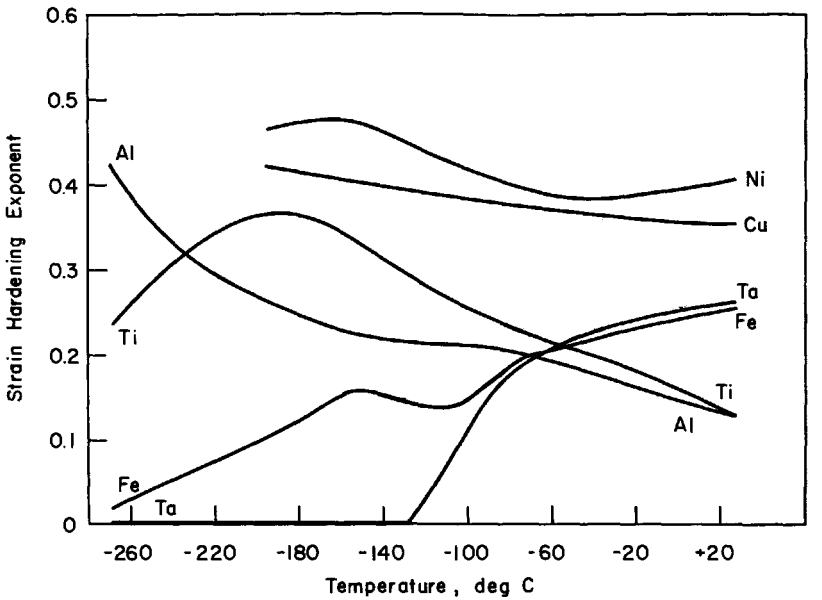

FIG. 14—*Influence of testing temperature on the strain-hardening exponents of various commercially pure metals. (Ni and Cu curves are from unpublished data by J. Nunes.)*

temperature. Figure 14 is a plot of the strain-hardening exponent for various high-purity polycrystalline metals. These and other data [5] show that face-centered cubic metals generally exhibit a steady increase of strain-hardening exponent with decrease in temperature. The body-centered cubic metals generally undergo a transition to very low values at the lower test temperatures. The temperature at which this transition occurs varies from metal to metal, and in some cases may be absent, as in the Ta-10W alloy of Figs. 5 and 6.

The behavior of the hexagonal metals varies. Titanium shows a sharp increase attributable to the onset of twinning at low temperatures. If no twinning occurs, the change with temperature is less.

In commercial alloys, the same general behavior is often found. For

many metals, there is an inverse relationship between strength level and strain-hardening exponent. As the strength level is increased by solid-solution strengthening or by precipitation hardening, the strain-hardening exponent decreases. The increased strength level at low temperatures for body-centered cubic metals is undoubtedly a contributing factor to the decrease in strain-hardening exponent at these temperatures. It is not the sole factor, however, since the data for the Ta-10W alloy in Figs. 5 and 6 show a strong increase in yield stress with no change in strain-hardening exponent.

The increase in strain-hardening exponent at low temperatures for the face-centered cubic metals is also manifested in the fact that the true stress-strain curves, such as Fig. 2, tend to diverge with increasing strain. This means that the temperature sensitivity of the flow stress increases with the strain at which the flow stress is measured, and that the temperature sensitivity of the tensile strength is greater than that of the yield stress [*3*].

Discussion

It is well known that the crystallography of slip depends primarily on the crystal structure [*6*]. Hence it is not surprising that metals of the same crystal structure often show a similar dependence of plastic-flow properties on temperature. Face-centered cubic metals generally slip on the most densely packed planes, {111}, in the close-packed directions, ⟨101⟩. Body-centered cubic metals slip in the close-packed directions, ⟨111⟩. The slip plane varies depending on composition and temperature. As the temperature increases, the slip planes tend to change from {112}, to {110}, to {123} for some metals. In iron, however, all three slip planes are active at room temperature. At low temperatures, slip in body-centered cubic metals may be interrupted by deformation twinning. Hexagonal metals generally slip on the basal planes, (0001), in the $\langle 11\bar{2}0 \rangle$ directions if the ratio of the lattice parameter, c/a, is higher or lower than ideal. At intermediate values of c/a, prismatic slip, $\{10\bar{1}0\}$ $\langle 11\bar{2}0 \rangle$, is generally encountered. At low temperatures, twinning becomes an important deformation mechanism. These are general behaviors, and in any given case the effects of composition, strain rate, and temperature are important.

Etch-pit studies and, especially, transmission electron microscopy have revealed important information on dislocation structures in metals. For face-centered cubic metals, after a small amount of deformation, the dislocations tend to arrange themselves in a cell structure [*7*]. Further straining leads to an increase in dislocation density, with most of the dislocations in the cell walls, and a decrease in cell size. A limiting value of cell size is reached at a given temperature. The cell size decreases as the deformation temperature lowers.

Most investigations have shown a linear dependence of dislocation density ρ on strain

$$\rho = k\epsilon \quad \ldots\ldots\ldots\ldots\ldots\ldots\ldots\ldots (1)$$

Similarly, the dependence of flow stress on dislocation density has been found to be

$$\sigma = k'Gb\rho^{1/2} \quad \ldots\ldots\ldots\ldots\ldots\ldots\ldots\ldots (2)$$

where G is the shear modulus, and b the Burger's vector.

Similar behavior has been encountered with body-centered cubic metals. In these metals, however, while the dislocation density varies linearly with strain (Eq 1) the variation of flow stress with dislocation density is given by

$$\sigma = \sigma_0 + k''Gb\rho^{1/2} \quad \ldots\ldots\ldots\ldots\ldots\ldots\ldots\ldots (3)$$

where σ_0 is the extrapolated value of σ at zero dislocation density.

In body-centered cubic metals such as iron, cell formation is observed at room temperature after sufficient strain. The cell size decreases with decreasing temperature as in face-centered cubic metals, but the strain required for cell formation is found to increase as the temperature is lowered. The dislocation distribution tends to be more uniform at the lower temperatures, and the dislocations may be relatively straight and lie on definite crystallographic planes [*8*].

Thus it is apparent that on a microscopic scale there are important distinctions as to dislocation arrangements during straining metals of different crystal structure. While there is similarity between different metals of the same structure, important differences can also arise here based on composition, temperature, stacking-fault energy, and so forth.

The Hall-Petch equation

$$\sigma = \sigma_i + kd^{-1/2} \quad \ldots\ldots\ldots\ldots\ldots\ldots\ldots\ldots (4)$$

has generally been used to explain the variation of flow stress, σ, on grain diameter, d. The term σ_i is a friction stress which depends on temperature and strain rate, and k is a constant which depends only slightly on temperature. The friction term, σ_i, in turn can be separated into two components

$$\sigma_i = \sigma^* + \sigma_\mu \quad \ldots\ldots\ldots\ldots\ldots\ldots\ldots\ldots (5)$$

where σ^* is a thermal component depending on temperature and strain rate, and σ_μ an athermal term. This athermal term depends on temperature only through its dependence on the shear modulus, G.

An interpretation of σ^* and σ_μ can be obtained in terms of dislocation theory. The athermal component, σ_μ, is associated with obstacles to plastic flow, where the energy from thermal fluctuation is not enough to over-

come the obstacles. Generally there are long-range stress fields associated with these obstacles, which may be such things as large precipitates, or dislocations on intersecting or parallel slip planes. The thermal component of the stress σ^* is associated with short-range obstacles, where thermal fluctuations can provide the energy to overcome the obstacles. Such obstacles include the Peierls-Nabarro stress, forest dislocations, the motion of jogs in screw dislocations, cross-slip of screw dislocations, and climb of edge dislocations.

Recognition that plastic flow is thermally activated has stimulated attempts to determine the rate-controlling mechanisms for plastic flow under various conditions. A review of this area has recently been published by Conrad [*9*]. The macroscopic strain rate, ϵ, can be expressed as a function of the dislocation velocity

$$\dot{\epsilon} = \phi b \rho \dot{s} = \phi \nu \exp\left(\frac{-H}{kT}\right) \quad \ldots\ldots\ldots\ldots\ldots\ldots (6)$$

where ϕ is an orientation factor, about 0.5 for tensile strain; b is the Burgers vector; ρ is the density of moving dislocations; s the average velocity of the dislocations; ν the frequency factor; H the activation enthalpy (energy); and T = absolute temperature. By conducting tension tests where the temperature or strain rate is changed, or creep tests where the temperature or stress is changed, it is possible to experimentally determine the activation energy, H, the frequency factor, ν, and an activation volume, v. The experimentally determined values can then be compared to calculated values for various assumed dislocation mechanisms.

For the face-centered cubic metals it is found that the Cottrell-Stokes law is approximately valid [*10*]. This states that the ratio of the flow stresses at two temperatures is approximately constant, independent of strain. Furthermore, the athermal part of the flow stress, σ_μ, is greater than the thermal part, σ.* This is supported by the yield-stress curves in Figs. 9 and 11, which show that the thermal part of the flow stress is quite small. It has not definitely been determined what the rate-controlling mechanism is, although the intersection of dislocations is undoubtedly important. It is also possible that the conservative motion of jogs plays a role [*3*].

Body-centered cubic metals show a much larger thermal component of the stress than do the face-centered cubic metals, as is evident from Figs. 10 and 11. At low temperatures below $T/T_m = 0.1$, the thermal component is larger than the athermal component, but at somewhat higher temperatures, $T/T_m \geqq 0.2$, the athermal component is larger. Impurities appear to play a minor role for iron and some metals in Group VI-A, but are less important for the Group V-A metals, where the solubility of interstitials is higher [*3*]. It is now apparent that direct impurity-dislocation reactions are not responsible for the high flow stresses at low temperatures. The

rate-controlling mechanism appears to be overcoming the Peierls-Nabarro stress, presumably by the production of double kinks in straight dislocation lines [*11*].

Studies such as this have been useful in trying to understand the rate-controlling processes for deformation, but in most cases the exact mechanisms have not been pinned down with certainty. In all cases, the experimentally determined values have to be compared with values calculated for various assumed dislocation configurations. Besides the obvious difficulties in making theoretical calculations of this sort, it is often found that experimentally determined values are compatible with several dislocation mechanisms. Nevertheless this approach is capable of extending our knowledge of low-temperature plastic flow.

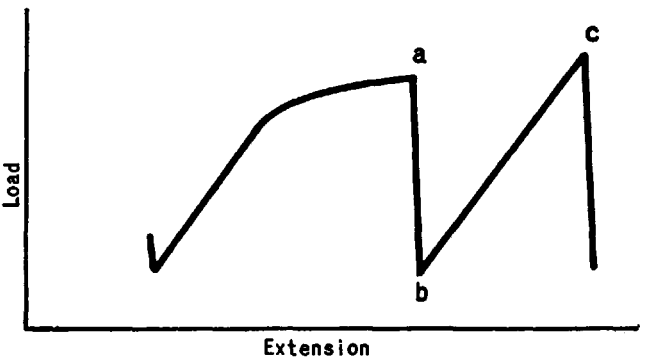

FIG. 15—*Schematic of serrations in load-extension curve at −269 C.*

Serrated Yielding

Probably the most interesting phenomenon encountered during tension testing at low temperatures is the occurrence of serrated stress-strain curves, observed in Figs. 1, 3, 5, and 7. These serrations are somewhat similar in appearance to serrations observed during elevated-temperature testing of metals that are undergoing strain aging. The serrations can take the form of many small serrations, or two or three very large serrations. In some cases the serrations start immediately upon yielding, in other cases only after considerable plastic deformation.

This is true discontinuous yielding, and the drop in load occurs very rapidly, in about 1.5×10^{-4} sec [*12*]. Since the total distance between the crossheads of the tensile machine remains constant during the load drop, or increases by an amount consistent with the crosshead velocity, there must be an elastic relaxation of the specimen and the rest of the system between the crossheads. There must be also a plastic extension of equal magnitude in the specimen to keep the total length constant (or increasing

at the rate the crossheads are moving). Thus, there is an effective exchange of elastic strain for plastic strain, and this plastic strain is generally found to be localized at one point along the length of the specimen.

An extensometer on the specimen will measure an increase in length caused by the plastic strain during the load drop, *a–b*, in Fig. 15. Further straining will be on an elastic line, *b–c*, until a load is reached that is generally slightly above the load at which the previous serration occurred. Another serration may appear immediately, or there may be a region of homogeneous straining along the normal stress-strain curve before another serration appears. With succeeding serrations, the region which undergoes localized straining may change along the length of the specimen, or the deformation may continue to be localized in one region.

Since the plastic extension equals the elastic relaxation, the elastic stiffness of the specimen and testing system determines the amount of plastic strain occurring during a given load drop. By inserting springs in series with the specimen, Rutherford et al were able to replace the sharp load drops by periods of extended straining at almost constant load [*13*]. The whole question of system stiffness has been extensively treated by Chin et al [*14*], who showed how the stiffness influenced the character of the serrated yielding and even the fracture stress.

There have been a number of explanations offered for the cause of these serrations, or instabilities. Deformation twinning [*15*], martensite formation [*16*], and "burst" dislocation formation [*17*] have all been suggested as possibilities, although now it is generally agreed that the serrations are caused by adiabatic heating [*12*]. Strain localization by adiabatic heating has been long recognized [*18*], but Basinski showed how the peculiar conditions of low heat capacity and high temperature sensitivity of the flow stress at low temperatures can lead to this being a general phenomenon [*12*].

That portion of the energy of plastic deformation not remaining in the specimen as stored energy is converted into heat. Since the heat capacity of metals is very low at temperatures approaching absolute zero, this thermal energy leads to a very large temperature rise, unless it can be rapidly dissipated by conduction along the length of the specimen or through the surface to the surrounding cooling medium. Furthermore, most metals have a high rate of change of flow stress with temperature, $d\sigma/dT$, in this temperature region. If the thermal softening caused by heating during deformation is greater than the strain hardening, the specimen soon has an applied load greater than necessary for continued deformation at the then-current temperature. This is an unstable situation, and the load suddenly drops, at a rate determined by the elastic stiffness of the system. When the applied load has dropped below that required for continued deformation at the then-current temperature, plastic flow ceases, and the specimen cools down to that of the surrounding medium. The specimen is

then loaded elastically until the flow stress is again reached, plastic deformation and concomitant heating occur, and the whole process repeats itself.

For 24S aluminum alloy, Basinski calculated the length of flowing region necessary for plastic flow under adiabatic conditions, the temperature rise, and the magnitude of the load drops, all of which gave reasonable agreement with measured values.

The fact that serrated yielding occurs under adiabatic conditions does not necessarily prove that adiabatic flow is the cause of the serrations. Some difficulty may be encountered in accepting this concept, if one thinks in terms of gross effects instead of infinitesimal rates of change, since the plastic deformation and temperature rise, which presumably cause the load drop, occur *after* the load has started to drop. Basinski [*12*] and Erdman and Jahoda [*19*, *20*] have experimentally measured thermal effects during serrated yielding, and have shown that the temperature starts to rise when the load drops. Using "transient calorimetry," Erdman and Jahoda were able to identify the location and magnitude of the heat generated during each load drop. Basinski recognized this problem and postulated a "nucleating deformation" that would occur before the serration [*12*].

Chin et al extended Basinski's concept and considered the relaxation of load applied by the machine [*14*]. Discontinuous flow would be possible when

$$dF_T + dF_{SH} \leqq dF_M \quad \ldots\ldots\ldots\ldots\ldots\ldots\ldots\ldots (7)$$

where dF_T is the load decrease caused by thermal softening, dF_{SH} the load increase caused by strain hardening, and dF_M is the relaxation of load applied by the machine, which is proportional to the spring constant of the system.

Other authors neglected the area change and did not consider serrated yielding as a true maximum-load condition leading to necking. They were concerned with the balance between strain hardening and thermal softening. It is possible to consider serrated yielding as a series of maximum loads, and by this to explain not only the serrations, but also the change in position of the deforming region during straining.

The load F on a bar undergoing uniaxial straining is

$$F = \sigma A \quad \ldots\ldots\ldots\ldots\ldots\ldots\ldots\ldots\ldots\ldots (8)$$

where σ is the true stress, and A the instantaneous area. The incremental load change as the bar is strained is

$$dF = \sigma dA + A d\sigma \quad \ldots\ldots\ldots\ldots\ldots\ldots\ldots\ldots (9)$$

where $Ad\sigma$ is the load change due to strain hardening, and σdA is the (negative) load change due to decrease in cross-sectional area. If the

definition of true strain

$$d\epsilon = -dA/A \quad \ldots\ldots\ldots\ldots\ldots\ldots\ldots\ldots (10)$$

is substituted, this leads to the normal condition for maximum load and necking

$$\frac{d\sigma}{d\epsilon}\Big|_{dF=0} = \sigma \quad \ldots\ldots\ldots\ldots\ldots\ldots\ldots\ldots (11)$$

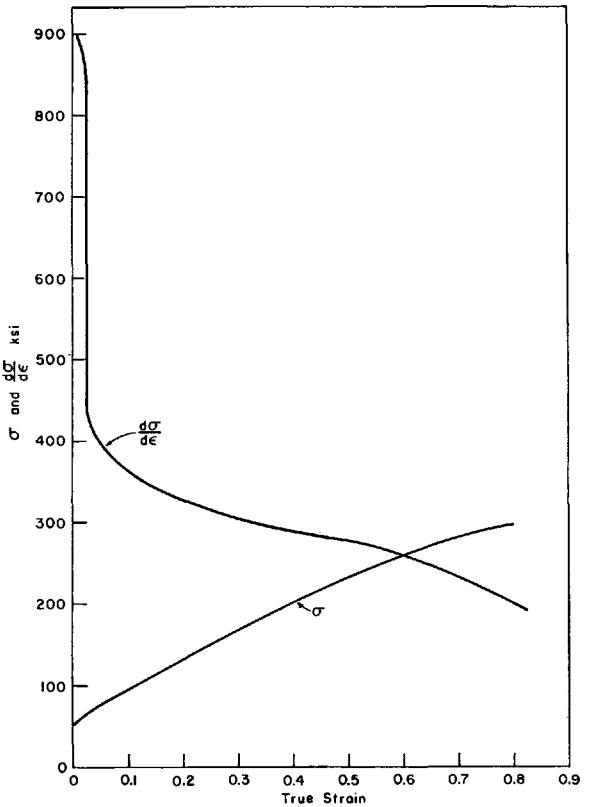

FIG. 16—*True stress and rate of strain hardening versus true strain for iodide titanium at −269 C.*

During straining, however, the flow stress, σ, depends not only on the strain, but also on the temperature, T, the strain rate, $\dot{\epsilon}$, and the structure (if there is a transformation during straining). Neglecting any change in structure during straining, Eq 9 can be rewritten

$$dF = \sigma dA + A[(\partial\sigma/\partial\epsilon)_{\dot{\epsilon},T}d\epsilon + (\partial\sigma/\partial\dot{\epsilon})_{\epsilon,T}d\dot{\epsilon} + (\partial\sigma/\partial T)_{\epsilon,\dot{\epsilon}}dT] \ldots (12)$$

Substituting Eq 10 in Eq 12

$$dF = Ad\epsilon[(\partial\sigma/\partial\epsilon)_{\dot{\epsilon},T} - \sigma + (\partial\sigma/\partial\dot{\epsilon})_{\epsilon,T}d\dot{\epsilon}/d\epsilon + (\partial\sigma/\partial T)_{\epsilon,\dot{\epsilon}}dT/d\epsilon] \ldots (13)$$

Any terms that increase the right side of Eq 13 will favor a positive dF and hence uniform deformation, whereas terms that decrease the right side and make it negative will promote a decreasing load and localized plastic flow. A maximum load will occur whenever the sum of the terms within the brackets equals zero, or

$$\sigma = (\partial\sigma/\partial\epsilon)_{\dot{\epsilon},T} + (\partial\sigma/\partial\dot{\epsilon})_{\epsilon,T}d\dot{\epsilon}/d\epsilon + (\partial\sigma/\partial T)_{\epsilon,\dot{\epsilon}}dT/d\epsilon \quad (14)$$

If dF becomes zero, and then sufficiently negative so that it is equal to the relaxation of load applied by the machine

$$dF_M = -k\,dl \quad (15)$$

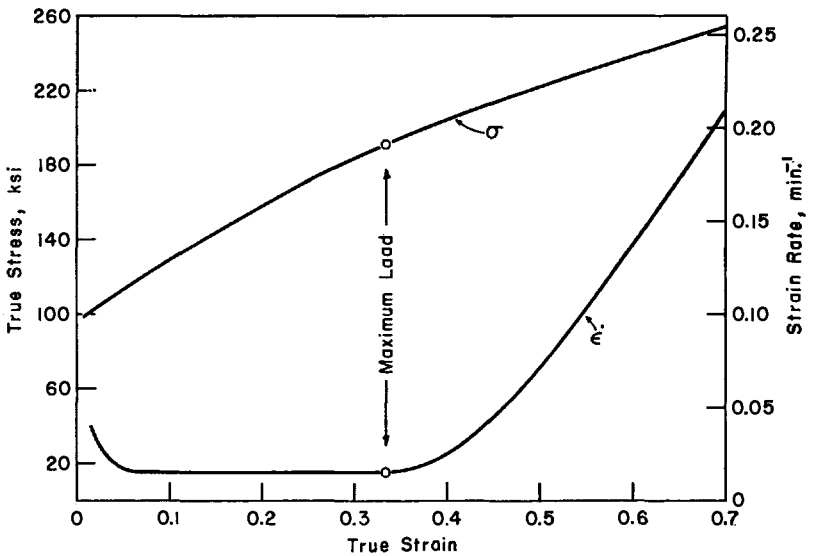

FIG. 17—*True stress and strain rate versus true strain of commercially pure titanium at −196 C.*

where k is the spring constant of the system, and dl the length change occurring during a strain $d\epsilon$, a plastic-elastic instability will occur, and the load will drop at a rate determined by the elastic characteristics of the machine, as discussed by Chin et al [*14*]. This is exactly analogous to the condition for high-velocity ductile fracture or neck development at strains exceeding maximum load when the testing machine "runs away" as described by Orowan [*21*]. It should be noted that, for serrations to occur before the normal or ultimate maximum load, dF from Eq 13 must first become zero then so negative that it satisfies Eq 15. Beyond the ultimate maximum load, dF is already negative, and discontinuous yielding will occur whenever dF equals dF_M. It is apparent that dF is undergoing a series of oscillations during the course of discontinuous yielding.

The various terms that contribute to strain hardening in Eqs 13 and 14

will now be considered individually. The first term is the strain-hardening term, $(\partial\sigma/\partial\epsilon)_{\dot{\epsilon},T}$. This is simply the slope of the stress-strain curve, and is shown in Fig. 16 plotted against the strain. It has very high values at initial yielding, and decreases during straining.

The term $-\sigma$ is the "geometrical softening," and $-\sigma A d\epsilon$ is the decrease in load-carrying ability due to the decreasing cross-sectional area. When this term is equal to the strain-hardening term (Fig. 16), in the absence of strain rate and thermal effects, a normal maximum load and necking will occur. When the term $[(\partial\sigma/\partial\epsilon)_{\dot{\epsilon},T} - \sigma]Ad\epsilon$ in Eq 13 is equal to the relaxation of load applied by the machine, Eq 15, high-velocity ductile failure as described by Orowan [*21*] may occur.

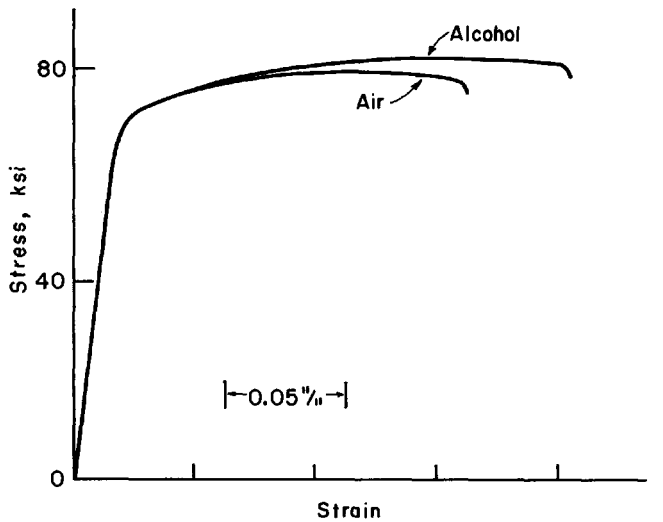

FIG. 18—*Stress-strain curves of commercially pure titanium in air and alcohol at 5 in./min.*

The third term represents the effect of strain rate, $(\partial\sigma/\partial\dot{\epsilon})_{\epsilon,T}d\dot{\epsilon}/d\epsilon$. The first factor, $\partial\sigma/\partial\dot{\epsilon}$, can be obtained by changing the strain rate during a tension test. Data reviewed by Conrad [*9*] and data for body-centered cubic metals of Christian and Masters [*11*] show that this term is much lower for face-centered cubic metals than for body-centered cubic metals, but that in both cases it extrapolates to zero at absolute zero. The second factor, $d\dot{\epsilon}/d\epsilon$, represents the change of strain rate with strain during a test. Figure 17 shows the strain rate as a function of strain during a tension test at a constant head speed. The strain rate during initial yielding is high, but decreases rapidly and attains a value consistent with the head speed during homogeneous straining. Because of the increasing length of the specimen, the strain rate is decreasing slightly, and $d\dot{\epsilon}/d\epsilon$ is slightly negative prior to maximum load. After maximum load, when necking occurs, the strain rate increases rapidly and $d\dot{\epsilon}/d\epsilon$ is positive. But at maximum load, when dF is

zero, $d\dot{\epsilon}/d\epsilon$ is exactly zero and hence can safely be neglected in calculating maximum load. Once a serration is underway, the product $(\partial\sigma/\partial\dot{\epsilon})_{\epsilon,T}d\dot{\epsilon}/d\epsilon$ will have a small positive value and hence tend to stop the serration.

The last term in Eqs 13 and 14, $(\partial\sigma/\partial T)_{\epsilon,\dot{\epsilon}}\, dT/d\epsilon$, represents the thermal softening. Even at room temperature the effect of this term can be significant, as can be seen from Fig. 18. Two specimens of commercial-purity titanium wire 0.060 in. diameter and 7 in. long were tested at a head speed of 5 in./min. The specimen temperature rise may have been greater. The other specimen was tested in alcohol in an attempt to maintain isothermal conditions. The significant differences in dF at each strain and in the whole stress-strain curve are apparent.

At low temperatures the effect of the thermal softening is much more important. The factor $(\partial\sigma/\partial T)_{\epsilon,\dot{\epsilon}}$ should be obtained by changing the temperature during a tension test. It is extremely difficult to obtain such data accurately at temperatures approaching absolute zero, but values can be approximated from isothermal tests conducted at a series of temperatures. As can be seen from Figs. 9 to 12 and from data in such sources as Refs. [3] and [11], $\partial\sigma/\partial T$ at yielding can have quite large negative values at temperatures approaching absolute zero, especially for the body-centered cubic metals. Values may be as large as 1400 psi/deg C. Equally important, however, the values become greater (more negative) as the temperature decreases.

The second factor in the thermal-softening term represents the temperature rise with strain and can be rewritten

$$dT/d\epsilon = \alpha\sigma/\rho c \qquad (16)$$

where α is the fraction of the work of plastic deformation which is converted to heat and retained in the deformation region, ρ is the density, and c is the specific heat. Under adiabatic conditions, the maximum value that α can attain is one minus the ratio of stored energy to expended energy. Appleton and Bever [22] have shown that this ratio of stored to expended energy increases as the temperature decreases, and is in the range of 0.13 to 0.18 for a gold-silver alloy at −269 C. Erdmann and Jahoda [19, 20] report that the ratio of stored to expended energy for copper-nickel alloys was 0.38 to 0.49 for uniform plastic deformation, and 0.59 to 0.69 for serrated yielding. Based on these results, the maximum value that α can have is about 0.87 and may even be as low as 0.31. In any actual case these values can be reduced still further if the deformation process is not completely adiabatic.

The specific heat, c, is very low at low temperatures and extrapolates to zero at absolute zero. In the low-temperature region, the specific heat is proportional to the temperatures raised to the third power, so that small increases in temperature give rise to proportionally large changes in the heat capacity.

For the titanium shown in Fig. 16, a maximum load can occur whenever

$\partial\sigma/\partial\epsilon - \sigma$ is equal to the thermal softening. Using values of -360 psi/deg C for $\partial\sigma/\partial T$, 0.5 for α, and 0.0001 cal/g deg C for ρc, $(\partial\sigma/\partial T)(dT/d\epsilon)$ calculates to be almost -4×10^7 psi, more than enough to ensure a maximum load already at yielding, which was observed. Notice in this case that dF can be negative already at initial yielding, so no prior deformation is required. It is difficult to accurately calculate the stress necessary for initiation of discontinuous yielding. While σ and $\partial\sigma/\partial\epsilon$ can be measured rather precisely as a function of strain, the factors in the thermal-softening term, $\partial\sigma/\partial T$, c, and especially α, are often not known to a sufficiently high degree of precision.

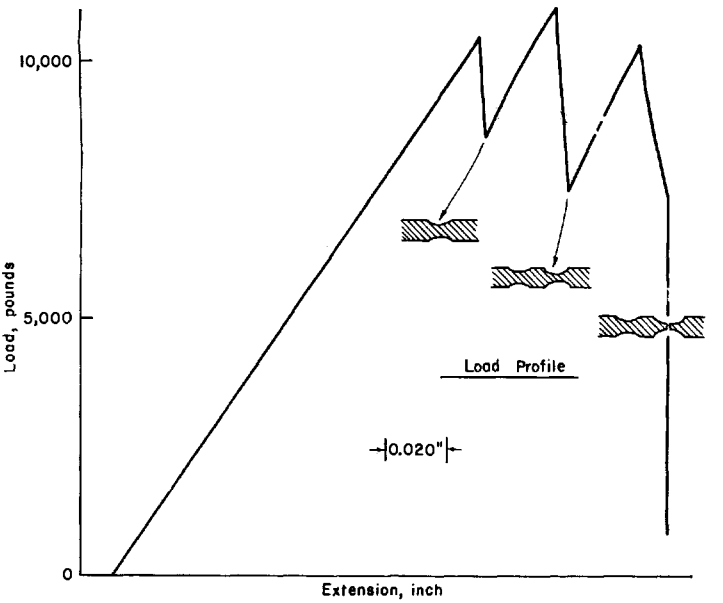

FIG. 19—*Load extension and specimen profile of AISI 416 at −269 C.*

Klyavin and Stepanov have recently reported on the effect of surface condition on serrated yielding at temperatures approaching absolute zero [*23*]. They compared as-machined, etched, and electrolytically polished surfaces, and found that the strain at the first serration and the number of serrations varied with these conditions. It is generally recognized that surface defects can lead to strain initiation and concentration. Their results can be at least partially explained by considering that surface defects can lead to the "nucleating deformation" of Basinski [*12*], or to an effectively higher value of α, which increases the magnitude of the thermal-softening term.

A load drop will stop when the load has fallen to a value less than that required for deformation at the then-current temperature. Alternatively,

it can be seen that the load drop will cease when the magnitude of the thermal-softening term becomes less than $\partial\sigma/\partial\epsilon - \sigma$. This occurs during the heating, since $\partial\sigma/\partial T$ will decrease in magnitude, and c will increase with the cube of the absolute temperature. These oscillations in the thermal-softening term allow a series of maximum loads to occur during straining.

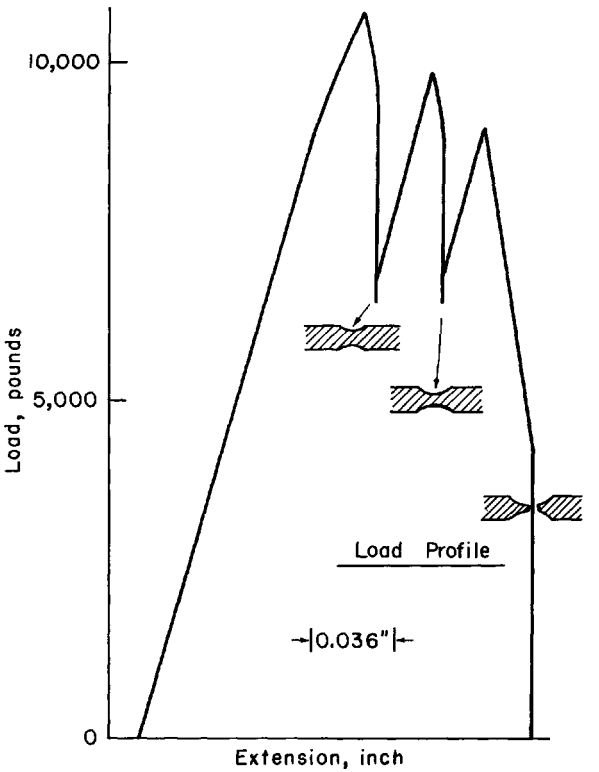

FIG. 20—*Load extension and specimen profile of AISI 416 at −269 C.*

Provided that the deformation during the serration is large enough, the specimen will appear to have formed a neck. If the true stress at the second serration is less than $\partial\sigma/\partial\epsilon$, or the load is greater than that at the initiation of the first serration, the region that deformed during the first load drop will have strain hardened sufficiently so that the load-carrying ability at that section is greater than at other sections. The deformation during the second load drop will therefore occur at another, weaker cross section, forming a second neck. As long as the upper envelope of the load serrations continues to increase, or the stress at the initiation of a serration is less than $\partial\sigma/\partial\epsilon$, the location of the deforming zone will change along the length of

the specimen. When the ultimate maximum load is reached, σ will be equal to $\partial\sigma/\partial\epsilon$, and further deformation will be localized at one neck. This will be true for all serrations after maximum load.

This can be seen from Figs. 19 and 20, which show two stress-strain curves for Type 416 stainless steel tested at −269 C. Several large serra-

FIG. 21—*Microstructure of iodide titanium after first serration (approximately 0.10-in. extension).* (×500).

tions are visible, and the accompanying sketch of the specimen profile shows where the deformation has occurred during each serration. It is evident that there is a change in the location of the deformation for those serrations occurring before the ultimate maximum load, whereas after maximum load the deformation occurs only at one location.

Since the conditions for describing serrated yielding have been described completely in terms of Eq 13, it appears that the deformation mechanism plays no role. Thus whether deformation occurred by slip, twinning, or martensite formation is not important. The deformation mechanism does play a secondary role, in that the terms σ, $\partial\sigma/\partial\epsilon$, $\partial\sigma/\partial T$, and so forth are influenced by the exact mechanism. But Eq 13 can be satisfied, and serrated yielding can occur, no matter what the nature of the deformation mechanism.

This can be seen by microstructural examination of specimens deformed at −269 C. A sample of iodide titanium was deformed to a strain of 0.10, at which point the first serration appeared. The microstructure showed that deformation had occurred by twinning (Fig. 21) in addition to slip. Further straining led to a series of serrations, so that the deformation occurred almost exclusively by discontinuous yielding. Micro-examination revealed that further twinning occurred during this discontinuous yielding. Since twinning occurred both before and after the onset of the serrations, twinning is clearly not a necessary condition for discontinuous yielding.

A similar conclusion can be drawn from the results of Reed and Guntner, who deformed 18 Cr-8 Ni stainless steel at −269 C [*24*]. Measurements revealed that plastic straining was accompanied by formation of the body-centered cubic martensite or hexagonal close-packed epsilon phases throughout the range of straining. Since serrations were initiated only after a strain of about 0.15, it is obvious that the martensite or epsilon formation contributed to the strain in the uniform-strain region as well as in the region of serrated yielding.

Conclusions

A study of the mechanical properties of metals at temperatures approaching absolute zero is extremely interesting but presents many experimental difficulties. For example, there are practically no results reported for temperatures below −269 C, and even very few for temperatures between the boiling points of helium and hydrogen. Temperature-change tests are especially difficult to conduct in this range. Many materials of interest are brittle at these temperatures and fracture on yielding, or else start to neck immediately on yielding, so that strain or strain-rate control is difficult. More important, however, as Basinski pointed out [*12*], this thermal instability at low temperatures means that it is almost impossible to conduct tests under isothermal conditions or with controlled strain rate.

Acknowledgments

The authors would like to thank Hans Conrad for kindly providing a copy of his manuscript prior to its publication, also Walter Backofen, and Joseph Bluhm for their helpful discussions on serrated yielding.

References

[1] F. R. Schwartzberg, S. H. Osgood, R. D. Keys, and T. I. Keifer, *Cryogenic Materials Data Handbook*, Technical Document Report ML-TDR-280, August 1964.

[2] H. M. Rosenberg, "Research on the Mechanical Properties of Metals at Liquid-Helium Temperatures," *Metallurgical Reviews*, Vol. 3, No. 12, 1958, pp. 357–379.

[3] H. Conrad, "The Cryogenic Properties of Metals," *Proceedings*, Second International Materials Symposium, 15–18 June 1964. University of California, Berkeley, Calif.

[4] J. Nunes, A. A. Anctil, and E. B. Kula, "Low Temperature Flow and Fracture Behavior of Tantalum," *Advances in Cryogenic Engineering*, Plenum Press, Inc., New York, N.Y., Vol. 10, 1964.

[5] F. R. Larson and E. B. Kula, "Strain Hardening of High Purity Metals," *Metallurgia*, October 1961, pp. 159–164.

[6] C. S. Barrett, "*Metallurgy and Metallurgical Engineering Series*," McGraw-Hill Book Co., Inc., New York, N.Y., 1952, pp. 336.

[7] P. R. Swann, "Dislocation Arrangement in Face-Centered Cubic Metals and Alloys," *Electron Microscopy and Strength of Crystals*, Interscience Publishers, New York, N.Y. 1963, pp. 131–181.

[8] A. S. Keh and S. Weissmann, "Deformation Structure in Body-Centered Cubic Metals," *Electron Microscopy and Strength of Crystals*, Interscience Publishers, New York, N.Y., 1963, pp. 231–300.

[9] H. Conrad, "Thermally Activated Deformation of Metals," *Journal of Metals* July 1964, pp. 582–588.

[10] A. H. Cottrell and R. J. Stokes, "Effects of Temperature on the Plastic Properties of Aluminum Crystals," *Proceedings*, Royal Society of London, Series A, Vol. 233, 1955, pp. 17–33.

[11] J. W. Christian and B. C. Masters, "Low Temperature Deformation of Body-Centered Cubic Metals," Parts I and II, *Proceedings*, Royal Society of London, Series A, Vol. 281, 1964, pp. 223–256.

[12] Z. S. Basinski, "The Instability of Plastic Flow of Metals at Very Low Temperatures," *Proceedings*, Royal Society of London, Series A, Vol. 240, 1957, pp. 229–257.

[13] J. L. Rutherford, R. L. Smith, and M. Herman, "Properties of Zone-Refined Titanium and Zirconium," Part I, *FIL Interim Report I-A1878-6*, July 1960.

[14] G. Y. Chin, W. F. Hosford, Jr., and W. A. Backofen, "Influence of the Mechanical Loading System on Low-Temperature Plastic Instability," *Transactions*, American Institute of Mining, Metallurgical, and Petroleum Engrs., Vol. 230, 1964, pp. 1043–1048.

[15] T. H. Blewitt, R. R. Coltman, and J. K. Redman, "Low-Temperature Deformation of Copper Single Crystals," *Journal of Applied Physics*, Vol. 28, No. 6, June 1957, pp. 651–660.

[16] S. C. Collins, F. D. Ezekiel, O. W. Sepp, and J. W. Rizika, "The Strength of Certain Stainless and Carbon Steels at Low Temperatures," *Proceedings*, Am. Soc. Testing Mats., Vol. 56, 1956, pp. 687–703.

[17] E. T. Wessel, "Some Exploratory Observations of the Tensile Properties of Metals at Low Temperatures," *Transactions*, American Society for Metals, Vol. 49, 1957, pp. 149–172.

[18] C. Zener and J. H. Hollomon, "Effect of Strain Rate upon Plastic Flow of Steel," *Journal of Applied Physics*, Vol. 15, 1944, pp. 22–32.

[19] J. C. Erdmann and J. A. Jahoda, "Calorimetry of Instantaneous Heat Sources Arising from Plastic Tensile Deformation at Low Temperatures," *Document D1-82-0311*, Boeing Scientific Research Laboratory, October 1963.

[20] J. C. Erdmann and J. A. Jahoda, "Calorimetry of Transient Phenomena in Metals at Low Temperatures," *Document D1-82-0384*, Boeing Scientific Research Laboratory, October 1964.

[21] E. Orowan, "Condition of High-Velocity Ductile Fracture," *Journal of Applied Physicals*, Vol. 26, July 1955, pp. 900–902.

[22] A. S. Appleton and M. B. Bever, "The Energy Relations in the Deformation by

Torsion of a Gold-Silver Alloy," *Transactions*, American Institute of Mining, Metallurgical, and Petroleum Engineers, Vol. 227, 1963, pp. 365–371.

[23] O. V. Klyavin and A. V. Stepanov, "Surface Condition as Affecting the Irregular Deformation of Aluminum at T = 1.3°K," *The Physics of Metals and Metallography*, Vol. 17, No. 4, 1964, pp. 106–113.

[24] R. P. Reed and C. J. Guntner, "Stress-Induced Martensite Transformation in 18Cr-8Ni Steel," *Transactions*, American Institute of Mining, Metallurgical and Petroleum Engineers, Vol. 230, 1964, pp. 1713–1720.

[25] M. A. Adams, A. C. Roberts, and R. E. Smallman, "Yield and Fracture in Polycrystalline Niobium," *Acta Metallurgica*, Vol. 8, May 1960, pp. 328–337.

E. T. Wessel[1]

Some Basic and Engineering Considerations Regarding the Fracture of Metals at Cryogenic Temperatures

REFERENCE: E. T. Wessel, **"Some Basic Engineering Considerations Regarding the Fracture of Metals at Cryogenic Temperatures,"** *Behavior of Materials at Cryogenic Temperatures, ASTM STP 387,* Am. Soc. Testing Mats., 1966, p. 32.

ABSTRACT: In this paper, factors affecting the fracture characteristics of metals at cryogenic temperatures are reviewed, and the use of fracture mechanics for predicting performance of defect-containing structures is discussed. The phenomenon of serrated yielding and the effect of phase transformations on cryogenic properties are also discussed. At cryogenic temperatures, the resistance to plastic flow of body-centered-cubic metals and most close-packed-hexagonal metals increases sharply. This increased resistance causes a corresponding decrease in fracture strength. At these subtransition temperatures, brittle fracture strength is always less than the extrapolated yield strength, and only microscopic amounts of plastic deformation precede fracture. Data from smooth-tension, notched-tension, and cracked-plate tests performed on a Ni-Mo-V forging steel indicate that the temperature and stress at which fracture occurs is strongly dependent on the severity of the test conditions—the size and acuity of defects. Since fracture strength is a variable quantity, load-bearing capacity is better evaluated using fracture toughness, a basic material parameter. Quantitative predictions of load-bearing capacity can be made using the fracture-toughness parameter with expressions relating to toughness, defect size, applied stress, and relative geometry.

KEY WORDS: cryogenics, metals, defects, fracture toughness, fracture mechanics

With the advent of the space age, rigorous application and design requirements demand that the utmost performance be extracted from available materials. This situation requires an intimate knowledge of the performance capabilities of the materials involved. In recent years it has been recognized that the level and state of stress, the defect size and location, and the inherent fracture resistance of the material, have profound influ-

[1] Fellow engineer, Metallurgy Department, Research and Development Center, Westinghouse Electric Corp., Pittsburgh, Pa.

ence on a metal's performance characteristics, particularly fracture behavior. Since fracture is one of the primary items of concern in the structural application of metals at cryogenic temperatures, an understanding of the factors controlling fracture at these temperatures is essential for efficient and effective use of metals.

This paper will attempt an insight into the basic factors of metal fracture at cryogenic temperatures. Equivalent emphasis will also be given to this subject on an engineering level. In the first section dealing with basic factors, attention is focused on the inherent fracture toughness of the metal, the effects of flaws or defects, a physical description of what is occurring in the vicinity of flaws, and the influence of these factors upon the bulk properties of metals. Since the ultimate performance of a material is based primarily upon the load-bearing capacity of a structure, one particular bulk property, the fracture strength, is of major concern. As will be seen, the measured bulk fracture strength is not a unique basic material property reproducible from one situation to another. It is, rather, a highly variable criterion that represents the gross product of complex mechanical and metallurgical interactions.

Dealing with the subject on an engineering level, the second section will show how fracture-strength data, properly interpreted into terms of a basic material parameter related to fracture toughness, then properly applied with a knowledge of the prevailing defects and applied stresses can be a useful engineering tool for quantitatively establishing the performance characteristics of a structure. This discussion of the fracture problem on an engineering level will emphasize the use of the recently evolved fracture-mechanics principles, concepts, and expressions. The fracture-mechanics approach is discussed in terms of material section, design of components and structures, establishment of inspection procedures and acceptance standards, and ultimate evaluation of the integrity and expected performance of the structures.

Basic Considerations of the Fracture of Metals

This section of the paper is intended to provide a general physical description of the basic factors in metal fracture. Its purpose is to explain the fracture process to facilitate application of present knowledge to practical engineering problems. No attempt is made to cover all details of the atomistic and theoretical aspects of the flow and fracture processes. A brief general discussion of fracture on the atomic scale, however, is necessary to set the stage for subsequent discussion on fracture at cryogenic temperatures.

Origin of the Fracture Strength of a Metal

The fracture strength of metals arises from the forces or bonds between the atoms. The actual stress required to rupture these bonds is believed

to be quite high. The theoretical fracture strength of metal containing no defects or imperfections has been calculated [*1*][2] to be of the order of 0.1 to 0.5 Young's modulus. A review [*2*] of other estimates reveals similarly high values of breaking strength. On this basis, in iron for example, theoretical fracture stresses of the order of 3,000,000 psi or greater would be expected. Since the perfect metal with no defects or imperfections has never been achieved, however, fracture strengths of this order of magnitude have never been measured. The closest approach to obtaining the estimated fracture strengths has been in metal-whisker crystals that are relatively free of defects or imperfections. Brenner [*3*] reports that, in general, the strengths of the more perfect whiskers are equal within at least a factor of ten to the estimated or calculated strengths of perfect crystals.

Much speculation has centered around the discrepancies between theoretical and measured fracture strengths. It appears that the failure of metals

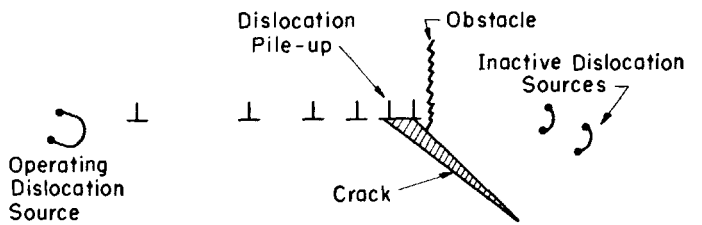

FIG. 1—*Generalized concept of crack initiation by dislocation pile-up.*

to achieve their respective theoretical strengths can be attributed to the presence of defects or imperfections of one sort or another. Early concepts and experiments [*4*] supported the idea that stress concentrations at the tip of small inherent cracks caused the low measured values of strength. Other types of internal flaws may similarly contribute to producing low fracture stresses [*3*]. These earlier concepts based on inherent cracks have, however, generally given way to the commonly accepted explanation that localized stress concentrations in regions of dislocation pile-ups become high enough to exceed the theoretical strength of the metal and initiate a crack in some local region.

Concept of Fracture Initiation

Many detailed descriptions of the dislocation-pile-up type of crack initiation may be found [*5–9*]. Generally these various concepts agree that it is the local stresses in the vicinity of dislocation pile-ups that become high enough to rupture the bonds between atoms and initiate a brittle

[2] The italic numbers in brackets refer to the list of references appended to this paper.

crack. Because of the presence of these lattice-structure imperfections or defects, the average applied stresses necessary to produce high local fracture-causing stresses can be considerably less than the theoretical strength.

A general qualitative description of the dislocation-pile-up mechanism of brittle crack initiation is given in Fig. 1. As stress is applied to a metal, some dislocation sources are activated and dislocations start to move through the lattice. A minute amount of localized plastic strain is associated with the movement of these dislocations through the lattice. It is believed that such movement occurs in some favorable regions at applied stresses well below conventionally measured yield strengths. These dislocations may encounter a barrier such as a grain boundary, subgrain boundary, hard particle, hard phase, or other dislocation group, which restricts further motion and causes the dislocations to pile up. High local stresses develop in the regions at the head of these pile-ups. As the applied stress is increased, one of two things can happen. The local stress concentrations can be relieved by local plastic deformation. This may be accomplished by the activation of new, formerly inactive sources in adjoining material or by the pile-up breaking through from its barrier. On the other hand, if the adjoining material is highly resistant to plastic flow because of orientation, temperature, lack of sources, or other possible characteristics, the high local stresses can exceed the inherent strength of the metal and open up cracks. These cracks may grow catastrophically or become stable depending upon the metal and prevailing conditions. This will be discussed later.

It is apparent that the true origin of the strength of a metal involves the forces or bonds between the atoms. Because of the presence of lattice defects or imperfections leading to high local-stress concentrations when the metal is stressed, however, the theoretical strength is never measured in an actual test.

The Fracture Strength of Metals in Simple Tension

In the light of the foregoing discussion, let us consider the nature of the fracture strength of a metal as it is measured under simple (uniaxial) tensile-loading conditions. Fracture and plastic deformation (yielding) can be visualized as similar but competitive processes. One or the other must occur if a metal is loaded to a sufficiently high stress. Since the inherent resistance of some metals to plastic flow is highly dependent on temperature, their respective fracture characteristics must be also.

In the temperature range below about 0.2 of the melting temperature (absolute), many metals exhibit a marked increase in their resistance to plastic deformation. This is evidenced by a pronounced rise in the yield and flow stresses with decreased temperature. For many of the metals of practical interest, this behavior occurs in the cryogenic-temperature range.

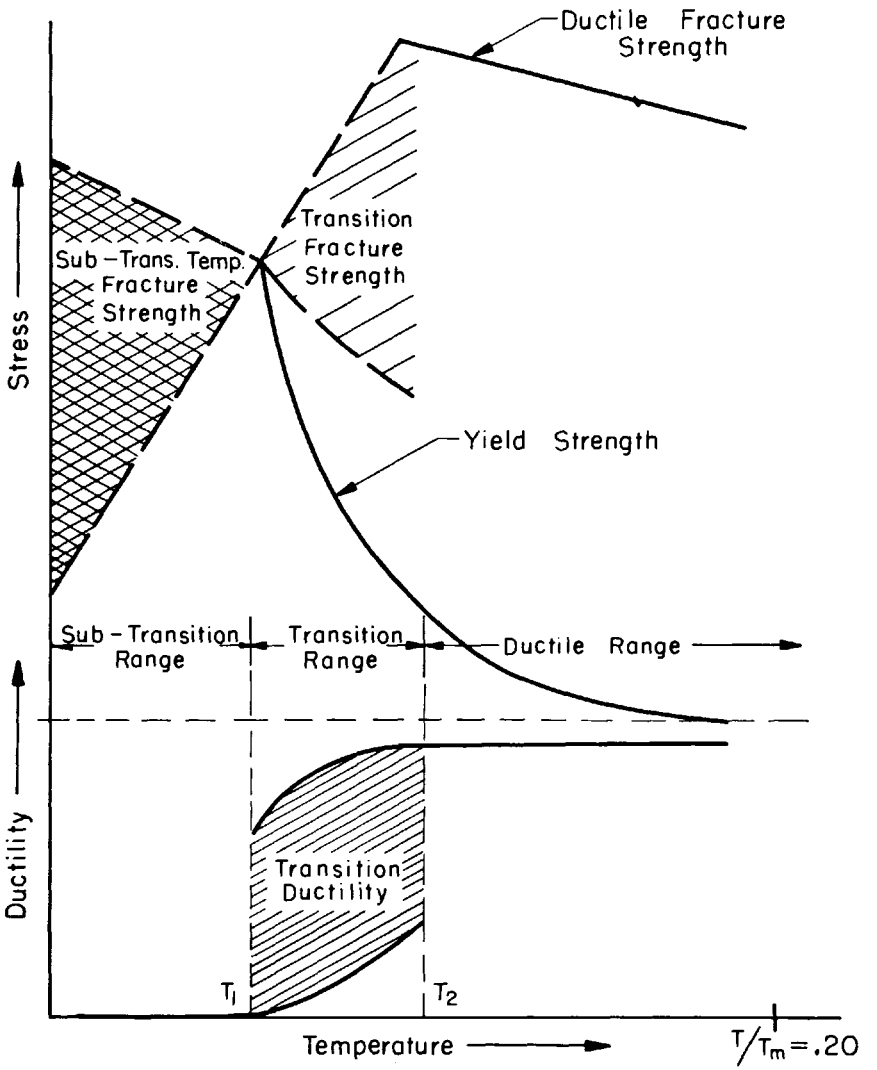

FIG. 2—*Schematic of variations in fracture behavior in different temperature ranges for bcc metals tested in uniaxial tension.*

Such a behavior is characteristic of all body-centered-cubic (bcc) and some close-packed-hexagonal (cph) metals. It is unknown in pure, single-phase, face-centered-cubic (fcc) metals where the yield strength is relatively insensitive to temperature and brittle, cleavage fractures do not occur. This strong temperature dependence of the yield strength is believed [*10–13*] to be associated with increased inherent resistance to the movement of dislocations through the lattice. At cryogenic temperatures, the resistance to plastic flow becomes so great that the local stresses encountered in the vi-

cinity of dislocation pile-ups are not readily relieved by local plastic flow, and crack formation becomes the more favorable process.

Effects of Lattice Structures

Metals having the bcc lattice structures are most susceptible to low-temperature brittleness, so it is appropriate to discuss these first. The general fracture-strength behavior [*12*] for bcc polycrystalline metals is shown in Fig. 2. Although this is a schematic representation, it is based on a large amount of experimental data from a large number of metals. It is intended primarily to illustrate the rather pronounced differences (cross-hatched areas) in fracture strength that can be observed depending on the metal, its metallurgical condition, and the test temperature.

The subtransition range lies below T_1 of Fig. 2. A marked difference in brittle fracture strength behavior is observed between two different metals, or in different metallurgical conditions of one metal. The various metals have one thing in common in this range, however: they all fail at applied stresses below the predicted or extrapolated yield strength. In this range, total fracture occurs during the very early stages of plastic flow (nil amounts by conventional standards), and the measured fracture strength can vary considerably depending upon the amount of microstrain (plastic) occurring prior to fracture. High local stresses are relieved by local plastic strain. Therefore, with increased amounts of plastic strain, larger applied stresses are required before the critical local stress concentration for crack initiation is achieved. In general, materials with very high resistance to plastic flow fail after very little microscopic plastic flow at relatively low applied stresses. These metals exhibit fracture strengths in the lower regions of the cross-hatched area of Fig. 2. Their fracture strength generally decreases with decreased temperature in this subtransition range. If the resistance to plastic flow is somewhat weaker, larger amounts of microscopic plastic deformation occur prior to fracture, and this in turn permits somewhat higher levels of applied stress to prevail. Thus, metals of this nature tend to exhibit fracture stresses lying in the upper regions of the cross-hatched area of Fig. 2. Mild steels [*14,15,18,19*] fall in this latter category and show a slight increase in fracture strength with decreased temperature. Molybdenum [*20*] and tungsten [*21*] have been reported to have a temperature-independent subtransition fracture strength, whereas columbium [*16,22*] and some alloy steels [*17*] exhibit fracture strengths that decrease markedly. Thus it appears that in the subtransition range fracture stresses may be any value on the stress-strain curve between the upper yield point and a much lower value possibly below currently measurable elastic limits depending on the metal.

It is believed that in the subtransition range the first or one of the first microcracks to be initiated leads directly to total fracture. Once a microcrack is formed, propagation apparently occurs with relative ease at these

low temperatures. Several metals subjected to brittle fracture in the subtransition-temperature range have been examined, and no microcracks were observed in the deformed regions of the test specimens. Cracks directly adjacent to the main fracture were occasionally found, but these were associated with the passing of the main fracture and had not occurred prior to the primary fracture. It is possible, however, for submicroscopic cracks to have existed prior to the main fracture. It is also possible for very small cracks to have closed up when the stress was relaxed by the specimen breaking. Further work is required to establish this point on submicroscopic cracks. Judging by the existing experimental evidence, however, it appears that the initiation of the first microcrack of a size visible in a light microscope controls fracture in this subtransition range, whereas, in the transition range, some metals can contain many stable microcracks prior to total fracture.

The transition range lies at higher temperatures (between T_1 and T_2 of Fig. 2). In this range, some macroscopic amount of plastic straining always precedes total fracture, and the applied stresses required for fracture are always equal to or greater than the conventional yield strength of the metal. Depending upon the metal and its particular condition, markedly different fracture strengths and ductilities are again observed. In this range, the temperature dependence of the yield strength is always quite strong signifying a rapidly increasing resistance to plastic flow with lowered temperatures.

If the resistance to crack formation is relatively low, the brittle-fracture strengths and ductilities tend to lie in the lower region of their respective transition-range hatched areas, and it is generally observed [*14,15,19,23*] that cleavage microcracks are initiated during the early stages of plastic deformation. In this case, the fracture strength may be independent of temperature or even increase as the temperature decreases. Usually the microcracks are first apparent in the region just behind the passing of the Lüders band. During subsequent deformation and the associated increase in applied stress, these cracks grow in size and number and develop into a larger, more continuous network, until eventually the critical-size conditions for total fracture are achieved. In this case, it appears that the propagation of microcracks is more difficult than their initiation, therefore, the propagation phase controls total fracture. Large microcracks and networks of cracks prior to total fracture have been observed in mild steel [*14,15,19*], some lots of molybdenum [*12*], chromium [*23*], and rhenium.

If, on the other hand, the material has a high resistance to crack initiation, it will exhibit fracture strengths and ductilities lying in the upper portions of the hatched areas (transition range, Fig. 2). Fracture strength may increase, by varying degrees, with increased temperature. In this case microcracks generally are not initiated until considerable deformation and the associated increase in applied stress has occurred. Then, because

of the relatively high stresses that prevail, the first microcracks to form readily propagate catastrophically to total fracture. Some examples of metals exhibiting this behavior are columbium [*16*], some lots of molybdenum [*12,20*], and alloy steels. In this transition range, it is apparent that stable microcracks may or may not exist prior to total fracture, de-

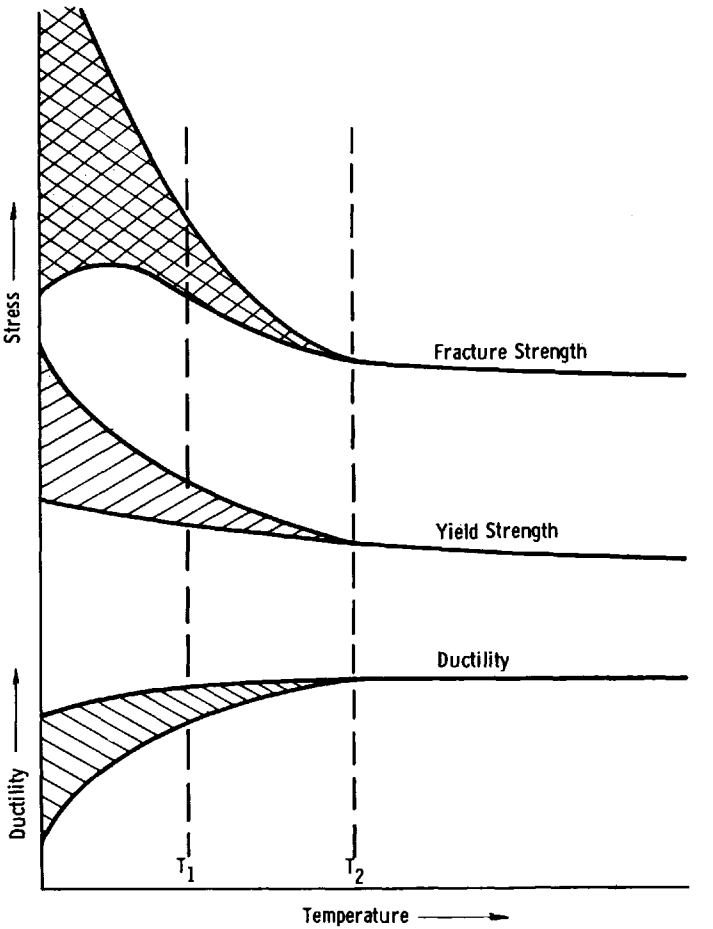

FIG. 3—*Schematic of variations in fracture behavior in different temperature ranges for fcc metals tested in uniaxial tension.*

pending upon the metal, its condition, or both, and corresponding differences in fracture strength and prefracture ductility may be expected.

As will be discussed in more detail in the following paper,[3] twinning can become the preferred mode of plastic straining for many of these metals at temperatures in the transition and subtransition ranges. For

[3] See p. 60.

simplicity in the preceding discussions, plastic strain has been considered to be either slip, twinning, or combinations of the two. For the purposes of illustration, the stress concentration at the ends of twins or at the heads of slip systems are assumed to have similar effects.

In the ductile range (above T_2 of Fig. 2), the temperature dependence of the yield strength is not extremely strong, and the fracture strength and ductility are quite high. In this range, plastic deformation is obviously more favorable than brittle crack initiation. Gross plastic deformation, including necking, precedes the initiation of ductile shear cracks that subsequently propagate to produce a ductile shear rupture.[4] The behaviors of various metals or different lots of a given metal are fairly consistent in this range.

The foregoing discussions have described the general behavior of bcc metals. The same behavior trends apply to some cph metals, but other cph metals tend to behave like fcc metals. To provide the proper perspective, some discussion of the relative behavior (uniaxial tension) of fcc metals is warranted at this time. A schematic representation of the general behavior of fcc metals is provided in Fig. 3, where the temperatures T_1 and T_2 correspond to those shown in Fig. 2.

The relatively pure, single-phase metals tend to exhibit only a slight increase in resistance to plastic flow (mild temperature dependence of yield strength) at low temperatures. Correspondingly, these metals exhibit high fracture strengths and ductilities and lie in the upper portions of the cross-hatched sections of fracture-strength and ductility ranges shown in Fig. 3. If the temperature dependence of the yield strength (increased resistance to plastic flow) is increased due to impurities, alloying, or cold work, the fracture strengths and ductilities are reduced, and their respective values lie in the lower regions of the ranges shown. In contrast to the bcc metals, there is no abrupt transition to a brittle behavior, and the fracture strength always exceeds the yield strength even at extremely low temperatures. The only exceptions would be where the metals have a pronounced increased resistance to plastic flow because of extreme amounts of alloying, cold work, or impurities. In general, compositional or microstructural changes that tend to increase the yield strength and its temperature dependence will tend to cause these metals to behave more and more like bcc structures. Some of the high-strength precipitation-hardened stainless steels are examples of this latter behavior.

Other Factors Affecting the Uniaxial Tensile Behavior of Metals at Cryogenic Temperatures

Unconventional Modes of Plastic Flow

There is an additional factor of concern from the viewpoint of fracture and design in the use of some metals at low temperatures although they

[4] In some cases [*14,17*] the propagating shear crack may convert to a brittle cleavage crack during the rupture process.

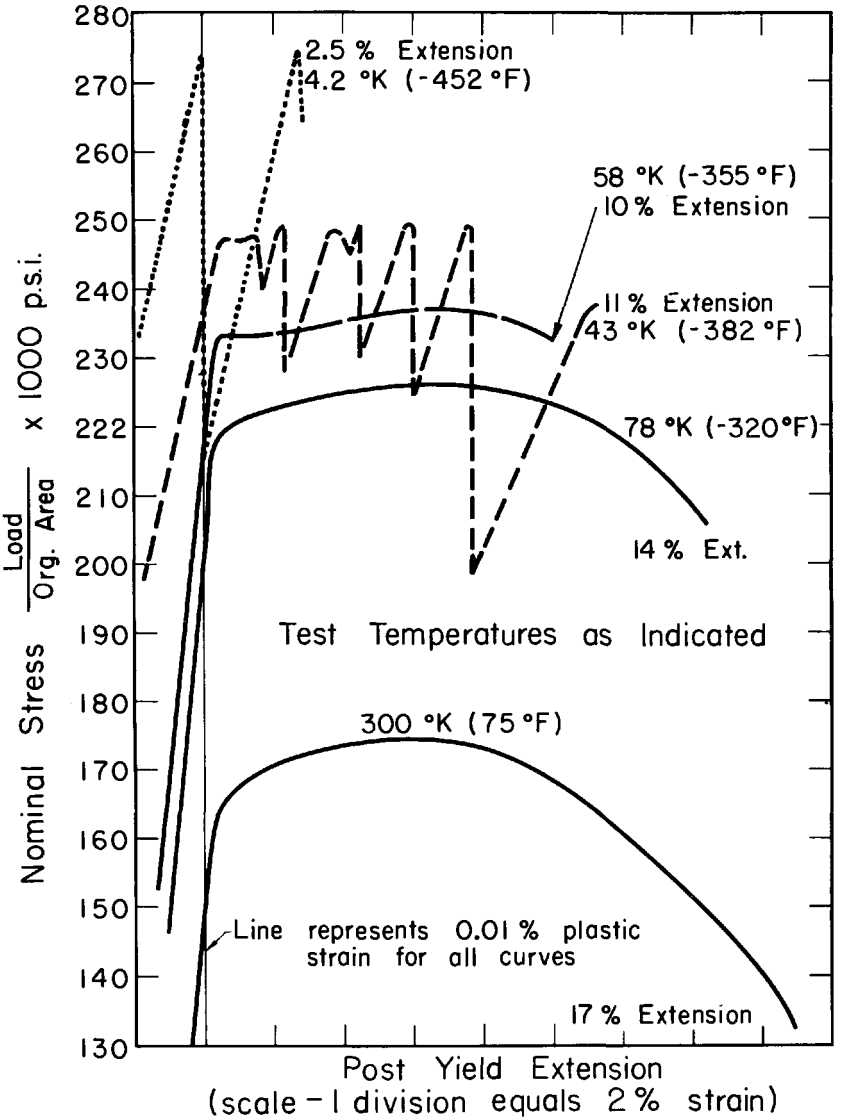

FIG. 4—*The effect of temperature on the stress-strain curves of a quenched and tempered alloy steel.*

remain quite ductile. This problem is related to an unstable type of plastic flow observed for many metals at very low temperatures [*24*]. This behavior is illustrated for an alloy steel (bcc) by the stress-strain curves of Fig. 4. Above −364 F, the normal smooth type of stress-strain curve is obtained, but a substantial decrease in work hardening with decreased temperature is apparent. Below −364 F, plastic flow becomes quite irregular in nature, and the stress-strain curve consists of a series of discontinu-

ous yields (drop in load). A large amount of highly localized plastic flow is associated with each yielding. At −452 F only one very pronounced yielding occurs prior to total rupture. Several other tests of steels at −452 F resulted in failure of the specimen during the first yielding. In these cases, large reductions in area, little elongation, and ductile shear fractures were observed. Similar behaviors have been reported in other metals [*24*] and by other investigators [*25–27*]. Smith and Rutherford [*25*] report that the fracture behavior in ultra-high-purity iron tested at −452 F had all the rapidity and outward appearances of being brittle, but an examination of the failed specimen showed a local reduction in area of 85 per cent with a ductile rupture occurring during the one sudden catastrophic yielding.

The bcc metals seem to be most prone to this type of low-temperature behavior, whereas the flow instability in fcc metals is much less pronounced. Repeated discontinuous yielding also occurs in nickel (fcc) at −452 F, however, the magnitudes of the yields are far less pronounced than those observed in the steels (bcc). Without going into the details of the probable mechanism of this unstable flow, it can be concluded that the severity of the catastrophic yieldings can be related to the ability of the metal to work (strain) harden at low temperatures. BCC metals are known to lose their ability to work harden at low temperatures. Hence, once yielding starts at some local region, there is little resistance in the form of work hardening to prevent or even slow down the catastrophic process of flow. Undoubtedly local heating from the plastic flow also contributes to the catastrophic nature of the yielding by decreasing the flow stress of the metals being deformed. In contrast to the bcc metal, the ability of fcc metals to work harden increases with decreased temperature. Thus, when plastic flow starts in some local region, the metal in this region work hardens and plastic flow stops, and an increase in load is required before any further flow can occur in this region. This process may be repeated many times throughout the entire specimen resulting in large amounts of general flow. If the yield strength of an fcc metal is appreciably raised by alloying or precipitation hardening, its stress-strain curve and work-hardening characteristics would tend to be more like the bcc metals. It is therefore likely that these high-yield-strength fcc metals would exhibit a greater tendency for unstable plastic flow at low temperatures as shown by the data of Collins et al [*27*] for some stainless steels.

Thus from the viewpoint of application, it appears that this form of unstable plastic flow at low temperatures could represent as serious a problem as does brittle fracture. For example, if the stresses were high enough to cause plastic flow to occur at some local region, as they undoubtedly would be at the root of a sharp notch or defect, a sudden catastrophic rupture could occur without an increase in load or any general plastic straining. For the lack of a better term this type of failure is identified as "catastrophic shear."

Metallurgical Stability

The last general category of low-temperature problems to be discussed is concerned with phase transformations and associated changes in mechanical properties. It is known that phase changes occur in some metals at low temperatures. Such changes can occur as a result of cooling alone, and in general, the ability to transform is enhanced when plastic deformation accompanies the cooling.

Barrett [*28*] has developed apparatus in which a metal can be cooled to temperatures as low as −452 F, plastically deformed at the low temperature, and examined with X-ray techniques for evidence of phase transformations. The work that has been reported [*28*] has been concerned with phase transformations in bcc alkali metals. Several of these were found to transform from bcc to cph to fcc when subjected to plastic deformation at very low temperatures. Beta brass was also found to undergo similar transformations which could be compared to corresponding changes in fracture resistance as measured by notched-impact tests.

From free-energy considerations, it would appear that the general tendency would be for transformations on cooling to proceed in the direction of closest packing. There are exceptions in metals where there are strong magnetic effects, however. In these cases, the transformations are in an unfavorable direction from the low-temperature mechanical-property viewpoint. That is, upon cooling, cold plastic deformation, or both, the changes are from the ductile fcc structure to the undesirable bcc structure, where low-temperature brittleness is a problem. The iron-nickel system has this type of behavior. The relative temperatures for transformation (fcc to bcc) shown for varying amounts of nickel have been reported by Kaufman and Cohen [*29*]. A number of other references to low-temperature transformations may be found in Barrett's summary paper [*28*], and several detailed papers describing the influence of prior mechanical and thermal history on transformations in iron-nickel alloys have been published [*30*].

These transformations can be reversible and are influenced by many factors. Among these are: the temperatures encountered, the rates of heating and cooling, the amount of associated plastic strain (warm or cold), general composition, and impurity effects. Undoubtedly many of these aspects will require investigation for specific applications, particularly the degree of transformation and the brittleness of the transformed product. Some experimental work [*26*] suggests that the degree of transformation in some commonly used austenitic stainless steels, the properties of the transformed products, or both, do not present problems of severe brittleness. On the other hand, a pronounced embrittlement is reported [*31*] for austenitic Cr-Mn-N-Fe alloys as a result of the martensitic transformation. A commercial Type 347 stainless steel tested at −452 F in notched tension ($K_t = 3.2$) exhibited no embrittlement even though 25 per cent of the

material in the region of the notch had transformed [*32*]. Hence it is apparent that the effects of martensitic-type transformations can vary between materials depending upon the many factors involved. The important aspects are: phase transformations can occur at low temperatures and may be reversible upon subsequent heating; these transformations are enhanced by plastic deformation; and changes from bcc to fcc should have associated changes in fracture behavior that are in a favorable direction, while those going from fcc to bcc could produce undesirable effects.

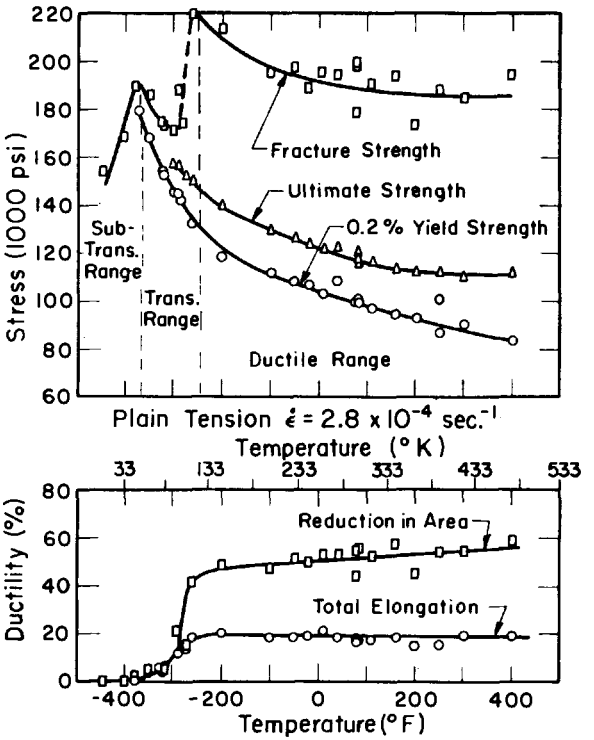

FIG. 5—*The temperature dependence of the uniaxial tensile properties of a Ni-Mo-V forging steel.*

Effects of Notches (Defects) on the Fracture Behavior

To gain some insight into the role of defects and the problem of how metals fail in practice at very low applied stresses particularly at cryogenic temperatures, let us consider the behavior of a given metal under various test conditions leading to brittle fracture. Since the bcc metals are most susceptible to low-temperature brittleness, a ferritic steel serves as a convenient example. The particular metal to be described is a Ni-Mo-V forging steel. The pertinent metallurgical characteristics and detailed data have been described elsewhere [*17*].

Simple Tension

The engineering tensile (uniaxial) data for this metal are shown in Fig. 5. Note the correspondence of these data to the generalized fracture-strength behavior of Fig. 2. In the ductile range above −250 F, the fracture strength and ductility are quite high. In the transition range between −250 and −380 F, total brittle fractures (cleavage) are encountered, and ductility decreases markedly with decreasing temperature. After an abrupt

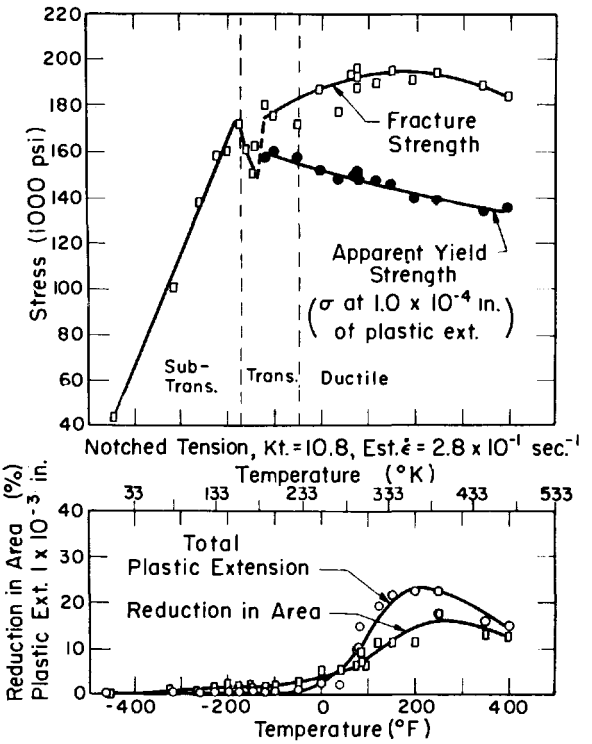

FIG. 6—*The temperature dependence of the notched tensile properties of a Ni-Mo-V forging steel.*

drop upon entering the transition range, fracture strength increases with decreased temperature, corresponding to the lower limit of the hatched transition area of Fig. 2. Below −380 F, in the subtransition range, fracture strength decreases markedly, and the ductilities are essentially nil. Of greatest significance in Fig. 5 is the fact that the stresses required for brittle fracture are nowhere near the low stresses at which the type of material has failed in practice at ambient temperatures.

Machined Notch in Tension

To take a step closer to the conditions that could prevail in practice, a sharp notch is machined in a cylindrical tension specimen to provide a

theoretical elastic stress concentration factor, K_t, of 10.8. A series of these specimens tested over a range of temperatures yields the results shown in Fig. 6. Total-cleavage fractures are now encountered at all temperatures below about −50 F. The transition range is approximately −50 to −150 F, the subtransition range being, obviously, below −150 F. Of particular significance from the cryogenic viewpoint is the very pronounced decrease in fracture strength in the subtransition-temperature range. Below about −250 F, the notched-bar fracture strength is less than the yield

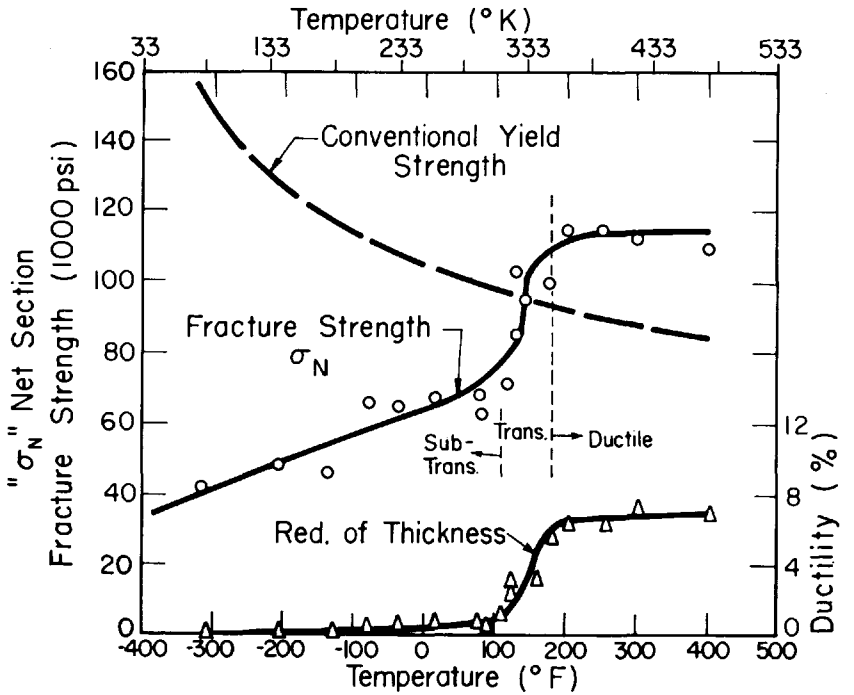

FIG. 7—*Fracture strength and ductility in the crack-notch condition for a Ni-Mo-V forging steel.*

strength of the plain bar (Fig. 5). The rapid decrease of fracture strength in the subtransition range is associated with the inherent increased resistance of the metal to plastic flow, abetted by the general plastic restraint around the notch. In addition to the highly localized, atomic-scale, stress concentrations around dislocation pile-ups, there is an additional general, macroscopic-scale, stress concentration in the vicinity of the machined notch. As the plastic resistance of the material increases with decreased temperature, the general stress concentration due to the notch also becomes greater, since there is less stress relief by plastic flow. In effect, a larger and larger percentage of the theoretical elastic stress concentration factor is realized.

The fracture processes occurring on the atomic scale are the same for plain and notched tension. Owing to the presence of the notch, however, an increase in the general stress concentration and a localization of the plastic strain facilitate development of the critical, highly local stress conditions around dislocation pile-ups. Therefore, fracture comes at applied stresses much lower than those required in simple tension.

Cracked Plates in Tension

To achieve more severe test conditions, a large flat tension specimen containing sharp cleavage edge cracks is employed. This provides ex-

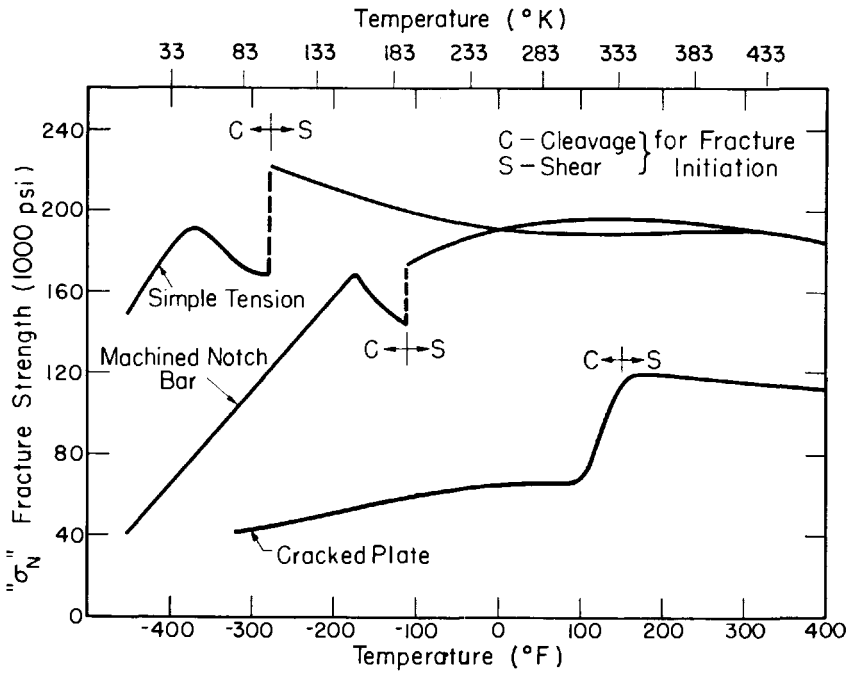

FIG. 8—*Fracture strength of a Ni-Mo-V forging steel for different test conditions.*

tremely severe notch acuity and stress concentration. Such sharp cracks or crack-like defects are likely to exist in large metal members and structures as weld cracks, inclusions, flakes, shrinkage cracks, forging bursts, and so forth. The method of preparing and testing these crack-notch specimens has been described elsewhere [*17*].

The pertinent results obtained when a series of crack-notch specimens of constant geometry are tested over a temperature range are illustrated in Fig. 7 for the Ni-Mo-V forging steel. The fracture-strength behavior is most significant. The net section fracture strength, σ_N, represents the average applied stress required to initiate fracture at the root of the pre-existing crack. The values are obtained by dividing the applied load at the

onset of rapid fracture (fracture initiation) by the uncracked area between the notches. In the transition-temperature range (approximately 100 to 200 F), σ_N undergoes an abrupt drop from values above to values well below the conventional yield strength. A corresponding loss in ductility occurs in the same temperature range. Likewise a change in the mode of fracture from a ductile shear tearing (fracture at an angle of about 45 to specimen axis) to a flat brittle cleavage fracture occurs in this transition-temperature range. The fracture strength continues to decrease in the temperature range below the abrupt transition.

Comparison of Different Tests of Same Material

To see how various test conditions affect the brittle-fracture strength, let us compare the data obtained in the three series of experiments described in this section. Figure 8 shows the fracture strength for the plain-tension, the cylindrical-notched-tension, and the crack-notch-plate tests. It is seen that, as the severity of test conditions is increased, brittle fractures occur at progressively higher temperatures and lower applied stresses. Since the specimen size is essentially the same, the difference in the fracture strength and the transition temperature, C/S, between the plain-tension and cylindrical-notched tests (*top two curves*) can be attributed primarily to the presence of the notch and its associated effect of concentrating the fracture processes in a local region. The rather drastic lowering of the fracture strength and the pronounced rise in the transition temperature illustrated by the crack-notch data (*bottom curve*) may be attributed to the combined effect of the more severe notch (crack) and the increased section size.

Thus, the rather pronounced effects of mechanical variables on brittle-fracture behavior are demonstrated. While the data provided are for a given metal, the behavior pattern is typical of the general trend for bcc metals. The temperature dependence of the fracture stresses for identical test conditions can also vary between metals. Some fcc and cph metals also exhibit behavior trends similar to bcc metals with respect to notch and section-size effects [*33,34*]. In view of these results, one can better appreciate the contributions of cracks and defects to the brittle failures that have occurred in practice, especially at low temperatures and at unexpectedly low stresses. Likewise, it is readily apparent that the measured fracture strength of a given metal can vary markedly from one type of test to another. Similarly, various metals or one metal in various metallurgical conditions can exhibit drastic differences in fracture strength even when tested under identical conditions.

At this point it must be emphasized that the notch-fracture strengths shown in Fig. 8 were obtained for particular specimen geometries and crack-sizes. In their present form, these data cannot be used for specific evaluation or design. They are intended only to illustrate behavior pat-

terns and trends. It is necessary to consider the interrelationships of fracture strength, crack lengths, section sizes, stress states, and possibly other influential factors before experimental data obtained for any given set of conditions can be utilized for specific evaluation or design. In the next section, some consideration is given to use of fracture-strength data in determining the load-bearing capacity of structures containing defects or flaws.

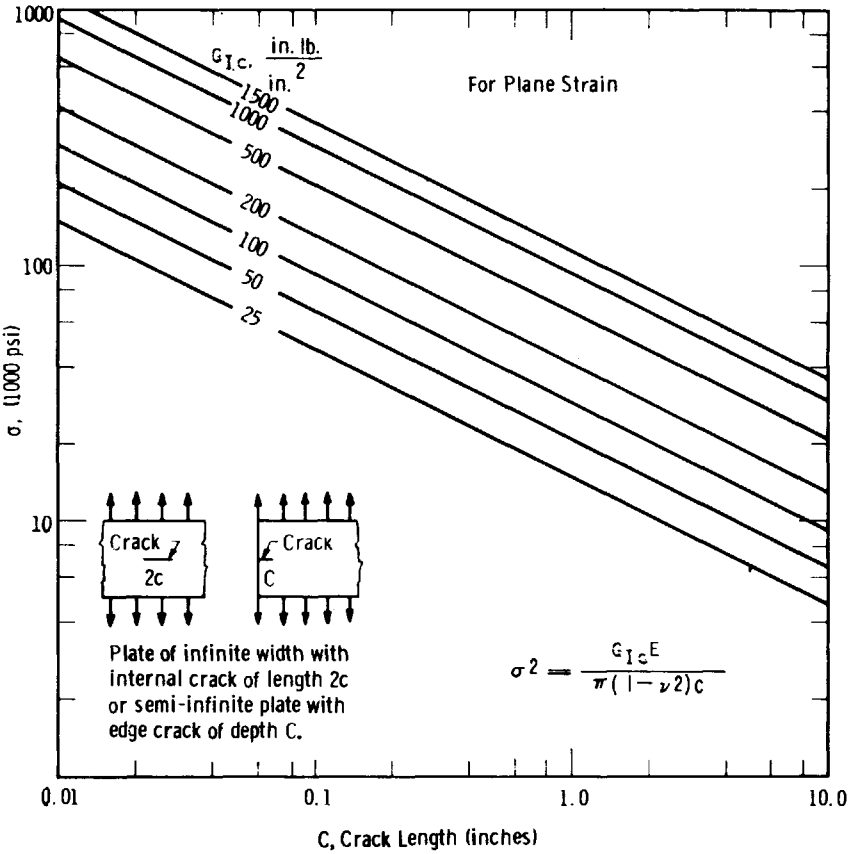

FIG. 9—*The relationship of fracture strength to crack size for different levels of fracture toughness.*

The Load-Bearing Capacity of Structures Containing Defects

The Fracture-Toughness (Fracture-Mechanics) Concept

The foregoing discussion has demonstrated that the load-bearing capacity (fracture strength) of a metal can be drastically affected by varia-

tions in specimen geometry and the type of notch or defect that prevails. How then is it possible to evaluate the load-bearing capacity of a structure or member containing known defects? The fracture-mechanics or fracture-toughness approach to the general problem of fracture appears to be the most promising means available for this purpose, since it facilitates quantitative estimates of the critical combinations of defect sizes

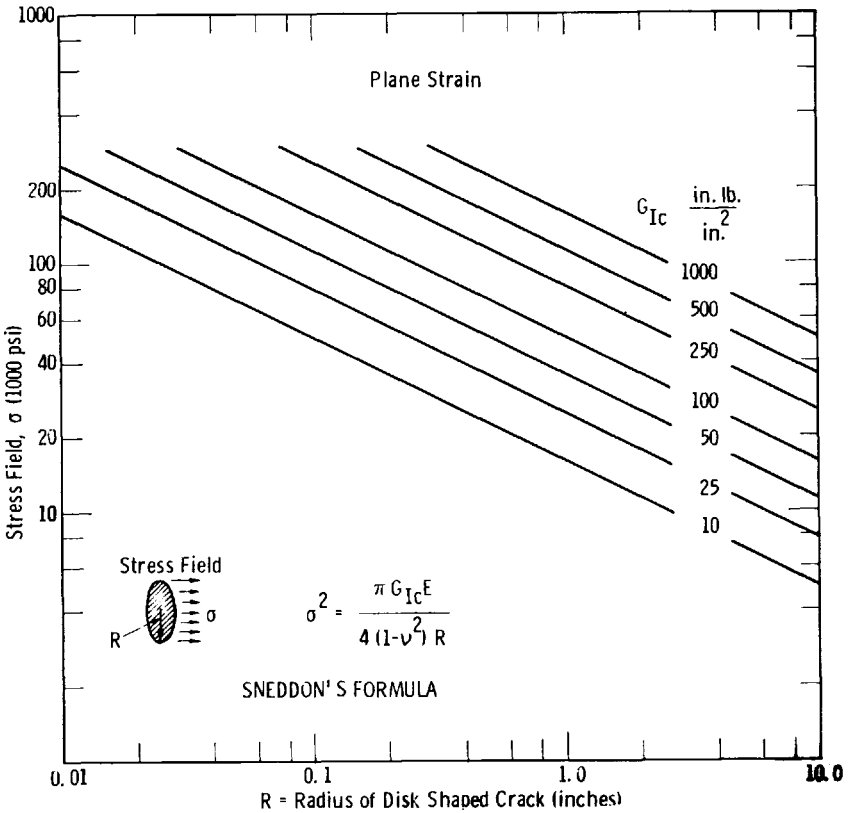

FIG. 10—*The relationship of fracture strength to crack size for different levels of fracture toughness. (For a thin disk-shaped crack of radius* R *embedded in a stress field* σ *of large extent as compared with* R.) (*From Ref. 45.*)

and applied stresses required for catastrophic failure. This approach would appear to be particularly suited to cryogenic applications where the susceptibility of most metals to a brittle behavior is considerably enhanced.

It is beyond the intended scope of this paper to discuss the complex details of the fracture-toughness concept—a comprehensive review of this subject has recently been published [*35*]. My primary intent is to illustrate the practical applicability of fracture mechanics to cryogenic applications. A brief general description of the concept is necessary, however, before

its use can be illustrated. More specific information is available [*35–42*]. The basis of the concept is that the fracture toughness of a material can be expressed as a material parameter[5] analogous to yield strength. This parameter is usually described in terms of "G_c" (critical crack-extension force, in psi), or of "K_c" (critical stress-intensity factor, psi $\sqrt{\text{in.}}$). Either

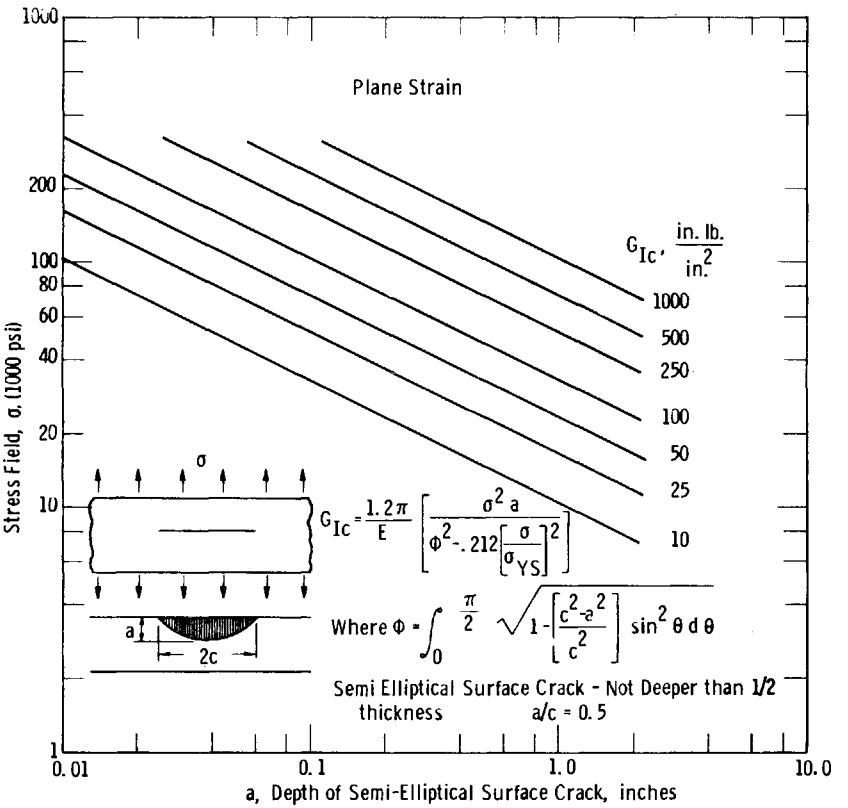

FIG. 11—*The relationship of fracture strength to crack size for different levels of fracture toughness. (For catastrophic failure at* $\sigma = \frac{1}{2}$ *YS with semi-elliptical surface crack of geometry* a/c = *0.5.) (From Ref 3.7.)*

G_c or K_c is commonly referred to as "fracture toughness." [6] Once properly determined under one set of conditions, the fracture toughness is applicable to other conditions of geometry, flaw size, and loading, since it

[5] The evidence to date substantiates the hypothesis that the fracture toughness, when properly measured, can be considered as a material constant for practical engineering purposes.

[6] There are many subscripts used to denote various aspects of G_c or K_c, therefore, an intimate knowledge of this terminology is essential to the proper use of these parameters.

is a material parameter. Several types of specimens and loading conditions have been successfully employed to obtain measurements of fracture toughness [*35–42*].

Application of Fracture Mechanics

Expressions relating the fracture toughness and the load-bearing capacity of defect-containing structures or components are available for a number of geometries, loading conditions, and types of defects. Such expressions nearly always involve the following terms: the fracture toughness, the applied stress, the elastic modulus, the yield strength of the material, a linear dimension of the crack or defect, and a proportionality term dependent only on the manner of loading and the relative geometry of the defect and structural component. Some examples of the expressions [*35–46*] derived and available in the literature are: infinite or semi-infinite plates with central or edge cracks loaded in tension [*36,38,41*], notched disks or shafts in rotation [*43,44*], notched bars in bending [*35,41*], notched cylindrical members in tension [*35,39*], a small flaw imbedded in a large body in tension [*43,45*], and semi-elliptical surface or internal flaws in sheets or plates in tension [*35,37,40,41*]. For simplicity, some of these solutions are shown in graphical form in Figs. 9 to 11. In the case of the semi-elliptical surface flaw (Fig. 11), boundary conditions for the stress field and flaw geometry had to be applied for ease of simplified graphical representation. It is, therefore, of limited applicability, but it does serve to demonstrate the general relationship of crack size to critical stress for the various levels of toughness, G_c .

The implementation of the fracture-toughness approach for determining load-bearing capacity is readily apparent from the graphs provided in Figs. 9 to 11. Knowing the fracture toughness of the material in question for the temperature range of interest and the size of the defects from a nondestructive evaluation, it is possible to evaluate the load-bearing capacity in terms of the average applied stress prevailing in the structure. Conversely, knowing the toughness and applied stress, it is possible to estimate the critical-defect sizes required for catastrophic failure. These, in turn, can be compared with performance capabilities of the nondestructive test techniques that may be employed. As seen in Figs. 7 to 9, at a given level of toughness, G_{Ic} , the applied stress required for catastrophic fracture decreases as the crack size increases. Similarly, for a given defect size, a decrease in toughness results in a lower applied stress for fracture. Thus, an estimate of the critical combination of defect size and applied stress required for fracture may be readily determined if one knows the toughness of the material and either one of the other two variables.

It should be realized that the foregoing paragraph is intended only to provide a general idea of the application of the fracture-toughness approach and to emphasize the interplay between toughness and defect size

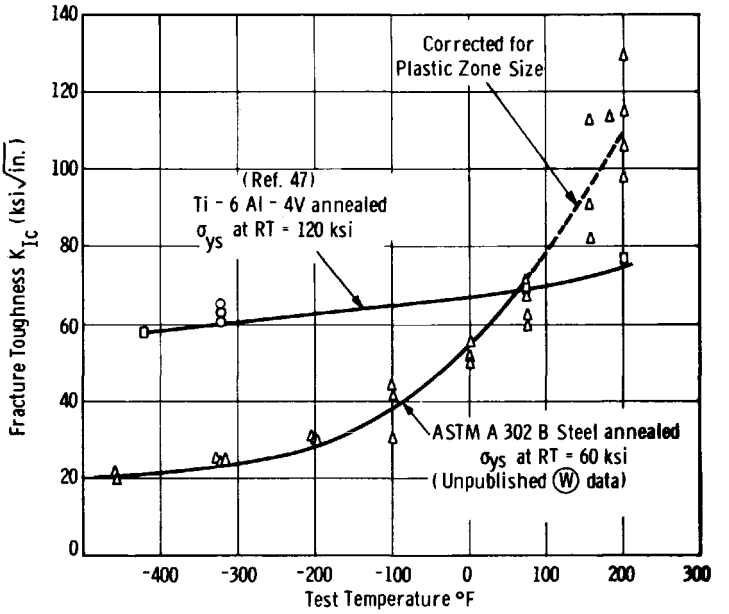

FIG. 12—*Comparison of the temperature dependence of* K_{Ic} *for a steel and a titanium alloy.*

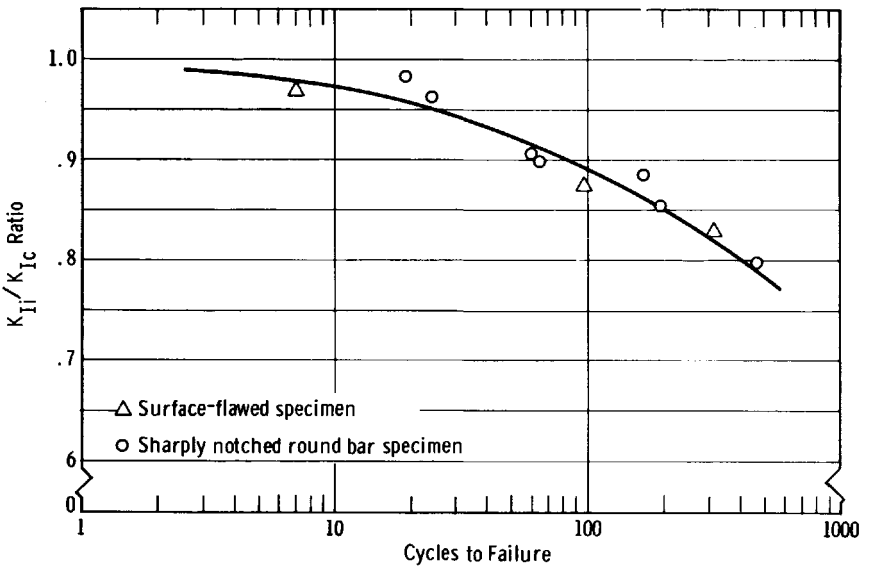

FIG. 13—*Cyclic flaw growth data of 6Al-4V titanium plate tested at −320 F (Ref. 47).*

in determining the load-bearing capacity of a structure. For a precise evaluation of any specific situation, considerably more detailed information is required regarding: the temperature dependence of the fracture toughness, K_{Ic} or G_{Ic}, in the range of interest; the location, size, shape, orientation, and type of defect; the direction and magnitude of the applied (and possibly residual) stresses acting on the defect; the slow-growth characteristics of a subcritical-size flaw under sustained or cyclic loading at the application temperatures; the relative geometry of the structural member and the defect; and the proper criterion of fracture toughness (plane stress or plane strain and fracture mode) to be employed.

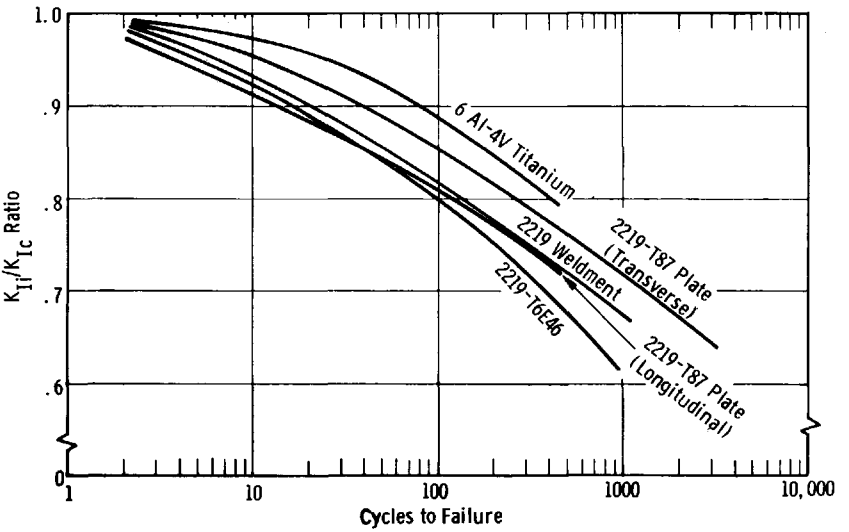

FIG. 14—*Comparison of cyclic flaw growth data for various materials at −320 F (Ref. 47).*

Some good examples of the application of fracture mechanics to the solutions of cryogenic engineering problems, particularly as related to storage vessels, may be found [*35,40,47,48*]. The same considerations can also be applied to any cryogenic structural problems. Basic fracture-toughness data, K_{Ic} or G_{Ic}, for some materials and cryogenic temperatures are also available [*35–40,47–49*].

Figures 12 to 14 are examples of fracture-toughness data for the cryogenic-temperature range. Figure 12 illustrates the difference in the temperature dependence of K_{Ic} for metals having different lattice structures, steel (bcc) and titanium (cph).[7] The relative behavior exhibited by the

[7] The Ti-6Al-4V is an $\alpha + \beta$ alloy, but in the annealed condition and at low temperatures the α phase is predominant. Hence it is primarily a cph-lattice structure.

steel and titanium alloy is what would be expected from the fundamental aspects of fracture discussed earlier in the paper. BCC metals characteristically exhibit a strong increase in resistance to plastic flow with decreasing temperature. Thus, a correspondingly strong decrease in fracture toughness, K_{Ic}, with decreased temperature is to be expected. Conversely, the titanium alloy exhibits a relatively mild increase in resistance to plastic flow, hence, a mild decrease in fracture toughness.

Figures 13 and 14 illustrate the effect of the initial stress-intensity factor, K_{Ii}, upon the life of several metals under conditions of cyclic loading. A similar behavior occurs under sustained loading conditions. For this description, the ordinate is given in terms of the ratio of the initial stress-intensity factor, K_{Ii}, to the critical stress-intensity factor, K_{Ic}, which is the basic material-toughness parameter. As may be seen, the higher the ratio of K_{Ii} to K_{Ic}, the shorter the life expectancy of the material. In essence, this means that the closer the initial conditions (stress and flaw size) are to the critical conditions for catastrophic failure, the less slow-crack growth or increased stress the metal can tolerate.

Data of the type shown in Figs. 13 and 14 are essential for evaluating the performance and useful life of structures or components. For example, by using an expression appropriate to the given situation of component and defect geometry, the designer can compute K_{Ii} (initial stress-intensity factor) from a knowledge of the nominal stresses prevailing in the region of the defect and a knowledge of the defect size, shape, and orientation obtained from nondestructive inspection. The computed K_{Ii} coupled with a known value of K_{Ic} and appropriate slow-crack-growth data of the type illustrated in Figs. 13 and 14 then permits the designer to quantitatively evaluate the reliability and life expectancy of the component in question.

Summary

The origin of the fracture strength (load-bearing capacity) of a metal involves the forces or bonds between atoms. Accordingly, the stresses required to rupture these bonds are quite high. Because of highly localized stress concentrations brought about by the presence of atomic-scale defects or imperfections, however, the theoretical strength of a metal is never achieved.

The fracture strength of a given metal may be related to its inherent resistance to plastic flow (plastic resistance). Since the plastic resistance of some metals is markedly temperature dependent, their respective fracture characteristics must be also. Such behaviors are characteristic of all bcc metals and most of the cph metals. A strong increase in the plastic resistance with decreased temperature gives rise to a brittle behavior at cryogenic temperatures.

As measured in a simple tension test, various metals or various lots of a given metal may exhibit markedly different brittle fracture strengths in

different temperature regions. Their individual behavior depends on their particular plastic resistance characteristics. There are some features, however, that are common in the bcc metals and also in some cph metals. In the transition-temperature range, some macroscopic amount of plastic deformation always precedes brittle fracture, and the brittle fracture strength is always equal to or greater than the conventional yield strength. In this range, stable microcracks may or may not exist prior to total fracture. At subtransition temperatures, the brittle fracture strengths are always less than the conventional yield strength, and only microscopic amounts of plastic deformation precede fracture. In this range, it appears that the first microcrack immediately grows catastrophically to total fracture. Depending upon the metal, the cryogenic-temperature range could incorporate both the transition and subtransition behaviors.

In the more practical situation where notches or defects of a macroscopic nature are likely to prevail initially, the same general atomic-scale fracture processes occur. The attainment of the critical conditions governing these processes is abetted by the general stress or strain concentrations prevailing in the vicinity of the macroscopic defect. Consequently, the fracture strength of a given metal as measured in a given type of notched test is not some unique basic material property reproducible from one type of test to another. It is, rather, a highly variable criterion representative of the gross product of complex interactions of several influential factors, namely: the inherent plastic resistance (toughness) of the metal at the temperatures of interest; the size, shape, orientation, and acuity of the notch or defect; the relative size and geometry of the defect and the specimen; and the manner and rate of loading the specimen. In general, as the severity of the test conditions increases to larger and more acute notches, larger specimens, higher rates of loading, and so forth, brittle fractures will occur at progressively higher temperatures and lower applied stresses. In the cryogenic-temperature range, these applied stresses can be exceptionally low.

In evaluating the load-bearing capacity of defect-containing components or structures, the problem of variable fracture strengths may be circumvented by the use of a basic material parameter that describes the inherent fracture toughness of a material. This fracture-toughness parameter used with appropriate expressions relating the toughness, defect size, applied stress, and relative geometry factors make it possible to make quantitative evaluations of the load-bearing capacity of structures containing defects. This technique is commonly called the "fracture-mechanics" or "fracture-toughness" approach. While the employment of fracture-mechanics concepts, expressions, and data may initially appear to be quite complex to the uninitiated designer or materials engineer, familiarity with the subject and systematic consideration of all factors can evolve a relatively simple and quantitative engineering procedure. The approach can be readily used

in a quantitative manner in several areas: establishment of design configurations and design stresses, evaluation of materials, selection of optimum material for a given application, establishment of required nondestructive inspection procedures, development of inspection standards and acceptance limits, quality control, purchase specifications, and, ultimately, overall evaluation of the integrity and performance characteristics of components and structures.

References

[1] F. Seitz and T. A. Read, "Theory of the Plastic Properties of Solids III," *Journal of Applied Physics*, Vol. 12, 1941, p. 470.

[2] C. S. Barrett, *Structure of Metals*, McGraw-Hill Book Co., New York, 1943, p. 319.

[3] S. S. Brenner, "The Properties of Whiskers," *Growth and Perfection of Crystals*, John Wiley and Sons, Inc., New York, 1958, p. 161.

[4] E. Orowan, "The Solid State of Matter," *International Conference on Physics, Vol. II*, Physical Society of London, 1935, p. 89.

[5] C. Zener, "The Micro-Mechanism of Fracture," *Fracturing of Metals*, Am. Soc. Metals, Cleveland, 1952, pp. 3–31.

[6] N. J. Petch, "The Cleavage Strength of Polycrystals," *Journal Iron and Steel Institute*, Vol. 174, 1953, p. 25.

[7] A. N. Stroh, "The Formation of Cracks as a Result of Plastic Flow," *Proceedings*, Royal Soc., London, Vol. A223, 1954, p. 404.

[8] A. H. Cottrell, "Theory of Brittle Fracture in Steel and Similar Metals," *Transactions*, Am. Inst. Mining, Metallurgical and Petroleum Engrs., Vol. 212, 1958, p. 192.

[9] E. T. Wessel, "Abrupt Yielding and the Ductile-to-Brittle Transition in Body-Centered-Cubic Metals," *Transactions*, Am. Inst. Mining, Metallurgical and Petroleum Engrs., Vol. 209, 1950, p. 930.

[10] J. J. Gilman, "Dislocation Motions and the Yield Strength of Solids," *Properties of Crystalline Solids, ASTM STP 283*, Am. Soc. Testing Mats., 1960, p. 69.

[11] J. Heslop and N. J. Petch, "The Stress to Move a Free Dislocation in Alpha Iron," *Philosophical Magazine*, Vol. 1, 1956, p. 866.

[12] J. H. Bechtold, E. T. Wessel, and L. L. France, "The Mechanical Behavior of Refractory Metals," *Refractory Metals and Their Alloys*, Interscience Publishers, New York, 1961, p. 25.

[13] H. Conrad and W. Hayes, "Correlation of the Thermal Component of the Yield Stress of the BCC Metals," *Transactions*, Am. Soc. Metals, Vol. 56, No. 1, March 1963.

[14] E. T. Wessel, "A Tensile Study of the Brittle Behavior of a Rimmed Structural Steel," *Proceedings*, Am. Soc. Testing Mats., Vol. 56, 1956, p. 540.

[15] W. S. Owen, M. Cohen, and B. L. Averbach, "Brittle Fracture of Mild Steel in Tension at −196°C," *Transactions*, Am. Soc. Metals, Vol. 50, 1958, p. 634.

[16] E. T. Wessel, L. L. France, and R. T. Begley, "The Flow and Fracture Characteristics of Electron Beam Melted Columbium," *Columbium Metallurgy*, Interscience Publishers, New York, 1961, pp. 459–502.

[17] E. T. Wessel, "The Influence of Pre-Existing Sharp Cracks on Brittle Fracture of a NiMoV Forging Steel," *Transactions*, Am. Soc. Metals, Vol. 52, 1960, pp. 277–306.

[18] A. S. Eldin and S. C. Collings, "Fracture and Yield Stress of 1020 Steel at Low Temperatures," *Journal of Applied Physics*, Vol. 22, No. 10, October 1951, p. 5705.

[19] G. T. Hahn, B. L. Averbach, W. S. Owen, and M. Cohen, "Initiation of Cleavage Microcracks in Polycrystalline Iron and Steel," *Fracture*, Technology Press, Massachusetts Institute of Technology and John Wiley and Sons, Inc., New York, 1959, p. 91.

[20] J. H. Bechtold and E. T. Wessel, "The Ductile-to-Brittle Transition in Molybdenum," *The Metal Molybdenum*, Am. Soc. Metals, Cleveland, 1958, p. 241.

[21] J. H. Bechtold and P. G. Shewmon, "The Flow and Fracture Characteristics of Annealed Tungsten," *Transactions*, Am. Soc. Metals, Vol. 46, 1954, p. 397.

[22] E. T. Wessel and D. D. Lawthers, "The Ductile-to-Brittle Transition in Columbium," *Technology of Columbium*, John Wiley and Sons, Inc., New York, 1958, p. 66.

[23] M. J. Marcinkowski and H. A. Lipsitt, "The Plastic Deformation of Chromium at Low Temperatures," *Acta Metallurgica*, Vol. 10, 1962, p. 95.

[24] E. T. Wessel, "Some Exploratory Observations of the Tensile Properties of Metals at Very Low Temperatures," *Transactions*, Am. Soc. Metals, Vol. 49, 1957, p. 149.

[25] R. L. Smith and J. L. Rutherford, "Tensile Properties of Zone Refined Iron in the Temperature Range From 298° to 4.2°K," *Transactions*, Am. Inst. Mining, Metallurgical and Petroleum Engrs., Vol. 209, 1957, p. 857.

[26] R. H. Kropschot, "The Mechanical Properties Testing Program at the NBS-AEC Cryogenic Engineering Laboratory," *Proceedings*, 1954 Cryogenic Engineering Conference, Boulder, Colo., September 1954, (NBS *Report No. 3517*), p. 164.

[27] S. C. Collins, F. D. Ezekiel, O. W. Sepp, and J. W. Rizika, "The Strength of Certain Stainless and Carbon Steels at Low Temperatures," *Proceedings*, Am. Soc. Testing Mats., Vol. 56, 1956, p. 687.

[28] C. S. Barrett, "Metallurgy at Low Temperatures," *Transactions*, Am. Soc. Metals, Vol. 49, 1957, p. 53.

[29] L. Kaufman and M. Cohen, "The Martensitic Transformation in the Iron-Nickel System," *Transactions*, Am. Inst. Mining, Metallurgical and Petroleum Engrs., Vol. 206, 1956, p. 1393.

[30] B. Ya. Lyubon, "Problems of Metallography and the Physics of Metals," *Fourth Symposium, Atomic Energy Commission Translation 2924*, Moscow, 1955.

[31] F. W. Schaller and V. F. Zachay, "Low-Temperature Embrittlement of Austenitic Cr-Mn-N-Fe Alloys," *Transactions*, Am. Soc. Metals, Vol. 51, 1959, pp. 476–494.

[32] E. T. Wessel and W. H. Pryle, "Tensile Properties of AISI Types 304 and 347 Stainless Steels at Moderate Temperatures for Section Sizes Ranging From Bars to Extremely Large Forgings," *Transactions*, Am. Soc. Mechanical Engrs., *Journal Basic Engineering*, Vol. 83(d), 1961, p. 489.

[33] "Effects of Low Temperatures on Structural Metals," *NASA Technology Utilization Report, NASA SP-5012*, NASA Technology Utilization Division, December 1964.

[34] *Evaluation of Metallic Materials in Design for Low Temperature Service, ASTM STP 302*, Am. Soc. Testing Mats., 1961.

[35] *Fracture Toughness Testing and Its Applications, ASTM STP 381*, Am. Soc. Testing Mats., April 1965.

[36] ASTM Committee on Fracture Testing of High-Strength Sheet Materials, "Fracture Testing of High-Strength Sheet Materials," *ASTM Bulletin*, January 1960 (Part I) and February 1960 (Part II), pp. 29–61 and pp. 18–28.

[37] ASTM Committee on Fracture Testing of High-Strength Sheet Materials, "The Slow Growth and Rapid Propagation of Cracks," *ASTM Bulletin*, May 1961, pp. 389–393.

[38] ASTM Committee on Fracture Testing of High-Strength Materials, "Fracture Testing of High-Strength Sheet Materials," *ASTM Bulletin*, November 1961, pp. 877–885.

[39] ASTM Committee on Fracture Testing of High-Strength Materials, "Screening Tests for High-Strength Alloys Using Sharply Notched Cylindrical Specimens," *ASTM Bulletin*, March 1962, pp. 196–204.

[40] ASTM Committee on Fracture Testing of High-Strength Materials, "Progress in Measuring Fracture Toughness and Using Fracture Mechanics," *Materials Research & Standards*, March 1964, pp. 107–134.

[41] G. R. Irwin, "Relation of Crack Toughness Measurements to Practical Applications," *Welding Journal, Research Supplement*, Vol. 41, No. 11, November 1962, p. 519s.

[42] Am. Soc. Mechanical Engineers Subcommittee on Brittle Fracture, "A Review of Engineering Approaches to Design Against Brittle Fracture," *ASME Special Publication,* May 1965.

[43] D. H. Winne and B. M. Wundt, "Application of the Griffith-Irwin Theory of Crack Propagation to the Bursting Behavior of Disks, Including Analytical and Experimental Studies," *Transactions*, Am. Soc. Mechanical Engrs., Vol. 80, 1958, p. 1643.

[44] G. O. Sankey, "Spin Fracture Tests of NiMoV Rotor Steels in the Brittle Fracture Range," *Proceedings*, Am. Soc. Testing Mats., Vol. 60, 1960, p. 721.

[45] I. N. Sneddon, "The Distribution of Stresses in the Neighborhood of a Crack in an Elastic Solid," *Proceedings*, Royal Soc., Vol. A187, 1946, p. 229.

[46] E. T. Wessel, "Correlation of Laboratory Determinations of Fracture Toughness With the Performance of Large Steel Pressure Vessels," *Welding Journal*, Research Supplement, Vol. 43, No. 9, September 1964, p. 415.

[47] C. F. Tiffany and P. M. Lorenz, "An Investigation of Low-Cycle Fatigue Failures Using Applied Fracture Mechanics," *ML-TDR-65-53,* Air Force Materials Laboratory, Wright-Patterson Air Force Base, May 1964.

[48] "Thick Section Fracture Toughness," *ML-TDR-64-236,* Air Force Materials Laboratory, Wright-Patterson Air Force Base, October 1964.

[49] *Aerospace Structural Metals Handbook,* Vols. I and II, Syracue University Press, Syracuse, 1963.

R. P. Reed[1] *and J. F. Breedis*[2]

Low-Temperature Phase Transformations

REFERENCE: R. P. Reed and J. F. Breedis **"Low-Temperature Phase Transformations,"** *Behavior of Metals at Cryogenic Temperatures, ASTM STP 387,* Am. Soc. Testing Mats., 1966, p. 60.

ABSTRACT: Changes in crystallographic structures can occur solely at low temperatures by a diffusionless, shear-type of transformation to a product structure termed martensite. This paper presents a review of martensitic transformations which occur in ferrous and nonferrous alloys. Specifically, kinetic, structure, and the theoretical approaches to describing diffusionless transformations are treated.

The kinetic characteristics pertinent to this class of transformations include dependence upon temperature, time, applied stress, and chemical composition. The structural aspects of martensitic transformations include their morphology and crystallography. Four general types of martensite transformation morphology have been observed in steels and in nonferrous alloys. With particular reference to steels, the product structures may be morphologically described as either: (1) plates, (2) sheets comprised of martensite crystals or laths, (3) homogeneous sheets, or (4) surface martensite. Theories pertaining to martensitic transformations relate either to the initiation or to the subsequent growth of the product. Theories employing thermodynamic analyses or dislocation models generally are concerned with nucleation, while crystallographic theories attempt to predict the mode of growth and the final orientations of the product. Both approaches are discussed.

Approximately 650 references appear in the extended bibliography which lists almost all articles published in English after 1940, in addition to major articles published in other languages. Tables which attempt to classify articles are also included to simplify research of martensite literature.

KEY WORDS: cryogenics, metals, phase transformations, crystal structure, martensite

The sole change in crystallographic structure that can occur in the solid state at low temperatures involves no long-distance transport of the atom species. The product of this mode of transformation is termed martensite and has been observed to form at temperatures where kT is only 0.005 ev or less. Theoretical understanding of the crystallography of the martensitic transformation has developed to date almost independently from its

[1] Physical metallurgist, Cryogenics Div., National Bureau of Standards, Institute for Materials Research, Boulder, Colo.

[2] Assistant professor, Department of Metallurgy, Massachusetts Institute of Technology, Cambridge, Mass.

thermodynamic requirements and vice versa; no complete theory for the transformation has been formulated yet. The purpose of this review is to discuss the present status of each approach together with the experimentally observed kinetic and structural characteristics of the martensitic transformation.

The martensitic transformation may be described as a reaction in which a new crystallographic structure is produced by the coordinated shear of many atoms through small distances relative to their neighbors. Consequently, any given lattice point in the parent structure is related to a specific point in the martensitic product lattice. This lattice correspondence is not, in general, associated with other types of phase transitions. Implicit with the absence of long-range diffusion is constant chemical composition between the parent and product structures. One characteristic of a shear-type transformation has been the production of surface relief effects or a macroscopic shape change during transformation [*104*].[3] Therefore the observation of surface relief has been proposed [*57,104,626*] for experimentally distinguishing martensitic transformations from other reactions. This criterion is not totally exclusive, however, since surface-relief effects have also been found for a few reactions which require some short-range atom diffusion, such as the formation of proeutectoid ferrite [*700*], bainite [*701*], and an Au-Cu ordering reaction [*702*].

It is preferable to identify a martensitic transformation as a crystallographic change brought about by the coordinated shear of many atoms, but without diffusion. The following general characteristics (with some exceptions) are typical of such a transformation:

1. A macroscopic shape change or surface relief.
2. No composition gradient between parent and product.
3. Unique crystallographic relations between parent and product.
4. Unique transformation morphology.
5. Transformation possible near absolute zero.
6. Incomplete transformation possible, even near absolute zero, in certain alloys.
7. Transformation possible over a wider temperature range by applied elastic stress or plastic strain.
8. Accommodation stress effects in product, parent, or both.

Kinetic Characteristics

A considerable amount of experimental data has accumulated regarding the kinetic characteristics of martensite transformations (see Tables 1 and 5). These effects can be divided into those of a general nature and those which are influenced by a specific parameter. The parameters thought to be the most fundamental are temperature, time, applied stress, and chemical

[3] The italic numbers in brackets refer to the list of references appended to this paper.

TABLE 1—*Classification of papers containing*

Structural Change on Cooling	Alloy System	Composition Range for Spontaneous Transformation, weight per cent	M_s, M_d, A_s, A_d Data	Stress
fcc → hcp	Co	...	*4, 49, 105, 150, 225, 234, 382, 516, 587, 634*	*225, 382, 467*
	Co-Ni	≦35Ni	*52, 225, 506*	...
	Co-Fe	...	...	*524*
	La	...	*634, 639*	...
fcc → {hcp / bcc}	Fe-Mn	$\epsilon \geqq$ 10Mn $\alpha' \leqq$ 20Mn	*26, 259, 515*	...
	Fe-Mn-C	C lowers M_s^{ϵ} and $M_s^{\alpha'}$	*182, 247, 306, 307, 310, 354, 359, 368, 470, 573, 574*	*310, 470, 557, 573*
	Fe-Mn-Ni	Ni lowers M_s^{ϵ}	*63, 94, 155, 308, 310, 470, 497*	*310, 447, 470*
	Fe-Mn-Ni-Cr	Cr raises M_s^{ϵ}	*65, 66*	*66*
	Fe-Cr-Ni	...	*5, 80, 83, 108, 109, 139, 151, 156, 157, 167, 183, 184, 208, 209, 296, 312, 366, 367, 442, 443, 473, 494, 520, 607, 655*	*5, 18, 43, 44, 61, 81, 83, 106–109, 157, 185, 207, 211, 294, 309, 312, 360–362, 373, 385, 429, 441, 443, 473, 494, 495, 529, 607*
	Fe-Cr-Mn	...	...	...
	Fe-Ru, Os, Pt, Ir	...	*628, 645, 646*	*628*
fcc → bcc	Fe	...	*50, 105, 141, 257*	*257, 616*
	Fe-Ni	≦34Ni	*19, 24, 80, 83, 95, 96, 111, 176, 183, 184, 250, 259, 261, 269, 271, 290, 291, 294, 295, 338, 355, 375, 414, 427, 453, 464, 499, 503, 611, 614, 616*	*19, 83, 95, 185, 269, 271, 294, 295, 355, 414, 464, 611, 616*
	Fe-Ni-Co	...	*184*	...
	Fe-Ni-(Ti, Nb, V, Si)	...	*572*	...
	Fe-Si	≦2Si	*176, 509*	*509*
	Fe-Cr	≦15Cr	*176*	*616*
	Fe-Co-W-Cr	...	*505*	...
fcc → bct	Fe-C	<2.5C	*1, 26, 50, 64, 190, 194, 197, 222, 235, 248, 250, 359, 363, 370, 428, 434, 455, 553, 593*	*428, 434*
	F-C-N	...	...	...
	F-C-H	...	...	...

kinetic martensitic transformation data.

Particle Size	Isothermal Holding	Cooling Rate	Composition	Temperature	Tempering Effects
...	*234, 516*	*49, 516*	...	*150, 234, 382, 467, 516*	...
...	...	...	*52, 225, 506*	*506*	...
...	...	...	...	...	...
...	...	...	...	...	...
26	...	*259*	*259, 411*	*247, 259, 411, 515, 574, 575*	...
537, 573	*182, 247, 306, 307, 310, 461, 470, 574–576*	*574*	*368, 557*	*182, 306, 307, 310, 354, 461, 470, 557, 576*	...
...	*63, 94, 308, 310, 470*	...	*497*	*94, 155, 308, 310, 470, 497*	...
...	...	...	*65, 66*	*65, 66*	...
208, 451	*45, 108, 139, 156, 157, 296, 312, 442, 494*	...	*5, 45, 80, 108, 151, 157, 211, 366, 367, 429, 441, 442, 520, 607, 655*	*5, 18, 43, 45, 61, 81, 83, 108, 109, 157, 183, 184, 208, 211, 294, 296, 309, 312, 361, 362, 368, 373, 441–443, 473, 494, 495*	*45, 107, 109, 139, 607*
...	...	...	*236*	...	...
...	...	...	*628*	*628*	...
...	*490*	*50*	...	*257, 490*	...
24, 95, 96, 261, 537	*146, 250, 290, 355, 567, 571, 648*	*503, 571, 577*	*111, 176, 259, 269, 290, 291, 453, 489, 503, 567, 591, 614*	*24, 83, 95, 146, 183, 184, 250, 259, 261, 269, 271, 290, 291, 294, 295, 333, 355, 427, 464, 567*	*250*
...	...	...	...	*184*	...
...	...	...	*572*	...	...
...	...	*176*	*176*	...	...
...	...	*176*	*176*	...	...
...	...	...	*505*	...	...
26, 363	*190, 222, 235, 237, 250, 370, 511, 553*	*50, 363, 194*	*1, 64, 145, 190, 194, 197, 216, 233, 235, 247, 293, 434, 439, 448, 455–457, 593*	*190, 222, 235, 237, 248, 250, 293, 370, 428, 434*	*1, 46, 216, 222, 248, 250, 277, 439, 517, 555*
...	...	...	*381*	...	...
...	*181*	...	*181*	*181*	...

TABLE 1—*Classification of papers containing*

Structural Change on Cooling	Alloy System	Composition Range for Spontaneous Transformation, weight per cent	M_s, M_d, A_s, A_d Data	Stress
fcc → bct *Continued*.....	Fe-C-(Mn, Cu, Si, Ni, Cr, Mo, V, W, Al, Co)	...	*190, 416, 435, 496, 526, 649, 650*	*650*
	Fe-Cr-C	...	*26, 42, 86, 206, 212, 222, 279, 281, 359, 419, 578*	*20, 202, 343, 578*
	Fe-Cr-C-H	...	...	...
	Fe-Ni-C	...	*16, 17, 86, 147, 183, 184, 187, 222, 235, 250, 331, 359, 370, 414, 430, 554*	*16, 17, 218, 331, 414, 430, 554*
	Fe-Ni-C-H	...	...	...
	Fe-Cu-C	...	...	...
	Fe-Si-C	...	...	...
	Fe-Cr-Ni-C	...	*354*	...
	Fe-Ni-Cr-Mo-C	...	*297, 460*	*474*
	Fe-N	...	*604*	...
fcc → {hcp / fcc}.....	Ce	...	*204, 353, 634*	*353*
fcc → fct.....	Mn-Cu	≦30Cu	*37*	...
	In-Tl	18–23Tl	*90, 215, 369*	*90*
	In-Tl-Li	...	*369*	...
fct → fct.....	In-Pb	12–14.5Pb	*369*	...
bcc → hcp.....	Na	...	*2, 30, 32, 133, 158, 205, 242, 342*	*32, 133, 242*
	Zr	...	*105, 141, 166, 491, 525*	...
	Zr-(Nd, Y, Dg, Ho, Er)	...	*245*	...
	Tl	...	*104, 141*	...
	Hf	...	*140, 166, 602*	...
	Ti	...	*48, 105, 141, 166, 491*	*561*
	Ti-H_2	<50H_2	*314*	...
	Ti-Al	<16.5Al	*595*	...
	Ti-Cu	<8Cu	*186, 491*	...
	Ti-Cr	<6.5Cr	*143, 407*	*407*
	Ti-Fe	<6Fe	*143, 423, 424*	...

kinetic martensitic transformation data.—Continued.

Particle Size	Isothermal Holding	Cooling Rate	Composition	Temperature	Tempering Effects
...	*461, 616, 649, 653*	...	*190, 416, 435, 496, 526*	*190, 435, 461, 526, 616, 649, 650*	...
26, 206	*20, 212–214, 578, 648*	*213*	*42, 86, 578*	*20, 206, 212, 213, 578*	*20, 231*
...	*181*	...	*181*	*181*	...
...	*17, 147, 222, 235, 237, 250, 286, 370, 404, 419, 461, 648*	*147, 222, 286, 451 589*	*17, 86, 214, 235, 237, 281, 331, 370, 456*	*16, 17, 147, 183, 184, 187, 214, 222, 235, 237, 250, 278, 286, 331, 370, 404, 414, 554*	*222, 223, 237, 250, 278, 285, 555*
...	*181*	...	*181*	*181*	...
...	*189*	...	*189*	*189*	*189*
...	*461*	...	...	*461*	...
...	*404*	...	...	*354, 404*	...
...	*460*	*460*	*297*	*460*	*474*
...	...	...	...	*604*	...
...	*353*	*204*	...	*204, 353*	...
37	*37*	...	*466*	*37, 466*	...
39	*90*	...	*215, 369*	*90, 369*	...
...	...	...	*369*	...	...
...	...	...	*369*	*369*	...
...	...	...	...	*205, 342, 30, 32, 133*	...
...	...	*141*	...	...	...
...	...	...	*245*	*245*	...
...	...	*141*	...	...	...
...	...	...	...	*602*	...
...	*48*	*48, 141*	...	...	...
...	...	...	*314*	*314*	...
...	...	...	...	*595*	...
...	...	...	*491*	*186*	...
...	...	...	*143*	*21*	...
424	...	...	*423, 143*	...	...

TABLE 1—*Classification of papers containing*

Structural Change on Cooling	Alloy System	Composition Range for Spontaneous Transformation, weight per cent	M_s, M_d, A_s, A_d Data	Stress
bcc → hcp *Continued*.....	Ti-Mn	<6.4Mn	*143, 169*	...
	Ti-Mo	<12Mo	*130, 141, 143*	*228*
	Ti-Zr	0–100Zr	*142, 202*	...
	Ti-V	<15V	*143*	*228*
	Ti-Al-V	...	*508*	...
	Ti-Al-V-Mn	...	*508*	...
	Ti-Al-Cr	...	*510*	...
	Ti-Cr-Mo	...	...	*228*
	Ti-Ta, Nb, W	<25W, <50Ta, <36Nb	*143*	...
	Zr-U	...	*132*	...
	Cu-Al-Ni	...	*100, 240, 452*	*8*
bcc → ?.....	Cu-Al-Fe	...	*262*	...
bcc → {monoclinic / orthorhombic}.....	Cu-Al	9–14.5Al	*120, 201, 335, 376, 379, 475, 610*	*345*
	Ag-Cd	46–51Cd	*346, 349*	*347, 349*
bcc → {orthorhombic / tetragonal}.....	Au-Cd-Cu	...	*380*	...
	Au-Cd	46–52Cd	*99, 596, 597*	...
bcc → {hcp / fcc}.....	Li	...	*28, 32–34, 69, 134, 135, 158, 178, 242, 341*	*28, 32, 34, 135, 178, 242*
	Li-Mg	<23Mg	*33, 34, 135, 340, 348*	*33, 34, 135*
	Cu-Zn	38–52Zn	*238, 345, 426, 513, 586*	*31, 345, 498*
bcc → ?.....	Cu-Zn-Ga	...	...	...
	Cu-Sn	16–26Sn?	*7*	...
	Au-Zn	50Zn	*660*	...
hcp → fcc.....	A-N_2	1–55N_2	*35*	...
tetragonal → orthorhombic.....	U	...	*105*	...
	U-Cr	<3Cr	*558*	...
rhombohedral → bct.....	Hg	...	*504, 641*	*504, 641*
Possible Transformations: face centered orthorhombic → monoclinic....	Pu	...	*226, 413*	...

kinetic martensitic transformation data.—Concluded.

Particle Size	Isothermal Holding	Cooling Rate	Composition	Temperature	Tempering Effects
...	...	...	*143, 169*	...	...
...	...	*141*	*130, 141, 143*	...	...
...	...	*142*	*142, 202*	...	...
...	...	...	*143*	...	...
...	...	...	...	...	...
...	...	...	...	...	...
...	...	...	*510*	...	...
...	...	...	...	...	...
...	...	...	*143*	...	...
...	...	...	*132*	*132*	...
...	...	...	...	...	*240*
...	...	...	...	...	...
...	...	...	*345, 376, 610*	*200, 201*	*120*
...	*347*	...	*346, 347*	*346, 347, 349*	...
...	...	...	*380*	*380*	...
...	...	...	*99, 596, 597*	*98, 99, 596*	...
...	...	...	...	*28, 32, 34, 134, 135, 341*	...
...	*33*	*33*	*34, 348*	*33, 34, 135, 340*	...
...	...	...	*345, 426, 586*	*426, 498, 513*	...
...	...	...	...	...	*188*
...	...	...	...	...	...
...	...	...	...	...	...
...	...	...	*35*	...	...
...	...	...	...	...	...
...	...	...	*558*	...	...
...	...	...	...	*504*	...
...	...	...	...	...	...

TABLE 2—*Structural data for martensitic transformations.*

Structural Change on Cooling	Alloy System	Composition Range, weight per cent	Habit Plane	Orientation Relationship	Internal Structure and Morphology of Product, M	Internal Effects in Parent, P	References
fcc → hcp.....	Co	...	$(111)_P$	$(111)_P \parallel (00.1)_M$, $[1\bar{1}0]_P \parallel [11.0]_M$	Faults. Narrow sheets on $(111)_P$, all four variants are found. Surface tilts observed.	Faults.	*4, 51–54, 149, 173, 234, 272, 468, 527, 528*
	Co-Ni	<30.5Ni	$(111)_P$	$(111)_P \parallel (00.1)_M$, $[1\bar{1}0]_P \parallel [11.0]_M$	Surface tilt of product implies three $\langle a/6\rangle[11\bar{2}]$ partials responsible per sheet. Sheets on $(111)_P$.	...	*52, 173, 506, 613*
fcc → bcc } → hcp }	Fe-Mn	18.5–20Mn	hcp$(111)_P$	$(111)_P \parallel (00.1)_M$, $[1\bar{1}0]_P \parallel [11.0]_M$	HCP forms in sheets, bcc in plate- or lath-like form. It appears that bcc is contained within $(111)_P$ sheets.	BCC grows in both fcc and hcp.	*110, 327, 411, 412, 557*
	Fe-Mn-C	10–12Mn, 0.5–1.1C	hcp$(111)_P$ bcc$(259)_P$?	$(111)_P \parallel (00.1)_M$, $[1\bar{1}0]_P \parallel [11.0]_M$	Decreasing carbon promotes hcp. Thin sheets of hcp.	Faults in P.	*327, 386, 449, 557*
	Fe-Ni-Cr	11–19Cr, 7–16Ni	hcp$(111)_P$ bcc$(225)_P$ to $(112)_P$	$(111)_P \parallel (00.1)_M$, $[1\bar{1}0]_P \parallel [11.0]_M$ $(111)_P \parallel (101)_M$, $[1\bar{1}0]_P \parallel [11\bar{1}]_M$	Narrow sheets of product ∥ to $(111)_P$, composed of long, lath-like crystals. Long axis of laths ∥ to $\langle 110\rangle_P \pm 5$ deg., plane of lath ∥ to approximately $(225)_P$. Adjacent laths may be twin-related. No internal twinning. Volume within sheets that has not transformed to bcc is either hcp or extensively faulted fcc. Definite scatter of habit plane. Faults in hcp.	Accommodation faults and dislocations in P. Nucleation of M in hcp sheets. bcc grows through both fcc and hcp. Higher Ni alloys exhibit much less faulting and little, if any, hcp.	*80–83, 127, 128, 144, 185, 273–275, 277, 312, 443, 523, 528*
	Fe-Cr-Ni	16.5Cr, 8.5Ni, 0.7Mo, 0.1C	hcp$(111)_P$ bcc~$(259)_P$?	same as above	same as above	Less faulting in P.	*312*
	Fe-Cr-Ni	2.3Cr, 27–30Ni	...	...	BCC plate-like product is formed. Internal twinning on $\{112\}_M$ and dislocation substructure along $\langle 110\rangle$ $[\bar{1}11]_M$.	...	*144*
	Fe-Cr-Ni	5–10Cr, 16–23Ni	...	...	BCC needles or thin plate-like product, which form almost exclusively on the surface.	...	*144*

	Fe-Mn-Cr-Ni	12Mn, 10Cr, 4Ni	hcp(111)$_P$ bcc(112)$_P$	...	Sheets ∥ to [111]$_P$ containing laths ∥ to $\langle 1\bar{1}0\rangle_P$ of habit plane about (112)$_P$. The hcp contain few faults.	...	*273*
	Fe-Cr-Mn	14Cr, 14Mn, 1C	hcp(111)$_P$	...	...	Preferential nucleation of bcc in hcp sheets.	*459*
fcc → bcc.....	Fe-Ni	29–33Ni	~(3, 10, 15)$_P$ to (1, 3, 4)$_P$ (0.80, 0.57, 0.18)$_P$	$(111)_P:(011)_M$ − 1 deg, $[0\bar{1}1]_P:[1\bar{1}1]_M$ − 6 deg, $[1\bar{0}1]_A:[1\bar{1}1]_M$ − 4 deg $(111)_P:(011)_M$ − 2.4 deg, $[1\bar{2}1]_P:[0\bar{1}1]_M$ − 1 deg, $(111)_P:(011)_M$ − 0.3 deg, $[1\bar{2}1]_P:[0\bar{1}1]_M$ − 2.2 deg, $[01\bar{1}]_P:[11\bar{1}]_M$ − 2.4 deg	Plate-like product. Fragmented internal twinning on (112)$_M$[11$\bar{1}$]$_M$. Twins are usually not uniform throughout plate but are approximately 30 to 70 A thick and spaced approximately 100 to 400 A apart. Extent of twinning increases with Ni content. Evidence indicates $\{112\}_M$ twins slip along $\langle 111\rangle_M$. Dislocations on $\{110\}$ $\langle\bar{1}11\rangle$ in regions where there are no twins. Midrib composed of high density of twins. Midrib coherent across annealing fcc twin boundary. Deformation twins in bcc on (112)$_M$ [11$\bar{1}$]$_M$.	Nucleation of *M* at twin boundaries. Accommodation dislocations. Slip lines in *P* after transformation. Possible slow growth of *M* plates in low C, 29 Ni parent.	*84, 148, 185, 198, 287, 332, 357, 384, 390–393, 395, 402, 415, 421, 472, 489, 538, 552, 570, 609*
	Fe-Ni	30Ni, 0.04C	...	...	Surface martensite, forms as long ∥ needles which lie on (112)$_P$ planes.	...	*282*
	Fe-Ni	6–25Ni	...	...	Plates not well defined. High dislocation density in cell structure in *M*. Adjacent cells almost twin-related.	Slip lines in *P* after transformation	*148, 489*
	Fe-Ni	14–28Ni	...	(111)$_P$∥(011)$_M$, [$\bar{2}$11]$_P$∥[0$\bar{1}$1]$_M$	Thin film transformation. $\{112\}_M$ twins spaced about 60A apart.	...	*375*
	Fe-Ni-Cr	2–12Cr, 16–36Ni	...	...	Plates with midrib. Internal twinning and slip.	No faults in *P*.	*80, 128, 385*
	Fe-Ni	30Ni	...	*a*) (001)$_P$∥(001)$_M$, [100]$_P$∥[110]$_M$ *b*) (110)$_P$∥(112)$_M$, [100]$_P$∥[110]$_M$	...	(*a*) Specimen compressed with [100] as axis. (*b*) Specimen compressed with [110] near axis.	*67*
	Fe	...	...	(111)$_P$∥(101)$_M$, [1$\bar{1}$0]$_P$∥[11$\bar{1}$]$_M$	Needles ∥ to $\langle 110\rangle_P$ or plates ∥ to (111)$_P$	...	*25, 145, 153, 351, 362, 583*

TABLE 2—*Structural data for martensitic transformations—Continued.*

Structural Change on Cooling	Alloy System	Composition Range, weight, per cent	Habit Plane	Orientation Relationship	Internal Structure and Morphology of Product, *M*	Internal Effects in Parent, *P*	References
fcc → bcc *Continued*.....	Fe-Ni	31Ni	...	$(001)_P \parallel (001)_M$, $[010]_P \parallel [\bar{1}10]_M$ $(001)_P \parallel (1\bar{1}0)_M$, $[110]_P \parallel [\bar{1}\bar{1}2]_M$	Thin foil transformation. Twinning in *M*.	...	*394*
fcc → bct.....	Fe-C	≦ 0.3C	...	...	Surface relief indicates narrow striations on $(111)_P$. Needlelike, ∥ to $\langle 111 \rangle_M$ or $\langle 110 \rangle_P$. A few twins. Number of plates increases with carbon. Tendency for needles to arrange themselves in sheets.	...	*198, 276, 277, 351*
	Fe-C	0.3–0.95C	$\sim(225)_P$	...	Lath-like product with long axis ∥ to $\langle 110 \rangle_P$. Laths within $\{111\}_P$ sheets. Some internal twinning.	...	*198, 275–277, 358, 482*
	Fe-C	1–1.4C	$(225)_P$	$(111)_P \parallel (101)_M$, $[1\bar{1}0]_P \parallel [11\bar{1}]_M$	Plate-like product. Twins on $\{112\}_M$. Slip on $\{111\}_M$, sometimes two sets of $\{112\}_M$ twins. Midrib, when present, is not prominent. Habit plane spread.	...	*25, 70, 78, 198, 274–277, 311, 351, 359*
	Fe-C	1.5–1.8C	$(124)_P$	...	Plates with midribs, internally twinned. Habit plane spread which may depend on transformation temperature.	...	*196, 198, 276, 325, 359*
	Fe-C	0.7–1C	...	$(110)_P \parallel (101)_M$, $[1\bar{1}0]_P \parallel [11\bar{1}]_M$	Thin foil transformation.	...	*421, 482*
	Fe-N C	1.5N	...	$(110)_P \parallel (112)_M$, $[\bar{1}10]_P \parallel [111]_M$	Fine twins on $\{112\}_M$. Transformation in thin foils.	...	*420–422*
	Fe-Cr-C	28.3Cr, 1.5C	$\sim(124)_P$ (0.26, 0.38, 0.89) (0.30, 0.41, 0.86)	$(111)_P : (011)_M$ — 3 deg $[01\bar{1}]_P : [11\bar{1}]_M$ — 2.8 deg $[\bar{1}10]_P : [\bar{1}\bar{1}1]_M$ — 6.1 deg	Plates with dislocation substructure. May be more lath-like at higher transformation temperatures. Deformation twins in *M*.	Slip lines in *P*.	*198, 256, 281, 399, 402, 406*

				$(111)_P : (011)_M$ — 1 deg $[0\bar{1}1]_P : [1\bar{1}1]_M$ — 7 deg $[101]_P : [1\bar{1}1]_M$ — 3 deg			
	Fe-Cr-C	7.9Cr, 1.1C	$(449)_P$	$(111)_P : (011)_M$ — 5 deg $[01\bar{1}]_P \parallel [11\bar{1}]_M$	Long, narrow plates with small spikes.	...	*544*
	Fe-Ni-C	20–24Ni, 0.6–1C	$\sim(225)_P$ at −95 C $\sim(259)_P$ at −196 C	$(111)_P \parallel (101)_M$, $[1\bar{1}0]_P \parallel [11\bar{1}]_M$ ——— $(111)_P : (011)_M$ — 1 deg $[1\bar{1}0]_P : [11\bar{1}]_M$ — 2.5 deg $[11\bar{2}]_P : [10\bar{1}]_M$ — 2 deg	Long, narrow plates with many ∥ striations. Twins in M on $\{112\}_M$, about 100 to 1000 A apart. Twins in some cases are continuous, in others are fragmented.	...	*193, 199, 274, 275, 277, 415, 552, 606*
	Fe-Ni-C	11Ni, 1.2C	$\sim(259)_P$	...	...	Slip lines in P.	*148, 198*
fcc → fct.....	Mn-Cu	≦30Cu	$(110)_P$	$(111)_P \parallel (111)_M$, $[01\bar{1}]_P \parallel [01\bar{1}]_M$	Banded structure of continuous twins on $\{110\}_M$. Bands may grow by introducing temperature gradient.	...	*37, 569*
	In-Tl	18–23Tl	$(110)_P$	$(111)_P \parallel (111)_M$, $[01\bar{1}]_P \parallel [01\bar{1}]_M$	Twinned product. Single or double interface between P and M, movable by temperature gradient or applied stress. Lamellar structure ∥ to $\{110\}_P$ containing striations also ∥ to other $\{110\}_P$.	...	*39, 72, 90, 215, 369*
bcc → hcp fcc.....	Li	...	$(441)_P$	$(110)_P \parallel (00.1)_M$, $[\bar{1}11]_P \parallel [[[11.0]_M$	FCC product is faulted and is induced by cold work. HCP appears needle-like.	...	*32, 69, 179*
bcc → hcp fcc or ortho-rhombic...	Cu-Zn	40–46.....	fcc-(2, 11, 12)$_P$ or orthorhombic	$(101)_P : (111)_M$ — 4 deg $(011)_P : (111)_M$ — 10 deg $(110)_P : (010)_M$ — 7 deg	Zig-zag array of plates. FCC phase has $(011)_P$ midrib.	...	*172, 195, 238, 241, 258, 300, 345, 426*
		45–52	hcp?		Faulting in hcp plane. Twins or faults in M about 25 A apart.		
bcc → hcp.....	Na	...	...	...	Diagonal sub-bands observed on plates. Product is faulted.	...	*30, 32, 243*
	Zr	...	$\sim(334)_P$ or $(569)_P$ (0.46, 0.50, 0.73)	$(011)_P \parallel (00.1)_M$, $[1\bar{1}1]_P : [1\bar{2}.0]_M$ — 1 deg	Fine ∥ striations in M, Lamellar M appearance.	...	*89, 174, 180*

TABLE 2—*Structural data for martensitic transformations—Concluded.*

Structural Change on Cooling	Alloy System	Composition Range, weight, per cent	Habit Plane	Orientation Relationship	Internal Structure and Morphology of Product, *M*	Internal Effects in Parent, *P*	References
bcc → hcp *Continued*	Ti	. . .	(8, 9, 12) $_P$	(110) $_P$: (00.1) $_M$ − 0.5 deg, [111] $_P$ ‖ [11.0] $_M$	Surface striations in *M*.	Accommodation slip.	*246, 320, 352, 383, 560, 634*
	Ti-Mo	10–15Mo	(334) $_P$ and (344) $_P$	(011) $_P$ ‖ (00.1) $_M$, [111] $_P$ ∼ ‖ [11.0] $_M$ ——— ($1\bar{1}$0) $_P$: (00.1) $_M$ − 14 deg, [110] $_P$: [10.0] $_M$ − 1 deg	Habit plane of α phase. Feather-like product appearance, narrow plates. Sub-boundaries in *M* on (01.2) $_M$. Only (344) $_P$ habit plane was found after cooling to −186 C.	Accommodation slip.	*174, 321, 551, 566, 634*
	Ti-alloys (ω phase)	7–10Cr; 10Mo; 4–5Fe; 6–9Ni; 50Zr; 16V	(111) $_P$	(110) $_P$ ‖ (11.0) $_M$, [111] $_P$ ‖ [00.1] $_M$	Product forms usually as a result of plastic deformation. Plate-like form.	. . .	*21, 22, 476, 566*
	Ti-Fe	. . .	∼(334) $_P$	. . .	Long, narrow plates.	. . .	*219, 321*
	Ti-Al-Ni	14.4Al; 4.75Ni	. . .	. . .	Single interface.	. . .	*8*
	Ti-Cr	6Cr	(334) $_P$	(111) $_P$ ‖ (00.1) $_M$, (110) $_P$ ‖ (11.0) $_M$	Long, narrow plates. Thicker plates formed after deformation.	. . .	*22, 321*
	Ti-Mn	4–5Mn	(334) $_P$ and (344) $_P$	(110) $_P$ ‖ (00.1) $_M$, [$\bar{1}$11] $_P$: [11.0] $_M$ < 0.5 deg ($1\bar{1}$0) $_P$: (00.1) $_M$ − 14 deg, [110] $_P$: [10.0] $_M$ − 1 deg	No midrib. Plates composed of thin, ‖ striations. Long, narrow plates.	. . .	*320*
bcc → hcp or orthorhombic	Cu-Al-Ni	12.8Al, 7.7Ni	β'-(155) $_P$	. . .	Striations on plates. Product β' plates are very fine.	. . .	*240, 452*
		15.6Al, 9.9Ni	γ' between (133) $_P$ and (144) $_P$	. . .	. . .	. . .	*240, 452*
	Cu-Al	9–10.1Al	∼(331) $_P$	. . .	β' monoclinic, faults about 100 A apart. Acicular plates may be twin-related. Midrib corresponds to plane normal {501} $_P$, twin plane down middle. No optically observed striations.	. . .	*191, 259, 274, 299, 302, 377, 378, 388, 389, 501, 502, 559, 615, 631, 640*

		10.8–13.7Al	~(331)$_P$	(110)$_P$~‖(00.1)$_M$, [1$\bar{1}$1]$_P$‖[11.0]$_M$	β_1' same as β' except contains superlattice. Parent phase ordering inherited. May be converted to γ' by deformation.	...	*191, 259, 274, 299, 302, 377, 378, 388, 389, 501, 502, 559, 615, 631, 640*
		12.9–14.7Al	~(221)$_P$	(110)$_P$‖(00.1)$_M$, [1$\bar{1}$1]$_P$‖[01.0]$_M$	γ' basically hcp; considering superlattice orthorhombic. {121}$_M$ orthorhombic, or {1$\bar{1}$.1}$_M$ hcp twins. Higher order twinning also observed. Plates contain striations. Domain structure observed.	...	*191, 259, 274, 299, 302, 377, 378, 388, 389, 501, 502, 559, 615, 631, 640*
	Cu-Al-Ni	13–14.5Al, 3.8 Al	(221)$_P$ to (331)$_P$	(101)$_P$‖(001)$_M$, [010]$_P$‖[010]$_M$	May be single interface (γ'), thermoelastic growth. May appear as plates. Large plates are γ'. Fine plates are β'. Striations in γ'.	Considerable plastic deformation	*8, 100, 137, 240, 323*
	Cu-Sn	26Sn	(133)$_P$	...	Long, thin plates.	...	*195*
	Au-Cd	47–49Cd	(133)$_P$	(100)$_P$‖(100)$_M$, [$\bar{1}\bar{1}$1]$_P$‖[1$\bar{1}$0]$_M$	Single interface.	...	*99*
	Au-Zn-Cu	31Zn, 21Cu	(133)$_P$ to (011)$_P$	[10$\bar{1}$]$_P$‖[100]$_M$, [010]$_P$‖[010]$_M$, [101]$_P$‖[001]$_M$	Single interface.	...	*138*
tetragonal → orthorhombic....	U	...	(123)$_P$	(0$\bar{1}$1)$_P$‖(001)$_M$, [Ref *229*, Fig. 12]	Slow, isothermal plate growth.	...	*229*
	U-Cr	1.4Cr	(123)$_P$, (144)$_P$	(817)$_P$‖(001)$_M$, (12, 3, 4)$_P$ ~‖(010)$_M$	Plate-like product.	...	*91*
bcc → fct.....	Fe_3Al	...	(0.0$\bar{6}$, 0.88, 0.48)$_P$	(110)$_P$‖(112)$_M$, [$\bar{1}$1$\bar{1}$]$_P$‖[$\bar{1}$10]$_M$	Superlattice preserved.	...	*338*
cubic → tetragonal.....	Au-Mn	70–80Au	(110)$_P$	...	Lamellar appearance with internal striations (twins). Twins are 60 deg from (110)$_P$ habit planes.	...	*483*

TABLE 3—*Estimated or experimentally determined energies of martensitic transformations.*

Type of Energy	Alloy System	Value	Units	Temperature, deg K	Method or Assumptions	References
Interfacial, σ	Fe alloys	2.4×10^{-5}	cal/cm²	...	estimation of a maximum value	*118*
		4.8×10^{-6}	cal/cm²		from Frank's dislocation model [*168*]	*115, 283, 618*
		5.8×10^{-7}	cal/cm²		coherent interface	*163, 301*
		7.9×10^{-6}	cal/cm²		core energy of screw dislocations	*624*
Strain parameter, A	Fe alloys	440	cal/cm³	...	uniform elastic strain	*618*
		500 or $\mu/38$	cal/cm³		elasticity theory after Kröner [*625*] (μ = shear modulus)	*270, 283*
A'		$1.24\ \mu/38$			where μ = shear modulus, from Eshelby [*621*] and Christian [*103*] treatment elasticity theory	*267*
A		1 200	cal/cm³		uniform elastic strain	*163*
Activation energy of stabilization	Fe-Ni-C	11 000	cal/mole	...		*419*
	Fe-30Ni-C	15 500 ± 3 000	cal/mole		assume straight line fit of $1/T$ versus stabilization rate constant	*567*
	Fe-1.1C-5Ni	28 000	cal/mole		0% prior martensite	*250*
	Fe-1.1C-5Ni	23 000	cal/mole		~60% prior martensite	*250*
	Fe-1.1C-5Ni	30 000	cal/mole		0% prior martensite	*370*
	Fe-1C-1.5Cr	22 000	cal/mole		~95% prior martensite	*231*
Activation energy of growth, Δf_g	Fe alloys	2 000	cal/mole	...	calculated, assuming coherent growth	*163*
	Fe-6Mn-0.6C	1 600	cal/mole		experimental	*306*
	Fe-23Ni-3.4Mn	600	cal/mole		temperature <223 K	*308*
	Fe-23Ni-3.4Mn	940	cal/mole		temperature <223 K	*63*
Activation energy of isothermal nucleation	Fe-23Ni-3.6Mn	6 150	cal/mole	80	assumed $\Delta f_g = 0$	*94, 470*
		9 150	cal/mole	130	assumed $\Delta f_g = 0$	*94, 470*
		13 800	cal/mole	180	assumed $\Delta f_g = 0$	*94, 470*
	Fe-23Ni-3.4Mn	0, 700, 1 400	cal/mole	223, 243, 273	Δf_g = 600 cal/mole	*308*
	Fe-23Ni-3.4Mn	2 400, 4 700	cal/mole	120, 223	Δf_g = 940 cal/mole	*63*

Activation energy of initial isothermal nucleation.....	Fe-23Ni-3.6Mn	6 150	cal/mole	80	assumed classical rate equation	*94, 470*
		9 150	cal/mole	130	assumed classical rate equation	*94, 470*
		13 800	cal/mole	180	assumed classical rate equation	*94, 470*
Free energy change, $\Delta G^{P\rightarrow M}$, due to applied stress.....	...	−1.42	cal/mole	...	1000 psi-uniaxial tension-theoretical	*414*
		−0.96	cal/mole		1000 psi-uniaxial compression-theoretical	*414*
		+0.47	cal/mole		1000 psi-hydrostatic pressure-theoretical	*414*
Chemical energy, $\Delta F^{P\rightarrow M} = \Delta f^{P\rightarrow M}$/particle volume.....	Fe-31.3Ni-5.7Co	−95	cal/mole	258	from heat of transformation experimental data	*183*
	Fe-30Ni	−175	cal/mole	243	from heat of transformation experimental data	*183*
	Fe-25.1Ni-0.26C	−665	cal/mole	217	from heat of transformation experimental data	*183*
	Fe-11.7Ni-15.1Cr	−1 700	cal/mole	215	from heat of transformation experimental data	*183*
Chemical difference, F^{m}-$F^{ferrite}$..	Fe	300 ± 70	cal/mole	300	from electromotive force cell of martensite and ferrite	*477*

composition. The following discussion in this section relates the effects of each of these parameters on martensite transformations.

In an Fe-29Ni-0.5C alloy, the transformation proceeds at speeds about one third the limit of elastic wave propagation in solids [*88*], even at very low temperatures. It is thought that most martensitic transformations in other ferrous alloys and in most nonferrous alloys proceed equally as fast. In these alloys, audible clicks are usually heard as the transformation proceeds. There is abundant evidence in some nonferrous systems, however,

TABLE 4—*The suggested minor, second shears in the fcc → bcc (bct) transformation.*

Transformation Mechanism	Author(s)	References
$(1\bar{2}1)_M$, $[111]_M$, and 8.9% in $[1\bar{2}1]_M$	Kelly and Nutting	*277*
Homogeneous deformations consisting of principal strains (0.082, 0.082, −0.177) along $[100]_M$, $[010]_M$, and c axis $[001]_M$	Lagneborg	*312*
$(112)_M$, $[11\bar{1}]_M$, plus small dimensional adjustments	Jaswon	*253*
6.4% $[21\bar{1}]_M$, −2.3% $[1\bar{1}1]_M$, −2.3% $[011]_M$	Venables	*523*
$(112)_M$, $[11\bar{1}]_M$	Bowles	*70*
Heterogeneous shear generated by screw dislocations of $b = (a/2)[01\bar{1}]_P$ on $(011)_P$	Frank	*168*
$\frac{1}{8}a\langle 110\rangle_M$ preceded by $(a/18)[12\bar{1}]_P$ of $(111)_P$ planes	Bogers and Burgess	*627*

TABLE 5—*Reference guide for martensitic transformation—review papers.*

Subject	References
Thermodynamic	*270, 303, 533*
Crystallographic	*58, 59, 71, 221, 336, 542*
Electron microscopy	*80*
Entire subject	*28, 29, 57, 114, 387, 440, 514, 619, 626, 652, 654*
Ferrous alloys	*177, 210, 220, 305, 416, 435–437, 600*
Strength of martensite	*116, 117*
Kinetics	*270, 298, 301–305, 533, 598, 638*
Other	*36, 104, 285, 337, 398, 468, 605*

that the rate of transformation is much slower. In these systems (Au-Mn, Au-Cd, In-Tl, Mn-Cu, Cu-Al-Ni) the transformation rate is proportional to the rate of cooling; the single interface connecting the transformed and untransformed regions advances or retracts as the temperature is lowered or raised.

The product retains the chemical composition of the parent phase, at least initially. Stabilization and isothermal transformation observations suggest, however, that the interstitial concentrations are not preserved and that interstitial diffusion does occur between product and parent.

The transformation in many systems never proceeds to completion, and

in other systems a transformation range of over 200 K is needed for complete conversion of the parent to martensite. The amount of transformation product is primarily dependent on the temperature, and not upon the time held at a given temperature. At a particular temperature, martensite may form in the morphology of plates, laths, or needle-shaped crystals. Normally, transformation proceeds via the process of nucleation and rapid growth to a final size. Subsequent transformation proceeds also by nucleation followed by growth and does not proceed by continued growth of previously formed crystals. Exceptions to this are found in the Au-Mn, Au-Cd, In-Th, Mn-Cu, and Cu-Al-Ni alloys mentioned earlier. In these alloys, the position of a given transformation interface can be controlled by an elastic stress or temperature gradient. Another exception occurs in the U-Cr system, where martensite plates grow while the temperature is held constant.

Nucleation usually controls martensitic reactions. The possible sites at which the transformation is initiated have been the subject of considerable speculation. Many have reported that, in ferrous alloys, the product prefers to form at annealing twins, stacking faults, or at the hexagonal close-packed phase found in low stacking-fault energy materials. Further, small amounts of prior strain may enhance the transformation. The transformation in fine powder specimens of Fe-Ni alloys was entirely suppressed on cooling [*24,95,206,261*]. Presumably this was caused by a lack of nucleation sites. These results imply that the nucleation event is heterogeneous.

Temperature Dependence

The temperature at which martensite begins to spontaneously form on cooling (athermal transformation) in a time-independent manner is called the M_s temperature. This temperature is well defined for a given chemical composition, provided that isothermal transformation is not present. In all systems, the amount of transformed product is dependent on the temperature. In some alloys, however, martensite can form isothermally above the M_s temperature [*229,296,306,308,470*]. Factors which influence the M_s temperature for a given alloy are listed below. (References can be found in Table 1 under M_s Data.)

1. Thin foils and films exhibit M_s temperatures which are higher than those of bulk materials.

2. Transformation at free surfaces occurs at temperatures higher than the bulk M_s temperature.

3. Austenitizing time-temperature treatments influence the M_s temperature.

4. The M_s temperature is usually independent of the cooling rate, except in some cases such as low-carbon steels [*571*], pure iron [*50*], and titanium [*48*], where rapid rates suppress this temperature. Conversely, very slow cooling may suppress the M_s temperature if stabilization occurs.

5. Decreasing grain or particle size lowers the M_s temperature.

6. Prior plastic deformation above the M_s temperature can either suppress or raise the M_s temperature.

7. The application of hydrostatic pressure depresses the M_s temperature.

8. Neutron irradiation usually lowers the M_s temperature [*427,486,576*].

9. In ferrous alloys, the application of a magnetic field raises the M_s temperature [*167,454*].

The same factors that influence the M_s temperature also influence in a similar manner the amount of transformation which occurs below the M_s temperature.

A martensitic transformation is reversible, with a temperature hysteresis which depends on the alloy system. The exception to this is the Fe-C system, where diffusion-controlled nucleation and growth of carbon precipitates occur below A_s, the temperature at which the original parent phase begins to form on heating. In single interface transformations such as Au-Cd, Ag-Cd, and In-Tl, the temperature hysteresis is slight (2 to 50 C); however, in ferrous alloys the hysteresis is as much as 600 C.

Time Dependence

Two time-dependent transformation phenomena are: (1) stabilization, and (2) isothermal transformation.

1. *Stabilization*—When an alloy is held at a given temperature either slightly above or below the M_s temperature, the subsequent amount of transformation may be retarded. This phenomenon of product retardation is termed "thermal stabilization." Since it has been found to occur above the M_s temperature, accommodation stress relaxation at potential nucleation sites cannot be the general mechanism involved in thermal stabilization. Woodilla et al [*567*] and Bogaceva and Sadovskij [*648*] have demonstrated the absence of stabilization in ferrous alloys substantially free of interstitial solutes. Izumiyama [*250*] indicated that the activation energy associated with the stabilization process is apparently a function of amount of prior martensite. The activation energy in Fe-C alloys with no prior transformation is close to the activation energy for diffusion of carbon in austenite (about 30,000 cal/mole), while the energy for nearly 100 per cent prior martensite approximately equals the activation energy for diffusion of carbon in martensite (about 21,000 cal/mole). Table 3 lists some experimentally determined activation energies. Therefore, it seems reasonable to account for thermal stabilization in terms of interstitial diffusion. Mechanical stabilization, or product retardation by strengthening the parent matrix, is discussed in the next section, on *Stress Dependence*.

2. *Isothermal Transformation*—The transformation of martensite at constant temperature (below and sometimes above the M_s temperature) has now been reported for practically all alloy systems (Table 1, Isothermal Holding). Isothermal transformation exhibits typical C-curve behavior

when plotted as temperature versus time for a constant amount transformed. In general, the amount of martensite formed athermally is greater than that formed isothermally. However, the transformation has been reported to proceed entirely in an isothermal manner in Fe-Mn-C [*306*], Fe-Ni-Mn [*94,308,470*], and U-Cr [*229,371*] systems. With the exception of the U-Cr system, the isothermal transformation occurs by the formation of new plates, and not by the growth of existing plates.

Stress Dependence

Applied stress influences diffusionless transformation in three basic ways: (1) If the temperature is below T_0, the chemical equilibrium temperature, the application of stress provides another driving energy to promote the transformation. (2) If the applied stress is above the yield stress of the parent material, the parent phase will strain plastically and work harden. The increased density of defects in the parent material acts to increase the restraining energy on the transformation. (3) In some materials sufficient heterogeneous nucleation sites are not available, and small amounts of plastic deformation evidently provide these sites through the introduction of more imperfections. These three effects are sometimes singularly apparent, but usually all are present. Their contributions result in the following general characteristics. (For a comprehensive list of references see Table 1 under Stress.)

Depending upon the state of elastic stress [*125,164,414*], martensite can form above the M_s temperature. Below this temperature, it can form in larger amounts than when it is in the stress-free state. In some cases, such as beta-brass [*444*] and In-Tl [*90*], stress-induced plates disappear with the removal of the stress. This behavior is not observed in iron alloys. Nucleation of the martensitic transformation under elastic stress has been reported in many ferrous systems. Recent work [*83*] determined the variation of the resolved shear stress for yielding with temperature for Fe-Ni and Fe-Cr-Ni single crystals above the M_s temperature. It was found that the Fe-Cr-Ni alloy exhibited a drastic reduction in the apparent resolved shear stress above the M_s temperature, while the resolved shear stress of the Fe-Ni alloy did not decrease. Presumably the difference in behavior under stress between the two alloys can be explained by more detailed knowledge of their transformation mechanisms.

The application of plastic strain to the parent phase may alter the transformation characteristics in several ways. If the parent phase is strained plastically below T_0 but above M , the transformation is induced. The amount of martensite formed increases with larger strains and with lower deformation temperatures. The highest temperature at which transformation can occur during extensive plastic strain is called the M_d temperature. This temperature has been associated with T_0. Below the M_s temperature, plastic strain produces additional transformation at the straining tempera-

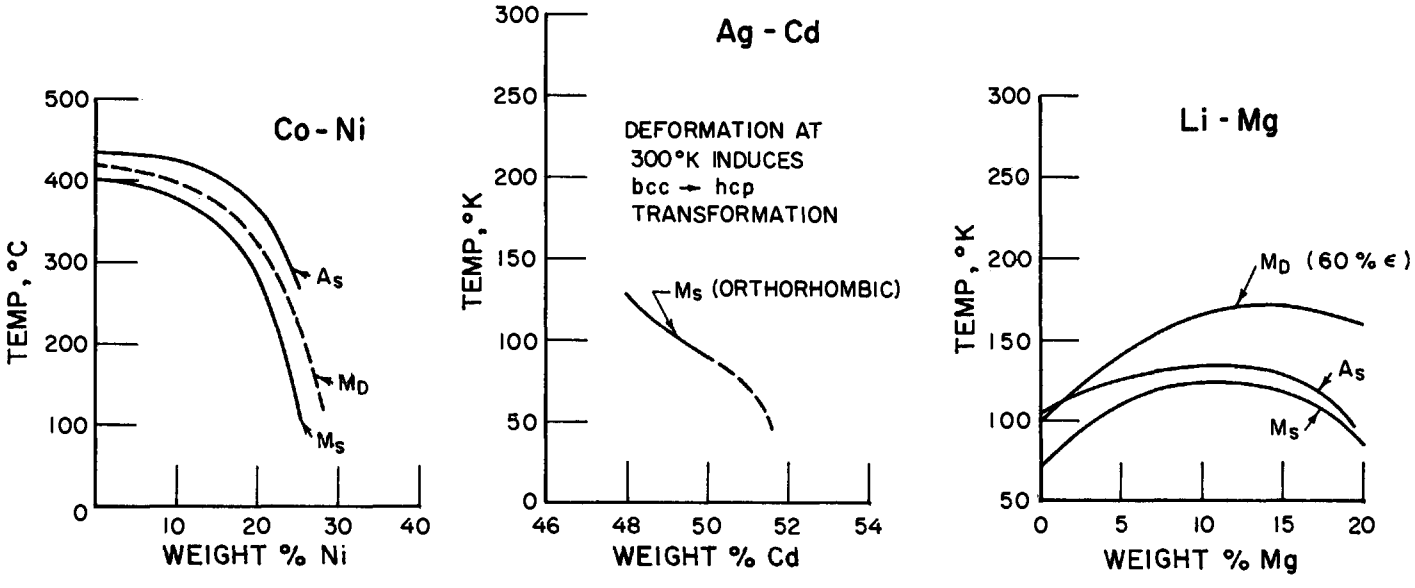

FIG. 1—*The dependence of the martensitic transformation temperatures on chemical composition: for Co-Ni according to Bibring et al [52], Hess and Barrett [225], and also Takeuchi and Honna [506]; for Ag-Cd according to Masson [346]; for Li-Mg according to Barrett and Trautz [34].*

ture. Lowering of the deformation temperature does not necessarily lead to more complete transformation, because suppression at very low temperatures may result [*441*]. Regardless of the temperature of plastic deformation, subsequent spontaneous transformation produced on cooling is usually suppressed. This suppression, associated with hardening of the parent phase, is called mechanical stabilization.

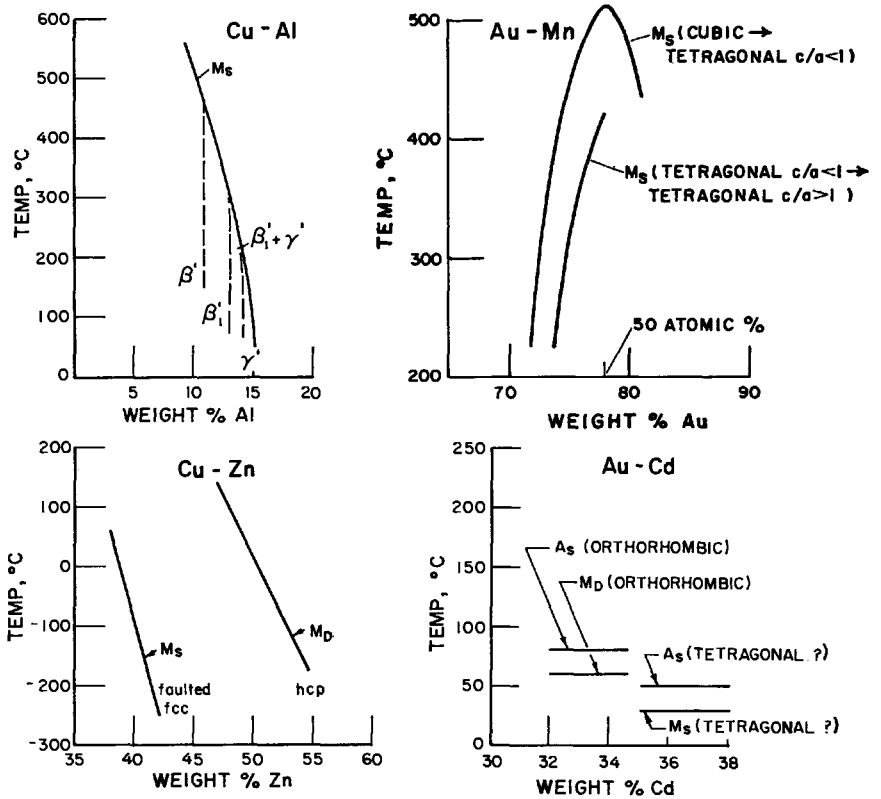

FIG. 2—*The dependence of the martensitic transformation temperatures on chemical composition: for Cu-Al according to Nakanishi [376–379], Swann and Warlimont [502], and Wilkens and Warlimont [559]; for Cu-Zn according to Massalski and Barrett [345] and Pops and Massalski [426]; for Au-Mn according to Smith and Gaunt [483]; for Au-Cd according to Chang and Read [99] and Koster and Schneider [596].*

Small plastic deformations can act to stimulate martensitic transformation in certain alloys, however [*81,157,312,443,636*]. In Fe-Cr-Ni alloys, this stimulation has been correlated with dislocation substructure [*81*]. Planar dislocation arrays and Lomer-Cottrell barriers are more prevalent in lower stacking-fault-energy alloys, and long-range shear stress fields on $(111)_{fcc}$ slip planes exist after deformation. These stress concentrations are throught to aid the nucleation process, since increased transformation of up to 500 per cent occurs on cooling after 2 to 6 per cent strain. No en-

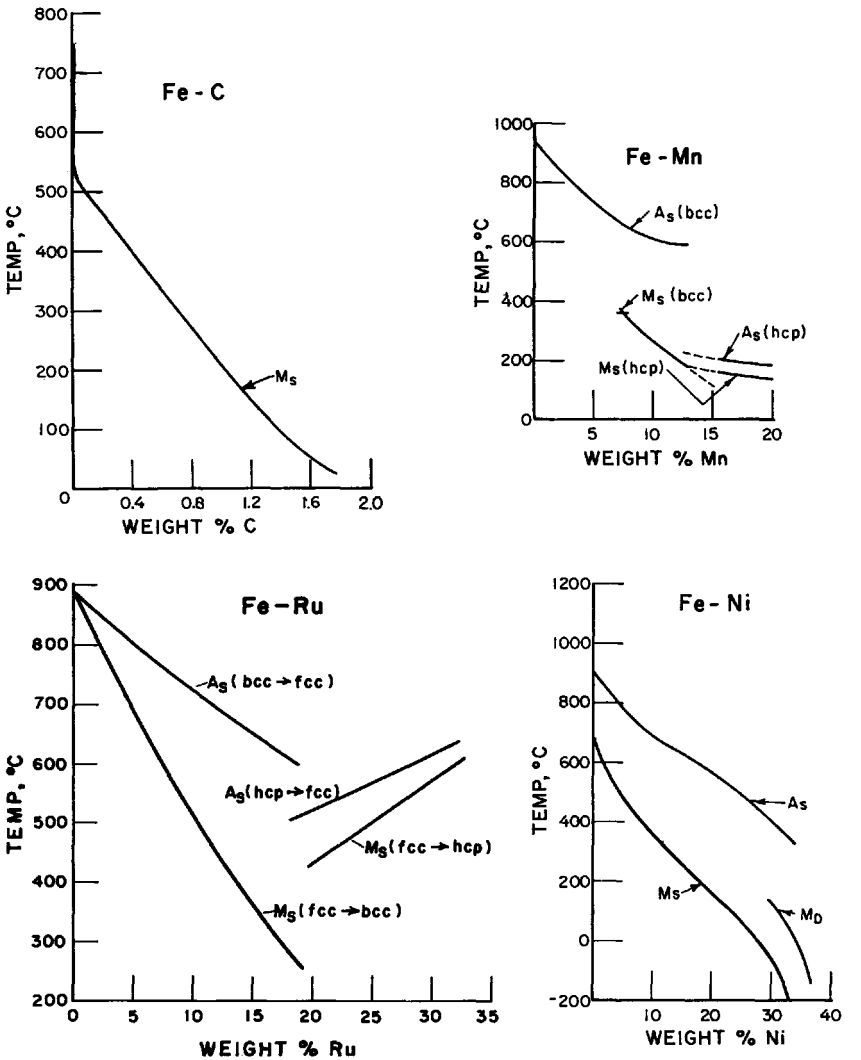

FIG. 3—*The dependence of the martensitic transformation temperatures on chemical composition: for Fe-C according to Bibby and Parr* [50], *Kaufman and Cohen* [270], *and Troiano and Greninger* [514]; *for Fe-Ni according to Kaufman and Cohen* [269] *and Swanson and Parr* [503], *see also Yeo* [571] *and Jones and Pumphrey* [259]; *for Fe-Ru according to Blackburn et al* [628], *Raub and Platte* [644], *Fallot* [645], *and Martelly* [646]; *for Fe-Mn according to Jones and Pumphrey* [259] *and Troiano and McGuire* [515].

hancement of the transformation on subsequent cooling is observed in alloys that form cell structures during deformation. Stimulation of the transformation does not continue indefinitely but is maximum in Fe-Cr-Ni alloys after polycrystalline specimens are elongated approximately 3 to 6 per cent. Depending upon composition and temperature of deformation,

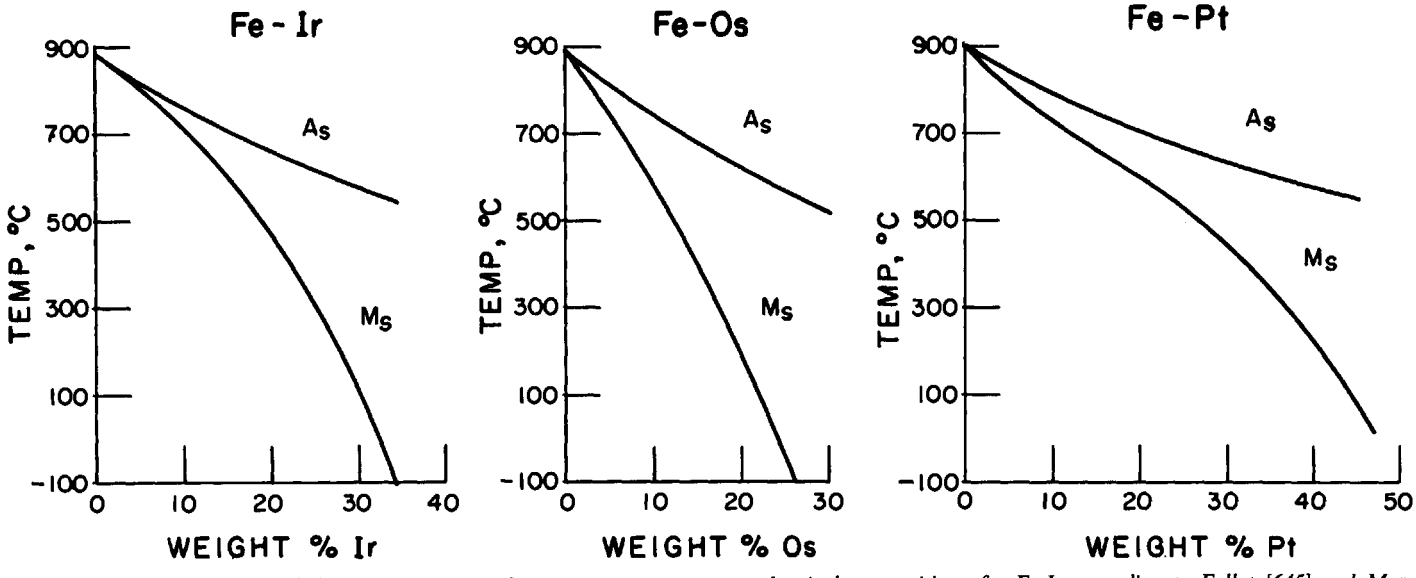

FIG. 4—*The dependence of the martensitic transformation temperature on chemical composition; for Fe-Ir according to Fallot* [645] *and Martelly* [646]; *for Fe-Os according to Fallot* [645] *and Martelly* [646]; *for Fe-Pt according to Fallot* [645] *and Martelly* [646].

suppression of the transformation does not occur until the plastic strain exceeds 8 to 14 per cent.

Prior plastic deformation of the parent phase can influence the crystallography of the transformation on cooling below the M_s temperature. After the release of an applied stress in Fe-31.7Ni single crystals strained 30 per cent at room temperature [*611*], transformation occurred in bursts at slightly higher M_s temperatures (−49 to −32 C). Furthermore, large

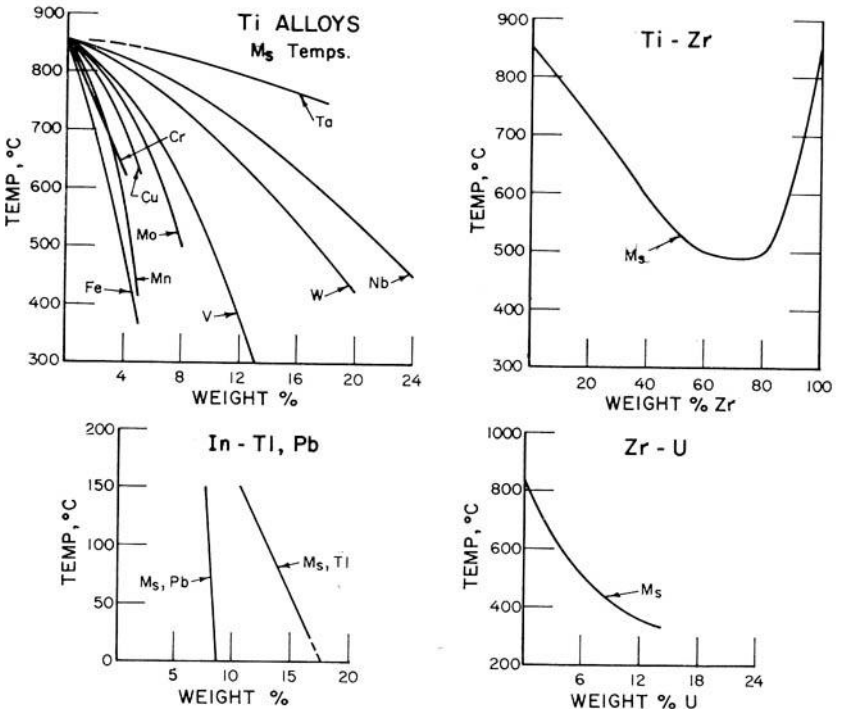

FIG. 5—*The dependence of the martensitic transformation temperature on chemical composition: for Ti alloys according to Duwez [143] and Srivastava [491]; for Ti-Zr according to Duwez [142]; for In-Tl and In-Pb according to Guttman [215] and Moore et al [369]; for Zr-U according to Douglas et al [132].*

volumes in the strained single crystals transformed in cooperative fashion to groups of four habit plane variants most closely aligned with a given $\langle 110 \rangle_{fcc}$ direction (discussed in the following section).

Work in Li-Mg alloys has produced some peculiar results compared with ferrous alloys [*34*]. In these materials, the stress-induced transformation from bcc to hcp and fcc can be initiated at temperatures about 40 C higher than the A_s temperature. Therefore, it would appear that the M_d temperature may be considerably higher than T_0 in some alloy systems.

Recent experiments show that application of hydrostatic pressure as the specimen is cooled suppresses both the M_s temperature and the amount of

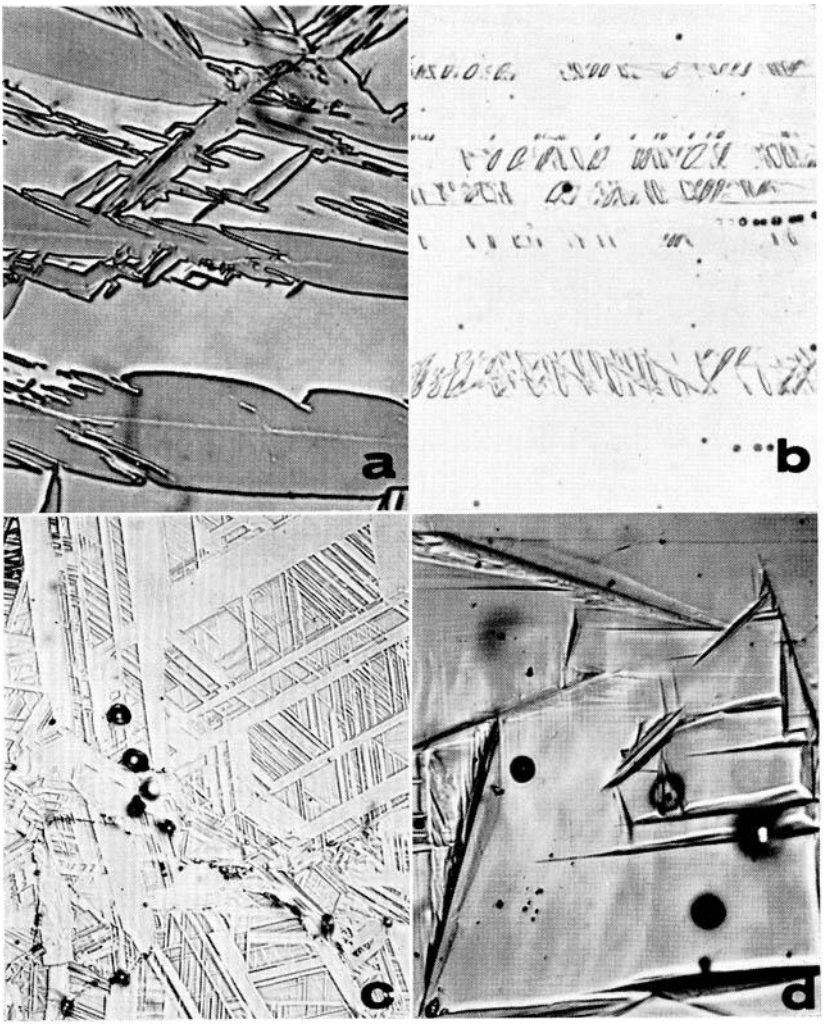

(*a*) Plate martensite. Fe-3Cr-27Ni. Magnification 1000×. (Ref. *144*.)
(*b*) Lath martensite. Fe-18Cr-8Ni. Magnification 1200×.
(*c*) Sheet martensite. Fe-19Ru. Magnification 500×.
(*d*) Surface martensite. Fe-7.5Cr-19Ni. Magnification 500×. (Ref. *144*.)

FIG. 6—*Various types of ferrous alloy martensite morphologies.*

athermal and isothermal transformation [*271,430,434,497,616,628*]. The transformation was entirely suppressed at 76 K in Fe-30Ni alloys (M_s temperature about 127 K), held under 25 and 50 kilobars hydrostatic pressure at high temperatures (550 to 650 C), then cooled under pressure to room temperature. If the initial pressure was applied at temperatures of 500 C or below, however, no suppression occurred. The transformation on cooling between 100 and 0 C was apparently stabilized in an Fe-0.75C

TABLE 6—*Reference guide for martensitic*

Structural Change on Cooling	Alloy System	Electron Microscopy: Transmission, **Replica**	Optical Microscopy	X-ray	Resistivity
fcc → hcp	Co	**51**, *68, 527, 528*	*4, 52–54, 173, 272, 634*	*4, 149, 150, 173, 234, 272, 492, 516*	...
	Co-Ni	**51**	*52, 173, 506, 613*	*225, 613*	...
	Co-Fe	*524*	...	...	...
	Cu-Si	...	*630, 633*	...	*633*
	La	...	...	*584, 642*	...
→ {hcp / bcc}	Fe-Mn	...	*26, 110, 412*	*110, 259, 327, 411, 412, 515*	...
	Fe-Mn-C	*387, 449, 537, 539*	*110, 247, 359, 400, 481, 539, 557, 573–575*	*110, 247, 327, 359, 373, 400, 485, 557, 573, 574*	*247, 354, 470*
	Fe-Mn-Cr	**459**	*110, 236, 459*	*110, 459*	...
	Fe-Mn-Ni	...	*63, 94, 110*	*110*	*470*
	Fe-Mn-Cr-Ni	*273*	*65, 66*	...	...
	Fe-Cr-Ni	*79–81, 127, 128, 273, 274, 275, 277, 312, 372, 373, 522, 523, 529, 531*	*44, 45, 80, 82, 83, 108, 109, 128, 139, 157, 170, 183, 294, 312, 360, 364, 400, 404, 441, 443, 473, 607*	*43, 44, 61, 80, 83, 108, 109, 139, 183, 185, 207, 208, 211, 288, 312, 313, 400, 441, 443, 473*	*157, 296, 366*
	Fe, Ru, Os, Pt, Ir	...	...	...	*628*
fcc → bcc	Fe	*562*	*47, 50, 358, 490, 543, 583, 616*	*583*	...
	Fe-Ni	*80, 118, 144, 171, 238, 274, 275,* **289**, *292, 375, 391–394,* **395**, *415, 421, 447, 472, 489, 537, 538,* **643**	*80, 83, 84, 95, 110, 119, 176, 183, 198, 282, 289, 290, 332, 333, 355, 357, 359, 370, 384, 385, 402, 409, 415, 464, 570, 609, 611, 616*	*24, 67, 80, 83, 84, 95, 110, 119, 146, 183, 185, 198, 249, 259, 261, 287, 292, 294, 295, 357, 375, 384, 385, 402, 609*	*19, 88, 269, 291, 295, 333, 355, 414, 427, 567, 611, 614*
	Fe-Ni-(Ti, Nb, V, Si, Al, Cu, Mo)	*488*, **488**	...	*488*	...
	Fe-Ni-Co	...	...	...	...
	Fe-Si	...	*509*	..	...
	Fe-Cr	...	*616*	...	...
	Fe-Co-W-Cr	...	*505*	...	...
fcc → bct	Fe-C	**1**, *25, 274–277,* **276**, *421, 517, 629*	*1, 26, 50, 70, 78, 194, 196, 197, 222, 224, 235, 237, 248, 319, 322, 325, 351, 356, 359, 363, 370, 434, 482, 511, 600*	*9, 145, 196, 216, 233, 311, 319, 359, 359, 417, 418, 448, 455, 462, 482, 555, 556, 591, 593*	*428*

transformation—experimental papers.

Magnetic	Dilatometry	Other	Lattice Parameters, Ultrasonics	Mechanical Properties	Single Crystals
...	*272, 382, 467*	*49*	**468**, *587, 634*	*105, 587, 634*	*173, 382, 634*
...	*506*	...	...	...	*173*
...	...	...	...	...	...
...	...	...	...	...	...
...	*634, 639*	...	*642*	...	...
...	*259*	...	**411**. *412*, **515**	...	...
182, 306, 307, 310, 573, 576	*247, 461, 574*	*576*	...	*368, 481, 557, 573*	...
463	...	...	...	*463*	...
308, 310, 497	*94*	...	*155*	...	...
...	*65, 66*	...	...	...	...
5, 18, 43, 61, 81, 106–109, 139, 156, 167, 209, 211, 309, 312, 360–362, 373, 429, 441–443, 494, 495, 520	*43, 45, 151, 364, 438*	*183, 209*	**108, 157**, *184*, **185, 400, 443**	*5, 43, 44, 81, 83, 106–108, 211, 288, 360–362, 364, 494, 520, 529, 530, 607*	*43, 45, 151, 364, 438*
645, 646	...	...	...	...	...
...	...	*152, 257, 374, 477, 616*	*521*	*50, 105, 260*	*583*
88, 96, 250, 261, 427, 512	*111, 146, 250, 259, 571, 648*	*88, 176, 183, 261, 271, 594, 616*	*184*, **185**, *375*, **402**. *409. 512*	*19, 83, 119, 290, 295. 464. 489*	*67, 282, 287, 384, 611*
443	*572*	...	...	*488*	...
...	...	*183*	*184*	...	...
...	...	*176*	...	...	...
...	...	*176, 616*	...	...	...
...	...	...	...	*505*	...
250, 454, 593, 649	*250, 276, 511*	*64, 194, 203, 224, 231, 363, 553, 594*	*46*, **116**, *233, 293*, **319**, *374, 439*, **448**, **455**, *493, 534*, **555**	*1, 50, 248, 274, 428, 457, 511, 593*	...

TABLE 6—*Reference guide for martensitic*

Structural Change on Cooling	Alloy System	Electron Microscopy: Transmission, **Replica**	Optical Microscopy	X-ray	Resistivity
fcc → bct *Continued*	Fe-C-N	...	*153*	...	...
	Fe-C-H	...	...	...	...
	Fe-N	*420, 421*	*604*	*604*	...
	Fe-Cr-C-H	*223, 343*	*20, 26, 42, 86, 113, 212–214, 222, 237, 256, 274, 281, 343, 354, 399, 402, 406, 419, 544, 578*	*207, 231, 256, 279, 359, 399, 402, 544*	*419, 578*
	Fe-Cr-Ni-C	...	*404*	...	*354*
	Fe-Cr-Mo-Si-Ni-Mn-C	...	*190, 496*	...	...
	Fe-Ni-C-H	*274, 275, 277, 415, 552*	*86, 148, 149, 183, 187, 190, 193, 197, 218, 331, 400, 404, 410, 431, 446, 451, 456, 577*	*183, 193, 197, 359, 400, 453, 485, 555, 564, 577*	*331, 414, 554, 564*
	Fe-Cu-C	...	*189*	...	...
	Fe-Cr-Ni-Mo-C-H	...	*297*	...	*460*
fcc → {hcp / fcc}	Ce	...	...	*353*	...
fcc → fct	Mn-Cu	...	*37, 569*	*37*	...
	In-Tl-Li	...	...	*369*	...
	In-Tl	...	*39, 72, 90, 215, 369*	*39, 72, 215, 369*	...
fct → fct	In-Pb	...	...	*369*	...
bcc → hcp	Na	...	*30, 243, 244*	*32*	*2, 133, 136, 205, 242*
	Zr	...	*89, 174, 180*	*89, 174*	*585*
	Tl	...	...	...	...
	Hf	...	...	*140*	*585, 602*
	Ti	...	*48, 246, 383, 560, 561, 565, 634*	*352, 383, 560, 634*	...
	Ti-O, N, H	...	*3, 314*	...	...
	Ti-Al	...	*595*	*595*	*595*
	Ti-Cu	...	*186, 491*	...	*186*
	Ti-Co	...	*500*	*500*	...
	Ti-Cr	...	*407*	*21, 22, 407*	...

transformation—experimental papers.—Continued.

Magnetic	Dilatometry	Other	Lattice Parameters, Ultrasonics	Mechanical Properties	Single Crystals
...	...	...	...	*381*	...
...	*181*	...	...	...	...
604	*604*	...	*604*	*604*	...
20, 206, 419, 589	*181, 419, 438, 461*	...	**145, 279, 402, 462, 544**	*20, 214, 343, 578*	...
...	...	...	...	...	...
616, 526, 650	*461, 535, 648*	*616*	...	...	...
16, 17, 250	*181, 250, 278, 331*	*16, 183, 331, 430*	*184,* **555**	*218, 446, 453, 554, 564, 576*	...
...	...	...	...	...	...
...	...	...	...	*474*	...
...	*204, 634*	...	**204.** *353*	...	...
466	...	...	**37,** *466*	*466*	...
...	...	...	**369**	...	...
...	...	...	**72. 215.** *369*	...	*39*
...	...	...	**369**	...	...
...	...	*41, 158, 339, 342*	**32**	*242*	...
...	*166, 525, 585*	*141, 491, 585*	**89.** *166,* **326**	*105*	...
...	...	*141*	...	*105*	...
...	*166*	*140*	*166*	...	...
...	*85, 166*	*85, 141*	*166, 246, 491*	*48, 105, 561, 565*	...
...	...	*314*	...	*314*	...
...	...	...	...	...	...
...	...	*491*	...	...	...
...	...	...	...	*500*	...
...	*21*	*143*	**21**	...	*22*

TABLE 6—*Reference guide for martensitic*

Structural Change on Cooling	Alloy System	Electron Microscopy: Transmission, **Replica**	Optical Microscopy	X-ray	Resistivity
bcc → hcp *Continued*	Ti-Fe	...	*219, 423, 424*	*423*	...
	Ti-Mn	...	*169, 230, 320, 328*	*21, 320*	...
	Ti-Mo	...	*130, 174, 228, 334, 551, 566*	*551, 566*	...
	Ti-Ni	...	*425*	*425*	...
	Ti-Zr	...	*202*	...	*202*
	Ti-Ta, Nb, W, V	...	...	...	...
	Ti-Mo-Cr	...	*228*	...	...
	Ti-V	...	*228*	...	...
	Ti-Al-V	...	*508*	*508*	*508*
	Ti-Al-Mo-V	...	*508*	*508*	*508*
	Ti-Al-Cr	...	...	...	...
	Zr-U	...	*132*	...	...
	Zr-Nd, Y, Dy, Ho, Er	...	...	...	*245*
	Cu-Al-Fe	...	*262*	...	...
	Cu-Al-Ni	...	*8, 100, 137, 240, 452, 651*	*137, 240, 323*	...
bcc → {monoclinic / ortho- / rhombic}	Cu-Al	*274, 388, 389, 501, 502, 559, 615, 630, 631*	*120, 191, 200, 201, 280, 299, 335, 376–378*	*191, 280, 376–379, 559, 610, 640*	*377, 379, 475*
	Ag-Cd	...	...	*346, 347, 349*	...
bcc → {hcp / fcc}	Li	...	*69, 179, 243*	*27, 28, 32, 34*	*134–136, 242*
	Li-Mg	...	...	*33, 34, 348*	*135*
	Cu-Zn	*238, 239, 258*	*172, 195, 241, 258, 345, 426, 444, 586*	*31, 172, 195, 258, 300, 344, 345, 586, 612*	*426, 498, 513*
bcc → ?	Cu-Ga	...	*344*	...	...
	Cu-Zn-Ga	...	*344*	*188, 344*	...
	Cu-Sn	...	*7, 195, 651*	*195*	...
	Au-Zn	...	*660*	*660*	...

transformation—experimental papers.—Continued.

Magnetic	Dilatometry	Other	**Lattice Parameters,** Ultrasonics	Mechanical Properties	Single Crystals
...	...	*143*	...	*423, 424*	...
...	...	*143*	...	*230, 328*	...
...	...	*141, 143*	...	*228*	...
...	...	...	...	...	...
...	*202*	*142*	...	...	...
...	...	*143*	...	...	...
...	...	...	...	*228*	...
...	...	...	...	*228*	...
...	...	*508*	...	*508*	...
...	...	*508*	...	*508*	...
...	...	...	*510*	...	...
...	...	...	...	...	...
...	...	...	...	...	...
...	...	...	...	...	...
...	...	**137**	*432*	*8, 137, 323*	
377	*201, 379*	*376, 475*	...	*120, 475*	...
...	...	...	**349**	...	...
...	*599*	*34, 41, 131, 158*	**27, 28, 32, 34**	*178, 242, 599*	...
...	...	*34, 340*	**34**, *348*	*34*	...
...	...	*426*	**31**. **586**	*498*	*300*
...	...	...	...	...	...
...	...	...	...	...	...
...	...	...	...	...	...
...	...	...	...	...	...

TABLE 6—*Reference guide for martensitic*

Structural Change on Cooling	Alloy System	Electron Microscopy: Transmission, Replica	Optical Microscopy	X-ray	Resistivity
bcc → {ortho-rhombic tetragonal} ...	Au-Cd	...	*98, 99*	*97, 99, 596, 597*	*99*
	Au-Cd-Cu	...	...	...	*380*
bcc → orthorhombic ...	Au-Cu-Zn	...	*138*	*138*	...
hcp → fcc	A-N_2	...	...	*35*	...
bcc → {tetragonal ($c/a < 1$) tetragonal ($c/a > 1$)} ...	Au-Mn	...	*483*	*483*	...
tetragonal → orthorhombic ...	U	...	*371*	...	...
	U-Cr	...	*91, 229*	*91, 229*	...
rhombohedral → bct. .	Hg	...	...	...	...
hexagonal → monoclinic ...	V_2O_5	...	...	*536*	...
Possible Transformations: bcc → bcc ...	Mn_3Si	...	*129*	*129*	...
face centered orthorhombic → monoclinic ...	Pu	...	...	*226, 413, 603*	...
cubic → fct ...	Fe_3Al	*338*	...	...	...
monoclinic → triclinic ...	WO_3	...	*507*	*507*	...
bcc → hcp ...	Ti-V	...	...	*476*	...
(ω phase) ...	Ti-Cr	...	...	*21, 22*	...
	Ti-Mn	...	*320, 328*	*21, 320*	...
	Be-8Ni	...	*410*	*410*	...

alloy under high pressure (42 kilobars) after about 30 per cent completion. Lower-carbon alloys were not stabilized by such a treatment.

Chemical Composition Dependence

The chemical composition influences diffusionless phase transformations through changes in the relative chemical and nonchemical energy differences between the parent and product phase. Figures 1 through 5 give the

transformation—experimental papers.—Concluded

Magnetic	Dilatometry	Other	Lattice Parameters, Ultrasonics	Mechanical Properties	Single Crystals
...	...	...	97, 596	*99*	...
...	...	...	...	...	...
...	...	...	138	...	*138*
...	...	...	...	...	...
483	...	...	...	...	...
...	...	...	...	*105*	...
...	*558*	...	...	...	...
...	...	*465, 504, 641*	465	...	...
...	...	...	*536*	...	...
...	...	...	...	...	...
...	...	...	...	...	...
...	...	...	338	...	...
...	...	...	...	...	...
...	...	...	476	...	...
...	*21*	...	21	...	*22*
...	...	...	...	*328*	...
...	...	...	410	...	...

variation of the M_s, A_s, and M_d temperatures (when available) as a function of the amount of alloying element. The M_s temperature is depressed in all cases by alloying in binary systems. There appears to be a slight discrepancy between the extrapolated M_s temperature values of pure iron and iron alloys. The M_s temperatures for very dilute Fe-C alloys have recently been measured [*150*], and these results imply that the M_s temperature rises very abruptly below about 0.005 per cent C. This abrupt rise

would put the Fe-C extrapolated M_s at about the same temperature as for the other iron alloys.

Structural Aspects of the Martensitic Transformation

The morphology and the crystallographic aspects of martensitic transformations are dependent upon the structures of the parent and product lattices and their composition. These structural aspects of the martensitic transformation will be discussed in this section and are compiled in Table 2.

Martensite Morphology

Most interest has centered upon martensitic transformations which occur in a variety of iron alloys. Four general types of transformation morphology have been observed in steels. These product structures can be described as: plates (Fig. 6*a*), sheets comprised of martensitic crystals in the shape of laths (Fig. 6*b*), sheets (Fig. 6*c*), or surface martensite (Fig. 6*d*). Martensite plates are formed in iron alloys containing approximately 1.1 weight per cent carbon or more, or at least 25 weight per cent nickel [*540*], and in Ni-C, Cr-C, Mn-C, and certain Ni-Cr steels (Table 2). In both types of sheet martensite, the plane of the sheets is parallel with {111} planes of the parent austenite. Sheet martensite which contains many small, slender bcc crystals has been reported in Fe-Cr-Ni, Fe-Ru, Fe-Mn, Fe-Mn-Ni, and Fe-Mn-Cr alloys. The sheets can also contain an hcp structure in regions between the martensite crystals. It has been suggested that the hcp structure found in Fe-Cr-Ni alloys arises from faulting of the austenite during transformation to martensite [*128,144*]. On the other hand, some [*82,108,110,312,313,443*] have suggested that the hcp structure may form prior to any bcc martensite in this system. Both approaches agree that this close-packed structure can act to nucleate transformation.

Martensitic transformations which are confined to surfaces have been reported for Fe-Ni and Fe-Cr-Ni alloys. The appearance of surface martensite in the latter case is illustrated by Fig. 6*d*. In Fe-Ni alloys, individual surface martensite crystals were observed to grow at speeds many orders of magnitude slower than martensite plates forming within bulk specimens [*570*]. The surface martensite crystals extended to depths of 30 to 100μ from the surface.

The formation of martensite plates demands that the macroscopic shape change accompanying transformation closely approximate an invariant plane strain. The interfacial boundary (or habit plane) of the plate is the invariant plane. Since the lattice deformation associated with the change in crystal structure is not usually an invariant plane strain, a second or lattice invariant shear (also called an inhomogeneous shear), such as slip or twinning, is required. Transmission electron microscopy has played a

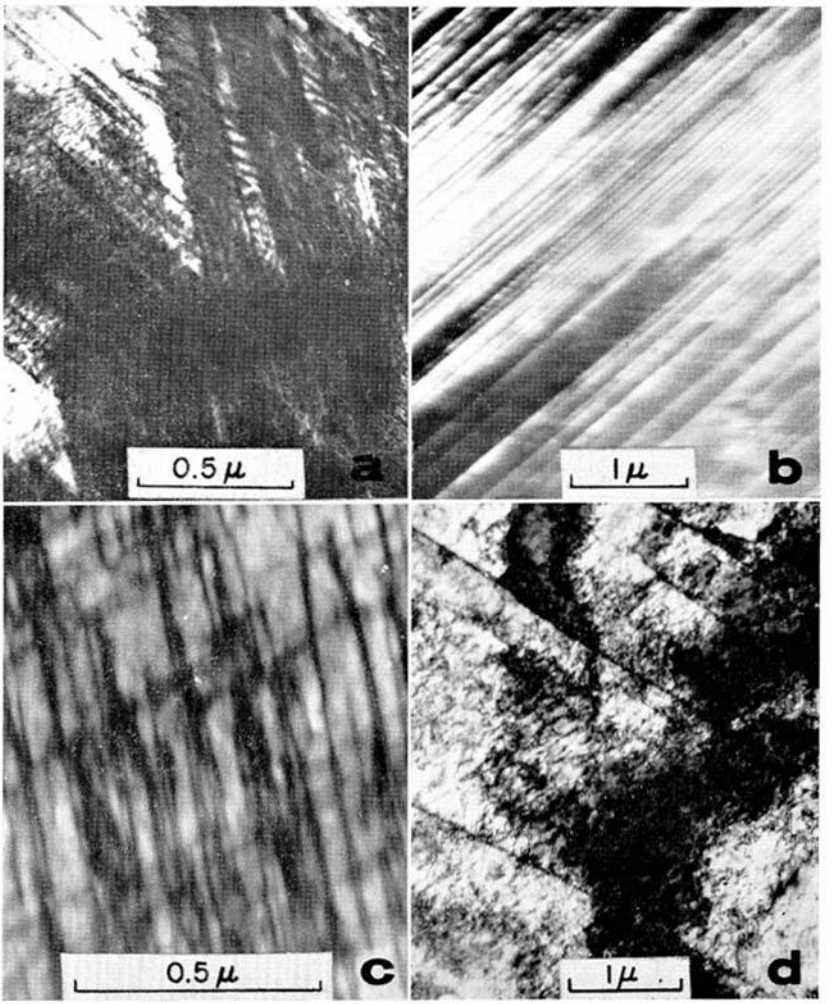

(*a*) Fragmented twins. Electron transmission, Fe-31Ni.
(*b*) Continuous twins. Electron transmission, dark field using (002)*m* twin reflection, {112}*m* twins, Fe-33Ni.
(*c*) Uniform dislocation structure. Electron transmission, Fe-3Cr-27Ni. (Ref. *140.*)
(*d*) Cellular dislocation structure. Electron transmission, Fe-8Cr-16Ni. (Ref. *144.*)

FIG. 7—*Internal structures of ferrous alloy martensite.*

significant role in determining the character of the internal deformation structure of martensite. The studies of alloys and pure metals in which martensitic-transformation products have been examined with this technique are referenced in Table 6.

The internal deformation structure of martensite plates can be comprised of thin twins, approximately 100 A or less in thickness, in beta brass and in certain iron alloys. Twinned structures in Fe-Ni martensite are illustrated

by Figs. 7*a* and 7*b*. In view of the crystallographic theory for the martensitic transformation, it is reasonable to consider that the continuous twinning represents the lattice invariant shear accompanying transformation. However, fragmented twins and variable twin densities and spacings within given martensite plates have been reported in Fe-Ni [*144,472,538*] and in certain Fe-Ni-Cr [*144*] alloys. In numerous cases, twin densities are found to be highest near the central region of the martensite plate. Patterson and Wayman [*415*] have suggested that the uniformity of internal twinning is dependent upon the temperature at which a martensite plate forms in Fe-Ni alloys. Increased carbon content (increased martensite tetragonality) also favors more complete twinning, according to these investigators. More or less regular arrays of dislocations appearing as a cross-hatched pattern (Fig. 7*c*) occur in those portions of martensite plates not containing twins. Analysis [*144,538*] of the dislocation substructure in martensite plates suggests that the active slip systems are of the type $\{110\}\langle 111\rangle$. The dislocation substructures can be associated with either accommodation effects or with the lattice invariant shear. Dislocations producing the lattice invariant shear would comprise the interface, and they can react with dislocations in the surrounding austenite to produce dislocations such as those shown in Fig. 7. The reasons behind the choice of twinning or slip to produce the lattice invariant shear are not established.

Martensite sheets comprised of many crystals or laths have been studied by electron microscopy in Fe-Cr-Ni [*128,144,277,312,523*]. Martensite in Fe-18Cr-9Ni is exhibited in Fig. 6*b*. The plane of the sheets is parallel with a $(111)_{fcc}$ plane; the martensite crystals are lath-like or needle-like in appearance and contain high densities of randomly arranged dislocations. The long axes of the crystals deviate up to 5 deg from $\langle 110\rangle_{fcc}$ directions.

Based upon observations of foils prepared from transformed bulk specimens, Speich and Swann [*489*] have observed another type of martensite morphology in Fe-Ni alloys containing between 6 and 25 weight per cent nickel. Surface relief not unlike plate martensite is observed. Upon etching, blocky transformed regions are observed, which are comprised of large cells, some of which appear to be twin-related. This type of microstructure has also been observed [*144*] in Fe-8Cr-16Ni. The latter is illustrated in Fig. 7*d*. Each martensite unit consists of high dislocation densities which do not possess the regularity found in the martensite plates discussed previously. Under the assumption that the surface relief is associated with this internal morphology and that there is no complication with surface martensitic transformations, this structure is considered to result from another martensitic-type transformation. The results of Swanson and Parr [*503*] on the influence of quenching rates upon the mode of transformation support the presence of martensitic transformations at such low nickel contents.

In addition to twinning and slip, the lattice invariant shear can also ap-

pear as deformation faults. This mode is illustrated by the ordered bcc (β) to distorted hcp (monoclinic β') martensitic transformation in Cu-Al alloys. The martensitic plates were considered to be either randomly [*502*] or nonrandomly [*559,631*] faulted. In particular, Nishiyama and Kajiwara [*631*] suggested that the fcc structure of β_1' martensite is faulted every three layers.

Electron microscopy is not required to determine the nature of the lattice invariant shear in all cases. For instance, twins can be directly observed in the light microscope in martensites found in Au-Cd [*98,99,318*], Au-Mn [*483*], and In-Tl [*39,72,90,215,392*].

Martensite Crystallography

In addition to possessing characteristic morphologies and shape distortion, martensite products have definite lattice orientation relationships and a specific interfacial (or habit) plane with the parent structure. The most significant aspect of these crystallographic features is that they are not represented by rational Miller indices of planes and directions. An example of the irrational nature of the transformation crystallography is illustrated in iron alloys. The earliest works on the fcc to bcc or bct martensitic transformations implied that the only lattice orientation relationships which exist were either the Kurdjumov-Sachs relationship:[4]

$(111)_P$ parallel to $(101)_M$

$[1\bar{1}0]_P$ parallel to $[11\bar{1}]_M$

or the Nishiyama relationship:

$(111)_P$ parallel to $(101)_M$

$[1\bar{2}1]_P$ parallel to $[10\bar{1}]_M$

These relationships were found in certain Fe-C and Fe-Ni steels, where the habit planes were given the rational indices, $\{225\}_P$ and $\{259\}_P$, respectively. Precise measurements have shown that actual orientation relationships lie between these two extremes (which in cubic martensite are related to one another by a rotation of 5.27 deg about the $[101]_M$ direction). Similarly, interface planes for martensite plates are observed to lie in the vicinity of and between $\{225\}_P$ and $\{135\}_P$, which are separated by approximately fourteen degrees. Interface planes are more logically expressed in terms of the direction cosines of their normals rather than by angular deviations from some neighboring plane having rational Miller indices. There appears to be a true scatter in measured interface plane direction cosines, which is beyond the limits of experimental error [*84,406, 443*]. The most pertinent measurements of martensite crystallography are those where the orientation relationship is determined from a martensite plate whose particular interface plane direction cosines are known [*84,193*]. A complication is the irregular appearance of the interface plane when

[4] The symbols *P* and *M* refer to parent and product lattices, respectively.

viewed in the light microscope. A typical example is presented in Fig. 6*a*. In contrast, the interface in Au-Cd is perfectly planar. The reasons for deviation from planar interfaces in iron alloys have not been rationalized. Light microscopy of etched plates reveals that midrib planes are considerably more planar than interfacial planes. Therefore, some have restricted their measurements to the plane of the midrib [*84,198*]. In Fe-Ni alloys, the interface plane is not necessarily continuous where the martensite plate crosses an annealing twin boundary, but the midrib is always continuous across this coherent boundary [*84*]. This may imply that the midrib represents a thin planar region in which transformation begins.

The crystallographic aspects of the transformation to sheets containing lath-like or needle-like martensite are more complicated. The orientation relationship determined for stainless steel [*82*] is close to the Kurdjumov-Sachs relationship. Some have proposed that the individual crystals are in the form of laths (Fig. 6*b*). The habit plane determined for this shape of crystal is close to $\{225\}_P$ (Ref. [*443*]), $\{112\}$ (Ref. [*273*]), or both.

The orientation relationship has been determined for austenitic Fe-Mn and Fe-Mn-C alloys which transform to sheets of hcp martensite. This lattice relationship is given in Table 2. This relationship is also found between equivalent parent and product structures in Fe-Cr-Ni [*82,634*], Co-Ni [*613*], and Co [*4,149*]. The hcp structure in all cases forms parallel to $\{111\}_P$ planes.

Transformation in Thin Foils

Spontaneous transformation during the preparation of thin foils for electron microscopy has been reported in certain iron alloys [*80,171,537*] and in metastable beta-brass [*239*]. The morphological appearance of martensite formed during electrothinning is similar to the transformation structure observed in evaporated films [*375,421,422*]. The spontaneous transformation during thinning is confined mostly to the thinnest regions of the foil and is recognized through an accompanying shape distortion.

With the accuracy possible in electron diffraction, Pitsch [*421,422*] found the same orientation relationship and morphology in three evaporated iron alloy foils containing approximately 1.5 N, 1 C, 30 N. The Pitsch orientation relationship can be written:

$\{110\}_P$ parallel to $\{112\}_M$

$\langle 110\rangle_P$ parallel to $\langle 111\rangle_M$

The orientation relationship in the first two alloys is different from that observed in the Fe-Ni alloy when transformation occurs in bulk specimens. A second orientation relationship, termed the Bain relationship, which is written:

$\{110\}_P$ parallel to $\{100\}_M$

$\langle 100\rangle_P$ parallel to $\langle 100\rangle_M$

was also found in thin foil martensites in iron alloys. While more precise

measurements may demonstrate that they are variants of the same relationship, recent work by Bogers [*627*] indicates that these represent two distinct orientation relationships.

On the other hand, the transformation in certain Fe-Cr-Ni alloys is suppressed during rapid quenching or slow cooling in foils thinner than $4 \pm 1\mu$ [*79,80*]. This stabilization phenomenon, which has been attributed to the destruction or modification of transformation nuclei during thinning, has been observed thus far only in steels that transform to lath-type martensite.

THEORETICAL APPROACHES TO DIFFUSIONLESS TRANSFORMATIONS

Theories pertaining to martensitic transformations relate either to the initiation or to the subsequent growth of the product. Theories employing thermodynamic analyses or dislocation models generally are concerned with nucleation, while crystallographic theories attempt to predict the growth pattern and the final orientations of the product. Thermodynamic and crystallographic theories have been covered rather extensively in past reviews (Table 4). A brief review of these theories is presented, pertinent newer developments are considered, and other theoretical approaches are discussed.

Thermodynamic Theories

All thermodynamic theories attempt to apply classical equilibrium theory to diffusionless, nonequilibrium, solid-state transformations. Therefore, the Boltzmann equation and thermodynamic equilibrium conditions are assumed, enabling one to use the terms and standard expressions for free energy, driving force, etc. While such formulations are not rigorously correct, new experimental results or new theories have not supplanted them.

Classical Nucleation

The hypothesis that martensitic transformations are described by classical nucleation theory analogous to homogeneously nucleated condensed vapor systems has been expressed mainly by Fisher, Hollomon, Turnbull, and Kurdjumov (see Table 5 for references). Reviews of classical nucleation have been presented by Kaufman and Cohen [*270*], Hollomon and Turnbull [*232*], and Walker and Borland [*533*].

According to classical nucleation theory, the total free energy change in the transformation from the parent phase, P, to the martensitic product, M, is given by

$$\Delta F_T^{P\text{-}M} = 2\pi r^2\sigma + \frac{4}{3}\pi r c^2 A + \frac{4}{3}\pi r^2 c\,\Delta f \frac{\text{cal}}{\text{particle}} \quad \ldots\ldots\ldots (1)$$

The interfacial free energy is represented by $2\pi r^2\sigma$, where r is the radius

of a thin oblate spheroid product plate and σ is the specific interfacial free energy. The next term is the expression for the strain free energy, $4/3(\pi r^2 c)$ is the volume of the particle of width c, while $A \approx \mu/38$. (The shear modulus of the parent structure is μ, and Ac/r is the strain energy per unit volume of product phase. The parameters μ and σ are always positive.) The last term, $4/3(\pi r^2 c\ \Delta f)$, is the available chemical energy. The term Δf represents the difference in free energy between martensite and the parent phase, $(f^M - f^P$, per volume of product. It is assumed that the free energy of martensite equals the free energy of equiaxed ferrite when applied to ferrous alloy transformations. Below T_0, Δf is negative.

Critical values of the free energy and embryo sizes obtained by minimizing Eq 1 with respect to r and c are

$$\left.\begin{aligned} \Delta F^* &= \frac{32\pi A^2\sigma^3}{3\Delta f^4}\ \frac{\text{cal}}{\text{particle}} \\ r^* &= \frac{4A\sigma}{\Delta f^2}\ \text{cm} \\ c^* &= \frac{-2\sigma}{\Delta f}\ \text{cm} \end{aligned}\right\} \qquad (2)$$

If the nucleation process is assumed to be random, the rate of nucleation may be expressed as

$$\dot{N} = \frac{N_0}{V}\,\nu' \exp\left(\frac{-\Delta F^*}{kT}\right) \frac{\text{nuclei}}{\text{cm}^3\ \text{sec}} \qquad (3)$$

where N_0/V is the number of atoms per cubic centimeter and ν' is the lattice vibration frequency equivalent to the number of attempts to scale the free energy barrier, ΔF^*, per second per atom. The M_s temperature is identified as the temperature at which $\dot{N} = 1$ nucleus/cm^3 sec. Thus, the M_s temperature is the temperature at which the rate of martensitic transformation becomes relatively appreciable and the nucleation process is essentially an isothermal process. Equation 3 predicts C-curve behavior for the nucleation process.

Several assumptions of classical theory should be emphasized. First, the energy for nucleation is assumed to be supplied from either thermal vibrations or from a temperature change (making Δf more negative). Second, the energy needed for growth of the embryo is assumed to be negligible; that is, the term $\exp(-\Delta f_g/kT)$ in which Δf_g is the activation energy per unit growth step is assumed equal to unity. Third, the positive energy terms in Eq 1 are usually large. Therefore, a large negative free-energy difference is required for nucleation. In interstitial alloys, such as Fe-C, it is assumed that the embryos form in carbon-free regions. If the volume of such a region exceeds V^* with radius, r^*, and thickness, c^*, a nucleus is formed which will evolve rapidly into a plate. Transformation

will cease when nuclei are no longer available. At lower temperatures, the critical nucleus size, V^*, is decreased, thus enabling smaller embryos to become nuclei.

The application of classical nucleation theory to diffusionless transformations has been criticized by Kaufman and Cohen [*270*]. They point out that calculations of the activation energy of nucleation, ΔF^*, for Fe-30Ni, using $\sigma = 200$ ergs/cm^2, $\Delta F = -44$ cal/cm^3 or -315 cal/mole, $A = 2 \times 10^{10}$ ergs/cm^3, and an oblate spheroid product geometry, give values for

TABLE 7—*Reference guide for martensitic transformation—theoretical papers.*

Subject	References
Thermodynamic:	
Classical nucleation	*112, 159–164, 232, 303, 518, 519, 618, 656, 658*
Operational nucleation	*103, 113, 115, 118, 165, 183, 267–271, 329–331, 333, 414, 433, 477–479, 521, 616*
Free energy versus composition or versus temperature calculations	*259, 264–266, 396, 408, 484, 568, 608, 659*
Other	*92, 126, 154, 227, 408, 477–479, 582, 590, 592, 601*
Crystallographic:	
Dislocation models	*38, 55–57, 78, 93, 101, 121, 168, 252–254, 277, 312, 468, 469, 489, 506, 524*
Wechsler-Liebermann-Read theory	*102, 316–318, 401, 403, 405, 540, 541, 544, 545–549*
Bowles-MacKenzie theory	*73–78, 102, 103, 403, 487, 540, 541, 606*
Coherent-lattice-rearrangement theory	*10–15*
Bullough-Bilby-Crocker theory	*60, 87, 122–124*
Lattice-orientation-relationship theories	*23, 39, 70, 72, 89, 97, 193, 199, 225, 255 311, 324, 384, 421, 422, 445, 613*
Geisler theory	*40, 175, 588*
Other	*125, 332, 334, 458, 499, 581, 642, 657*
Quantum mechanical	*131, 133, 136, 397, 617*
Other	*62, 224, 315, 563, 580, 581, 621–623, 625*

ΔF^* of 9×10^{-9} ergs/nucleus or 13×10^7 cal/mole. This value is extremely large, and the probability that thermal fluctuations can provide this amount of energy is very low.

On this basis, heterogeneous nucleation must be assumed. However, it is not consistent to combine heterogeneous nucleation with classical theory. Fe-Ni-Mn isothermal data [*94,470*] indicate a range of activation energies from 6000 to 15,000 cal/mole, while the computed ΔF^* values range from 8×10^7 to 1.4×10^7 cal/mole in the same temperature region [*116*]. If heterogeneous nucleation is assumed, and the proper size embryo parameters are assumed to correlate the data for one temperature, these same

embryos are found to be impotent at all other temperatures. However, isothermal transformation occurs over a considerable temperature region (60 to 200 K) for this alloy. This implies that thermal fluctuations alone cannot account for martensite kinetics, but that the embryo size (energy) must also be a variable. The operational nucleation model initiated by Knapp and Dehlinger [*283*], endorsed and expanded by Kaufman and Cohen [*270*], Christian [*103*], and Kaufman [*267*], and reviewed by Walker and Borland [*533*] is such a model.

Operational Nucleation

In this approach (see Table 7 for references) it is assumed that the free energy of nucleation, ΔF^*, is too large to be reached by thermal fluctuations and that heterogeneous nucleation is necessary. These existing embryos (nucleation sites) are presumed to transform via a dislocation mechanism.

The total energy change of the transformation $\Delta W^{P\to M}$ is defined as the difference between the chemical (driving) and the nonchemical (restraining) energies. For an embryo in the form of an oblate spheroid, this energy is given by

$$\Delta W^{P\to M} = \underbrace{2\pi r^2\sigma + \frac{4}{3}\pi r c^2 A' + \frac{4}{3}\pi r^2 c\Delta g_\Delta}_{\text{restraining } (\Delta g)} + \underbrace{\frac{4}{3}\pi r^2 c\Delta f}_{\text{chemical } (\Delta f)} \frac{\text{ergs}}{\text{embryo}} \quad \ldots(4)$$

The nonchemical terms represent the interfacial energy, σ, the strain energy, and a dilatation correction term, Δg_Δ. Kaufman, using Christian's generalized work, has calculated the strain energy constant A' to be

$$A' = \mu\left[\frac{\pi(2-\nu)}{8(1-\nu)}\epsilon^2 + \frac{\pi\xi^2}{1(1-\nu)} + \frac{\pi(1+\nu)}{3(1-\nu)}\Delta\xi\right]\frac{\text{ergs}}{\text{cm}^3} \quad \ldots\ldots(5)$$

where: ν is Poisson's ratio, ϵ is the homogeneous shear strain, ξ is the strain normal to the habit plane, and Δ is the uniform dilatation. A further discussion of the terms ϵ, ξ, and Δ is given in the Bowles-Mackenzie series of papers [*73–77*].

The positive term Δg_Δ represents the correction for the dilatation, Δ, and is given by the expression

$$\Delta g_\Delta = \frac{2\mu}{9}\frac{(1+\nu)}{(1-\nu)}\Delta^2\frac{\text{ergs}}{\text{cm}^3} \quad \ldots\ldots(6)$$

The requirements for minimizing ΔW with respect to the volume parameters and the dilatation are

$$\frac{\partial\Delta W}{\partial c} = \frac{\partial\Delta W}{\partial r} = \frac{\partial\Delta W}{\partial\Delta} = 0 \quad \ldots\ldots(7)$$

Applying the first two partials, one obtains

$$\frac{\sigma}{A'} = \frac{c^2}{r} \text{ cm} \quad \ldots\ldots\ldots\ldots\ldots\ldots\ldots\ldots (8a)$$

$$\Delta f + \Delta g_\Delta = -2\left(\frac{c}{r}\right) A' \frac{\text{ergs}}{\text{cm}^3} \quad \ldots\ldots\ldots\ldots\ldots\ldots (8b)$$

Equation 8*b* is very similar to the expression obtained by Goldman and Robertson [*183*], $\Delta F = -5/2(c/r)A'$, if Δg_Δ is assumed to be negligible. Both Kaufman and Goldman and Robertson have suggested a small value of Δg_Δ in the neighborhood of 0.1 to 4 cal/mole.

Dividing the volume restraining energy expression (Eq. 4) by the embryo volume and using Eq 8*a* yields

$$\Delta g_{\min} = A'\left(\frac{3}{2} + 1\right)\frac{c}{r} + \Delta g_\Delta \frac{\text{ergs}}{\text{cm}^3} \quad \ldots\ldots\ldots\ldots\ldots\ldots (9)$$

If Δg_Δ is small, this indicates that about 60 per cent of the restraining energy is surface energy, while 40 per cent is elastic strain energy.

If Eq 8*b* is substituted into Eq 9, one obtains

$$\Delta g_{\min} = \frac{-5}{4}\Delta f - \frac{\Delta g_\Delta}{4} \frac{\text{ergs}}{\text{cm}^3} \quad \ldots\ldots\ldots\ldots\ldots\ldots (10)$$

Since Δg_Δ is negligible, $\Delta g_{\min} \approx -5/4(\Delta f)$.

The estimated value of A' is between 1 and 1.28 times $\mu/38$ (Table 3). By measuring the heat of transformation (Table 2) and the shear moduli, μ, of several ferrous alloys, Goldman and Robertson have applied their expression, nearly equivalent to Eq 8*b*, to estimate the c/r ratios. They obtained values of $c/r = 1/75$, $1/50$, and $1/15$ for Fe-31.3Ni-5.7Co, Fe-30Ni, and Fe-25.1Ni-0.26C alloys, respectively.

Activation energies must be estimated before operational nucleation theory can be applied to available kinetic athermal and isothermal data. If Eq 4 is minimized with respect to the product phase radius and thickness, then

$$\left.\begin{aligned} \Delta W^* &= \frac{32\pi(A')^2\sigma^3}{3(\Delta f + \Delta g_\Delta)^4} \frac{\text{ergs}}{\text{embryo}} \\ r^* &= \frac{4A'\sigma}{(\Delta f + \Delta g_\Delta)^2} \text{ cm} \end{aligned}\right\} \quad \ldots\ldots\ldots\ldots (11)$$

It is argued that every embryo must have this energy above the M_s temperature, since the energy is too great (approximately 10^8 cal/mole) to be supplied by thermal activation.

Therefore, the embryo must attain another critical raidus greater than r^* in order to transform spontaneously. Operational nucleation theory supposes that this larger embryo size, but smaller activation energy, is con-

trolled by dislocation motion. The embryos are thought to contain interface dislocations, which provide the crystallographic matching between the parent and product lattices. Frank's analysis [*168*] envisions that the martensite embryo interface for the (225) habit plane consists of long circumferential dislocations spaced every sixth close-packed plane. For an embryo to grow spontaneously, the chemical free energy minus the strain energy (neglecting Δg_Δ) must be sufficiently large to move the interface

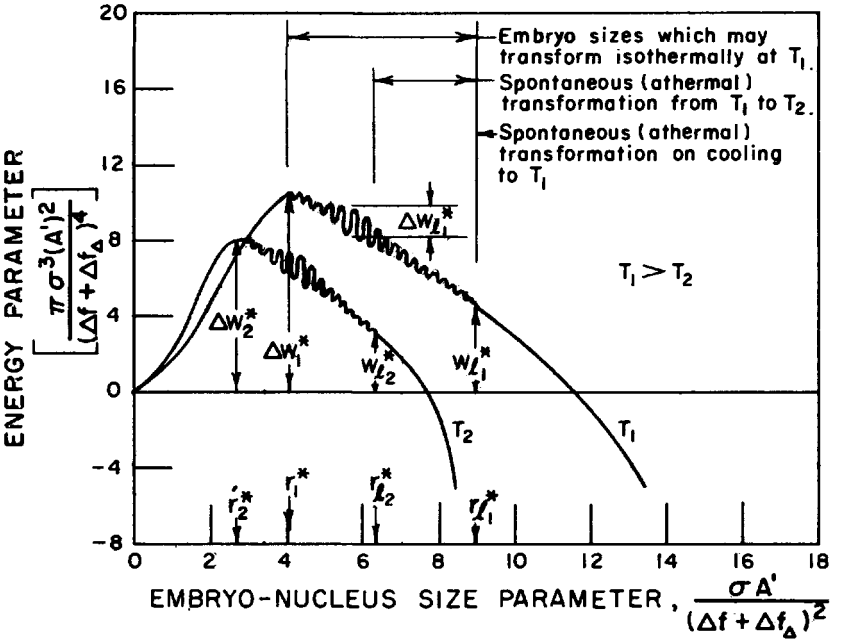

FIG. 8—*Illustration of operational nucleation theory parameters.*

dislocations, overcoming their line tension and shear resistance. The energy of a given dislocation loop equivalent to the equally spaced circumferential loops is given by

$$W_l = 2\pi\left(\frac{\mu b^2}{2}\right) - \pi r^2 b\tau \ \frac{\text{ergs}}{\text{loop}} \qquad \text{.....(12)}$$

where: $\mu b^2/2$ is the dislocation line tension (b is the magnitude of the Burger's vector of this loop), and τ is the shear stress on the loop and equals $\Delta f - cA'/r$ (the chemical driving force minus the strain energy per unit volume). Maximizing Eq 12 with respect to r, one obtains

$$\left.\begin{aligned} W_l^* &= \frac{9\pi\sigma^3(A')^2}{2\Delta f^4}\ \frac{\text{ergs}}{\text{loop}} \\ r_l^* &= \frac{9\sigma A'}{\Delta f^2}\ \text{cm} \end{aligned}\right\} \qquad \text{.....(13)}$$

An embryo that has a radius r_l^* or greater will grow spontaneously at a given temperature. Embryos larger than r^* but less than r_l^* will lower their total energy by growing but are not sufficiently large for their interface dislocations to propagate spontaneously (Fig. 8). As the temperature is lowered, the critical radii will decrease and enable smaller embryos to become active.

Thermal activation is needed at a given temperature for embryos with sizes between r^* and r_l^* to grow. This growth process is considered as the expansion of the interface dislocations in unit growth steps, that is, in units of 1 Burger's vector, as in slip. The energy for this incremental growth step is given by

$$\Delta W_l = \frac{5\pi b^2(\sigma r)^{3/2}}{2d^2(A')^{1/2}}\left[3 + \Delta f\left(\frac{r}{\sigma A}\right)^{1/2}\right]\frac{\text{ergs}}{\text{embryo growth step}} \quad \ldots(14)$$

where d is the average separation between interface dislocations. The maximum value of this energy is

$$\Delta W_l^* = \frac{0.11\pi\sigma^3 A'}{\Delta f^3}\frac{\text{ergs}}{\text{embryo growth step}} \quad \ldots\ldots\ldots(15)$$

when

$$r_+ = \frac{5\pi\sigma A'}{\Delta f^2}\text{ cm} \quad \ldots\ldots\ldots\ldots\ldots\ldots(16)$$

Embryos with sizes greater than r_+ but less than r_l^* will need correspondingly less energy for each unit growth step. Embryos with sizes between r^* and r_+ will need correspondingly more thermal energy for growth each step. Figure 8 shows the relative magnitude and embryo size dependence of the various energies.

To summarize, heterogeneous nucleation is necessary, since the overall energy barrier is much too large to be surmounted by chemical and thermal energy. Therefore, preexisting nucleation sites having a distribution of sizes must be present in the parent material, even above T_0. Athermal nucleation is explained by hypothesizing that the embryos are crystallographically matched with the parent material by a series of predominantly screw dislocation loops which completely surround martensite embryos. For the embryo to grow, the loops must expand, and the embryo critical radius required for spontaneous growth is r_l^*, which is approximately $2r^*$. Embryos with radii larger than r_l^* at a given temperature will grow spontaneously. At a lower temperature r_l^* decreases, therefore more embryos will be available to grow spontaneously, unless previous isothermal transformation has occurred at higher temperatures. Isothermal transformation is explained by considering the growth process for embryos having radii larger than r^* but smaller than r_l^*. The growth process is the unit expansion of the dislocation loops. Since this growth requires thermal

energy, fewer embryos of critical radius r_i^* are produced at low temperatures.

Several suggested alterations to the operational nucleation theory have been made. These are listed below.

1. Singh and Parr [*477*] obtained a value for the free energy difference

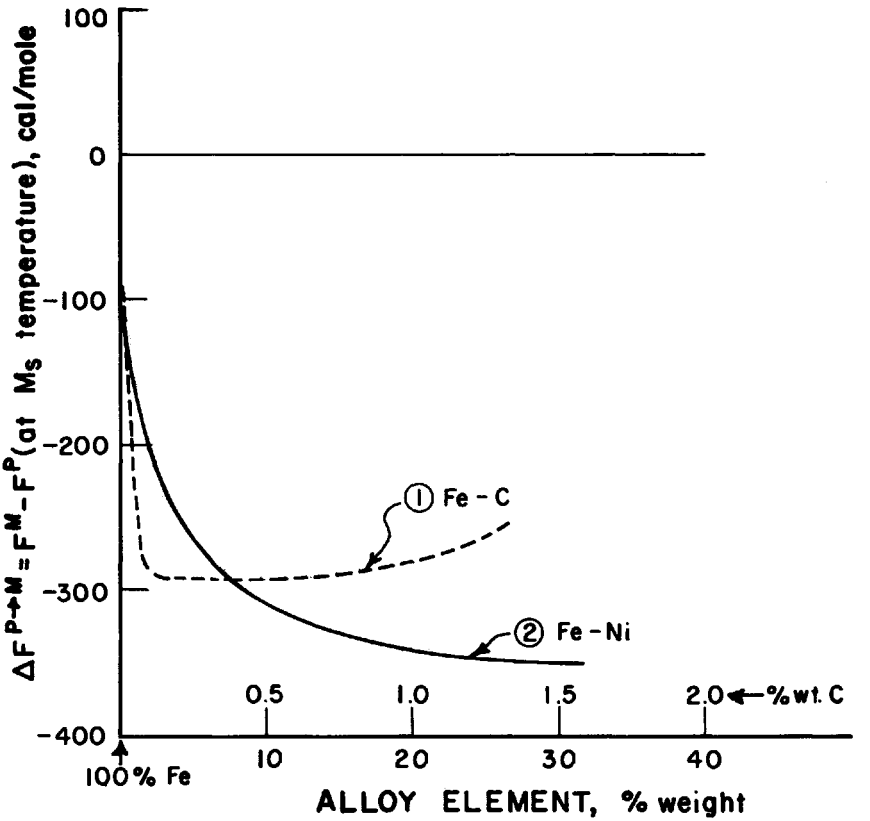

(*Curve 1*) Assumes Kaufman et al calculations [*659*] of ΔF versus T for constant concentrations and assumes Swanson and Parr's M_s values.

(*Curve 2*) Assumes Kaufman and Cohen's calculations [*269*] and Fig. 3 representation of M_s temperatures [*269, 503*].

FIG. 9—*Free-energy change versus composition for Fe-C and Fe-Ni alloys.*

between iron ferrite (α) and iron martensite (M) of 300 ± 70 cal/mole at 300 K. If this value is correct, then the previous calculations which assume that $F^\alpha = F^M$ are in error, though this value is only about one third of the calculated free energy difference [*269*] ($F^P - F^M \approx 1050$ cal/mole) between the austenite P and the martensite M at 300 K.

2. The rapid quenching experiments in iron-nickel alloys by Swanson and Parr [*503*] indicate that the M_s temperature is lower by about 150 C

than that previously found by Kaufman and Cohen [*269*]. In the low-nickel alloys, the M_s values obtained by the latter investigation coincide with the massive transformation results of Gilbert and Owen [*176*]. Using Kaufman and Cohen's [*269*] free energy versus temperature data and Swanson and Parr's M_s data, compatible values of the free energy difference $\Delta F^{P \to M}$ at the M_s temperature are not obtained for iron-nickel alloys (Fig. 9).

3. The same type of adjustment is needed in the Fe-C system. Bibby and Parr [*50*], using very pure iron specimens, have obtained M_s temperatures up to 750 C. Using Kaufman's calculations of $\Delta F^{P \to M}$ versus temperature for pure iron, one obtains values of about 90 cal/mole (Fig. 9). This is considerably less than the constant value assumed for all carbon contents, 290 cal/mole. By varying the cooling rate, Yeo [*571*] has found a critical dependence of the M_s temperature on carbon content in the Fe-Ni system. This dependence on cooling rate is apparent only for low carbon concentrations (<0.15 weight per cent C).

4. As a result of the simplifications employed in estimating the expressions for σ and A', only elastic moduli are used. A great deal of plastic deformation occurs in the course of the transformations, however, particularly in ferrous alloys. It would appear that consideration should be given to the stress required to move appreciable numbers of dislocations through the parent material. This is suggested by the behavior of Fe-18Cr-8Ni alloys [*441*] below the Neel temperature, about 40 K. In this case, the yield strength increases, the shear modulus decreases, while the stress-induced transformation is retarded.

Dislocation Models

Embryos of the product phase have been predicted with diameters up to 1000 A, although Bilby and Christian (57) have estimated their sizes to be as low as several atoms across. The large embryos should easily be seen with transmission electron microscopy. No conclusive evidence has yet been presented to substantiate their presence. Yet, if it is true that the embryo size is as low as 7 to 10 A, then individual dislocations, combinations of several dislocations, or stacking faults may serve as nucleation sites. This seems much more likely, and several models are discussed below.

FCC-HCP—It is generally agreed that the dissociation of an edge dislocation having a Burger's vector of $a/2[\bar{1}10]$ into its partials, $a/6[\bar{2}11]$ and $a/6[\bar{1}2\bar{1}]$, is the probable mechanism of martensite nucleation, since an hcp stacking of atoms exists between the partial dislocations. The energy to separate the partials is supplied by a reduction in the surface tension between the hcp and fcc atom arrangements; this energy is usually assumed to be the chemical free energy difference between the fcc and hcp structures. This difference does not need to be negative to achieve partial separation, however, since a repulsive force exists between the two partials of

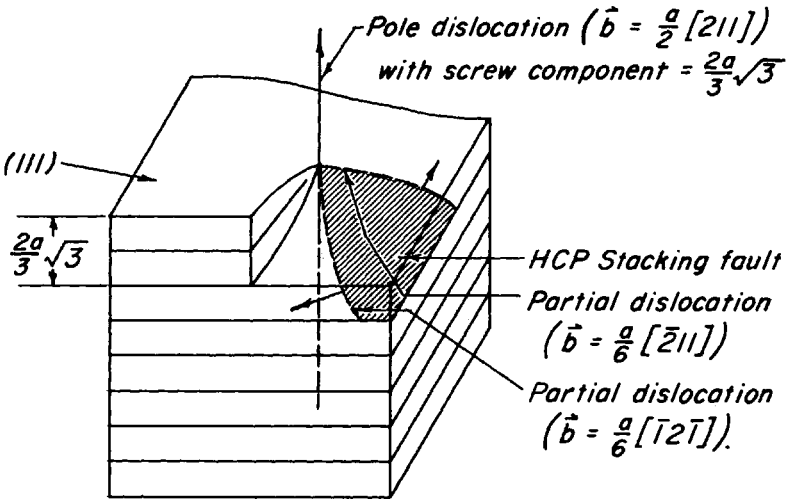

FIG. 10—*Illustration of operation of a pole mechanism for the fcc → hcp transformation.*

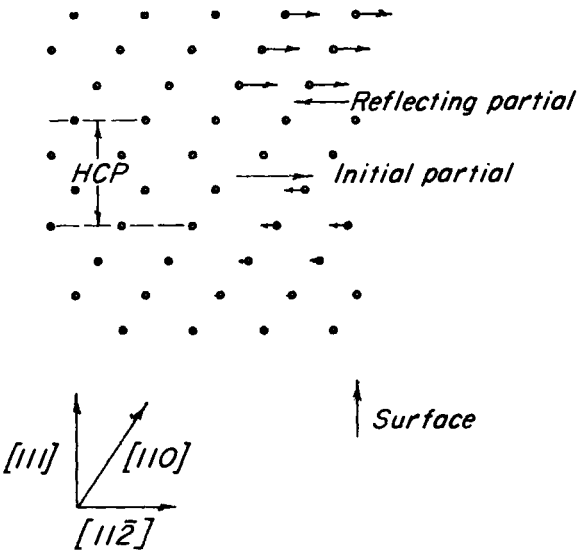

FIG. 11—*Illustration of reflecting partial dislocation mechanism for the fcc → hcp transformation.*

approximate magnitude equal to $\mu a^2/24\pi r$, where μ is the shear modulus, a is the lattice parameter, and r is the distance of separation of the two partials. Presumably, below T_0 the interfacial energy is negative, and the partials can separate until some barrier is met. An additional growth mechanism must operate for a macroscopic hcp plate or sheet to form. Alternate (111) fcc planes must fault to form a thick hcp product. Random nucleation by partial separation would not produce an hcp product.

Three different mechanisms have been proposed: pole mechanism, dynamic dislocation multiplication, and stacking-fault collisions.

1. In the pole mechanism model proposed by Bilby [*56*] and Seeger [*468*], the partials sweep in opposite directions about an anchored pole. One example of a pole is a dislocation lying in the [111] direction with a Burger's vector of $a/2[211]$. This dislocation has the required screw component of $2a/\sqrt{3}$ in the [111] direction and an edge component of $a/\sqrt{6}$ in the $[2\bar{1}\bar{1}]$ direction. As the partials sweep around the pole and meet each other on the other side, their separation in the [111] direction will now be $2/\sqrt{3}\,a$, which is the distance between alternate (111) planes.

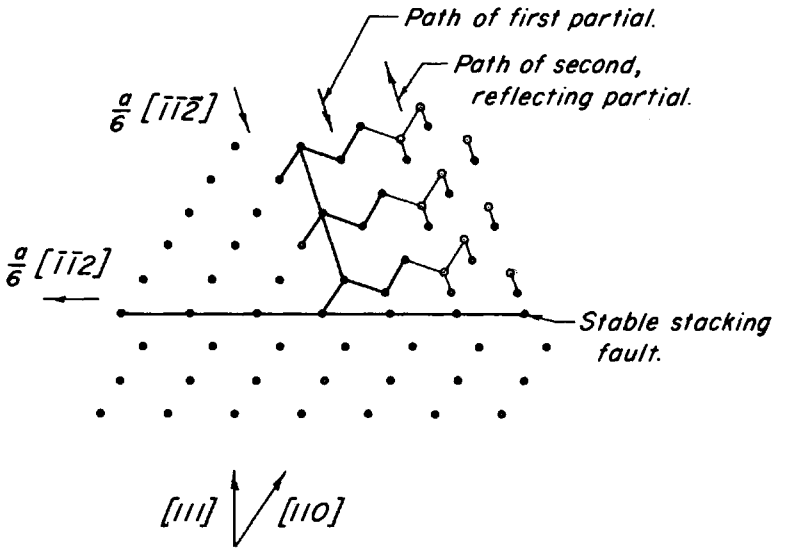

FIG. 12—*Illustration of moving partial-stacking fault collision mechanism for the fcc → hcp transformation.*

One partial dislocation spirals upward, while the other spirals downward. This is illustrated in Fig. 10. Growth proceeds, provided that the partial dislocations can overcome their mutual repulsion after one revolution.

2. Dynamic dislocation multiplication mechanisms forming an hcp structure from a fcc parent by means of dynamic nucleation of new dislocations have been proposed by Christian [*101*] and Bollmann [*68*]. Christian's model employs the hypothesis by Frank [*620*] that high-speed dislocations can be reflected from free surfaces. Bollmann's model visualizes stress-induced reflections of partial dislocations from stacking faults.

Christian proposed that partial dislocations will tend to reflect back into the crystal one or two planes from the original slip plane. When reflection occurs on alternate planes, an hcp product will be formed; if the reflection is only one plane away, an fcc twin is formed. Figure 11 illustrates this

process. The process requires high-speed dislocations which impart momentum to the slip plane atoms in the direction of the moving partial but which also produce overswing in the direction opposite to those atoms in the adjacent planes.

3. Bollmann [*68*] has pointed out that the radius of the extended dislocation needed to produce spontaneous growth and therefore high speed is of the order of several microns, which corresponds to the average grain size. He proposes that, if a moving extended dislocation collides with a stacking fault, a region of high local stress is created around the intersection. This

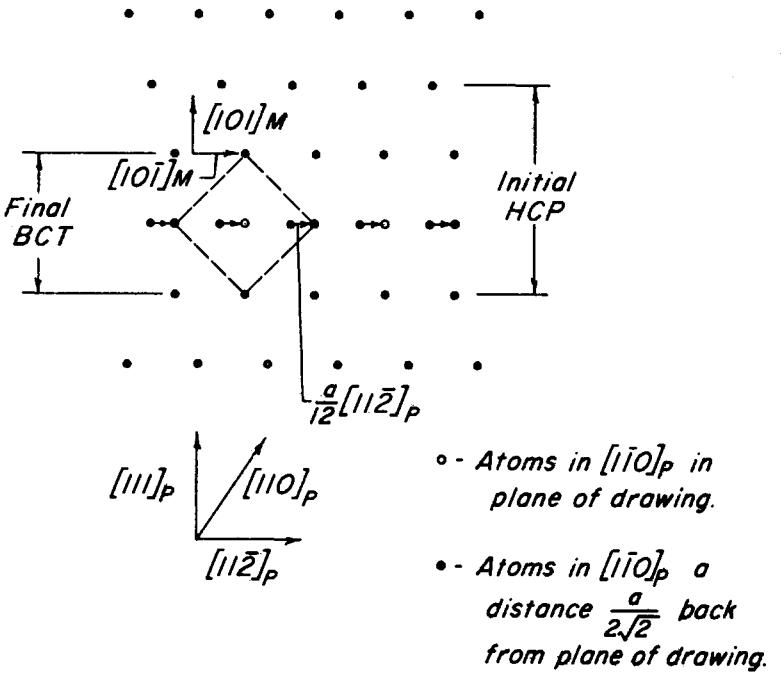

FIG. 13—*Atomic representation of fcc → bcc transformation.*

may be relieved by the production of a new fault lying parallel to the previously mobile extended dislocation. For the reflection process to continue, the newly created partial traveling in the opposite direction must obtain sufficient kinetic energy to collide with another fault, thereby creating another partial which moves back toward the original stable stacking fault. This process is illustrated in Fig. 12. In favor of this mechanism are the electron-microscope pictures of partial hcp transformations by Bollmann [*68*] and Votava [*527*]. Both authors show pictures of frequent narrow sheets of hcp bounded on both sides by stacking faults lying on another (111) set of planes.

FCC-BCC—Many authors have proposed that the fcc to bct or bcc

ferrous alloy transformations nucleate from stacking faults. In particular, Venables [*523*], Breedis [*144*], Reed [*443*], and Lagneborg [*312*] have suggested this as a result of experimental data. First Zener [*581*], followed by Bowles [*70*], Frank [*168*], Jaswon [*253*], and later by Venables [*523*], Kelly and Nutting [*277*], and Lagneborg [*312*] proposed basically the same crystallographic mechanism to produce the bcc (M) phase from fcc (P). Zener originally proposed that a shear along $(111)_P[1\bar{2}1]_P$ within a twin or fault region would produce, with small adjustments, the bcc structure. Jaswon put this shear in dislocation terminology by suggesting that the shear can be obtained by dissociation of a Shockley partial.

$$\frac{a}{6}[1\bar{2}1]_P \rightarrow \frac{a}{12}[1\bar{2}1]_P + \frac{a}{12}[1\bar{2}1]_P \quad \ldots\ldots\ldots\ldots (17)$$

This dissociation would be energetically feasible when the free energy of the bcc (area enclosed within the split partials) is less than the free energy of the fcc phase (below T_0). It is not expected that the partials begin splitting as T_0 is reached, since the parent material must be strained to accommodate the small atomic adjustments necessary to produce a bcc structure after the $[1\bar{2}1]$ shear. There have been many suggestions regarding the minor second shear, and these are listed in Table 3. It is probable that the second shear occurs along $(110)_M$, $(112)_M$, or both, since the intermediate structure is bct. Figure 13 illustrates the general atom movements involved in the transformation. It is interesting to note that, with some adjustment after the first shear in $(111)_P[1\bar{2}1]_P$, the Nishiyama orientation relationship exists, and that after the second shear, the Kurdjumov-Sachs relationship exists.

Frank [*168*] has proposed a dislocation model for growth of the product into the fcc lattice. In this model, the interface is essentially a tilt boundary composed of screw dislocations on every sixth (011) plane, each with a Burger's vector of $a/2[01\bar{1}]$. These misfit dislocations move into the fcc on a $(110)_P$ slip plane, but lie on $\{112\}_M$ bcc planes. Venables [*523*] has suggested a dislocation combination in which $[112]_P$ partials can dissociate to form split partials and $[011]_P$ screw dislocations. The reactions are

$$\frac{a}{6}[11\bar{2}] = \frac{a}{12}[\bar{1}2\bar{1}] + a[10\bar{1}] \quad \ldots\ldots\ldots\ldots\ldots (18)$$

$$\frac{a}{4}[10\bar{1}] + \frac{a}{4}[10\bar{1}] = \frac{a}{2}[10\bar{1}] : \frac{a}{2}[1\bar{1}1] \quad \ldots\ldots\ldots\ldots (19)$$

Bogers and Burgers [*627*] have suggested a different shear mechanism to achieve the bcc structure. If the magnitude of the $(111)_P[1\bar{2}1]_P$ displacement is one third of the twin shear (instead of one half as suggested above), and if the minor second shear is along $\langle 110 \rangle$ in the intermediate lattice, a final bcc structure is formed.

Application of Elastic Constants and Elastic Moduli to Thermodynamic Martensite Theory

The magnitudes of the elastic constants of the structures affect the interfacial and strain energies. Kröner [*625*], Eshelby [*621–623*], and Christian [*103*] have applied elasticity theory and have attempted to predict the associated strain energy as a function of known elastic constants or moduli. Zener [*581*] has related the elastic constants to chemical instability in the fcc-bcc system, and Nutkins [*397*] has derived an expression for the chemical free energy in terms of the elastic constants.

Zener has pointed out the following relationships relating elastic constants to thermodynamics. The elastic shear constant for a (110) $[1\bar{1}0]$ shear equals $2(S_{11} - S_{12})$ with S_{11} and S_{12} being elastic constants. When the elastic shear constant for the (110) $[1\bar{1}0]$ system in bcc materials is low, the thermally induced atomic vibrations in the $[1\bar{1}0]$ direction will be larger. This high amplitude of vibration corresponds thermodynamically to a high entropy. From the relationship $F = E - TS$, where F is the free energy, E is the internal energy, S is the entropy, and T is the temperature, a high entropy implies that the free energy will increase markedly as the temperature is lowered. This unusually high increase of free energy for the bcc phase may mean that the free energy of another phase, having a lower entropy of vibration, will be lower.

Corresponding to this free energy argument is the geometric fact that a shear on (110) bcc planes in the $[1\bar{1}0]$ direction will produce an atomic arrangement that is nearly fcc. If the elastic shear constants are very low for this system, this shear will require little driving energy. Following Zener's work, Barrett [*27,30,32*] and Barrett and Trautz [*34*] found such bcc-fcc transformations in lithium and sodium.

Using a quantum mechanical approach, Nutkins [*397*] calculates the elastic constants for the fcc and bcc for sodium. A relationship is then derived for the free energy of the phases as a function of temperature and the elastic constants. Assumed in this treatment is a free electron model and a given energy gap from the Fermi surface to the Brillouin zone boundary. Nutkins's final expression for the free energy, F, of either the bcc or fcc phase is

$$F = \frac{32k^4V}{h^3} T^4 I \left[\frac{\pi^4}{90} - Z\left(\frac{\theta_d}{T}\right)\right] \quad \ldots\ldots\ldots\ldots\ldots (20)$$

where k is Boltzmann's constant, h is Planck's constant, T is the absolute temperature, and V is the atomic volume. The characteristic temperature, θ_d, is given by $\theta_d = h/k(16/9\ VI)^{-1/3}$, where

$$I = \pi p/28[14S_{44} + 9/2(S_{11} - S_{12}) + 8/3(S_{11} + 2S_{12})],$$

p is the density, and S_{11}, S_{12}, and S_{44} are elastic constants. The function Z is expressed as an incomplete gamma function

$$\left.\begin{aligned} Z &= -\frac{1}{2}\int_y^\infty x^2 \log\,(1 - e^{-x})\,dx \\ y &= \frac{hS_i}{kT}\left(\frac{4\pi V}{3}\right)^{1/3} \end{aligned}\right\} \quad \ldots\ldots\ldots\ldots (21)$$

where $S_i = S_{44}$, $1/2(S_{11} - S_{12})$, and $1/3(S_{11} + 2S_{12})$. The function $Z \rightarrow 0$ as $T \rightarrow 0$. Nutkins applied this expression to sodium after solving also for the ground state energy, and predicted an equilibrium temperature in the range of 50 to 80 K, depending on the Fermi energy–Brillouin zone energy gap.

Although the elastic constant calculations depend on the electronic structure, the free energy expression is derived solely on the basis of the statistical mechanical relationship between the free energy and the lattice vibrations. This is valid if it is assumed that only the lattice vibrations contribute significantly to the temperature-dependent free energy. The free energy expression is solved in terms of the elastic constants. This approach provides fundamental chemical free energy versus temperature relations, provided that the elastic constants of the parent and product material are known.

Crystallographic Theories

Martensitic transformation mechanisms were thought at first to involve a sequence of lattice shears followed by suitable minor adjustments of interatomic distances. Such models were proposed for steels by Kurdjumov and Sachs [*311*], Nishiyama [*384*], and Bain [*23*]. These mechanisms did not produce all of the observed crystallographic features of the transformation, however. The present theoretical understanding of transformation crystallography stems from the critical observations reported in 1949 by Greninger and Troiano [*193*]. They were the first to show that the observed shape change, which corresponds to a shear of approximately 10^{-1}, cannot by itself convert the parent lattice into the martensite lattice in its proper orientation. The requirement of an additional heterogeneous shear on a fine scale to accomplish the total transformation is basic to the most recent formulations of transformation crystallography. Inhomogeneous distortion at the transformation interface to prevent accumulation of misfit strains is also preferred energetically to a homogeneous distortion where misfit strains can be large [*318*].

The phenomenological treatments of transformation to martensite were introduced independently by Wechsler et al. [*547*] and by Bowles and Mackenzie [*73,74*] over ten years ago. Both methods, reviewed recently by Wayman [*542*], are essentially equivalent, and no substantial changes have been made during this period. The transformation can be analyzed using matrix algebra, since the macroscopic change in shape accompanying transformation is equivalent to a homogeneous deformation. This type of defor-

mation can leave a particular plane (the interfacial or habit plane) neither rotated nor distorted. This is the basic assumption in the formulation by Wechsler et al. Using matrix algebra, the parent and product structures can be represented as a total lattice deformation, D, which is comprised of two parts. The first part is a pure strain, P, which is responsible for the change in crystal structure; the second is a rigid body rotation, R, between the product and parent lattices. The total lattice deformation can be written in matrix form as

$$D = RP \quad \ldots\ldots\ldots\ldots\ldots\ldots\ldots\ldots (22)$$

The characteristic feature of the martensitic transformation is the existence of a correspondence of planes and directions between the parent and product structures. Jaswon and Wheeler [*255*] were able to show that the Bain correspondence [*23*] best represents the pure strain component, P, for the fcc to bct or bcc transformation in steels, since it involves the smallest possible atomic displacements. Total lattice deformations are not usually invariant plane strains. An exception is the transformation in cobalt from fcc to hcp which can proceed by faulting on alternate $\{111\}_{fcc}$ planes. Usually, a critical amount of lattice invariant deformation, S, is combined with the total lattice deformation to yield an invariant plane strain which represents the total shape deformation, F.

$$F = RPS \quad \ldots\ldots\ldots\ldots\ldots\ldots\ldots\ldots (23)$$

Theory does not distinguish among lattice invariant deformations which are accomplished by slip, faulting, or twinning. Following convention, the lattice invariant deformation occurs before the structure change in the mathematics. It is actually immaterial whether the pure strain or lattice invariant deformation is mathematically treated first. Both are assumed to occur concomitantly during actual transformation. There are, in general, four solutions of Eq 23 which are not crystallographically equivalent. Each represents an irrational habit plane, an irrational orientation relationship, and a total shape deformation. The preferred solution is that which minimizes either the total shape change, the lattice invariant deformation, or both.

At this point the Wechsler et al approach and the Bowles-Mackenzie approach are identical, and both successfully predict transformation crystallography in In-Tl and Au-Cd alloys and in steels where the habit plane is close to $\{135\}_{fcc}$. The Bowles-Mackenzie approach has greater flexibility, since it can account for other transformation crystallographies with the use of an adjustable scalar quantity, δ. This parameter represents a uniform dilation in the interfacial plane and serves to uniformly adjust the lattice spacings of the parent and product structures in this plane. The dilatation parameter is included in the above formulation by multiplication with the matrix for the pure shear, or as δP. The predicted habit plane

direction cosines now vary along a great circle on a stereographic projection. In steels, the predicted habit plane direction cosines lie approximately between $\{135\}_{fcc}$ ($\delta = 1.000$) and $\{225\}_{fcc}$ ($\delta = 1.018$). Furthermore, the orientation relationship can be predicted from the theory with expressions such as [*84,256*]

$$[hkl]_{bcc} = \frac{[hkl]_{fcc}\,[\delta RP]^{-1}}{|\,[hkl]_{fcc}\,[\delta RP]^{-1}\,|} \qquad (24)$$

for planes. The corresponding expression relating directions is

$$[uvw]^{T}_{bcc} = \frac{[\delta RP]\,[uvw]^{T}_{fcc}}{|\,[\delta RP]\,[uvw]^{T}_{fcc}\,|} \qquad (25)$$

where T denotes the transpose of a matrix.

Use of a dilatation parameter in the crystallographic theory has been justified on thermodynamic requirements [*103,267*]. The total free energy can be minimized by including an additional dilation when transformation occurs under constraints by the parent structure. The dilation within the interface is otherwise independent of the overall volume change of the transformation which can be accommodated by an expansion or contraction normal to the interface. Therefore, the crystallographic features of martensitic transformations can be predicted by specification of the lattice pure strain, the elements of the lattice invariant deformation, and the dilatation parameter. The permutation of the habit plane direction cosines, the specific variant of the orientation relationship, and the specific elements of the lattice invariant deformation are rigidly related to one another. Therefore, the most significant information for use in a theoretical treatment involves the determination of all the crystallographic parameters from a single plate of the product phase [*316*].

Through determination of the habit or midrib plane direction cosines and the orientation relationship of specific martensite plates, the same mode of the lattice invariant deformation is found in steels in which plate martensite forms. This mode of deformation is found theoretically to be $\{112\}_{bcc}\langle 11\bar{1}\rangle_{bcc}$ or $\{101\}_{fcc}\langle 10\bar{1}\rangle_{fcc}$, if related to the parent structure through the lattice correspondence, in Fe-7.90Cr-1.11C (habit plane $\sim$ $\{225\}_{fcc}$) [*544*], Fe-31Ni (habit plane $\sim$ $\{135\}_{fcc}$) [*84*], and in Fe-3.09Cr-1.51C [*256*], where the habit plane lies between these two extremes. Twins have been observed on $\{112\}_{bcc}$ planes in martensite plates in most steels and on the required $\{112\}_{bcc}$ plane (with regard to the particular habit plane and orientation relationship variants) in Fe-3Cr-27Ni [*144*].

Using transmission electron microscopy, Kelly [*273*] was able to determine the habit plane of a martensite lath and the specific orientation relationship variant in stainless steel. For the variant of the Kurdjumov-Sachs relationship given in this section, the habit plane was found to lie close to $(\bar{1}\bar{1}2)_{fcc}$. For this orientation variant, the internally twinned martensite

plates discussed above would have an irrational habit plane close to $\{225\}_{fcc}$, which is nearly 65 deg from $(\bar{1}\bar{1}2)_{fcc}$. The crystallography of lath martensite, which is not internally twinned, can be understood through use of the Bowles-Mackenzie approach if the lattice invariant deformation is $(111)_{fcc}\,[\bar{1}2\bar{1}]_{fcc}$ [*273*]. This particular choice for shear plane and direction is preferred energetically to other possible modes, since it gives the minimum shape strain.

In general, the phenomenological theories predict rather well the observed crystallography of martensitic structures. The scatter observed in habit plane direction cosines over an area in a stereographic projection cannot be rationalized in terms of an isotropic dilation in the interface. Anisotropic dilations have been investigated by Otte [*403*] and by MacKenzie in an unpublished work summarized by Wayman [*542*]. It is not clear at the present time whether the reasons behind such discrepancies with theory arise through more complex forms of the lattice invariant deformation or through a more general interface distortion than an invariplane strain. In particular, Crocker and Bilby [*123*] have suggested that many experimental results could be explained if the lattice invariant deformation occurred on two or more planes in two or more directions. The resultant lattice invariant deformation can then be equivalent to shear on an irrational plane in an irrational direction. Finally, the influence of constraints by the parent lattice (which may not be inconsequential) have not as yet been included in the theory.

The phenomenological theories and the well known rapidity with which martensite plates form suggest that the martensite interface is comprised of a glissile array of dislocations. Bullough and Bilby [*87*] have considered a boundary comprised of parallel glissile dislocations of like but arbitrary Burgers vector which produces the total shape deformation as it moves into the parent lattice. Their treatment, which is equivalent to the Wechsler et al approach and the Bowles-Mackenzie approach, can predict the direction cosines of the interface plane, the orientation relationship between the phases, and the shape deformation. As in the Wechsler et al approach, Bullough and Bilby provide for no distortion within the interface. Frank [*168*] and Suzuki [*499*] have proposed two-dimensional models for a martensite interface which are comprised of specific dislocation arrays. Both models imply slight distortions in the interface which are not uniform in all directions. The nonuniformity in distortion arises from the need to accommodate the difference in lattice parameters of both structures by some distortion in the $[1\bar{1}0]_{fcc}$ direction. The Bullough-Bilby approach, which focuses attention on the structure of the interface, is also closely related to the prism matching method of Bilby and Frank [*60*]. Certainly, future work will attempt to describe in detail the precise nature of the parent-product interface.

Summary

The authors' purpose has been to present a critical survey of the literature pertaining to the martensitic transformation and to build upon the several comprehensive surveys already in print. While the characteristic features of the martensitic transformation are well known and documented, no unified theory for the mechanism involving growth of martensite crystals has yet been formulated.

References

In the course of the preparation of this manuscript, references were gathered and classified. The results of this compilation of literature are Tables 5 to 7 and 663 references. The reference list is, we hope, complete for articles published in English from 1940 to the present. Certain major articles published in other languages and significant articles published prior to 1940 are also included. The tables are an attempt to classify each article in order to simplify surveys of a topic which now contains a vast number of publications. Several factors should be mentioned. Many ferrous alloys, particularly carbon steels, have been grouped together, with only the major alloying elements listed. Therefore, when employing the tables for specific ferrous alloys, one should consider the various listed alloy groups in the broadest sense. Secondly, any attempt to categorize the work of others is in some cases somewhat arbitrary. The authors hope that any who have been offended by such a procedure will have sympathy with the cause for such an undertaking—to enable those doing research in the field to have at their disposal as much of the previously published literature as possible. This, we all know, is desirable.

[*1*] Aborn, R. H., *Trans.*, Am. Soc. Metals *48*, 51 (1956).
[*2*] Adler, J., Woods, S. B., *Can. J. Phys.*, *40*, 550 (1962).
[*3*] Albert, P. A., *Trans.*, AIME *197*, 1449 (1953).
[*4*] Anantharaman, T. R., Christian, J. W., *Phil. Mag.*, *43*, 1338 (1952).
Anderson, P. D., Hultgren, R., *Trans.*, AIME *224*, 842 (1962)—(Ref. [*618*]).
[*5*] Angel, T., *J. Iron Steel Inst.*, *177*, 165 (1954).
[*6*] Ansell, G. S., Arrot, A., *Trans.*, AIME *227*, 1080 (1963).
[*7*] Arbuzova, I. A., Khandros, L. G., *Prob. Phys. Met. Metal Studies*, *14*, 147 (1962).
[*8*] Arbuzova, I. A., Kurdjumov, G. V., Khandros, L. G., *Phys. Metals Metallog.*, *11*, No. 2, 116 (1961).
[*9*] Arbuzov, M. P., Lysak, L. I., Nesterenko, Ye. G., *Dokl. Akad. Nauk SSSR*, *90*, 375 (1953).
Arkharov, V. I., *Dokl. Akad. Nauk SSSR 1744* (1951) (as quoted in Ref. [*589*])—(Ref. [*654*]).
Arkharov, V. I., *Dokl. Akad. Nauk SSSR*, *70*, 8333 (1950)—(Ref. [*657*]).
[*10*] Arkharov, V. I., *Phys. Metals Metallog.*, *12*, No. 6, 65 (1961).
[*11*] Arkharov, V. I., *Phys. Metals Metallog.*, *13*, No. 4, 80 (1962).
[*12*] Arkharov, V. I., *Phys. Metals Metallog.*, *14*, No. 5, 56 (1962).
[*13*] Arkharov, V. I., *Phys. Metals Metallog.*, *15*, No. 6, 111 (1963).
[*14*] Arkharov, V. I., Kovendyaseva, Z. V., *Phys. Metals Metallog.*, *13*, No. 1, 86 (1962).
[*15*] Arkharov, V. I., Sidorenko, I. A., Izvestiya, V. V. Z., *Chernaya Metallurgiya*, 78 (1960).

[16] Arskii, V. N., *Phys. Metals Metallog.*, *6*, No. 3, 108 (1958)
[17] Arskii, V. N., Guliaev, A. P., *Phys. Metals Metallog.*, *6*, No. 5, 90 (1958).
Arskii, V. N., Metallog. *Processing Metals*, *11*, 26 (1956)—(Ref. [638]).
[18] Austin, J. B., Miller, D. S., *Trans.*, Am. Soc. Metals *28*, 743 (1940).
[19] Averbach, B. L., Cohen, M., *ASTIA Rept. No. AD 285459* (1962).
[20] Averbach, B. L., Kulin, S. A., Cohen, M., *Cold Working of Metals* (Am. Soc. Metals, Cleveland, Ohio, 1949), p. 290.
[21] Bagaryatskii, Y. A., Nosova, G. I., *Phys. Metals Metallog.*, *13*, No. 3, 92 (1962).
[22] Bagaryatskii, Y. A., Nosova, G. I., Tagunova, T. V., *Dokl. Akad. Nauk SSSR*, *105*, No. 6, 1225 (1955).
[23] Bain, E. C., *Trans.*, AIME *70*, 25 (1924).
[24] Bando, Y., *Trans.*, Japan Inst. Metals, *5*, 135 (1964).
[25] Baker, A. J., Kelly, P. M., Nutting, J., *Electron Microscopy and Strength o, Crystals*, (Interscience, New York, 1961), p. 899.
[26] Barnett, W. J., Troiano, A. R., *Trans.*, AIME *175*, 910 (1948).
[27] Barrett, C. S., *Phys. Rev.*, *72*, 245 (1947).
[28] Barrett, C. S., *Phase Transformations in Solids*, (J. Wiley & Sons, New York, 1951), p. 343.
[29] Barrett, C. S., *Structure of Metals*, (McGraw-Hill Book Company, Inc., New York, 1952), p. 559.
[30] Barrett, C. S., *J. Inst. Metals*, *84*, 43 (1955–1956).
[31] Barrett, C. S., *Inst. Metals Monograph No. 18*, 331 (1956).
[32] Barrett, C. S., *Acta Cryst.*, *9*, 671 (1956).
[33] Barrett, C. S., Clifton, D. F., *Trans.*, AIME *188*, 1329 (1950).
[34] Barrett, C. S., Trautz, O. R., *Trans.*, AIME *175*, 579 (1948).
[35] Barrett, C. S., Meyer, L., *J. Chem. Phys.*, *42*, 107 (1965).
[36] Barrett, C. S., *Imperfections in Nearly Perfect Crystals* (J. Wiley & Sons, New York, 1952), p. 97.
Barson, F., Legvold, S., Spedding, F. H., *Phys. Rev.*, *105*, 418 (1957)—(Ref. [639]).
[37] Basinski, Z. S., Christian, J. W., *J. Inst. Metals*, *80*, 659 (1951–1952).
[38] Basinski, Z. S., Christian, J. W., *Phil. Mag.*, *44*, 791 (1953).
[39] Basinski, Z. S., Christian, J. W., *Acta Met.*, *2*, 148 (1954).
[40] Basinski, Z. S., Christian, J. W., *Acta Met.*, *1*, 759 (1953).
[41] Basinski, Z. S., Verdini, L., *Phil. Mag.*, *4*, 1311 (1959).
[42] Bassett, J. B., Rowland, E. S., *Trans.*, AIME *185*, 341 (1949).
[43] Bastien, P. G., Dedieu, J. M. B., *J. Iron Steel Inst.*, *183*, 254 (1956).
[44] Bastien, P. G., Margerand, R., *Rev. Met.*, *56*, 463 (1959).
[45] Bastien, P. G., Sulmont, A., *Rev. Met.*, *56*, 40 (1959).
[46] Beaulieu, C. E., Dube, A., Letendre, G., *Trans.*, AIME *218*, 558 (1960).
Bedford, R. G., *J. Appl. Phys.*, *36*, 113 (1965)—(Ref. [602]).
[47] Bharucha, V., Mancini, G. A., Powell, G. W., Spretnak, J. W., *Trans.*, AIME *221*, 498 (1961).
[48] Bibby, M. J., Parr, J. G., *J. Inst. Metals*, *92*, 341 (1963–1964).
[49] Bibby, M. J., Parr, J. G., *Cobalt*, *20*, 111 (1963).
[50] Bibby, M. J., Parr, J. G., *J. Iron Steel Inst.*, *203*, 100 (1964).
[51] Bibring, H., *Acta Met.*, *7*, 684 (1959).
[52] Bibring, H., Lenoir, G., Sebilleau, F., *Rev. Met.*, *56*, 279 (1959).
[53] Bibring, H., Sebilleau, F., *Compt. Rend.*, *239*, 54 (1954).
[54] Bibring, H., Sebilleau, F., Buckle, C., *J. Inst. Metals*, *87*, 71 (1958–1959).
[55] Bilby, B. A., *Brit. J. Appl. Phys.*, *2*, 316 (1951).
[56] Bilby, B. A., *Phil. Mag.*, *44*, 782 (1953).
[57] Bilby, B. A., Christian, J. W., *Inst. Metals Monograph*, No. 18, 121 (1956).
[58] Bilby, B. A., Christian, J. W., *Iron & Steel*, *19*, 648 (1960).
[59] Bilby, B. A., Christian, J. W., *J. Iron Steel Inst.*, *197*, 122 (1961).
[60] Bilby, B. A., Frank, F. C., *Acta Met.*, *10*, 239 (1960).
[61] Binder, W. O., *Metal Progr.*, *58*, 201 (1950).
Blackburn, L. D., Kaufman, L., Cohen, M., *Acta Met.*, *13*, 533 (1965)—(Ref. [628]).

[62] Blanter, M. E., *Metalloved. i Term. Obrabotka Metal.*, No. 4, 2 (1960).
[63] Blanter, M. E., Novichkov, P. V., *Metalloved. i Term. Obrabotka Metal.*, No. 11, 12 (1961).
[64] Blickwede, D. J., *Trans.*, AIME *197*, 922 (1953).
Bogaceva, G. N., Sadovskij, V. D., *Dokl. Acad. Nauk SSSR, 83*, 569 (1952)—(Ref. [*648*]).
[65] Bogachev, I. N., Malinov, L. S., *Phys. Metals Metallog., 14*, No. 6, 27 (1962).
[66] Bogachev, I. N., Malinov, L. S., *Phys. Metals Metallog., 15*, No. 5, 32 (1963).
[67] Bogers, A. J., *Acta Met., 10*, 260 (1962).
Bogers, A. J., Burgers, W. G., *Acta Met., 12*, 255 (1964)—(Ref. [*627*]).
Bokros, J. C., Parker, E. R., *Acta Met., 11*, 1291 (1963)—(Ref. [*611*]).
[68] Bollmann, W., *Acta Met., 9*, 972 (1961).
[69] Bowles, J. S., *Trans.*, AIME *191*, 44 (1951).
[70] Bowles, J. S., *Acta Cryst., 4*, 162 (1951).
[71] Bowles, J. S., Barrett, C. S., *Progr. Metal Phys., 3*, 1 (1952).
[72] Bowles, J. S., Barrett, C. S., Guttman, L., *Trans.*, AIME *188*, 1478 (1950).
[73] Bowles, J. S., Mackenzie, J. K., *Acta Met., 2*, 129 (1954).
[74] Bowles, J. S., Mackenzie, J. K., *Acta Met., 2*, 138 (1954).
[75] Bowles, J. S., Mackenzie, J. K., *Acta Met., 2*, 224 (1954).
[76] Bowles, J. S., Mackenzie, J. K., *Acta Met., 5*, 137 (1957).
[77] Bowles, J. S., Mackenzie, J. K., *Acta Met., 10*, 625 (1962).
Bowles, J. S., Mackenzie, J. K., *Trans.*, AIME *194*, 1201 (1952)—(Ref. [*606*]).
[78] Bowles, J. S., Morton, A. J., *Acta Met., 12*, 629 (1964).
[79] Breedis, J. F., *Proc.*, Intern. Congr. Electron Microscopy, 5th (Academic Press, New York, 1962), *1*, HH5.
[80] Breedis, J. F., *Am. Soc. Metals Seminar on Thin Films* (1963).
[81] Breedis, J. F., *Acta Met., 13*, 239 (1965).
Breedis, J. F., *Trans.*, AIME *230*, 1583 (1964)—(Ref. [*144*]).
[82] Breedis, J. F., Robertson, W. D., *Acta Met. 10*, 1077 (1962).
[83] Breedis, J. F., Robertson, W. D., *Acta Met. 11*, 547 (1963).
[84] Breedis, J. F., Wayman, C. M., *Trans.*, AIME *224*, 1128 (1962).
Bridgman, P. W., *Phys. Rev., 48*, 893 (1935)—(Ref. [*641*]).
[85] Brock, E. G., *Phys. Rev., 100*, 1619 (1955).
[86] Brook, R., Entwisle, A. R., Ibrahim, E. F., *J. Iron Steel Inst., 195*, 292 (1960).
[87] Bullough, R., Bilby, B. A., *Proc.*, Roy. Soc. (London) *69*, 1276 (1956).
Bunshah, R. F., Lahteenkorva, E. E., Mehl, R. F., *ASTIA Rept. No. 32674* (1954)—(Ref. [*609*]).
[88] Bunshah, R. F., Mehl, R. F., *Trans.*, AIME *197*, 1251 (1953); Reply to Disc., *Trans.*, AIME *200*, 681 (1954).
[89] Burgers, W. G., *Physica, 1*, 561 (1934).
Burgers, W. G., Klostermann, J. A., *Acta Met., 13*, 568 (1965)—(Ref. [*647*]).
[90] Burkart, M. W., Read, T. A., *Trans.*, AIME *197*, 1516 (1953).
[91] Butcher, B. R., Rowe, A. H., *Inst. Metals Monograph No. 18*, 229 (1956).
Bystrom, A., Almin, K. E., *Acta Chem. Scand., 1*, 76 (1947)—(Ref. [*597*]).
[92] Cahn, J. W., *Acta Met., 4*, 572 (1956).
[93] Cahn, J. W., *Acta Met., 5*, 169 (1957).
Carpenter, H., Robertson, J. M., *Metals*, (Oxford University Press, 1939), p. 897—(Ref. [*600*]).
[94] Cech, R. E., Hollomon, J. H., *Trans.*, AIME *197*, 685 (1953); Reply to Disc., *Trans.*, AIME *200*, 683 (1954).
[95] Cech, R. E., Turnbull, D., *Trans.*, AIME *206*, 124 (1956).
[96] Cech, R. E., Turnbull, D., *Trans.*, AIME *212*, 395 (1958).
[97] Chang, L. C., *Acta Cryst., 4*, 320 (1951).
[98] Chang, L. C., *J. Appl. Phys., 23*, 725 (1952).
[99] Chang, L. C., Read, T. A., *Trans.*, AIME *191*, 47 (1951).
[100] Chen, C. W., *Trans.*, AIME *209*, 1202 (1957).
[101] Christian, J. W., *Proc.*, Roy. Soc., (London) *A206*, 51 (1951).
[102] Christian, J. W., *J. Inst., Metals, 84*, 386 (1955–56).
[103] Christian, J. W., *Acta Met., 6*, 377 (1958); Also *Acta Met., 7*, 218 (1959).

[*104*] Christian, J. W., *Decomposition of Austenite by Diffusional Processes* (Interscience, New York, 1962), p. 371.
[*105*] Chubb, W., *Trans.*, AIME *203*, 189 (1955).
[*106*] Chukhleb, A. N., Martynov, V. P., *Metalloved. i Term. Obrabotka Metal.*, *9*, 44 (1959).
[*107*] Chukhleb, A. N., Martynov, V. P., *Phys. Metals Metallog.*, *10*, No. 2, 80 (1960).
[*108*] Cina, B., *J. Iron Steel Inst.*, *177*, 406 (1954).
[*109*] Cina, B., *J. Iron Steel Inst.*, *179*, 230 (1955).
[*110*] Cina, B., *Acta Met.*, *6*, 748 (1958).
[*111*] Clark, C. A., *J. Iron Steel Inst.*, *193*, 11 (1959).
Clark, D., Jepson, K. S., Lewis, G. I., *J. Inst. Metals*, *91*, 197 (1962–63)—(Ref. [*595*]).
[*112*] Clemm, P. J., Fisher, J. C., *Acta Met.*, *3*, 70 (1955).
[*113*] Cohen, M., *Trans.*, Am. Soc. Metals *41*, 35 (1949).
[*114*] Cohen, M., *Phase Transformations in Solids* (J. Wiley & Sons, New York, 1951), p. 588.
[*115*] Cohen, M., *Trans.*, AIME *212*, 171 (1958).
[*116*] Cohen, M., *Trans.*, AIME *224*, 638 (1962).
[*117*] Cohen, M., *J. Iron Steel Inst.*, *201*, 833 (1963).
[*118*] Cohen, M., Machlin, E. S., Paranjpe, V. G., *Thermodynamics and Physical Metallurgy*, (Am. Soc. Metals, Cleveland, Ohio, 1949), p. 242.
[*119*] Cohen, M., Taranto, J., *ASTIA Rept. No. AD 418729* (1963).
[*120*] Cope, R. G., *J. Inst. Metals*, *87*, 330 (1958).
[*121*] Cottrell, A. H., Bilby, B. A., *Phil. Mag.*, *42*, 573 (1951).
[*122*] Crocker, A. G., *Acta Met.*, *10*, 113 (1962).
[*123*] Crocker, A. G., Bilby, B. A., *Acta Met.*, *9*, 678 (1961).
[*124*] Crocker, A. G., Bilby, B. A., *Acta Met.*, *9*, 992 (1961).
[*125*] Crussard, C., *Compt. Rend.*, *237*, 1709 (1953).
[*126*] Crussard, C., *Physica*, *15*, 184 (1949).
[*127*] Dash, J., Otte, H. M., *Proc.*, Intern. Congr. Electron Microscopy, 5th (Academic Press, New York, 1962), *1*, HH-4.
[*128*] Dash, J., Otte, H. M., *Acta Met.*, *11*, 1169 (1963).
[*129*] Dauydov, K. N., Sidorenko, F. A., Gel'd, P. V., *Phys. Metals Metallog.*, *12*, No. 3, 108 (1961).
Dehlinger, U., *Theoretical Metallography*, AEC-Tr-4500 (U. S. Atomic Energy Comm., 1958)—(Ref. [*619*]).
[*130*] Delazaro, D. J., Hansen, M., Riley, R. E., Rostoker, W., *Trans.*, AIME *194*, 265 (1952).
[*131*] DeSorbo, W., *Acta Met.*, *1*, 459 (1953).
Doi, M., Nishiyama, Z., *Mem.*, Inst. Sci. Ind. Res., Osaka Univ., *11*, 153 (1954).
Dornen, P., Hofman, W., Arch. *Eisenhuettenw.*, *30*, 627 (1959)—(Ref. [*145*]).
[*132*] Douglass, D. L., Marsh, L. L., Manning, G. K., *Trans.*, Am. Soc. Metals *50*, 305 (1957).
Dreyer, G. A., Polonis, D. H., *Trans.*, AIME *221*, 1074 (1961)—(Ref. [*633*]).
[*133*] Dugdale, J. S., Gugan, D., *Proc.*, Roy. Soc. (London) *254*, 184 (1960).
[*134*] Dugdale, J. S., Gugan, D., Okumura, K., *Proc.*, Roy. Soc. (London) *263*, 407 (1961).
[*135*] Dugdale, J. S., Gugan, D., *Cryogenics*, *2*, 103 (1961).
[*136*] Dugdale, J. S., Gugan, D., *Proc.*, Roy. Soc. (London) *270*, 186 (1962).
[*137*] Duggin, M. J., Rachinger, W. A., *Acta Met.*, *12*, 529 (1964).
[*138*] Duggin, M. J., Rachinger, W. A., *Acta Met.*, *12*, 1015 (1964).
[*139*] Dulis, E. J., Smith, G. V., *Trans.*, Am. Soc. Metals *44*, 621 (1951).
[*140*] Duwez, P., *J. Appl. Phys.*, *22*, 1174 (1951).
[*141*] Duwez, P., *Trans.*, AIME *189*, 765 (1951).
[*142*] Duwez, P., *J. Inst. Metals*, *80*, 525 (1951–52).
[*143*] Duwez, P., *Trans.*, Am. Soc. Metals *45*, 934 (1953).
[*144*] Breedis, J. F., *Trans.*, AIME *230*, 1583 (1964).
[*145*] Dornen, P., Hofmann, W., *Arch. Eisenhuettenw.*, *30*, 627 (1959).
[*146*] Earley, C. C., *Symposium on Internal Stresses* (Inst. Metals, London, 1948), p. 233.

[*147*] Edmondson, B., *Acta Met.*, *5*, 208 (1957).
[*148*] Edmondson, B., Ko, T., *Acta Met.*, *2*, 235 (1954).
[*149*] Edwards, O. S., Lipson, H., *Proc.*, Roy. Soc. (London) *180*, 268 (1942).
[*150*] Edwards, O. S., Lipson, H., *J. Inst. Metals*, *69*, 177 (1943).
[*151*] Eichelman, G. H., Hull, F. C., *Trans.*, Am. Soc. Metals *45*, 77 (1952).
[*152*] Eichen, E., Spretnak, J. W., *Trans.*, Am. Soc. Metals *51*, 454 (1959).
[*153*] Entwisle, A. R., *Inst. Metals Monograph*, No. 18, 315 (1956).
Eshelby, J. D., *Proc.*, Roy. Soc. (London) *A241*, 376 (1957)—(Ref. [*621*]).
Eshelby, J. D., *Proc.*, Roy. Soc. (London) *A242*, 261 (1959)—(Ref. [*622*]).
Eshelby, J. D., *Progress in Solid Mechanics* (North Holland, Amsterdam, 1961), *2*.—(Ref. [*623*]).
[*154*] Estrin, E. I., *Phys. Metals Metallog.*, *15*, No. 4, 139 (1963).
[*155*] Estrin, E. I., Zueva, O. M., Maksimova, O. P., Piguzov, Yu. V., *Phys. Metals Metallog.*, *11*, No. 2, 98 (1961).
Fallot, M., *Ann. Phys.*, *10*, 291 (1938)—(Ref. [*645*]).
[*156*] Fel'dgandler, E. G., Pridantsev, M. V., *Phys. Metals Metallog.*, *11*, No. 4, 68 (1961).
[*157*] Fiedler, H. C., Averbach, B. L., Cohen, M., *Trans.*, Am. Soc. Metals *47*, 267 (1954).
[*158*] Filby, J. D., Martin, D. L., *Proc.*, Roy. Soc. (London) *276*, 187 (1963).
Fine, M. E., Greener, E. H., *Trans.*, AIME *212*, 476 (1958)—(Ref. [*587*]).
[*159*] Fisher, J. C., *Trans.*, AIME *185*, 688 (1949).
Fisher, J. C., *Thermodynamics in Physical Metallurgy* (Am. Soc. Metals, Cleveland, Ohio, 1949), p. 201.—(Ref. [*618*]).
[*160*] Fisher, J. C., *Trans.*, AIME *197*, 918 (1953); Reply to Disc., *Trans.*, AIME *200* 685 (1954).
Fisher, J. C., *Trans.*, Am. Soc. Metals *47*, 451 (1955)—(Ref. [*624*]).
[*161*] Fisher, J. C., *Acta Met.*, *1*, 32 (1953).
[*162*] Fisher, J. C., Hollomon, J. H., Turnbull, D., *Trans.*, AIME *175*, 911 (1948).
[*163*] Fisher, J. C., Hollomon, J. H., Turnbull, D., *Trans.*, AIME *185*, 691 (1949).
[*164*] Fisher, J. C., Turnbull, D., *Acta Met.*, *1*, 309 (1953).
[*165*] Fisher, J. C., Turnbull, D., *Trans.*, AIME *197*, 921 (1953).
[*166*] Fisher, E. S., Renken, C. J., *Phys. Rev.*, *135*, A482 (1964).
[*167*] Fokina, Y. A., Zavadskiy, E. A., *Phys. Metals Metallog.*, *16*, No. 2, 128 (1963).
Forster, F., Scheil, E., *Z. Metall.*, *32*, 165 (1940)—(Ref. [*594*]).
[*168*] Frank, F. C., *Acta Met.*, *1*, 15 (1953).
Frank, F. C., *Rept.*, Bristol Conf. on the Strength of Solids, (Phys. Soc. London, 1948), p. 57.—(Ref. [*620*]).
[*169*] Frost, P. D., Parris, W. M., Hirsch, L. L., Doig, J. R., Schwartz, C. M., *Trans.*, Am. Soc. Metals *46*, 1056 (1954).
[*170*] Gabler, D., Mitsche, R., *Metall-Verlag-GMBH*, *5*, 362 (1958).
[*171*] Gaggero, J., Hull, D., *Acta Met.*, *10*, 995 (1962).
[*172*] Garwood, R. D., Hull, D., *Acta Met.*, *6*, 98 (1958).
[*173*] Gaunt, P., Christian, J. W., *Acta Met.*, *7*, 529 (1959).
[*174*] Gaunt, P., Christian, J. W., *Acta Met.*, *7*, 534 (1959).
Gawranek, V., Kaminsky, E., Kurdjumov, G. V., *Metallwirtscheft*, *15*, 370 (1936)—(Ref. [*610*]).
[*175*] Geisler, A. H., *Acta Met.*, *1*, 260 (1953).
Geisler, A. H., *Acta Met.*, *2*, 639 (1954)—(Ref. [*588*]).
[*176*] Gilbert, A., Owen, W. S., *Acta Met.*, *10*, 45 (1962).
[*177*] Gilewicz, E. P., Fragetta, W. A., Mehra, V., Krohn, R., *ASD-TDR-62-996*, (Wright-Patterson AFB, Ohio, 1964).
[*178*] Gindin, I. A., Lazarev, B. G., Starodubov, Ya. D., *Phys. Metals Metallog.*, *10*, No. 3, 153 (1960).
[*179*] Gindin, I. A., Lazarev, B. G., Starodubov, Ya. D., *Phys. Metals Metallog.*, *11*, No. 1, 49 (1961).
Gindin, I. A., Lazarev, B. G., Starodubov, Ya. D., Khotkevich, V. I., *J. Exptl. Theoret. Phys. (USSR)*, *35*, 802 (1955)—(Ref. [*599*]).
[*180*] Ginneken, A. J. J. van., Burgers, W. G., *Acta Cryst.*, *5*, 548 (1952).
[*181*] Gladman, T., Moore, P., Quarrel, A. G., *J. Iron Steel Inst.*, *200*, 527 (1962).

[182] Glover, S. G., Smith, T. B., *Inst. Metals Monograph* No. 18, 265 (1956).
[183] Goldman, A. J., Robertson, W. D., *Acta Met., 13*, 391 (1965).
[184] Goldman, A. J., Robertson, W. D., *Acta Met., 12*, 1265 (1964).
Goldman, A. J., Robertson, W. D., Koss, D. A., *Trans.*, AIME *230*, 240 (1964)—(Ref. [209]).
[185] Goldman, A. J., Wagner, C. N. J., *Acta Met., 11*, 405 (1963).
[186] Gomez, M. P., Polonis, D. H., *Trans.*, Am. Soc. Metals *52*, 201 (1960).
[187] Gorbach, V. G., Butakova, E. D., *Phys. Metals Metallog., 16*, No. 2, 112 (1963).
[188] Govila, R. K., *Acta Met., 12*, 273 (1964).
[189] Grange, R. A., Lambert, V. E., Harrington, J. J., *Trans.*, Am. Soc. Metals *51*, 377 (1959).
[190] Grange, R. A., Stewart, H. M., *Trans.*, AIME *167*, 467 (1946).
[191] Greninger, A. B., *Trans.*, AIME *133*, 204 (1939).
[192]
[193] Greninger, A. B., Troiano, A. R., *Trans.*, AIME *185*, 590 (1949).
[194] Greninger, A. B., *Trans.*, Am. Soc. Metals *30*, 1 (1942).
[195] Greninger, A. B., Mooradian, V. G., *Trans.*, AIME *128*, 337 (1938).
[196] Greninger, A. B., Troiano, A. R., *Nature, 141*, 38 (1938).
[197] Greninger, A. B., Troiano, A. R., *Trans.*, Am. Soc. Metals *28*, 537 (1940).
[198] Greninger, A. B., Troiano, A. R., *Trans.*, AIME *140*, 307 (1940).
[199] Greninger, A. B., Troiano, A. R., *Trans.*, AIME *145*, 289 (1941).
[200] Gridnev, V., *Tech. Phys. (USSR), 5*, 761 (1938).
[201] Gridnev, V., Kurdjumov, G., *Tech. Phys. (USSR), 5*, 263 (1938).
[202] Gridnev, V. N., Trefilov, V. I., Minakov, V. N., *Dokl. Akad. Nauk SSSR, 134*, 1334 (1960).
Gridnev, V. N., Trefilov, V. I., *Dokl. Akad. Nauk SSSR, 95*, 741 (1954)—(Ref. [636]).
[203] Griffiths, E., Pallister, P. R., *J. Iron Steel Inst., 175*, 30 (1953).
[204] Gschneidner, K. A., Elliott, R. O., McDonald, R. R., *J. Phys. Chem. Solids*, (GB) *23*, 555 (1962).
[205] Gugan, D., Dugdale, J. S., *Can. J. Phys., 36*, 1248 (1958).
[206] Gulyaev, A. P., Zelenova, V. D., *Phys. Metals Metallog., 6*, No. 5, 175 (1958).
[207] Gulyaev, A. P., Shigarev, A. S., *Phys. Metals Metallog., 10*, No. 5, 54 (1960).
[208] Gulyaev, A. P., Zelenova, V. D., *Phys. Metals Metallog., 9*, No. 4, 44 (1960).
[209] Goldman, A. J., Robertson, W. D., Koss, D. A., *Trans.*, AIME *230*, 240 (1964).
[210] Gulyaev, A. P., *Metalloved. i Term. Obrabotka Metal., 11*, 5 (1959).
[211] Guntner, C. J., Reed, R. P., *Trans.*, Am. Soc. Metals *55*, 399 (1962).
[212] Gupta, S. C., Das, Lement, B. S., *Trans.*, AIME *191*, 727 (1951).
[213] Gupta, S. C., Das, Lement, B. S., *Trans.*, AIME *197*, 530 (1953); Reply to Disc. *Trans.*, AIME *200*, 687 (1954).
[214] Gupta, H. R. Sen, Gupta, S. C. Das., *Trans.*, Indian Inst. Metals *12*, 109 (1959).
[215] Guttman, L., *Trans.*, AIME *188*, 1472 (1950).
[216] Hägg, G., *J. Iron Steel Inst., 130*, 439 (1934).
[217]
[218] Hagiwara, I., Kanazawa, S., *Trans.*, Japan Inst. Metals *3*, 133 (1962).
[219] Hahn, G., *Senior Thesis*, (New York Univ., New York, 1952).
[220] Hall, A. M., *DMIC Rept. 194* (Battelle Memorial Inst., Columbus, Ohio, 1963).
[221] Hall, E. O., *Twinning* (Butterworths Scientific, London, 1954), p. 124.
[222] Harris, W. J., Cohen, M., *Trans.*, AIME *180*, 447 (1949); Reply to Disc. *Trans.*, AIME *185*, 344 (1949).
[223] Hauser, J. J., Capenos, J. M., Banerjee, B. R., *Trans.*, Am. Soc. Metals *54*, 514 (1961).
[224] Heidenreich, R. D., *J. Appl. Phys., 26*, 879 (1955).
[225] Hess, J. B., Barrett, C. S., *Trans.*, AIME *194*, 645 (1952); Reply to Disc. *Trans.*, AIME *197*, 729 (1953).
[226] Hill, J. D., *Nature, 186*, 304 (1960).
[227] Hillert, M., *Acta Met., 6*, 122 (1958).
[228] Hiltz, R. H., *Trans.*, AIME *216*, 138 (1959).
Hocheid, B., Tanon, A., Miard, F., *Acta Met., 13*, 144 (1965)—(Ref. [603]).

[229] Holden, A. N., *Acta Met.*, *1*, 617 (1952).
[230] Holden, F. C., Odgen, H. R., Jaffee, R. I., *Trans.*, AIME *200*, 169 (1954).
[231] Hollomon, J. H., Jaffe, L. D., Buffum, D. C., *J. Appl. Phys.*, *18*, 780 (1947).
[232] Hollomon, J. H., Turnbull, D., *Progr. Metal Phys.*, *4*, 333 (1953).
[233] Honda, K., Nishiyama, Z., *Sci. Rept.* (Tohoku Univ., Sendai, 1932), *21*, 299.
Also *Trans.*, Am. Soc. Steel Treat. *20*, 464 (1932).
Honda, K., Iwase, K., *Sci. Rept.* (Tohoku Univ., Sendai, 1927), *16*, 1.—(Ref. [589]).
Houdremont, I. E., Krisement, O., *Arch. Eisenhuettenw.*, *24*, 53 (1954)—(Ref. [590]).
[234] Houska, C. R., Averbach, B. L., Cohen, M., *Acta Met.*, *8*, 81 (1960).
[235] Howard, R. T., Cohen, M., *Trans.*, AIME *176*, 384 (1948).
[236] Hsiao, C. H., Dulis, E. J., *Trans.*, Am. Soc. Metals *50*, 773 (1958).
[237] Hucek, H. J., Fletcher, E. E., Watts, A. A., Elsea, A. R., Manning, G. K., *WADC Tech. Rept. No. 55-341* (Wright-Patterson AFB, Ohio, 1955).
[238] Hull, D., *Electron Microscopy and Strength of Crystals* (Interscience, New York, 1961), p. 936.
Hull, D., Bull. *Inst. Metals*, *2*, 134 (1954)—(Ref. [626]).
[239] Hull, D., *Phil. Mag.*, *7*, 537 (1962).
[240] Hull, D., Garwood, R. D., *J. Inst. Metals*, *86*, 485 (1957–58).
[241] Hull, D., Garwood, R. D., *Inst. Metals Monograph No. 18*, 219 (1956).
[242] Hull, D., Rosenberg, H. M., *Phil. Mag.*, *4*, 303 (1958).
[243] Hull, D., Rosenberg, H. M., *Cryogenics*, *1*, 27 (1960).
[244] Hull, D., Rosenberg, H. M., *Phys. Rev. Letters*, *2*, 205 (1959).
[245] Ianniello, L., Burr, A., *J. Appl. Phys.*, *33*, 2689 (1962).
[246] Ikeda, K., Ogawa, S., *Sci. Rept.* (Tohoku Univ., Sendai, 1956), *8*, 391.
Il'ina, V. A., Kritskaya, V. K., *Dokl. Akad. Nauk SSSR*, *85*, 997 (1952)—(Ref. [591]).
[247] Imai, Y., Saito, T., *Sci. Rept.* (Tohoku Univ., Sendai, 1962), *14*, 104.
Irvine, K. J., Llewellyn, D. T., Pickering, F. B., *J. Iron Steel Inst.*, *193*, 218 (1959)—(Ref. [607]).
[248] Irvine, K. J., Pickering, F. B., Garstone, *J. Iron & Steel*, *19*, 660 (1960).
Isaitschew, I., Kaminsky, E., Kurdjumov, G. V., *Trans.*, AIME *128*, 361 (1958)—(Ref. [586]).
[249] Izmaylov, Y. A., Gorbach, V. G., Yakhoutov, A. G., *Phys. Metals Metallog.*, *16*, No. 3, 24 (1963).
[250] Izumiyama, M., *Sci. Rept.* (Tohoku Univ., Sendai, 1962), *14*, 11.
[251] Jackson, J. K., *Thesis* (Purdue Univ., W. Lafayette, Ind., 1961).
Jan, J. P., Pearson, W. B., *Can. J. Phys.*, *42*, 220 (1964)—(Ref. [660]).
[252] Jaswon, M. A., *Trans.*, AIME *200*, 678 (1954).
[253] Jaswon, M. A., *Inst. Metals Monograph No. 18*, 173 (1956).
[254] Jaswon, M. A., *Research*, *11*, 315 (1958).
[255] Jaswon, M. A., Wheeler, J. A., *Acta Cryst.*, *1*, 216 (1948).
[256] Johnson, K. A., Wayman, C. M., *Acta Cryst.*, *16*, 480 (1963).
[257] Johnson, P. C., Stein, B. A., Davis, R. S., *J. Appl. Phys.*, *33*, 557 (1962).
[258] Jolley, W., Hull, D., *J. Inst. Metals*, *92*, 129 (1963–64).
[259] Jones, F. W., Pumphrey, W. I., *J. Iron Steel Inst.*, *163*, 121 (1949).
[260] Jong, M. de., Rathenau, G. W., *Acta Met.*, *9*, 889 (1961).
[261] Kachi, S., Bando, Y., Higuchi, S., Japan *J. Appl. Phys.*, *1*, 307 (1962).
Kaminskii, E., *Tech. Phys. (USSR)*, *5*, 953 (1938)—(Ref. [612]).
Kajiwara, S., Nishiyama, Z., Japan *J. Appl. Phys.*, *3*, 749 (1964)—(Ref. [615]).
[262] Kasberg, A. S., Mack, D. J., *Trans.*, AIME *191*, 903 (1951).
Kasen, M. B., Polonis, D. H., *Acta Met.*, *10*, 959 (1962)—(Ref. [630]).
[263] Kaufman, L., *Acta Met.*, *7*, 575 (1959).
[264] Kaufman, L., *Trans.*, AIME *215*, 218 (1959).
Kaufman, L., *ASTIA Rept. No. AD 144220* (1959)—(Ref. [608]).
[265] Kaufman, L., Ringwood, A. E., *Acta Met.*, *9*, 941 (1961).
[266] Kaufman, L., Cloughterty, E. V., Weiss, R. J., *Acta Met.*, *11*, 323 (1963).
[267] Kaufman, L., *Acta Met.*, *7*, 216 (1959).

[268] Kaufman, L., Cohen, M., *Inst. Metals Monograph No. 18*, 187 (1956).
[269] Kaufman, L., Cohen, M., *Trans.*, AIME *206*, 1393 (1956).
[270] Kaufman, L., Cohen, M., *Progr. Metal Phys.*, *7*, 165 (1958).
[271] Kaufman, L., Levenaar, A., Harvey, J. S., *Acta Met.*, *8*, 270 (1960).
Kaufman, L., Levenaar, A., Harvey, J. S., *Progress in Very High Pressure Research* (J. Wiley & Sons, New York, 1961), p. 90—(Ref. [616]).
Kaufman, L., Radcliffe, S. V., Cohen, M., *Decomposition of Austenite by Diffusional Processes* (Interscience, New York, 1962), p. 313—(Ref. [659]).
[272] Kehrer, V. J., Leidheiser, H., *J. Chem. Phys.*, *21*, 570 (1953).
[273] Kelly, P. M., *Acta Met.*, *13*, 635 (1965).
[274] Kelly, P. M., *Electron Microscopy and Strength of Crystals* (Interscience, New York, 1961), p. 917.
[275] Kelly, P. M., *Proc.*, Intern. Congr. Electron Microscopy, 5th (Academic Press, New York, 1962), *1*, HH3.
Kelly, P. M., Nutting, J., *J. Iron Steel Inst.*, *192*, 246 (1959)—(Ref. [629]).
[276] Kelly, P. M., Nutting, J., *Proc.*, Roy. Soc. (London) *A259*, 45 (1960).
[277] Kelly, P. M., Nutting, J., *J. Iron Steel Inst.*, *197*, 199 (1961).
[278] Kerlins, V., Alstetter, C., *Trans.*, AIME *227*, 94 (1963).
[279] Klier, E. P., *Trans.*, AIME *162*, 186 (1945).
[280] Klier, E. P., Grymko, S. M., *Trans.*, AIME *185*, 611 (1949).
[281] Klier, E. P., Troiano, A. R., *Trans.*, AIME *162*, 175 (1945).
[282] Klosterman, J. A., Burgers, W. G., *Acta Met.*, *12*, 355 (1964).
[283] Knapp, H., Dehlinger, U., *Acta Met.*, *4*, 289 (1956).
[284] Ko, T., *Acta Met.*, *2*, 75 (1954).
[285] Ko, T., *J. Iron Steel Inst.*, *174*, 351 (1953).
[286] Ko, T., Edmondson, B., *Acta Met.*, *1*, 466 (1953).
Kogan, L. I., Entin, R. I., *Dokl. Akad. Nauk SSSR*, *73*, 1173 (1950)—(Ref. [655]).
Koistinen, D. P., Marburger, R. E., *Acta Met.*, *7*, 59 (1959)—(Ref. [592]).
[287] Kochendorfer, A., Otto, G., *Arch. Eisenhuettenw.*, *29*, 775 (1958).
Koster, W., Schneider, A., *Z. Metall.*, *32*, 156 (1940)—(Ref. [596]).
[288] Krainer, H., Krainer, E., *Berg-Huettenmaenn. Monatsh. Montan.*, *99*, 247 (1954).
[289] Krauss, G., *Acta Met.*, *11*, 499 (1963).
[290] Krauss, G., Cohen, M., *Trans.*, AIME *224*, 1212 (1962).
[291] Krauss, G., Cohen, M., *Trans.*, AIME *227*, 278 (1963).
[292] Krauss, G., Pitsch, W., *Acta Met.*, *12*, 278 (1964).
Krisement, O., Houdremont, I. E., Wever, F., *Rev. Met.*, *51*, 401 (1954)—(Ref. [601]).
[293] Kritskaia, V. K., Nodia, N. M., Osipyan, Yu. A., *Phys. Metals Metallog. 6*, No. 1, 162 (1958).
Kroner, E., *Acta Met.*, *2*, 302 (1954)—(Ref. [625]).
[294] Kulin, S. A., Cohen, M., *Trans.*, AIME *188*, 1139 (1950).
[295] Kulin, S. A., Cohen, M., Averbach, B. L., *Trans.*, AIME *194*, 661 (1952).
[296] Kulin, S. A., Speich, G. R., *Trans.*, AIME *194*, 258 (1952).
[297] Kumar, R., *Inst. Metals Monograph No. 18*, 317 (1956).
[298] Kumar, R., *Trans.*, Indian Inst. Metals *11*, 21 (1958).
[299] Kumar, R., Balasubramanian, V., *Trans.*, AIME *218*, 185 (1960).
[300] Kunze, V. G., *Z. Metall.*, *53*, 329, 356, 396 (1962).
Kunze, V. G., *Z. Metall.*, *55*, 307 (1964)—(Ref. [617]).
Kurdjumov, G. V., *Trans.*, AIME *133*, 222 (1938)—(Ref. [640]).
[301] Kurdjumov, G. V., *Zh. Tekhn. Fiz.*, *18*, 999 (1948).
[302] Kurdjumov, G. V., *Zh. Tekhn. Fiz.*, *18*, 1004 (1948).
[303] Kurdjumov, G. V., *Zh. Tekhn. Fiz.*, *18*, 1011 (1948).
[304] Kurdjumov, G. V., *Trans.*, AIME *215*, 449 (1959).
[305] Kurdjumov, G. V., *J. Iron Steel Inst.*, *193*, 26 (1960).
Kurdjumov, G. V., Khandros, L. G., *Dokl. Akad. Nauk SSSR*, *66*, 211 (1949)—(Ref. [651]).
Kurdjumov, G. V., *Dokl. Akad. Nauk SSSR*, *60*, 1543 (1948)—(Ref. [652]).
Kurdjumov, G. V., Maksimova, O. P., *Stal (USSR)*, *10*, (1950). (as quoted in Ref. [598])—(Ref. [653]).

[306] Kurdjumov, G. V., Maksimova, O. P., *Dokl. Akad. Nauk SSSR, 61*, 83 (1948).
[307] Kurdjumov, G. V., Maksimova, O. P., *Dokl. Akad. Nauk SSSR, 81*, 565 (1951).
[308] Kurdjumov, G. V., Maksimova, O. P., *Dokl. Akad. Nauk SSSR, 73*, 95 (1950).
[309] Kurdjumov, G. V., Maksimova, O. P., Nikonorova, A. I., Palenko, Z. D., Yampoliskii, A. M., *Phys. Metals Metallog., 6*, No. 1, 85 (1958).
[310] Kurdjumov, G. V., Maksimova, O. P., Tagonova, T. V., *Dokl. Akad. Nauk SSSR, 73*, 307 (1950).
Kurdjumov, G. V., Perkas, M. D., Shamov, A. E., *Dokl. Akad. Nauk SSSR, 92*, 955 (1953)—(Ref. [593]).
[311] Kurdjumov, G., Sachs, G., *Z. Physik, 64*, 325 (1930).
[312] Lagneborg, R., *Acta Met., 12*, 823 (1964).
[313] Lashko, N. F., *Phys. Metals Metallog., 12*, No. 5, 143 (1961).
Lement, B. L., *Nuovo Cimento, 1*, 295 (1955)—(Ref. [598]).
[314] Lenning, G. A., Craighead, C. M., Jaffee, R. I., *Trans.*, AIME *200*, 367 (1954).
[315] Leont'yev, B. A., *Phys. Metals Metallog., 16*, No. 4, 20 (1963).
[316] Lieberman, D. S., *Acta Met., 6*, 680 (1958).
[317] Lieberman, D. S., Read, T. A., Wechsler, M. S., *J. Appl. Phys., 28*, 532 (1957).
[318] Lieberman, D. S., Wechsler, M. S., Read, T. A., *J. Appl. Phys., 26*, 473 (1955).
[319] Lipson, H., Parker, A. M. B., *J. Iron Steel Inst., 149*, 123 (1944).
[320] Liu, Y. C., Margolin, H., *Trans.*, AIME *197*, 667 (1953).
Liu, Y. C., *ASTIA Rept. No. AD 40224* (1954)—(Ref. [635]).
[321] Liu, Y. C., *Trans.*, AIME *206*, 1036 (1956).
Ljubov, B. J., *Dokl. Akad. Nauk. SSSR, 72*, 273 (1950)—(Ref. [658]).
Ljubov, B. J., *Dokl. Akad. Nauk. SSSR, 72*, 895 (1951)—(Ref. [656]).
[322] L'nianoi, V. N., Salli, I. V., *Phys. Metals Metallog., 9*, No. 3, 122 (1960).
[323] Lobodyuk, V. A., Khandros, L. G., *Fiz. Metal Metalloved., 14*, 133 (1962).
[324] Lomer, W. M., *Inst. Metals Monograph No. 18, 243* (1956).
[325] Lucas, F. F., *Trans.*, ASST (ASM) *6*, 669 (1924).
[326] Lustman, B., Kerze, F., *The Metallurgy of Zirconium* (McGraw-Hill Book Company, Inc., New York, 1955).
[327] Lysak, L. I., Nikolin, B. I., *Phys. Metals Metallog., 16*, No. 2, 81 (1963).
[328] Macgregor, E. R., Peters, B. F., Parr, J. G., *Trans.*, AIME *206*, 1324 (1956).
[329] Machlin, E. S., *Trans.*, AIME *200*, 684 (1954).
[330] Machlin, E. S., *Trans.*, AIME *194*, 277 (1952).
[331] Machlin, E. S., Cohen, M., *Trans.*, AIME *191*, 746 (1951); Reply to Disc., *Trans.*, AIME *194*, 519 (1952).
[332] Machlin, E. S., Cohen, M., *Trans.*, AIME *191*, 1019 (1951); Reply to Disc., *Trans.*, AIME *194*, 1201 (1952).
[333] Machlin, E. S., Cohen, M., *Trans.*, AIME *194*, 489 (1952).
[334] Machlin, E. S., Weinig, S., *Acta Met., 1*, 480 (1953).
[335] Mack, D. J., *Trans.*, AIME *175*, 240 (1948).
[336] Mackenzie, J. K., *J. Australian Inst. Metals, 5*, 90 (1960).
[337] Maksimova, O. P., Estrin, E. I., *Phys. Metals Metallog., 9*, No. 3, 90 (1960).
Maksimova, O. P., Nikonorova, A. I., *Dokl. Akad. Nauk. SSSR, 81*, 183 (1951)—(Ref. [632]).
Malyshev, K. A., *Fiz. Metal. i Metalloved., 18*, 238 (1964)—(Ref. [637]).
[338] Marcinkowski, M. J., Brown, N., *Phil. Mag., 8*, 891 (1963).
Martelly, J., *Ann. Phys., 9*, 318 (1938)—(Ref. [646]).
[339] Martin, D. L., *Phys. Rev. Letters, 1*, 4 (1958).
[340] Martin, D. L., *Can. J. Phys., 38*, 25 (1960).
[341] Martin, D. L., *Proc.*, Roy. Soc. (London) *A254*, 444 (1960).
[342] Martin, D. L., *Proc.*, Roy. Soc. (London) *A254*, 433 (1960).
[343] Martin, C. F., Gerberich, W. W., Camont, J. M., Harmon, E. L., *ASD-TDR-62-692* (Wright Patterson AFB, Ohio, 1963).
[344] Massalski, T. B., *Acta Met., 6*, 243 (1958).
[345] Massalski, T. B., Barrett, C. S., *Trans.*, AIME *209*, 455 (1957).
[346] Masson, D. B., *Trans.*, AIME *218*, 94 (1960).
[347] Masson, D. B., *Acta Met., 8*, 71 (1960).
[348] Masson, D. B., *Acta Met., 10*, 986 (1962).

[*349*] Masson, D. B., Barrett, C. S., *Trans.*, AIME *212*, 260 (1958).
[*350*] Mathieu, K., *Arch. Eisenhuettenw.*, *16*, 215 (1942).
[*351*] McDougall, P. G., Bowles, J. S., *Acta Met.*, *12*, 779 (1964).
[*352*] McHargue, C. J., *Acta Cryst.*, *6*, 529 (1953).
[*353*] McHargue, C. J., Yakel, H. L., *Acta Met.*, *8*, 637 (1960).
[*354*] McReynolds, A. W., *J. Appl. Phys.*, *17*, 823 (1946).
[*355*] McReynolds, A. W., *J. Appl. Phys.*, *20*, 896 (1949).
[*356*] Mehl, R. F., Barrett, C. S., Smith, D. W., *Trans.*, AIME *105*, 215 (1933).
[*357*] Mehl, R. F., Derge, G., *Trans.*, AIME *125*, 482 (1937).
[*358*] Mehl, R. F., Smith, D. W., *Trans.*, AIME *113*, 203 (1934).
[*359*] Mehl, R. F., Van Winkle, D. R., *Rev. Met.*, *10*, 466 (1953).
[*360*] Menard, J., *Thesis*, (Univ. of Grenoble, Grenoble 1961).
[*361*] Menard, J., Weil, L., *Proc.*, Cryogenic Engr. Conf. (Plenum Press, New York, 1960), *6*, 587.
[*362*] Menard, J., Weil, L., *Compt. Rend.*, *250*, 4160 (1960).
[*363*] Meyerson, M. R., Rosenberg, S. J., *Trans.*, Am. Soc. Metals *46*, 1225 (1954).
[*364*] Meyrick, G., Paxton, H. W., *Trans.*, AIME *230*, 1010 (1964).
[*365*]
[*366*] Monkman, F. C., Cuff, F. B., Grant, N. J., *ASTIA Rept. No. AD 102322* (1957)
[*367*] Monkman, F. C., Cuff, F. B., Grant, N. J., *Metal Progr.*, *71*, 94 (1957).
[*368*] Mookerjee, S. N., Rao, H. R. S., Paranjpe, V. G., Visvanathan, S., *Trans.*, Indian Inst. Metals *12*, 371 (1959).
[*369*] Moore, A., Graham, J., Williamson, C. K., Raynor, G. V., *Acta Met.*, *3*, 579 (1955).
[*370*] Morgan, E. R., Ko, T., *Acta Met.*, *1*, 36 (1953).
[*371*] Mott, B. W., Haines, H. R., *Rev. Met.*, *51*, 614 (1954).
[*372*] Mugnier, D., Geneste, J., *Compt. Rend.*, *254*, 2976 (1962).
[*373*] Mugnier, D., Weil, L., *Proc.*, Cryogenic Engr. Conf. (Plenum Press, New York, 1961), *9*, 98.
[*374*] Mura, T., Tamura, I., Brittain, J. O., *J. Appl. Phys.*, *32*, 92 (1961).
[*375*] Nagakura, S., Kikuchi, N., Kaneko, Y., Oketani, S., *J. Appl. Phys.*, *2*, 201 (1963).
[*376*] Nakanishi, N., *Bull.*, Univ. Osaka, Prefect. *A9*, 95 (1961).
[*377*] Nakanishi, N., *Bull.*, Univ. Osaka, Prefect. *A9*, 109 (1961).
[*378*] Nakanishi, N., *Trans.*, Japan Inst. Metals *2*, 79 (1961).
[*379*] Nakanishi, N., Mitani, H., *Bull.*, Univ. Osaka, Prefect. *A7*, 155 (1959).
[*380*] Nakanishi, N., Wayman, C. M., *Trans.*, AIME *227*, 500 (1963).
Nash, S. K., *Tech. Rept.*, (Met. Dept., Mass. Inst. Tech., Cambridge, Mass., 1951)—(Ref. [*604*]).
[*381*] Nehrenberg, A. E., Payson, P., Lillys, P., *Trans.*, Am. Soc. Metals *47*, 785 (1955).
[*382*] Nelson, J. O., Alstetter, C. J., *Trans.*, AIME *230*, 1578 (1964).
[*383*] Newkirk, J. B., Geisler, A. H., *Acta Met.*, *1*, 370 (1953).
[*384*] Nishiyama, Z., *Sci. Rept.* (Tohoku Univ. Sendai, 1934) *23*, 637.
Nishiyama, Z., *Sci. Rept.* (Tohoku Univ. Sendai, 1936) *25*, 79.—(Ref. [*613*]).
[*385*] Nishiyama, Z., *Sci. Rept.* (Tohoku Univ. Sendai, 1936) *25*, 94.
[*386*] Nishiyama, Z., Simizu, K., *J. Phys. Soc.*, Japan *15*, 1963 (1960).
[*387*] Nishiyama, Z., *Mem.*, Inst. Sci. Ind. Res., Osaka Univ., *17*, 125 (1960).
[*388*] Nishiyama, Z., Kajiwara, S., *Trans.*, Japan Inst. Metals *3*, 127 (1962).
[*389*] Nishiyama, Z., Kajiwara, S., *Mem.*, Inst. Sci. Ind. Res., Osaka Univ. *19*, 59 (1962).
Nishiyama, Z., Kajiwara, S., Japan *J. Appl. Phys.*, *2*, 478 (1963)—(Ref. [*631*]).
[*390*] Nishiyama, Z., Shimizu, K., *Acta Met.*, *6*, 125 (1958).
[*391*] Nishiyama, Z., Shimizu, K., *Acta Met.*, *7*, 432 (1959).
[*392*] Nishiyama, Z., Shimizu, K., *Mem.*, Inst. Sci. Ind. Res., Osaka Univ. *19*, 123 (1962).
Nishiyama, Z., Shimizu, S., *Mem.*, Inst. Sci. Ind. Res., Osaka Univ. *15*, 105 (1958)—(Ref. [*643*]).
[*393*] Nishiyama, Z., Shimizu, K., *Acta Met.*, *9*, 980 (1961).
[*394*] Nishiyama, Z., Shimizu, K., Sugino, K., *Acta Met.*, *9*, 620 (1961).
[*395*] Nishiyama, Z., Shimizu, K., Sato, S., *Mem.*, Inst. Sci. Ind. Res., Osaka Univ. *13*, 1 (1956).

[396] Novikov, I. I., *Phys. Metals Metallog.*, *6*, No. 4, 189 (1958).
[397] Nutkins, M. A. E., *Proc.*, Phys. Soc. (London) *72*, 810 (1958).
[398] Orowan, E., *Symposium on Internal Stresses in Metals and Alloys* (Inst. Metals, London, 1958), p. 47.
[399] Otte, H. M., *Acta Met.*, *2*, 349 (1954).
[400] Otte, H. M., *Acta Met.*, *5*, 614 (1957).
[401] Otte, H. M., *Trans.*, AIME *218*, 342 (1960).
[402] Otte, H.-M., *Acta Met.*, *8*, 892 (1960).
[403] Otte, H. M., *Acta Cryst.*, *16*, 8 (1963).
[404] Otte, H. M., Ko,-T., *J. Iron Steel Inst.*, *173*, 31 (1953).
[405] Otte, H. M., Massalski, T. B., *Acta Met.*, *6*, 494 (1958).
[406] Otte, H. M., Read, T. A., *Trans.*, AIME *209*, 412 (1957).
[407] Otte, H. M., *Nature*, *174*, 506 (1954).
[408] Owen, W. S., Gilbert, A., *J. Iron Steel Inst.*, *196*, 142 (1960).
[409] Papadakis, E. P., Reed, E. L., *J. Appl. Phys.*, *32*, 682 (1961).
[410] Papirov, I. I., Tikhinskiy, G. F., Finkel, V. A., *Phys. Metals Metallog.*, *15*, No 3, 120 (1963).
[411] Parr, J. G., *J. Iron Steel Inst.*, *171*, 137 (1952).
[412] Parr, J. G., *Acta Cryst.*, *5*, 842 (1952).
[413] Pascard, R., *Acta Met.*, *7*, 305 (1959).
[414] Patel, J. R., Cohen, M., *Acta Met.*, *1*, 531 (1953).
[415] Patterson, R. L., Wayman, C. M., *Acta Met.*, *12*, 1306 (1964).
[416] Payson, P., Grange, R. A., *Metals Handbook* (Am. Soc. Metals, Cleveland, Ohio, 1948), p. 611.
[417] Petch, N., *J. Iron Steel Inst.*, *145*, 111 (1942).
[418] Petch, N., *J. Iron Steel Inst.*, *147*, 221 (1943).
Petrosjan, P. P., *Dokl. Akad. Nauk SSSR*, *59*, 1109 (1948)—(Ref. [649]).
Philibert, J., *Compt. Rend.*, *241*, 190 (1955)—(Ref. [614]).
[419] Philibert, J., Crussard, C., *J. Iron Steel Inst.*, *180*, 39 (1955).
[420] Pitsch, W., *Phil. Mag.*, *4*, 577 (1959).
[421] Pitsch, W., *J. Inst. Metals*, *87*, 444 (1959).
[422] Pitsch, V. W., *Arch. Eisenhuettenw.*, *30*, 503 (1959).
[423] Polonis, D. H., Parr, J. G., *Trans.*, AIME *200*, 1148 (1954).
[424] Polonis, D. H., Parr, J. G., *Trans.*, AIME *203*, 64 (1955).
[425] Polonis, D. H., Parr, J. G., *Trans.*, AIME *206*, 531 (1956).
[426] Pops, H., Massalski, T. B., *Trans.*, AIME *230*, 1662 (1964).
[427] Porter, L. F., Dienes, G. J., *Trans.*, AIME *215*, 854 (1959).
[428] Porter, L. F., Rosenthal, P. C., *Acta Met.*, *7*, 504 (1959).
[429] Post, C. B., Eberly, W. S., *Trans.*, Am. Soc. Metals *39*, 868 (1947).
[430] Predmore, R. E., *ASTIA Rept. No. AD 447576* (1964).
[431] Priestner, R., Glover, S. G., *Acta Met.*, *5*, 536 (1957).
Prosvirin, V. I., *Zh. Tehkn. Fiz.*, *19*, 542 (1949)—(Ref. [650]).
[432] Rachinger, W. A., *Brit. J. Appl. Phys.*, *9*, 250 (1958).
[433] Radcliffe, S. V., Kaufman, L., Cohen, M., *Acta Met.*, *10*, 1110 (1962).
[434] Radcliffe, S. V., Schatz, M., *Acta Met.*, *10*, 201 (1962).
[435] Ramachandran, E. G., Dasarathy, C., *Acta Met.*, *8*, 274 (1960).
[436] Ramachandran, E. G., Dasarathy, C., *Acta Met.*, *8*, 666 (1960).
[437] Ramachandran, E. G., Dasarathy, C., *Acta Met.*, *8*, 729 (1960).
[438] Ramachandran, E. G., Dasarathy, C., *J. Iron Steel Inst.*, *200*, 235 (1962).
Raub, E., Platte, W., Z. Metall. *51*, 477 (1960)—(Ref. [644]).
[439] Rawlings, R., McGrath, J., *ASTIA Rept. No. AD 600848*, (1964) and *No. AD 462096* (1965).
[440] Read, T. A., *The Science of Engineering Materials* (J. Wiley & Sons, New York, 1957), p. 196.
[441] Reed, R. P., Guntner, C. J., *Trans.*, AIME *230*, 1713 (1964).
[442] Reed, R. P., Mikesell, R. P., *Advan. Cryog. Eng.* (Plenum Press, New York, 1960), *4*, 84.
[443] Reed, R. P., *Acta Met.*, *10*, 865 (1962).
[444] Reynolds, J. E., Bever, M. B., *Trans.*, AIME *194*, 1065 (1952).

[445] Richards, T. L., Roberts, W. T., *Inst. Metals Monograph No. 18*, 193 (1956).
[446] Richman, R. H., *Trans.*, AIME *227*, 159 (1963).
[447] Richman, M. H., Cohen, M., Wilsdorf, H. G. F., *Acta Met.*, *7*, 819 (1959).
[448] Roberts, C. S., *Trans.*, AIME *197*, 203 (1953).
[449] Roberts, W. N., *Proc.*, Intern. Congr. Electron Microscopy, 5th (Interscience New York, 1962), *1*, HH7.
[450] Roitburd, A. L., *Phys. Metals Metallog.*, *10*, No. 2, 1 (1960).
[451] Rosenberg, S. J., *Acta Met.*, *1*, 376 (1953).
[452] Ryder, D. A., *Inst. Metals Monograph No. 18*, 320 (1956).
[453] Sachs, G., Spretnak, J. W., *Trans.*, AIME *145*, 340 (1941).
[454] Sadovskij, V. D., Rodigin, L. V., Smirnov, L. V., Filonchik, G. M., Fakidov, I. G., *Phys. Metals Metallog.*, *12*, No. 2, 131 (1961).
[455] Sadovskij, V. D., Jakutovic, M. V., *Dokl. Akad. Nauk. SSSR*, *70*, 833 (1950).
[456] Sadovskij, V. D., Bogaceva, G. N., *Dokl. Akad. Nauk. SSSR*, *83*, 221 (1952).
[457] Sagisman, M., *Arch. Eisenhuettenw.*, *25*, 271 (1954).
[458] Samans, C. H., *Trans.*, AIME *128*, 357 (1938).
[459] Sanderson, G. P., Honeycombe, R. W. K., *J. Iron Steel Inst.*, *200*, 934 (1962).
[460] Sastri, A. S., West, D. R. F., *ASTIA Rept. No. AD 440782* (1964).
[461] Schaaber, O., *Trans.*, AIME *203*, 559 (1955).
[462] Schaller, F. W., *Trans.*, AIME *227*, 1465 (1963).
[463] Schaller, F. W., Zackay, V. F., *Trans.*, Am. Soc. Metals *51*, 609 (1958).
[464] Scheil, E. Z., *Z. Anorg. Allgem. Chem.*, *207*, 21 (1932).
[465] Schirber, J. E., Swenson, C. A., *Acta Met.*, *10*, 511 (1962).
[466] Schwaneke, A. E., Jenson, J. W., *J. Appl. Phys.*, *335*, 1350 (1962).
[467] Sebilleau, F., Bibring, H., *Inst. Metals Monograph No. 18*, 209 (1956).
[468] Seeger, A., *Z. Metall. 47*, 653 (1956), also *44*, 247 (1953).
[469] Seeger, A., *Inst. Metals Monograph No. 18*, 330 (1956).
[470] Shih, C. H., Averbach, B. L., Cohen, M., *Trans.*, AIME *203*, 183 (1955).
[471] Shih, C., Cohen, M., Averbach, B. L., *Trans.*, AIME *200*, 683 (1954).
[472] Shimizu, K., *J. Phys. Soc. Japan*, *17*, 508 (1962).
[473] Shinoda, G., Kawasaki, B., *Sci. Rept.* (Tohoku Univ., Sendai, 1958), *47*, 363.
[474] Shyne, J. C., Zackay, V. F., Schmatz, D. J., *Trans.*, Am. Soc. Metals *52*, 346 (1960).
[475] Sidorova, T. S., Panin, V. Ye., Bol'shanina, M. A., *Phys. Metals Metallog.*, *14*, No. 5, 97 (1962).
[476] Silcock, J. M., Davies, M. N., Haroy, H. K., *Inst. Metals Monograph No. 18*, 93 (1956).
[477] Singh, K. P., Parr, J. G., *Acta Met.*, *9*, 1073 (1961).
[478] Singh, K. P., Parr, J. G., *Acta Met.*, *10*, 1109 (1962).
[479] Singh, K. P., Parr, J. G., *Acta Met.*, *10*, 1111 (1962).
[480] Sleeswyk, A. W., *Phil. Mag.*, *7*, 1597 (1962).
[481] Smith, A. E. W., *J. Iron Steel Inst.*, *186*, 425 (1957).
[482] Smith, G. V., Mehl, R. F., *Trans.*, AIME *150*, 211 (1942).
[483] Smith, J. H., Gaunt, P., *Acta Met.*, *9*, 819 (1961).
[484] Smith, J. H., Paxton, H. W., McCabe, C. L., *Trans.*, AIME *230*, 1484 (1964).
[485] Smith, R. A., *J. Iron Steel Inst.*, *173*, 147 (1953).
[486] Smith, R., *J. Australian Inst. Metals*, *5*, 163 (1960).
[487] Smith, R., Bowles, J. S., *Acta Met.*, *8*, 405 (1960).
Speich, G. R., *ASTIA Rept. No. AD 72077* (1955)—(Ref. [*605*]).
[488] Speich, G. R., *Trans.*, AIME *227*, 1426 (1963).
[489] Speich, G. R., Swann, P. R., Submitted to *J. Iron Steel Inst.* (1965).
[490] Spretnak, J. W., *ASTIA Rept. No. AD 207248* (1958).
[491] Srivastava, L. P., Parr, J. G., *Trans.*, AIME *224*, 1295 (1962).
[492] Stadelmaier, H. H., Hock, R. C., *Acta Met.*, *4*, 223 (1956).
[493] Stark, P., Averbach, B. L., Cohen, M., *Acta Met.*, *3*, 91 (1955).
[494] Starr, C. D., Reporter, M., Dorn, J. E., *Tech. Rept. No. 15*, (Inst. Eng. Res. Univ. California, Berkeley, 1951).
[495] Starr, C. D., *Trans.*, AIME *197*, 654 (1953).
[496] Stevens, W., Haynes, A. C., *J. Iron Steel Inst.*, *183*, 349 (1956).

[497] Stregulin, A. I., Mel'nikov, L. A., *Phys. Metals Metallog. 8*, No. 3, 79 (1959).
[498] Suoninen, E. J., Genevray, R. M. Rever. M. B., *Trans.*, AIME *206*, 283 (1956).
[499] Suzuki, H., Sci. Rept. (Tohoku Univ. Sendai, 1954), *6*, 30. Also with Homma, T., *Trans.*, AIME *194*, 519 (1952).
[500] Swann, P. R., Parr, J. G., *Trans.*, AIME *212*, 276 (1958).
[501] Swann, P. R., Warlimont, H., *Electron Microscopy and Strength of Crystals*, (Interscience, New York, 1961), p. 933.
[502] Swann, P. R., Warlimont, H., *Acta Met., 11*, 511 (1963).
[503] Swanson, W. D., Parr, J. G., *J. Iron Steel Inst., 202*, 104 (1964).
[504] Swenson, C. A., *Phys. Rev., 111*, 82 (1958).
[505] Sykes, W. P., *Trans.*, Am. Soc. Metals *31*, 284 (1943).
[506] Takeuchi, S., Honna, T., *Sci. Rept.* (Tohoku Univ., Sendai, 1957), *9*, 492.
[507] Tanisaki, S., *J. Phys. Soc.*, Japan *14*, 680 (1959).
[508] Tanner, L. E., *Trans.*, AIME *221*, 74 (1961).
[509] Tanner, L. E., Kulin, S. A., *Acta Met., 9*, 1038 (1961).
[510] Taylor, J. L., Duwez, P., *Trans.*, AIME *197*, 253 (1953).
[511] Thompson, F. C., Stanton, L. R., *J. Iron Steel Inst., 159*, 133 (1945).
[512] Tino, Y., Meade, T., *J. Phys. Soc.*, Japan *18*, 955 (1963).
[513] Titchener, A. L., Bever, M. B., *Trans.*, AIME *200*, 303 (1954).
[514] Troiano, A. R., Greninger, A. B., *Metal Progr., 50*, 303 (1946).
[515] Troiano, A. R., McGuire, F. T., *Trans.*, Am. Soc. Metals *31*, 340 (1943).
[516] Troiano, A. R., Tokich, J. L., *Trans.*, AIME *175*, 728 (1948).
[517] Turkalo, A. M., *Trans.*, Am. Soc. Metals *54*, 344 (1961).
[518] Turnbull, D., *Trans.*, AIME *203*, 709 (1955).
[519] Turnbull, D., Fisher, J. C., *J. Chem. Phys., 17*, 71 (1949).
[520] Uhlig, H. H., *Trans.*, Am. Soc. Metals *33*, 947 (1941).
[521] Uhlig, H. H., *Acta Met., 10*, 1109 (1962).
[522] Venables, J. A., *J. Iron Steel Inst., 197*, 165 (1961).
[523] Venables, J. A., *Phil. Mag., 7*, 35 (1962).
[524] Vishnyakov, Y. D., Kurdjumov, G. V., *Fiz. Tverd. Tela, 6*, No. 1, 279 (1964).
[525] Vogel, R., Tonn, W., *Z. Anorg. Allgem. Chem., 202*, 292 (1931).
[526] Vorob'ev, V. G., Guljaev, A. P., *Zh. Tekhn. Fiz., 21*, 1157 (1951).
[527] Votava, E., *Acta Met., 8*, 901 (1960).
[528] Votava, E., *J. Inst. Metals, 90*, 129 (1961).
[529] Voyer, R., Weil, L., *Proc.*, Cryog. Eng. Conf. (Plenum Press, New York, 1965), *10*,
[530] Voyer, R., Weil, L., *Compt. Rend., 259*, 2430 (1964).
[531] Voyer, R., Bertaut, F., Geneste, J., *Compt. Rend., 258*, 4975 (1964).
[532]
[533] Walker, D. G., Borland, D. W., *J. Australian Inst. Metals, 5*, 75 (1960).
[534] Ward, R., Capus, J. M., *J. Iron Steel Inst., 201*, 1038 (1963).
[535] Ward, J. O., Jepson, M. D., Rait, J. R., *J. Iron Steel Inst., 170*, 1 (1952).
[536] Warekois, E. P., *J. Appl. Phys., 31*, 346S (1960).
[537] Warlimont, H., *Trans.*, AIME *221*, 1270 (1961).
[538] Warlimont, H., *Proc.*, Intern. Congr. Electron Microscopy, 5th (Academic Press, New York, 1962), *1*, HH-6.
[539] Warlimont, H., *Trans.*, AIME *224*, 495 (1962).
[540] Wassermann, G., *Mitt. K.-W. Inst. Eisenforsch., 17*, 149 (1935).
[541] Wayman, C. M., *Acta Met., 9*, 912 (1961).
[542] Wayman, C. M., *Introduction to the Crystallography of Martensitic Transformations*, (MacMillan Series in Mat. Sci., New York, 1964).
[543] Wayman, M., Allstetter, C. J., *Acta Met., 10*, 993 (1962).
[544] Wayman, C. M., Hanafee, J. E., Read, T. A., *Acta Met., 9*, 391 (1961).
[545] Wechsler, M. S., *Acta Met., 7*, 793 (1959).
[546] Wechsler, M. S., Otte, H. M., *Acta Met., 9*, 117 (1961).
[547] Wechsler, M. S., Lieberman, D. S., Read, T. A., *Trans.*, AIME *197*, 1503 (1953).
[548] Wechsler, M. S., Lieberman, D. S., Read, T. A., *Trans.*, AIME *200*, 680 (1954).
[549] Wechsler, M. S., Read, T. A., Lieberman, D. S., *Trans.*, AIME *218*, 202 (1960).
[550]

[551] Weinig, S., Machlin, E. S., *Trans.*, AIME *200*, 1280 (1954).
[552] Wells, M. G. H., *Acta Met.*, *12*, 389 (1964).
[553] Wells, M. G. H., West, D. R. F., *J. Iron Steel Inst.*, *200*, 472 (1962).
[554] Wells, M. G. H., West, D. R. F., *J. Iron Steel Inst.*, *200*, 710 (1962).
[555] Werner, F. E., Averbach, B. L., Cohen, M., *Trans.*, Am. Soc. Metals *49*, 823 (1957).
Wert, C. A., Alstetter, C. J., Nelson, J. O., Rashid, M. S., *ASTIA Rept. No AD 609017* (1964)—(Ref. [634]).
[556] Wheeler, J. A., Jaswon, M. A., *J. Iron Steel Inst.*, *163*, 161 (1947).
[557] White, C. H., Honeycombe, R. W. K., *J. Iron Steel Inst.*, *200*, 457 (1962).
[558] White, D. W., Jr., *Trans.*, AIME *203*, 1221 (1955).
[559] Wilkens, M., Warlimont, H., *Acta Met.*, *11*, 1099 (1963).
[560] Williams, A. J., Cahn, R. W., Barrett, C. S., *Acta Met.*, *2*, 117 (1954).
[561] Williams, D. N., Wood, R. A. Jaffee, R. I., *Trans.*, AIME *230*, 256 (1964).
[562] Wilman, H., *Inst. Metals Monograph No. 18*, 328 (1956).
[563] Winchell, P. G., Cohen, M., *Electron Microscopy and Strength of Crystals* (Interscience, New York, 1961), p. 995.
[564] Winchell, P. G., Cohen, M., *Trans.*, Am. Soc. Metals *55*, 347 (1962).
[565] Wiskel, S. J., Youdelis, W. V., Parr, J. G., *Trans.*, AIME *215*, 875 (1959).
[566] Wood, R. M., *Acta Met.*, *11*, 907 (1963).
[567] Woodilla, J., Winchell, P. G., Cohen, M., *Trans.*, AIME *215*, 849 (1959).
[568] Worner, H. W., *Acta Met.*, *2*, 310 (1954).
[569] Worrell, F. T., *J. Appl. Phys.*, *19*, 929 (1948).
[570] Yeo, R. B. G., *Trans.*, Am. Soc. Metals *57*, 48 (1964).
[571] Yeo, R. B. G., *Trans.*, AIME *224*, 1222 (1962).
[572] Yeo, R. B. G., *Trans.*, AIME *227*, 884 (1963).
[573] Yershova, L. S., Bogachev, I. N., Shklyar, R. S., *Phys. Metals Metallog.*, *12*, No. 5, 41 (1961).
[574] Yershova, L. S., *Phys. Metals Metallog.*, *15*, No. 4, 76 (1963).
[575] Yershova, L. S., Bogachev, I. N., *Phys. Metals Metallog.*, *13*, No. 2, 133 (1962).
[576] Zakharov, A. I., Maksimova, O. P., *Dokl. Akad. Nauk SSSR*, *114*, 1195 (1957).
[577] Zakharova, M. I., Ignatova, I. A., Khatanova, N. A., *Phys. Metals Metallog.*, *6*, No. 3, 89 (1958).
[578] Zanardi, T. J., *Thesis* (Dept. Met. Mass. Inst. Tech., Cambridge, 1952).
[579] Zener, C., *Trans.*, AIME *167*, 550 (1946).
[580] Zener, C., *Phys. Rev.*, *71*, 846 (1947).
[581] Zener, C., *Elasticity and Anelasticity of Metals* (Univ. Chicago Press, Chicago, 1948), p. 19.
[582] Zener, C., *Trans.*, AIME *203*, 619 (1955).
[583] Zerwekh, R. P., Wayman, C. M., *Acta Met.*, *13*, 99 (1965).
[584] Ziegler, W. T., Young, R. A., Floyd, A. L., *J. Am. Chem. Soc.*, *75*, 1215 (1953).
[585] Zwikker, C., *Physica*, *6*, 361 (1926).
[586] Isaitschew, I., Kaminsky, E., Kurdjumov, G. V., *Trans.*, AIME *128*, 361 (1938).
[587] Fine, M. E., Greener, E. H., *Trans.*, AIME *212*, 476 (1958).
[588] Geisler, A. H., *Acta Met.*, *2*, 639 (1954).
[589] Honda, K., Iwase, K., *Sci. Rept.* (Tohoku Univ., Sendai, 1927), *16*, 1.
[590] Houdremont, I. E., Krisiment, O., *Arch. Eisenhuettenw.*, *24*, 53 (1954).
[591] Il'ina, V. A., Kritskaya, V. K., *Dokl. Akad. Nauk. SSSR*, *85*, 997 (1952).
[592] Koistinen, D. P., Marburger, R. E., *Acta Met.*, *7*, 59 (1959).
[593] Kurdjumov, G. V., Perkas, M. D., Shamov, A. E., *Dokl. Akad. Nauk. SSSR*, *92*, 955 (1953).
[594] Forster, F., Scheil, E., *Z. Metall.*, *32*, 165 (1940).
[595] Clark, D., Jepson, K. S., Lewis, G. I., *J. Inst. Metals*, *91*, 197 (1962–63).
[596] Koster, W., Schneider, A., *Z. Metall.*, *32*, 156 (1940).
[597] Bystrom, A., Almin, K. E., *Acta Chem. Scand.*, *1*, 76 (1947).
[598] Lement, B. L., *Nuovo Cimento*, *1*, 295 (1955).
[599] Gindin, I. A., Lazarev, B. G., Starodubov, D., Khotkevich, V. I., *J. Exptl. Theoret. Phys. (USSR)*, *35*, 802 (1958).
[600] Carpenter, H., Robertson, J. M., *Metals* (Oxford Univ. Press., New York, 1939), p. 897.

[601] Krisement, O., Houdremont, I. E., Wever, F., *Rev. Met., 51*, 401 (1954).
[602] Bedford, R. G., *J. Appl. Phys., 36*, 113 (1965).
[603] Hocheid, B., Tanon, A., Miard, F., *Acta Met., 13*, 144 (1965).
[604] Nash, S. K., *Tech. Rept.* (Dept. Met. Mass. Inst. Tech., Cambridge, Mass., 1951)
[605] Speich, G. R., *ASTIA Rept. No. AD 72077* (1955).
[606] Bowles, J. S., MacKenzie, J. K., *Trans.*, AIME *194*, 1201 (1952).
[607] Irvine, K. J., Llewellyn, D. T., Pickering, F. B., *J. Iron Steel Inst., 193*, 218 (1959).
[608] Kaufman, L., *ASTIA Rept. No. AD 144220* (1959).
[609] Bunshah, R. F., Lahteenkorva, E. E., Mehl, R. E., *ASTIA Rept. AD 32674* (1959).
[610] Gawranrek, V., Kaminsky, E., Kurdjumov, G. V., *Metallwirtscheft, 15*, 370 (1936).
[611] Bokros, J. C., Parker, E. R., *Acta Met., 11*, 1291 (1963).
[612] Kaminsky, E., *Tech. Phys. (USSR), 5*, 953 (1938).
[613] Nishiyama, Z., *Sci. Rept.* (Tohoku Univ., Sendai, 1936) *25*, 79.
[614] Philibert, J., *Compt. Rend., 241*, 190 (1955).
[615] Kajiwara, S., Nishiyama, Z., *Japan J. Appl. Phys., 3*, 749 (1964).
[616] Kaufman, L., Leyenaar, A., Harvey, J. S., *Progress in Very High Pressure Research* (J. Wiley & Sons, New York, 1961), p. 90.
[617] Kunze, G., *Z. Metall., 55*, 307 (1964).
[618] Fisher, J. C., *Thermodynamics in Physical Metallurgy* (Am. Soc. Metals, Cleveland, Ohio, 1949), p. 201.
[619] Dehlinger, U., *Theoretical Metallography, AEC-Tr-4500* (U. S. Atomic Energy Comm., 1958).
[620] Frank, F. C., *Rept.* Bristol Conf. on the Strength of Solids (Phys. Soc., London, 1948), p. 57.
[621] Eshelby, J. D., *Proc.*, Roy Soc. (London) *A241*, 376 (1957).
[622] Eshelby, J. D., *Proc.*, Roy Soc. (London) *A242*, 261 (1959).
[623] Eshelby, J. D., *Progress in Solid Mechanics* (North Holland, Amsterdam, 1961), *2*.
[624] Fisher, J. C., *Trans.*, Am. Soc. Metals *47*, 451 (1955).
[625] Kröner, E., *Acta Met., 2*, 302 (1954).
[626] Hull, D., *Bull.*, Inst. Metals *2*, 134 (1954).
[627] Bogers, A. J., Burgers, W. G., *Acta Met., 12*, 255 (1964).
[628] Blackburn, L. D., Kaufman, L., Cohen, M., *Acta Met., 13*, 533 (1965).
[629] Kelly, P. M., Nutting, J., *J. Iron Steel Inst., 192*, 246 (1959).
[630] Kasen, M. B., Polonis, D. H., *Acta Met., 10*, 959 (1962).
[631] Nishiyama, Z., Kajiwara, S., Japan *J. Appl. Phys., 2*, 478 (1963).
[632] Maksimova, O. P., Nikonorova, A. I., *Dokl. Akad. Nauk. SSSR, 81*, 183 (1951).
[633] Dreyer, G. A., Polonis, D. H., *Trans.*, AIME *221*, 1074 (1961).
[634] Wert, C. A., Alstetter, C. J., Nelson, J. O., Rashid, M. S., *ASTIA Rept. No. AD 609017* (1964).
[635] Liu, Y. C., *ASTIA Rept. No. AD 40224* (1954).
[636] Gridnev, V. N., Trefilov, V. I., *Dokl. Akad. Nauk. SSSR, 95*, 741 (1954).
[637] Malyshev, K. A., *Fiz. Metal. i Metalloved., 18*, 239 (1964).
[638] Arskii, V. N., *Metallog. Processing Metals, 11*, 26 (1956).
[639] Barson, F., Legvold, S., Spedding, F. H., *Phys. Rev., 105*, 418 (1957).
[640] Kurdjumov, G. V., *Trans.*, AIME *133*, 222 (1938).
[641] Bridgman, P. W., *Phys. Rev., 48*, 893 (1935).
[642] Doi, M., Nishiyama, Z., *Mem.*, Inst. Sci. Ind. Res., Osaka Univ. *11*, 153 (1954).
[643] Nishiyama, Z., Shimizu, S., *Mem.*, Inst. Sci. Ind. Res., Osaka Univ. *15*, 105 (1958).
[644] Raub, E., Platte, W., *Z. Metall., 51*, 477 (1960).
[645] Fallot, M., *Ann. Phys., 10*, 291 (1938).
[646] Martelly, J., *Ann. Phys., 9*, 318 (1938).
[647] Burgers, W. G., Klostermann, J. A., *Acta Met., 13*, 568 (1965).
[648] Bogaceva, G. N., Sadovskij, V. D., *Dokl. Akad. Nauk. SSSR, 83*, 569 (1952).
[649] Petrosjan, P. P., *Dokl. Akad. Nauk SSSR, 59*, 1109 (1948).
[650] Prosvirin, V. I., *Zh. Tehkn. Fiz., 19*, 542 (1949).
[651] Kurdjumov, G. V., Khandros, L. C., *Dokl. Akad. Nauk. SSSR, 66*, 211 (1949).
[652] Kurdjumov, G. V., *Dokl. Akad. Nauk. SSSR, 60*, 1543 (1948).

[653] Kurdjumov, G. V., Maksimova, O. P., *Stal SSSR, 10,* (1950) (as quoted in Ref. [598]).
[654] Arkarov, V. I., *Dokl. Akad. Nauk. SSSR,* 1744 (1951) (as quoted in Ref. [598]).
[655] Kogan, L. I., Entin, R. I., *Dokl. Akad. Nauk. SSSR, 73,* 1173 (1950).
[656] Ljubov, B. J., *Dokl. Akad. Nauk. SSSR, 72,* 895 (1951).
[657] Arkarov, V. I., *Dokl. Akad. Nauk. SSSR, 70,* 8333 (1950).
[658] Ljubov, B. J., *Dokl. Akad. Nauk. SSSR, 72,* 273 (1950).
[659] Kaufman, L., Radcliffe, S. V., Cohen, M., *Decomposition of Austenite by Diffusional Processes* (Interscience, New York, 1962), p. 313.
[660] Jan, J. P., Pearson, W. B., *Can. J. Phys., 42,* 220 (1964).
[700] Miodownik, A. P., *Inst. Metals Monograph No. 18,* 319 (1956).
[701] Ko, T., Cottrell, S. A., *J. Iron Steel Inst., 172,* 307 (1952).
[702] Smith, R., Bowles, J. S., *Acta Met., 8,* 405 (1960).

H. W. Schadler[1] *and J. W. Livingston*[1]

Effect of Metallurgical Variables on the Superconducting Properties of Metals and Alloys

ABSTRACT[2]

This paper reviews the present understanding of the effects of metallurgical variables (composition, mechanical and thermal history, state of strain, etc.) on the superconducting properties of metals, alloys, and intermetallic compounds.

The discovery of the persistence of superconductivity to high magnetic fields in 1961 initiated a revolution in the understanding of superconductivity. Previously, any materials departing from the simple behavior of "soft" or Type I superconductors were called "hard" superconductors, and their properties, although sometimes characterized, were never explained or exploited. We now realize that some of this "hard" behavior resulted from Type II superconductivity, some from a superconducting surface sheath, and some from specimen inhomogeneities. These concepts are reviewed briefly, and the effects of metallurgical variables on superconducting properties are explained in terms of these concepts where possible.

The extreme structure sensitivity of superconducting properties has illuminated the need for further understanding of structure-property relations in superconductors and has given the metallurgist a unique opportunity to contribute both to the understanding and to the economic use of superconducting materials.

[1] General Electric Research Laboratory, Schenectady, N. Y.

[2] This paper is published in *Progress in Materials Science*, Vol. 12, No. 3, December, 1964.

Robert L. Powell[1]

Thermophysical Properties of Metals at Cryogenic Temperatures

REFERENCE: R. L. Powell, **"Thermophysical Properties of Metals at Cryogenic Temperatures,"** *Behavior of Metals at Cryogenic Temperatures, ASTM STP 387,* Am. Soc. Testing Mats., 1966, p. 134.

ABSTRACT: This paper is concerned with the specific heat and thermal conductivity of metals at cryogenic temperatures. A review of previous studies is complemented by the author's experience. Two internal energy forces affect specific heat—lattice interactions and electronic interactions. Since the lattice specific heat is related to T^3, it is very small at very low temperatures. The total conductivity of a metal is the sum of the electron thermal conductivity and the lattice thermal conductivity. Two factors that reduce electronic thermal conductivity are scattering of conduction electrons by thermal vibrations in the lattice, and scattering of electrons by defects and impurities present in the lattice. It is not yet possible to accurately predict thermal conductivity from fundamentals, but it is possible to make adequate predictions from thermal properties or electrical resistance of similar materials.

KEY WORDS: cryogenics, aluminum alloys, specific heat, thermal conductivity

The mechanical and fabrication properties of solids are of paramount importance for design of efficient cryogenic equipment for the chemical, military, and aerospace industries. The thermophysical properties are also important whenever heat loads, refrigeration, thermal fluctuations or stresses, or boiling cryogenic fluids must be considered. There is a relatively large amount of information available on the mechanical and structural properties of solids at cryogenic temperatures [*1*],[2] but unfortunately the opposite is true for thermophysical properties.

The solid materials for which there are complete thermophysical data are only a minor fraction of the total number that are important and commercially available. This dearth of information will undoubtedly continue in the future, in spite of increased interest, activity, and financial support for cryogenic research, because of the considerable difficulty and

[1] Supervisory physicist, Cryogenics Div., Institute for Materials Research, National Bureau of Standards, Boulder, Colo.

[2] The italic numbers in brackets refer to the list of references appended to this paper.

expense of the actual experimental measurements. It is, therefore, of the utmost importance that a design or materials engineer be able to estimate accurate values for new or untested materials. Unlike many mechanical or fabrication properties, the thermophysical properties (except thermoelectricity) for a given material may often be predicted from theoretical or semiempirical knowledge combined with data on similar materials.

This presentation stresses the basic phenomena and the fundamental concepts and assumptions. Each property is discussed with emphasis on temperature dependences and contributions to the total observed effect.

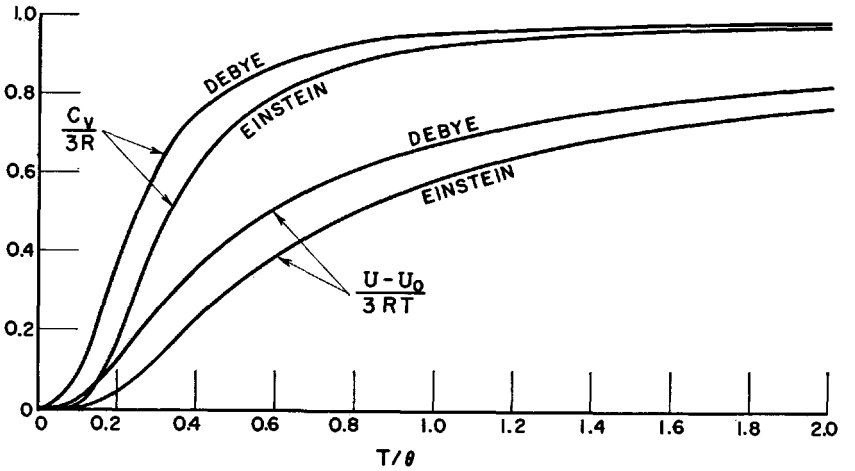

FIG. 1—*Typical heat capacity and internal energy curves for metals.*

Also noted are the interrelations between the various properties and the value of those interrelations as aids in prediction. Besides the usual references to articles and books, information is given on useful compilations and sources of specialized up-to-date bibliographies and data collections.

Because of the breadth of subject and limitations of space, it is impractical to give in this paper either a complete review of the data on various thermophysical properties of solids or a detailed explanation of the underlying assumptions and theories. To make the following discussions more manageable, the solid materials are limited to metals, and the thermophysical properties are limited to specific heat and thermal conductivity. As this is a review article, the subjects will not be confined to our own experimental programs and results.

Specific Heats

The specific heats of metals and alloys are fitted very well by existent theories, at least as far as engineering data are concerned. Therefore, it is common either to tabulate experimental values or to represent them on a

common, reduced temperature graph. Figure 1 is such a graph, but without specific metals or temperatures represented. The essential experimental problem is to ascertain the characteristic temperature, θ. Conversely, given values of the characteristic temperatures, values for specific heat are easily obtained.

The specific heat at constant volume of a metal may be defined as: $C_v \equiv (\partial U/\partial T)_v$, where U is the total internal energy of the metal or alloy system and T is the absolute temperature. The theoretical problem is then to determine the variation of the energy with temperature. There are two main types of energy variation. In the first type, the energy and consequently the specific heat are slowly varying functions of temperature, as shown in Fig. 1. In a metal, the internal energies of the ionic lattice and of the free or conduction electrons are typical examples. In the second type, a particular type of internal energy changes significantly only over a restricted temperature range. The energies of transformation for phase changes and magnetic ordering are examples of the latter type. The specific heat contribution for the transformation in these processes is observable only over the same restricted temperature range as the energy change. The restricted temperature range or anomalous specific heats are of tremendous importance for physics and chemistry research, but usually are not of great significance in commercial materials. In the following discussion, the anomalous specific heats will be omitted.

The lattice specific heat is much larger than the electronic specific heat at most temperatures. It will be discussed first. Einstein's representation of the ionic lattice as a system of independent oscillators led to the equation: $C_v = 3RE(\theta E/T)$, where θ is a characteristic temperature, R is the gas constant, and E is the Einstein function as defined by: $E(\theta/T) \equiv (\theta/T)^2 e^{\theta/T}/(e^{\theta/T} - 1)^2$. This gives a good fit at and above room temperatures, approximating the earlier observed Dulong-Petit universal value for heat capacity at high temperatures. It does not fit well at low temperatures, however.

The lattice of ions is known to interact. When this is taken into consideration and some simplifying approximations are made for the distributions of energies, the Debye theory is obtained. This theory is almost too good; its predictive ability was so successful that theoretical refinements were not considered seriously for many years. The Debye specific heat (for the lattice) is: $C_v = 3RD(\theta D/T)$, where the Debye function, D, is defined as:

$$D\left(\frac{\theta}{T}\right) \equiv 3\left(\frac{T}{\theta}\right)^3 \int_0^{\theta/T} \frac{x^4 e^x}{(e^x - 1)^2}\, dx$$

The Einstein and Debye specific heat and energy curves are shown in Fig. 1.

The main characteristics of the Debye curve are easily seen. At low temperatures the specific heat varies as T^3; at high temperatures it is ap-

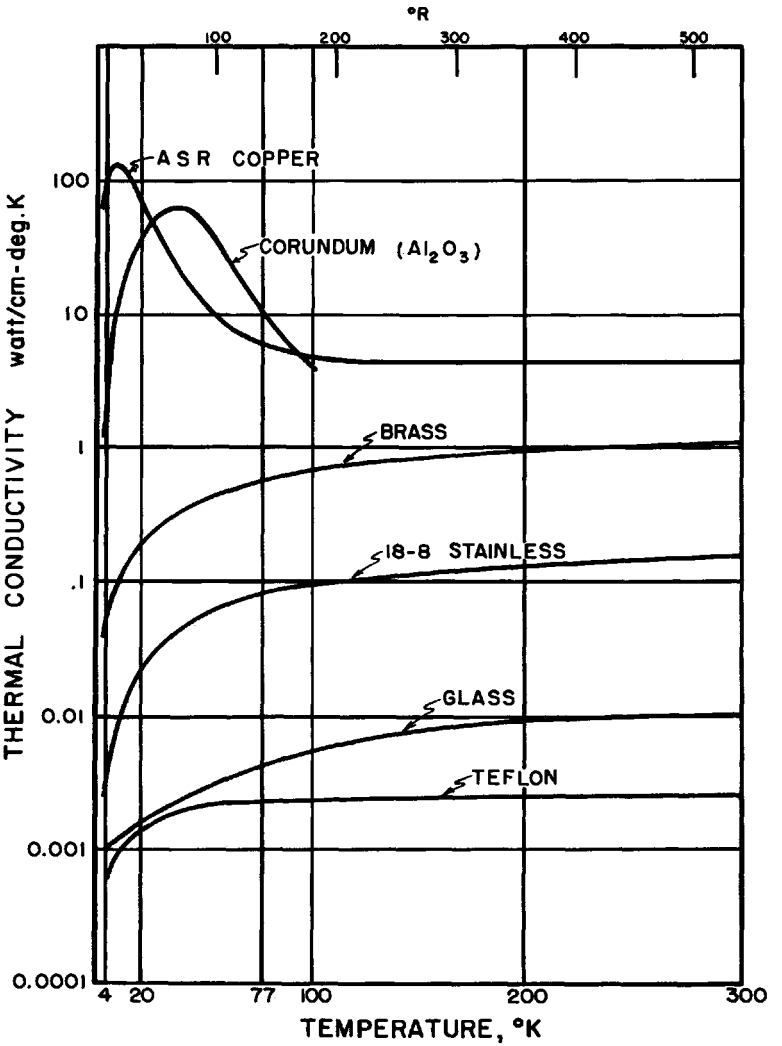

FIG. 2—*Thermal conductivity of several solids.*

proximately constant. The theory was developed for isotropic, homogeneous metals; how does it apply to alloys?

Near room temperature, the specific heat of an alloy is obtained quite well by the Kapp-Joule rule: the total specific heat is a linear combination of the specific heats of the constituents, each weighted according to its relative abundance. At low temperatures, one can either combine additively the actual specific heats of the constituents or take a weighted average of the characteristic temperatures. Either procedure will give approximately correct results.

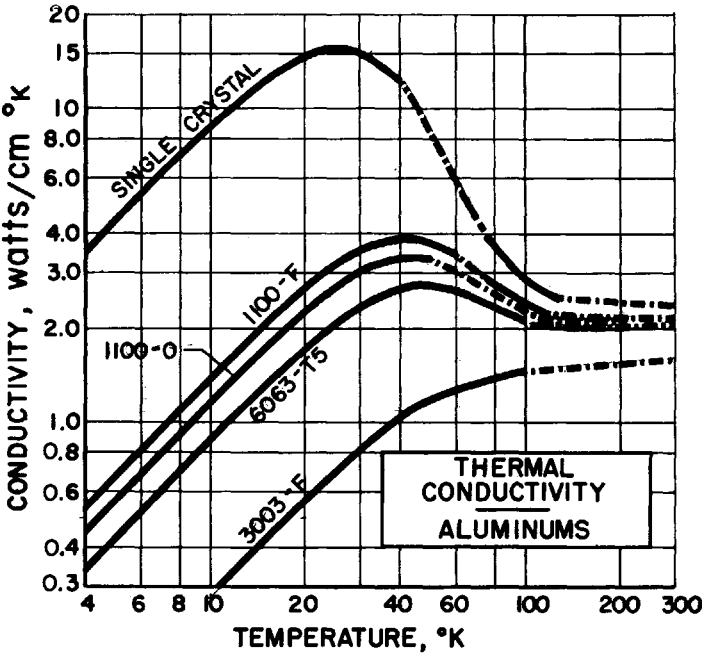

FIG. 3—*Thermal conductivity of aluminums.*

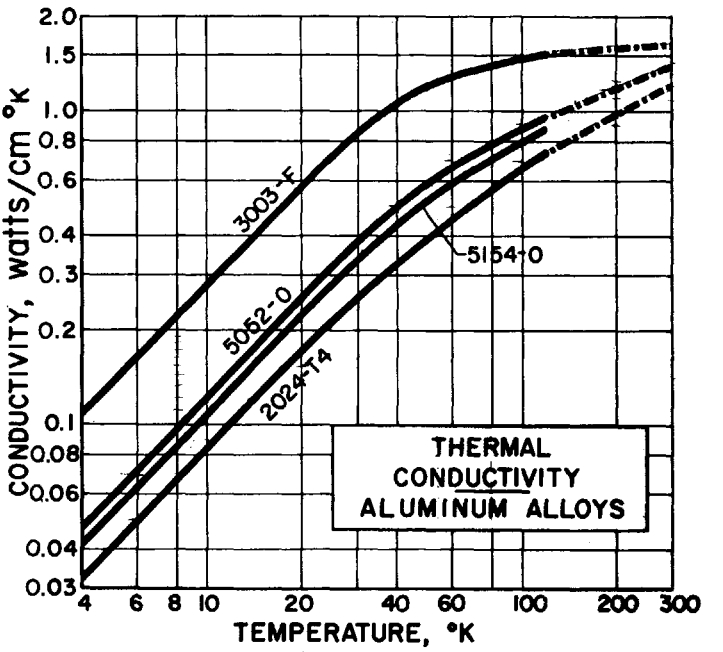

FIG. 4—*Thermal conductivity of aluminum alloys.*

The electronic specific heat is small compared to the lattice contribution at high temperatures, but it is linear in its temperature variation. Since the lattice term decreases as T^3, the electronic term will become significant only at the lowest temperatures. It is usually not significant for engineering applications.

The detailed theories for specific heat have been given in many references. The elementary discussions are covered in most solid-state textbooks; a recent review with emphasis on low temperatures has been given by Rosenberg [2]. Articles in the *Handbuch der Physik* by Blackman [3] and Keesom and Pearlman [4] are more thorough. Tables of the Einstein

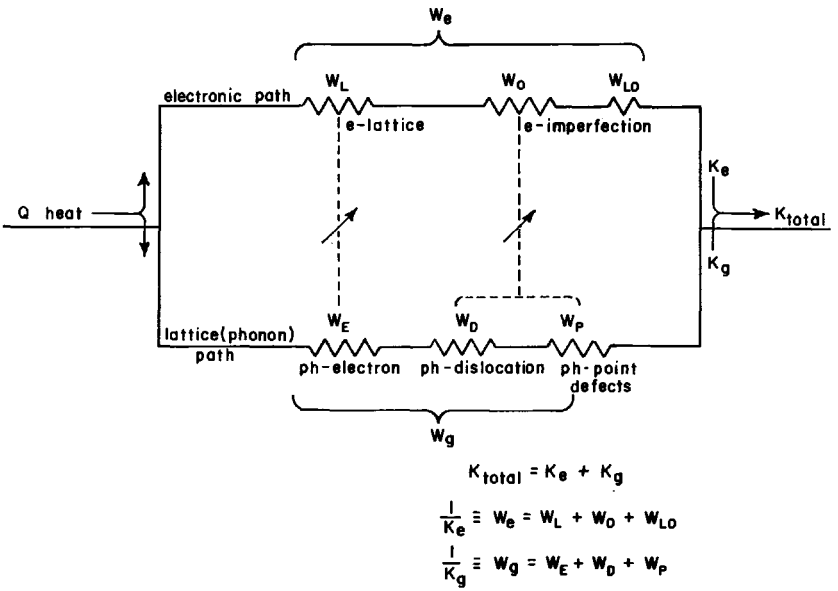

FIG. 5—*Electrical analog for thermal conduction. (The dashed lines with arrows indicate resistances that depend on the same basic scattering phenomena.)*

and Debye functions have been given by Landolt-Börnstein [5], Beattie [6], and by Rogers and Powell [7].

Actual experimental values for either the specific heat or the characteristic temperature have been given by Corruccini and Gniewek [8] and the NBS low-temperature compendium [9]. The Thermophysical Properties Research Center at Purdue University and the Cryogenic Data Center at the National Bureau of Standards in Boulder, Colo. are sources for current bibliographies and tabulated values.

Thermal Conductivity

The thermal conductivities of several solids are represented in Fig. 2. The variations in temperature dependences and absolute values are

obvious. Again restricting the materials to metals, Fig. 3 gives values for pure and commercial aluminums; Fig. 4 gives values for aluminum alloys. Even within those restrictions, there is considerable variation. Is it possible to make order out of this variety; is it possible to be able to predict reasonably well the thermal conductivity for new or untested materials? It is, if one utilizes knowledge of the fundamental phenomena.

Two parallel interdependent mechanisms are primarily responsible for the transport of heat in a metal at low temperatures. The first and most important is the electronic thermal conduction, the transport of thermal energy by the motion of conduction electrons. The second is the lattice thermal conduction, the transport by directional cooperative quantized vibrations (called phonons) of the thermally excited interacting lattice ions. These are the same phonons that are responsible for the observed specific heats and thermal expansions in metals. For pure metals and dilute alloys, the lattice thermal conductivity is insignificant compared to the electronic thermal conductivity. For alloys with several per cent, or more, of additives, the decreased electronic thermal conductivity allows the lattice contribution to become significant, though it is still small compared to the electronic contribution. For most metals and alloys, the total conductivity, K, is the sum of two terms, the electronic conductivity, K_e, and the lattice conductivity, K_g, (the subscript g stands for *Gitter*, the German word for lattice), that is, $K = K_e + K_g$. This equation is analogous to the one used in electrical circuit theory for the total conductance of two conductances in parallel. Both conduction mechanisms, K_e and K_g, are limited by various scattering processes, each process acting additively as a separate resistance in series. A representation of the analog is given in Fig. 5.

There are two main scattering processes that limit the electronic conductivity in the above expression. The first is the scattering of conduction electrons by thermal vibrations of the lattice (the phonons again), as represented by the electron-phonon resistivity, W_L, a characteristic property for a given metal. This scattering is most important at intermediate temperatures (about 40 to 80 K) and higher. The second process is the scattering of conduction electrons by imperfections (both impurity atoms and lattice defects), as represented by the electron-defect resistivity, W_0. This scattering is most important at the lower temperatures. The reciprocal of the total electronic thermal conductivity, K_e, is the total electronic thermal resistivity, W_e, which is assumed to be the sum of the two resistivities, W_L and W_0, plus a small deviation term, W_{L0}, that is, $1/K_e \equiv W_e = W_L + W_0 + W_{L0}$. This equation is analogous to the one used in electrical circuit theory for the total resistance of resistances in series.

The deviation term has been studied theoretically by Kohler [*10*] and independently in experiments by Powell et al [*11*]. It is of the form: $W_{L0} = \alpha W_L W_0/(\beta W_L + \gamma W_0)$, where α, β, and γ are constants of Order 1

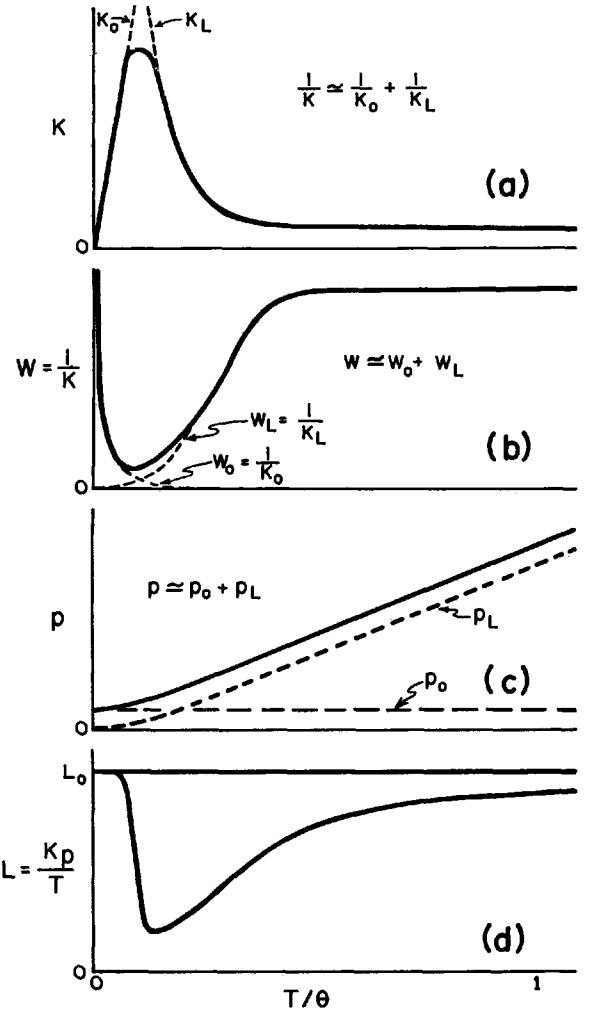

(*a*) Thermal conductivity.
(*b*) Thermal resistivity.
(*c*) Electrical resistivity.
(*d*) Lorenz ratio.

FIG. 6—*Matthiessen's rule for conductivities.*

and can be determined experimentally. Though theoretically significant, the term is numerically important only for very pure metals.

Whenever the interaction term W_{L0} is negligible, the thermal equivalent of Matthiessen's rule for electrical resistivity, $W_e = W_L + W_0$, is approximately correct. A graph of this relation and its equivalent for conductivity are given in Fig. 6. With knowledge of the two separate terms, prediction of the total electronic thermal resistivity becomes reasonable.

Both theoretical and experimental research have led to expressions for magnitudes and temperature dependences of the electron-phonon and electron-defect resistivities: $W_L = AT^n$ ($n \approx 2$ to 3, $T < 40$ K); $W_L \approx$ a constant (near room temperatures); $W_0 = B/T$ (at all temperatures). The constant A in the electron-phonon resistivity term is related to the intrinsic properties (including the characteristic temperature, θ) of a given metal and will not change for minor additions of chemical impurities or physical imperfections; B in the electron-defect resistivity term is related to the given amount of imperfections and residual electrical resistivity of the specific specimen. Above 40 K, the electron-phonon resistivity approaches a constant value, often labeled W_∞.

Figures 3 and 4 clearly show the effects of adding more impurities to a given metal, thereby increasing W_0. A detailed analysis would show that the electron-phonon term, W_L, did not change, that is, it is really intrinsic to aluminum. At low temperatures, the curves are parallel, with the higher impurity alloy lying lower. At higher temperatures, the curves approach each other, the differences decreasing approximately as $1/T$. The detailed methods of analysis and techniques for separation of electronic components of thermal resistivity have been outlined in a previous paper by Powell et al [*12*].

The shapes of the curves for aluminums in Fig. 3 are typical of pure metals: electronic conductivity is predominant, lattice conductivity is negligible. For a metal specimen with no chemical impurities or physical defects, the electron-phonon scattering component caused by the thermally excited ionic lattice, W_L, governs the temperature dependence of the conductivity. As the temperature is lowered, the resistivity decreases in approximate proportion to T^2; the conductivity rises equivalently. Superimposed on this decreasing ideal of electron-phonon resistivity is the electron-defect resistivity which increases as the temperature is decreased. At a minimum in the resistivity curve or maximum in the conductivity curve, the two scattering mechanisms are approximately equal. At higher temperatures, electron-phonon scattering is predominant; at lower temperatures, electron-defect scattering is predominant. The defects that limit conductivity at low temperatures can be quite varied: chemical impurities, inclusions, vacancies, interstitial atoms, dislocations, grain boundaries, external surface boundaries, and so on. Fortunately, for all but the last defect the scattering resistivity has the same temperature dependence, the B/T mentioned earlier. The boundary scattering is difficult to investigate and can be observed only in extremely pure metals at very low temperatures.

At the present, it is not possible to predict accurately the thermal conductivity of pure metals on the sole basis of their chemical analyses or physical specifications. The effect of each kind of chemical impurity is specific. Among other things, it depends on magnetic interactions and the

differences between host and impurity in ionic mass, ionic volume, and valence electrons. A great deal of work has been done on the specific effects of impurities in electrical resistivity, but little has been done in thermal conductivity. Sometimes even a chemical analysis is not of great help; a given impurity is much more effective as a scatterer if it is in solid solution rather than segregated at grain boundaries or in inclusions. This segregation effect is very pronounced in coppers [*13*]. Similar interpretive difficulties arise for physical defects.

The variations of thermal conductivity caused by relatively minor chemical impurities or physical imperfections are in sharp contrast to the relative insensitivity to defects observed in thermal expansions or specific heats. Successful prediction of thermal conuctivity, within about 10 to 20 per cent, is dependent on a skillful analysis of the probable scattering mechanisms and the availability of experimental results on a very similar metal or alloy. As will be shown later, low-temperature electrical resistivity data are also very valuable for predicting thermal conductivity.

Much of the pioneering experimental work on the separation of thermal conductivity components for pure metals was done at the Clarendon Laboratory, Oxford, by Rosenberg [*14*] and others. Research on commercial alloys of cryogenic importance is reported in References [*11,12,15, 16*]. There has been little additional experimental research on commercial alloys in the last few years. Reviews of the theoretical aspects of electronic conductivity and, in particular, basic expressions for the coefficients A and B have been given by Klemens [*17*] and Jones [*18*] in the *Handbuch der Physik* series, and by Rosenberg in his recent monograph [*2*].

Recently Cezairliyan and Touloukian [*19*] made a valuable contribution to the problem of engineering prediction of thermal conductivity with their original application of the principle of corresponding states. They simplified and separated the two main components of conductivity and expressed the results in easily used, graphic form. Their electron-phonon term was expressed as a function of reduced temperatures, T/T_m, where T is the absolute temperature and T_m is the experimentally determined temperature of maximum conductivity for a given metal.

In many low-conductivity alloys, the lattice thermal conductivity, K_g, is also measurable, and the separate scattering components for it may be resolved. For most alloys, there are three main processes that limit the lattice conductivity. The first process is scattering of the lattice waves by conduction electrons, as represented by the phonon-electron resistivity, W_E. This is the converse of electrons being scattered by phonons. The second process is scattering by dislocations, the phonon-dislocation resistivity, W_D. The third is scattering by point imperfections, the phonon-point imperfection resistivity, W_P. The first two processes will limit the lattice conductivity at lower temperatures; the third will limit it at higher temperatures.

The phonon-electron and phonon-dislocation resistivities have the same temperature dependence. Therefore, for one specimen, the two scattering mechanisms may not be unambiguously separated. For annealed specimens, the two resistivities will be of about the same magnitude; for unannealed specimens, the dislocation resistivity will greatly outweigh the phonon-electron resistivity. Below about 40 K, the lattice conductivity can be represented by: $1/K_g \equiv W_g = W_E + W_D + W_P = (E + D)T^{-2} +$

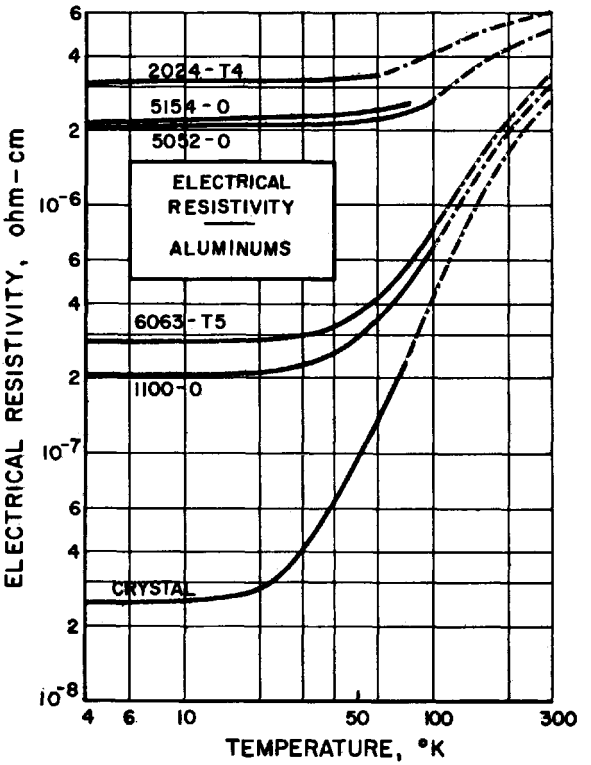

FIG. 7—*Electrical resistivity of aluminums.*

PT. Because of the T^{-2} dependences of the phonon-electron and phonon-dislocation resistivities, they are dominant at low temperatures and negligible at high temperatures. The maximum in lattice conductivity usually will occur between 50 and 100 K for most alloys. Above those temperatures, however, the lattice conduction cannot be easily separated experimentally from the electronic conduction because the latter has a much greater magnitude.

The shapes of the curves for aluminum alloys in Fig. 4 are typical; electronic conductivity is dominant, but lattice conductivity is observable. Again, the effects of additional impurities are clear. The detailed methods

of analysis and techniques for separation of electronic and lattice conductivity components and further separation of the various lattice resistivity terms have been outlined in a previous paper [*12*]. For aluminum alloys, the lattice conduction may be about 10 per cent of the total; for some nickel or iron alloys, it may be much higher. Discussions of the theoretical aspects of lattice conductivity in metals have been given by Klemens [*17*] and Rosenberg [*2*] in their general reviews and by Klemens [*20*] in a special review article.

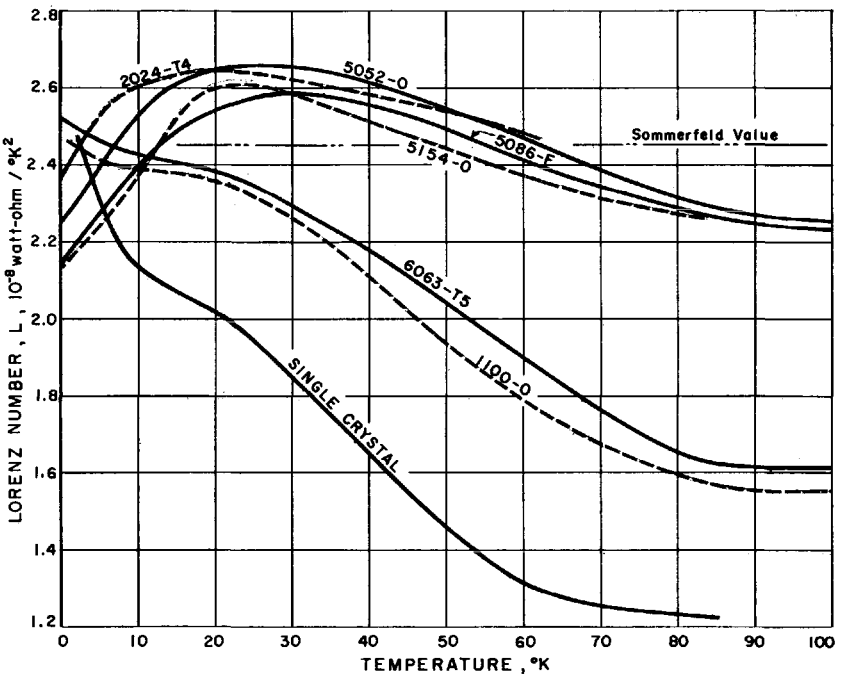

FIG. 8—*Lorenz ratio for aluminums.*

If there is no direct information on the thermal conductivity of a metal, then data on the electrical resistivity may be very helpful. The electrical resistivity may be related to the electronic thermal resistivity by means of the Wiedemann-Franz-Lorenz law: $\rho = LW_eT$, where L is the Lorenz ratio, assumed to be a fundamental constant given by the Sommerfeld value: $L = (\pi^2/3)(K/e)^2 = 2.44 \times 10^{-8}$ [watt-ohm/(deg K)^2].

A discussion of the separation of components and scattering mechanisms for electrical conductivity follows almost exactly that given above on the electronic thermal conductivity. The total electrical resistivity, ρ, is assumed to be the approximate sum of two separate resistivities, the intrinsic or electron-phonon resistivity, ρ_L, and the residual or electron-imperfec-

tion resistivity, ρ_0. In other words, Matthiessen's rule for electrical resistivity, $\rho = \rho_L + \rho_0$, is assumed to be approximately correct.

The expressions for the temperature dependences of the intrinsic and residual terms have been found to be given approximately by: $\rho_L = \alpha T^n$ ($n \approx 4$ to 5, $T < 40$ K); $\rho_L = \alpha' T$ (T near 300 K); $\rho_0 = \beta$ (constant). A graph of the separation of electrical resistivity components for a general metal is given in Fig. 6. Theoretical reviews and expressions for the coefficients α and β have been given by MacDonald [*21*], Gerritsen [*22*], and Rosenberg [*2*]. Experimental results for a typical series of alloys are given in Fig. 7.

Lorenz ratios may be calculated for the aluminums and aluminum alloys given in Figs. 2, 3, and 7. The numbers calculated, and shown in Fig. 8, express the ratios of the electrical resistivities to the total thermal resistivities. The extrapolated values L_0, however, should represent ratios of electronic terms only because the lattice contribution to the total thermal conductivity is greatly reduced at the lowest temperatures. A graph for Lorenz ratios for a general metal is given in Fig. 6.

It is seen that the Lorenz ratios for the high-conductivity specimens extrapolate to approximately the Sommerfeld value at 0 K but fall considerably below it at higher temperatures. The behavior of the low-conductivity alloys is different: the values between about 10 and 60 K are higher, but above 60 K the values are again lower. The regions where the ratios are above the Sommerfeld value indicate temperature ranges where lattice conductivity is important.

The Lorenz ratio should be constant if the conduction electrons are scattered elastically. That condition is approximately true at high temperatures, where there is a large amount of thermal vibration giving rise to large electron-phonon scattering, and at low temperatures, where the residual term is predominant in the electrical resistivity. At intermediate temperatures, the condition of elasticity no longer holds, and Lorenz ratios decrease considerably from the Sommerfeld value, if the lattice thermal conductivity is negligible. Any significant amount of lattice thermal conductivity will raise the Lorenz ratio above the value it would have had if only the electronic term in the thermal conductivity were considered.

Very little research has been reported on the Lorenz ratio of commercial alloys. Whenever electrical resistivities for a special material and Lorenz ratios for the general class of materials are available, however, reasonable predictions for thermal conductivity can be obtained.

It has been shown that at the present time it is not possible to accurately predict thermal conductivities for metals and alloys from the fundamentals. It is possible to make adequate predictions, however, if there are data on the thermal or electrical resistivities of similar materials and if one uses proper interpolation formulas and a knowledge of the effects of minor changes in the chemical impurities or physical imperfections. It is

imperative, of course, that good compendiums of experimental data exist. Fortunately, they do.

A convenient (but now out-of-date) desk pamphlet was published earlier by Powell and Blanpied [*23*]. More up-to-date but less thorough tables are included in the *American Institute of Physics Handbook* [*24*] and in the NBS low-temperature compendium [*9*]. Cezairliyan and Touloukian's report [*19*], which was mentioned earlier, has many valuable graphs on metals and dilute alloys. The giant of them all, a library in itself, is *Thermophysical Properties Research Center Data Book* [*25*], edited by Touloukian and his staff at Purdue University. These are exhaustive, containing thermal conductivities of all materials, in all phases, at all temperatures, wherever there is any reliable information. They are kept current with regularly issued addenda.

References

[*1*] See, for example, the other papers in this book and those presented in a similar session at the Sixty-seventh ASTM Annual Meeting, Chicago, Ill., June 21–26, 1964, as printed in *Materials Research & Standards*, Vol. 4, No. 10, October 1964, pp. 523–554.

[*2*] H. M. Rosenberg, *Low Temperature Solid State Physics*, Oxford Press, London, 1963.

[*3*] M. Blackman, "The Specific Heat of Solids," *Handbuch der Physik*, Vols. VII/1, Springer Verlag, Berlin, 1955, pp. 325–382.

[*4*] P. H. Keesom and N. Pearlman, "Low Temperature Heat Capacity of Solids," *Handbuch der Physik*, Vol. XIV, Springer Verlag, Berlin, 1956, pp. 282–337.

[*5*] Landolt-Börnstein, 6th ed., Vol. II, Part 4, Springer Verlag, Berlin, 1961, pp. 736–749.

[*6*] J. A. Beattie, "Six-Place Tables of the Debye Energy and Specific Heat Functions," *Journal of Mathematical Physics*, Vol. VI, 1926, p. 1.

[*7*] W. M. Rogers and R. L. Powell, "Tables of Transport Integrals," *Nat. Bur. Standards Circular 595*, July 1958.

[*8*] R. J. Corruccini and J. J. Gniewek, "Specific Heats and Enthalpies of Technical Solids at Low Temperatures," *Nat. Bur. Standards Monograph 21*, October 1960.

[*9*] V. J. Johnson, Ed., "A Compendium of the Properties of Materials at Low Temperatures, Part II, Properties of Solids," *WADD Technical Report 60–56*, July 1960. Available from Office of Technical Services, U. S. Dept. of Commerce, Washington 25, D. C.

[*10*] M. Kohler, "Allgemeine Theorie der Abweichungen von der Mathiessenschen Regel," *Zeitschrift der Physik*, Vol. 126, 1949, pp. 495–506.

[*11*] R. L. Powell, H. M. Roder, and W. J. Hall, "Low-Temperature Transport Properties of Copper and Its Dilute Alloys: Pure Copper, Annealed and Cold-Drawn," *Physical Review*, Vol. 115, July 1959, pp. 314–323.

[*12*] R. L. Powell, W. J. Hall, and H. M. Roder, "Low Temperature Properties of Commercial Metals and Alloys. II Aluminums.", *Journal of Applied Physics*, Vol. 31, March 1960, pp. 496–503.

[*13*] R. L. Powell, H. M. Roder, and W. M. Rogers, "Low Temperature Thermal Conductivity of Some Commercial Coppers," *Journal of Applied Physics*, Vol. 28, November 1957, pp. 1282–1288.

[*14*] H. M. Rosenberg, "The Thermal Conductivity of Metals at Low Temperatures," *Philosophical Transactions*, Royal Society, London, Vol. A247, March 1955, pp. 441–497.

[*15*] R. L. Powell, M. D. Bunch, and E. F. Gibson, "Low-Temperature Transport Properties of Commercial Metals and Alloys. III. Gold-Cobalt," *Journal of Applied Physics*, Vol. 31, March 1960, pp. 504–505.

[16] R. L. Powell, J. L. Harden, and E. F. Gibson, "Low-Temperature Transport Properties of Commercial Metals and Alloys. IV. Reactor Grade Be, Mo, and W," *Journal of Applied Physics*, Vol. 31, July 1960, pp. 1221–1224.

[17] P. G. Klemens, "Thermal Conductivity of Solids at Low Temperatures," *Handbuch der Physik*, Vol. XIV, Springer Verlag, Berlin, 1956, pp. 198–281.

[18] H. Jones, "Theory of Electrical and Thermal Conductivity in Metals," *Handbuch der Physik*, Vol. XIX, Springer Verlag, Berlin, 1956, pp. 227–315.

[19] A. Cezairliyan and Y. S. Touloukian, "Correlation and Prediction of Thermal Conductivity of Metals Through the Application of the Principle of Corresponding States," *Advances in Thermophysical Properties at Extreme Temperatures and Pressures*, Am. Soc. Mechanical Engineers, New York, 1965, pp. 301–313. Also *Technical Document Report ASD-TDR-63-291* available from Office of Tech. Services, U. S. Dept. of Commerce, Washington, 25, D. C.

[20] P. G. Klemens, "Thermal Conductivity and Lattice Vibrational Modes," *Solid State Physics*, Vol. 7, Academic Press, New York, 1958, pp. 1–98.

[21] D. K. C. MacDonald, "Electrical Conductivity of Metals and Alloys at Low Temperatures," *Handbuch der Physik*, Vol. XIV, Springer Verlag, Berlin, 1956, pp. 137–197.

[22] A. N. Gerritsen, "Metallic Conductivity, Experimental Part," *Handbuch der Physik*, Vol. XIX, Springer Verlag, Berlin, 1956, pp. 137–226.

[23] R. L. Powell and W. A. Blanpied, "Thermal Conductivity of Metals and Alloys at Low Temperatures," *Nat. Bur. Standards Circular 556*, September 1954. Now out of print, but available in depository libraries.

[24] R. L. Powell, "Sec. 4g. Thermal Conductivity," in *American Institute of Physics Handbook*, 2nd ed., McGraw-Hill, New York, 1963, pp. 4–76 to 4–101.

[25] Y. S. Touloukian, Ed., *Thermophysical Properties Research Center Data Book*, Vol. 1, "Metallic Elements and Their Alloys," Chap. 1, "Thermal Conductivity," Purdue University, Lafayette, Ind., 1964.

THIS PUBLICATION is one of many issued by the American Society for Testing and Materials in connection with its work of promoting knowledge of the properties of materials and developing standard specifications and tests for materials. Much of the data result from the voluntary contributions of many of the country's leading technical authorities from industry, scientific agencies, and government.

Over the years the Society has published many technical symposiums, reports, and special books. These may consist of a series of technical papers, reports by the ASTM technical committees, or compilations of data developed in special Society groups with many organizations cooperating. A list of ASTM publications and information on the work of the Society will be furnished on request.